Dynamic optimization based reactor synthesis and design under uncertainty for liquid multiphase processes

Dissertation

zur Erlangung des akademischen Grades

Doktoringenieur

(Dr.-Ing.)

von: Dipl.-Ing. Nicolas Maximilian Kaiser

geb. am: 24. September 1987

in: Aachen

genehmigt durch die Fakultät für Verfahrens- und Systemtechnik der Otto-von-Guericke-Universität Magdeburg

Promotionskommission: Prof. Dr. rer. nat. habil. Helmut Weiß (Vorsitz)
Prof. Dr.-Ing. habil. Kai Sundmacher (Gutachter)
Prof. Dr.-Ing. Robert Flassig (Gutachter)
Prof. Dr.-Ing. Magne Hillestad (Gutachter)

eingereicht am: 11. Dezember 2018

Promotionskolloquium am: 09. August 2019

Abstract

New process structures for the substitution of petrochemical feedstocks by renewables are required to cope with the upcoming scarcity of hydrocarbon resources and to decrease the anthropogenic impact on climate change. These challenges are triggered and increased by rising demands of a steadily growing world population and their increasing living standards. The development of therefore required innovative processes is a complex, interdisciplinary, multi-scale challenge including various fields of natural science and engineering. One of the main stimuli of and contributions to this endeavor are provided by computer-aided tools on every time and length scale of the process development procedure. With the Collaborative Research Center TR 63 “InPROMPT” a trans-regional project was founded (i) to investigate the utilization of innovative solvent systems for the functionalization of long chain substrates from renewable feedstocks and (ii) to develop the required tools for fast and efficient design of the corresponding process systems. As part of this project, the presented work had the goal to design an optimal reactor unit for the hydroformylation of 1-dodecene in a thermomorphic multicomponent solvent system. This process is an example of the very important class of homogeneously catalyzed liquid multiphase processes, which is highly promising for the task of substitution of petrochemical feedstocks. In order to accomplish this task, methodical approaches for the synthesis and design of chemical reactors have been developed and a detailed reactor design study as well as technical realization have been carried out.

An approach for the qualitative synthesis of reactor-networks was created within the process design framework of the methodology of *elementary process functions*. The key notion of the underlying methodology is the dynamic optimization of mass and energy control fluxes manipulating a Lagrangian fluid element on its way through the process in order to make it follow the optimal route in the thermodynamic state space. By analyzing the optimal control fluxes resulting from this dynamic optimization, the developed *flux profile analysis* enables the derivation of reactor-network candidates of different synthesis levels. This includes functions of reaction, separation, and recycling, and allows for a rational selection of promising reactor-network candidates based on reaction engineering fundamentals. The applicability of this approach was proven by comparison to well-known literature examples, which used the *attainable region* approach and *superstructure optimization*. Moreover, its application on the hydroformylation process revealed highly performing process candidates and gained interesting insights into the reaction characteristics.

The second methodical development touches the design of reactors under uncertainty within the aforementioned process design framework. Since past process design studies within this framework neglected the impact of arising uncertainties in the process model and disturbances of the process operation, the aspired development of a probabilistic design approach was necessary and reasonable. In order to include uncertainties in the dynamic optimization of the fluid element, the *unscented transformation* was used. For the reactor design under uncertainty the arising types and sources of uncertainty have been identified and classified with respect to their static or dynamic nature of appearance, and the mathematical formulation of the probabilistic dynamic optimization problem has been derived. The approach was applied on the hydroformylation process example considering model parameter uncertainties on the one hand, and imperfect realization of optimal control profiles on the other hand. Furthermore, the first study was extended in order to identify the most sensitive model parameters by a global sensitivity analysis.

In the final step, both novel approaches were applied to design an optimal reactor for an existing miniplant of the hydroformylation process. This retrofit included the synthesis of an optimal reactor-recycle-network and its detailed technical design and realization under the constraints of the miniplant. The resulting *in silico* design indicated an increase of the yield with respect to the desired

product of 17 % and 23 % for the operation without and with closed side product recycle, respectively, whereby the first prediction was experimentally validated and confirmed.

Within this work it is demonstrated how computer-aided synthesis and design tools significantly improve and accelerate the development of chemical processes, even for a complex liquid multiphase process. The presented dynamic optimization based approaches for reactor synthesis and design under uncertainty have proven to be expedient extensions for the methodology of *elementary process functions*, and they still provide potentials for further improvements and application on other processes.

Zusammenfassung

Es bedarf der Entwicklung neuer verfahrenstechnischer Prozesse zur Substitution petrochemischer durch regenerative Rohstoffe, um der allmählichen Verknappung von Kohlenwasserstoffressourcen zu begegnen und den anthropogenen Einfluss auf den Klimawandel zu reduzieren. Diese Problemstellungen werden durch steigende Bedürfnisse einer stetig wachsenden Weltbevölkerung und deren Lebensstandards ausgelöst und verstärkt. Die Entwicklung dieser innovativen Prozesse ist eine komplexe, interdisziplinäre, mehrskalige Herausforderung, die verschiedenste Bereiche der Naturwissenschaften und Ingenieurswissenschaften einspannt. Einen großen Antrieb und Beitrag zu dieser Bestrebung leisten dabei computergestützte Werkzeuge, die auf jeder Zeit- und Größenskala der Prozessentwicklung eine wichtige Rolle spielen. Mit dem Sonderforschungsbereich TR 63 „InPROMPT“ wurde ein transregionales Projekt gegründet, das die Nutzung innovativer Lösungsmittelsysteme für die Funktionalisierung langkettiger Substrate aus erneuerbaren Rohstoffen untersucht und die benötigten Werkzeuge für einen schnellen und effizienten Entwurf der entsprechenden verfahrenstechnischen Prozesse entwickeln soll. Als Teil dieses Projektes hatte die vorliegende Arbeit zum Ziel, einen optimalen Reaktor für einen Prozess zu entwerfen, der zur sehr wichtigen Klasse der homogenkatalysierten flüssigen Mehrphasenprozessen gehört. Ein Prozess mit vielversprechendem Potential für die Bewältigung der zuvor genannten Substitution petrochemischer Rohstoffe ist die Hydroformylierung von 1-Dodecene in temperaturgesteuerten Mehrkomponenten-Lösungsmittelsystemen. Mit diesem Ziel vor Augen wurden methodische Ansätze für die Synthese und den Entwurf chemischer Reaktoren entwickelt und eine detaillierte Reaktorentwurfsstudie sowie deren technische Realisierung durchgeführt.

Im Rahmen der Methode der *elementaren Prozessfunktionen* wurde ein Ansatz für die qualitative Synthese von Prozessstrukturen geschaffen. Die Schlüsselvorstellung der zugrundeliegenden Methode ist die dynamische Optimierung von Masse- und Energieflüssen, die ein Lagranges Fluidelement auf seinem Weg durch den Prozess steuern, um es eine optimale Trajektorie im thermodynamischen Zustandsraum folgen zu lassen. Durch die Analyse der optimalen Steuerflüsse dieser dynamischen Optimierung ermöglicht die hier entwickelte *Flussprofilanalyse* die Herleitung von Prozessstrukturkandidaten auf verschiedenen Synthesestufen. Diese beinhalten Funktionen wie Reaktion, Trennung und Rückführung und ermöglicht eine rationale Auswahl vielversprechender Prozessstrukturkandidaten auf Basis reaktionstechnischer Grundlagen. Die Anwendbarkeit dieser Methodik wurde durch den Vergleich mit bekannten Literaturbeispielen, die den Attainable Region Ansatz und Superstrukturoptimierung nutzten, bewiesen. Darüber hinaus lieferte ihre Anwendung auf den Hydroformylierungsprozess leistungsfähige Prozesskandidaten und interessante Einsichten in die Reaktionscharakteristiken.

Die zweite methodische Entwicklung befasst sich mit dem Entwurf unter Unsicherheiten auf Basis der zuvor genannten Entwurfsmethodik. Da deren bisherige Anwendungen in Entwurfsstudien die Auswirkungen von Unsicherheiten im Prozessmodell und des Prozessbetriebs vernachlässigten, ist die angestrebte Entwicklung eines probabilistischen Entwurfsansatzes notwendig und folgerichtig. Um die Unsicherheiten in die dynamische Optimierung zu integrieren, wurde die *Unscented Transformation* herangezogen. Für die Reaktorentwurfsmethode unter Unsicherheiten wurden die auftretenden Arten und Quellen von Unsicherheiten identifiziert, bezüglich ihrer statischen respektive dynamischen Natur klassifiziert und die mathematische Formulierung der probabilistischen dynamischen Optimierung hergeleitet. Die Methodik wurde auf den Hydroformylierungsprozess unter Berücksichtigung sowohl von Modellparameterunsicherheiten als auch ungenauer Optimalsteuerungs-realisierungen angewendet. Zusätzlich wurde erstere Studie erweitert, um die sensitivsten Modellparameter mit Hilfe einer globalen Sensitivitätsanalyse zu identifizieren.

Im letzten Schritt wurden die beiden neuen Methoden zur Entwicklung eines optimalen Reaktors für eine bereits bestehende Miniplant-Anlage des zuvor genannten Hydroformylierungsprozesses genutzt. Dieser Retrofit beinhaltet die Synthese eines optimalen Reaktor-Rückführungs-Netzwerks und dessen detaillierten technischen Entwurf unter den Einschränkungen der Miniplant. Der resultierende *In-silico*-Entwurf wies eine Ausbeutesteigerung des gewünschten Produkts von 17 % bzw. 23 % für den Betrieb ohne bzw. mit geschlossener Nebenproduktrückführung auf, wobei das erstgenannte Ergebnis auch im experimentellen Versuch bestätigt werden konnte.

Die Ergebnisse dieser Arbeit demonstrieren, wie computergestützte Synthese- und Entwurfsmethoden die Entwicklung chemischer Prozesse deutlich verbessern und beschleunigen können, selbst für einen komplexen flüssigen Mehrphasenprozess. Die vorgestellten auf dynamischen Optimierungen basierten Methoden für die Prozesssynthese und den Entwurf unter Unsicherheiten haben sich als zweckmäßige Erweiterungen der Methode der elementaren Prozessfunktionen herausgestellt und bergen noch weitere Verbesserungspotentiale und Anwendungsmöglichkeiten für andere Prozesse.

Content

Nomenclature

Within the following list symbols and abbreviations, which repeatedly occur within the text, are summarized. Notation, which is only locally relevant, is explained on the spot. Ambiguous notations can be concluded from the context.

Latin symbols

A	Collocation matrix	$[-]$
A_c	Cross sectional area	$[m^2]$
a	Correlation coefficient	$[various]$
a_m	Specific surface area	$[m^2\ m^{-3}]$
Cov	Covariance	$[-]$
c	Concentration	$[mol\ m^{-3}]$
D	Design, sensitivity index	$[-]$
D_{ax}	Axial dispersion coefficient	$[m^2\ s^{-1}]$
d	Diameter	$[m]$
E	Expected value	$[-]$
E_A	Activation energy	$[kJ\ mol^{-1}]$
G	Geometrical state	$[m^{-3}]$
g	Equality constraint function	$[-]$
H	Henry constant	$[bar\ ml\ mol^{-1}]$
h	Inequality constraint function, mapping function	$[-]$
h_A	Enthalpy flux	$[J\ mol^{-1}m^{-2}]$
I	Initial value function	$[-]$
j	Diffusion flux density	$[kg\ s^{-1}\ m^{-3}]$
K	Reaction rate parameter, equilibrium constant	$[-]$
k	Reaction rate constant	$[various]$
$k_L a$	Volumetric mass transfer coefficient	$[s^{-1}]$
L	Lagrangian type function	$[-]$
l	Length	$[m]$
M	Molar mass	$[g\ mol^{-1}]$
m	(Component) mass	$[kg]$
m_A	Mass flux	$[kg\ s^{-1}\ m^{-2}]$
N	Stoichiometric matrix	$[-]$
n	Amount of moles, dimensionality	$[mol], [-]$
n/iso	Ratio of linear to branched molecules	$[-]$
o	Objective	$[various]$
$Pé$	Péclet number	$[-]$
p	(Partial) pressure	$[bar]$
q	Heat flux	$[J\ s^{-1}\ m^{-2}]$

R	Universal gas constant	$[J\ mol^{-1}K^{-1}]$
r	Reaction rate, reaction flux	$[mol\ s^{-1}m^{-3}]$
S	Selectivity, section	$[-]$
STD	Standard deviation	$[-]$
T	Temperature	$[K]$
t	Time	$[s]$
u	Control variable	$[various]$
V	Volume	$[m^3]$
$\dot{V}$	Volumetric flow rate	$[m^3\ s^{-1}]$
Var	Variance	$[-]$
v	Velocity	$[m\ s^{-1}]$
W	Final value function	$[various]$
w	Mass fraction	$[-]$
w_t	Technical work	$[J]$
X	Conversion	$[-]$
x	State variable	$[various]$
y	Mass flux density	$[kg\ s^{-1}\ m^{-3}]$
Z	Number of separators	$[-]$
z	Removal flux density	$[kg\ s^{-1}\ m^{-3}]$

Greek symbols

α, β, κ	Tuning factors of UT	$[-]$
ΔG_i	Gibbs reaction enthalpy	$[J]$
ε	Hold-up	$[-]$
ε_{set}	Set point for sigmoidal function	$[-]$
θ	Uncertain variable	$[various]$
λ	Decision variable for sigmoidal function	$[-]$
ν	Stoichiometric coefficient	$[-]$
ξ	Process parameter	$[various]$
ρ	Density	$[kg\ m^{-3}]$
τ	Residence time	$[s]$
ϕ	Tuning factor for sigmoidal function	$[-]$
φ	Differential selectivity	$[-]$
ω	Sigmoidal function	$[-]$

Indices

α	Component index
B	Bottom stream
cat	Catalyst
D	Distillate stream

dec	Decanter
eff	Effective
eq	Equilibrium
f	Final point
gas	Gaseous
in	Inlet
L	Lower
liq	Liquid
m	Molar
max	Maximum
min	Minimum
out	Outlet
R	Reaction, Reactor
ref	Reference
S	Separation
set	Set point
st	Storage tank
t	Technical
tot	Total
U	Upper
V	Volumetric flow included
$*$	Interphase
0	Initial point, basic value

Abbreviations

AR	Attainable region
CAPE	Computer aided process engineering
CFR	Continuous flow reactor
CH	Hydrocarbons
CO	Carbon monoxide
COM	All components
COSMO-RS	Conductor-like screening model for real solvents
CP	Collocation point
CSBR	Cyclic semi-batch reactor
CSTR	Continuous stirred tank reactor
C10an	n-decane
const.	Constant
DMF	Dimethylformamide
DOP	Dynamic optimization problem
DR	Distributed recycled

DSR	Differential sidestream reactor
distr.	Distributed
dyn.	Dynamic
EPF	Elementary process functions
FE	Finite element
FPA	Flux profile analysis
GAS	Gas components
H_2	Hydrogen
HCTR	Helically coiled tube reactor
HJB	Hamilton-Jacobi-Bellman
IR	Initial recycled
iC12en	Isomeric dodecenes
iC13al	2-methyl-dodecanal
init.	Initial
MC	Monte Carlo
MIDO	Mixed integer dynamic optimization
MINLP	Mixed integer nonlinear programming
MORDOP	Multi-objective robust dynamic optimization problem
NLP	Nonlinear programming
nC12an	n-dodecane
nC12en	1-dodecene
nC13al	n-tridecanal
neg.	Negative
ODE	Ordinary differential equation
PDF	Probability density function
PFR	Plug flow reactor
PMP	Pontryagin's minimum principle
pos.	Positive
RBO	Reliability-based optimization
RDO	Robust design optimization
RDOP	Robust dynamic optimization problem
RTD	Residence time distribution
SP	Sigma points
SOL	Solvents
$scCO_2$	Supercritical carbon dioxide
TMS	Thermomorphic multicomponent solvent
TP	Temperature points
TPP	Triphenylphosphan
TPPTS	Tri-(natrium-meta-sulfonatophenyl)-phosphan
UQ	Uncertainty quantification
UT	Unscented transformation

WS	Weighted sum method
ε-CM	Epsilon constraint method

1 Introduction

Research vision

Every century of humankind is characterized by challenges whose solutions decide about the future prospects of societies. Thereby, the development of technologies is often the stimulus for both the faced challenges and the therefore developed solutions. Today, humankind faces new challenges, which are often of anthropogenic kind since they are mainly caused by the unsustainable use of technologies and exploitation of natural goods. The exhaustion of fossil hydrocarbon resources, which today's society is strongly dependent on, and the climate change, which is mainly caused by the unsustainable use of those resources, are the main global challenges we face in our century and, thus, the discussions about their impact and the seeking for solutions are omnipresent. Beside of that, there exist numerous other challenges which also seek for technological solutions, e.g. the supply of fresh water and healthy food for the increasing number of humans, the development of drugs for lethal diseases, satisfying the increasing energy demands around the world, etc. Most of these challenges have in common, that they require the efficient use of resources for production of consumer goods, food, pharmaceuticals, and energy. Hence, humankind aspires to dream processes, which allow for the optimal use of the resources and provide the basis for future generations to live a life without scarcity of vital supplies. All around the world scientists and engineers are working towards technological solutions in the fields of physics, chemistry, medical science, electrical engineering, etc. One of the most crucial building blocks for the development of dream processes is the field of process engineering, which utilizes the insights and knowledge of basic natural sciences to create process systems for the transformation of energy and material in chemical, biochemical, and electrochemical processes. The application areas of these process systems are numerous in industries of e.g. petroleum, pharmaceutical and health, environment, building materials, agriculture, food, water management, cosmetics, electronics, etc., since all of them require materials and energy of various kinds [1].

The major concerns of process engineering are on the one hand the analysis, understanding, and modeling of the physical, biological, and chemical phenomena, which are investigated in the corresponding natural sciences, and on the other hand the use of these mathematical models for the optimal design, control, and operation of process systems, which utilize these phenomena for material and energy conversion. A very crucial role for these purposes plays the *computer-aided process engineering* (CAPE) or *process systems engineering* which investigates the utilization and exploitation of computer-based methods in process engineering. Due to the continuously increasing computational power in the last decades their diversity, complexity, and sophistication increases as well. Their application covers all temporal and spatial scales. On the nano- and micro-scale they are used e.g. in computer-aided molecular design and quantum chemistry, on the meso- and macro-scale e.g. numerical solvers for simulation and optimization of process units and their control as well as computational fluid dynamics are employed, and on the industrial-scale entire processes and plants are simulated and even enterprise-wide decisions are based on mathematical programming results. Hence, the development of computer-aided tools as well as their expedient application in analysis and design frameworks provide a tremendous potential for the endeavor of creating efficient and maybe even dream processes. Vice versa, the current global challenges and requirements for improved computer tools invigorates the innovation in CAPE and paves the way to more sophisticated computer-based analysis, simulation, and optimization tools [2].

Intending to seek for new process structures, which are supposed to substitute petrochemical feedstocks by renewables, and develop procedures and computer-based tools for integrated process design, the trans-regional Collaborative Research Center of the German Research Foundation TR63 "InPROMPT" was founded. Within its structure it mirrors the interdisciplinary nature of the process

development task as it tackles the fundamental chemical and physical analysis of kinetics and thermodynamics, the design of optimal process units, and the systematic synthesis of overall process structures as well with regard to economic criteria. The main concern of this project is the utilization of innovative solvent systems for chemical processes, which intend to functionalize long chain molecules recovered from renewable feedstocks. The resulting liquid multiphase systems represent a complex and highly challenging process class including homogeneous transition metal catalysis, phase equilibria thermodynamics, and advanced process control strategies.

Goals of this work

Within the "InPROMPT" project the subproject this thesis arises from was supposed to design an optimal reactor for the hydroformylation reaction of 1-dodecene in a thermomorphic multicomponent solvent system, which should be set up and experimentally tested in a miniplant. In order to accomplish this task, the methodology of *elementary process functions* (EPF) shall be used which allows for the dynamic optimization based design of chemical reactors. The EPF methodology, introduced by Freund and Sundmacher [3], bases on the notion of a Lagrangian fluid element travelling through the process and being manipulated by optimal mass and energy control fluxes which are a result of a dynamic optimization of the fluid element within the thermodynamic state space. In addition, this method provides a systematic mathematical framework for the description of chemical processes and the inclusion of process intensification options, e.g. for the design of multifunctional reactors. Although a reactor design approach based on the EPF method was introduced before [4] and its applicability had been shown in several design examples (e.g. [5], [6]), the EPF based design framework is supposed to be extended within this thesis to exploit further potentials for process development.

The first aspect touches the synthesis of reactor-networks, i.e. the conceptual design of the optimal topology of the involved units. In contrast to the aforementioned design approach, which is located on the process unit level, the synthesis acts on the plant level and, thus, provides structural information about the process. Therefore, the results of the dynamic optimization of the EPF method, i.e. the optimal control fluxes of mass and energy, are supposed to be analyzed with respect to their features, subdivided in characteristic sections, and associated with generic idealized process units which can be combined to create candidates of optimal reactor-networks. The approach should be able to include different functions as they occur in process systems, i.e. reaction, separation, recycling etc., leading to process systems of different synthesis levels.

The second focus lies on the development of a dynamic optimization based design under uncertainty approach within the EPF framework. As so far all EPF based process designs have been of deterministic nature neglecting uncertainties, which arise due to inaccurate models or disturbances in operation, the extension towards a probabilistic design with the EPF method is a reasonable and necessary step. Therefore, the *unscented transformation* is tailored to the design approach. For the reactor design under uncertainty via dynamic optimization combined with the *unscented transformation* the mathematical formulation has to be derived. Furthermore, the uncertainties and their sources have to be identified and classified with regard to their treatment within the dynamic optimization.

Finally, an optimal reactor for the hydroformylation process is derived applying these novel synthesis and design under uncertainty approaches. Moreover, it is technically designed for the embedding in an existing miniplant setup to demonstrate its increased performance compared to the existing setup and, thus, the beneficial use of the model-based design approaches for the development of process systems.

Structure of the thesis

The thesis is separated into six chapters, whereby the first is satisfied with this introduction. In chapter 2 the methodical background of the EPF methodology is provided. Furthermore, state-of-the-art approaches for reactor synthesis and design under uncertainty are discussed allowing the classification of the presented approaches, and fundamental knowledge about the hydroformylation example process are given together with the required model basis for the following design studies. In the following, chapter 3 covers the novel approach for qualitative reactor synthesis within the EPF methodology. After its principles are introduced, the qualitative synthesis approach is applied to two literature examples for comparison purposes and to the hydroformylation process example intending the synthesis of reactor-network, reactor-recycle-network, and reactor-separator-recycle-network candidates. It closes with a discussion of the novel approach and future prospects. In chapter 4 the design under uncertainty approach is introduced. This includes the identification of uncertainty types and their nature of appearance. The mathematical basics of the *unscented transformation* are presented, and the mathematical formulation of the probabilistic dynamic optimization problem is discussed. The design under uncertainty approach is applied on the hydroformylation process example for the case of model parameter uncertainties and imperfect realization of temperature control profiles. The first is used as well to quantify impacts of individual parameters on the overall performance uncertainty to identify the most sensitive parameters. Finally in this chapter, both uncertainties are combined and a discussion of the approach as well as promising future research aspects is conducted. In chapter 5 both the qualitative synthesis approach and the reactor design under uncertainty approach are used to derive an optimal reactor for the retrofit of an existing miniplant. Therefore, optimal reactor-(recycle)-network candidates are derived and compared with regard to their selectivity-conversion behavior. The most promising candidate is designed in detail for technical realization. At the end of this chapter, the first experimental results of the optimal reactor embedded in the integrated overall process are briefly discussed and the successful performance improvement of the retrofit is indicated. Finally, chapter 6 summarizes the insights and achievements of the work and discusses interesting future prospects for model-based process design.

2 Background

Within this background chapter the fundament of this work is built. At first, the methodical framework of *elementary process functions*, on which the methodical contributions of this work base on, is introduced, and the motivation of these new contributions and their placement with respect to existing works are outlined in subchapter 2.1. Subsequently, subchapter 2.2 provides an overview of existing methods for reactor synthesis and design under uncertainty in order to allow for a classification of the new contributions and their novelties. Finally, the example process, which the novel synthesis and design under uncertainty approaches are applied to, is presented in subchapter 2.3. This includes basic information about the reaction and its catalysis, and covers existing process concepts and innovative process alternatives for the class of processes the example process is a kind of. In addition, the fundamentals of the example process are derived from previous works and the model equations used in the remainder of the work are given.

2.1 Methodical background

2.1.1 Elementary process functions

Chemical processes and their products are as manifold as their design and analysis is complex. All chemical processes have in common that they intend to transform a certain (raw) material into a higher valuable product material. The complexity of this transformation originates from the different occurring physico-chemical phenomena, the corresponding time and length scales, which vary between 10^{-15} to 10^{8} s and 10^{-9} to 10^{6} m, respectively [7], and the numerous operations which are required to realize this transformation. On the smallest scale, the molecular scale, the molecules of different components interact, e.g. by association, adsorption, etc., and react often accompanied by the presence of catalyst species. These interactions take place in one or more phases and/or at their interphases e.g. caused by transport phenomena. The thermodynamic states of the phases have to be controlled by energy and material streams in order to adjust the optimal conditions with respect to chemical and thermodynamic equilibria or to steer occurring chemical reactions. The contacting and/or separation and the control of the thermodynamic states, realized by transport of energy, mass, and momentum, is conducted in process units, which are mostly designed for a specific operation. These process units are interconnected by material and energy streams allowing for sequencing and parallelization of operations, recycling of required material and heat integration, respectively. The resulting process structure or plant might additionally be embedded in an even larger so called composite process which integrates energy, material and waste streams and shares energy and material supplies in a closed network of several different production processes. In order to order and classify these different aspects of a process system, Freund and Sundmacher [8] developed a hierarchical concept which subdivides the process system into four main levels – the molecular level, the phase level, the process unit level, and the plant level, see Fig. 2.1. On each level the process can be analyzed by experiments to gain insights into the process characteristics. The obtained experimental data is used to derive and identify suitable models and their parameters, which serve as a basis for process design procedures. Within this description, the analysis, identification, and design of the process can be carried out either on each level individually or joint for several levels.

Alternative concepts for systematic analysis and design of process systems chose other categories. For instance, Lerou and Ng [9] ordered crucial phenomena such as reaction or fluid dynamic and transport with respect to their time and length scales. Charpentier and McKenna [10] subdivided process systems into different organized levels of complexity, whereby on each level molecular processes are translated into phenomenological macroscopic laws. Other authors focused on

the task of process design and how it can be carried out hierarchically. For instance, Douglas [11] introduced a heuristic-based approach for synthesizing process flow sheets with different decision levels. Smith and Linnhoff [12] proposed the onion model putting the chemical reactor into the center of the process and extending the design problem step by step adding units such as separators, heat exchangers and auxiliary units. A phenomena-based modularization approach was introduced by Arizmendi-Sanchez and Sharratt [13], who subdivided the design procedure in the modules goal, function, structure, and behavior and included process intensification options. In a similar subdivision as shown in Fig. 2.1, Mangold et al. [14] suggest a structuring of models and model equations on different levels applying a network theoretical approach.

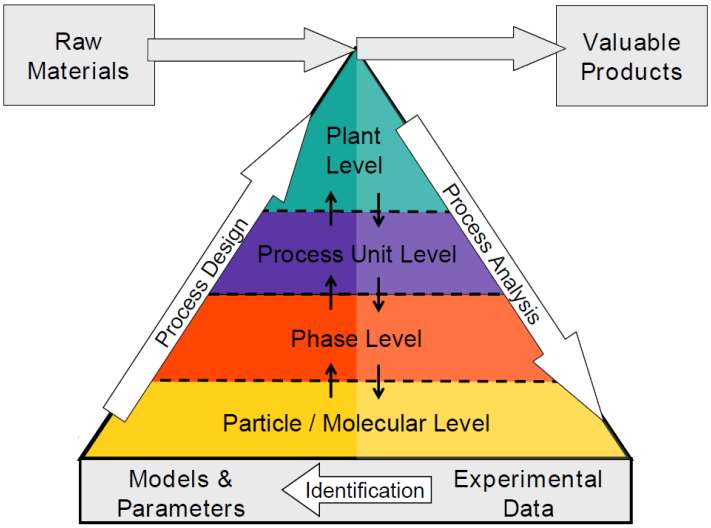

Figure 2.1: Pyramid of process analysis and design (adapted from [8])

As mentioned above, the process units, which are composed to a plant and in which the phases interact, are classically associated with specific operations and characteristics. These are, for instance, units for contacting of phases (e.g. mixers), for separation of phases (e.g. distillation columns, membranes), for heat supply/removal (e.g. heat exchangers), or chemical reaction with defined mixing behavior (e.g. continuous stirred tank reactor). These so called *unit operations* are the basis of classical process design approaches which search (i) for the best structure of predefined units composing the overall production process (e.g. flow sheet optimization, superstructure optimization) or (ii) for the region of all attainable state configurations (e.g. attainable region approach), see subchapter 2.2.1. Main drawbacks of the flow sheet or superstructure optimization are that optimal solutions have to be included in the predefined set of possible configurations, and that it is hardly possible to derive new, integrated or intensified apparatuses what might lead to suboptimal solutions of the optimization. The attainable region approach requires at first a search of all possible state configurations and does not intend to directly find an optimal configuration. Furthermore, it is mostly used for design problems with small dimensions. For higher dimensional problems it suffers from the curse of dimensionality. To overcome these drawbacks in process design and allow for the systematic inclusion of process intensification options, Freund and Sundmacher [3] developed the methodology of *elementary process functions*. Therein, they propose a shift from the use of *unit operations* towards *functional modules*, which are independent of existing apparatuses and instead focus on the functionalities that are required at certain steps along the production process, see Fig. 2.2. Thereby, each *functional module* can include one or several functionalities, e.g. contacting and reaction, or separation and heat removal, etc., depending on the task of the module and the chosen concept for its accomplishment.

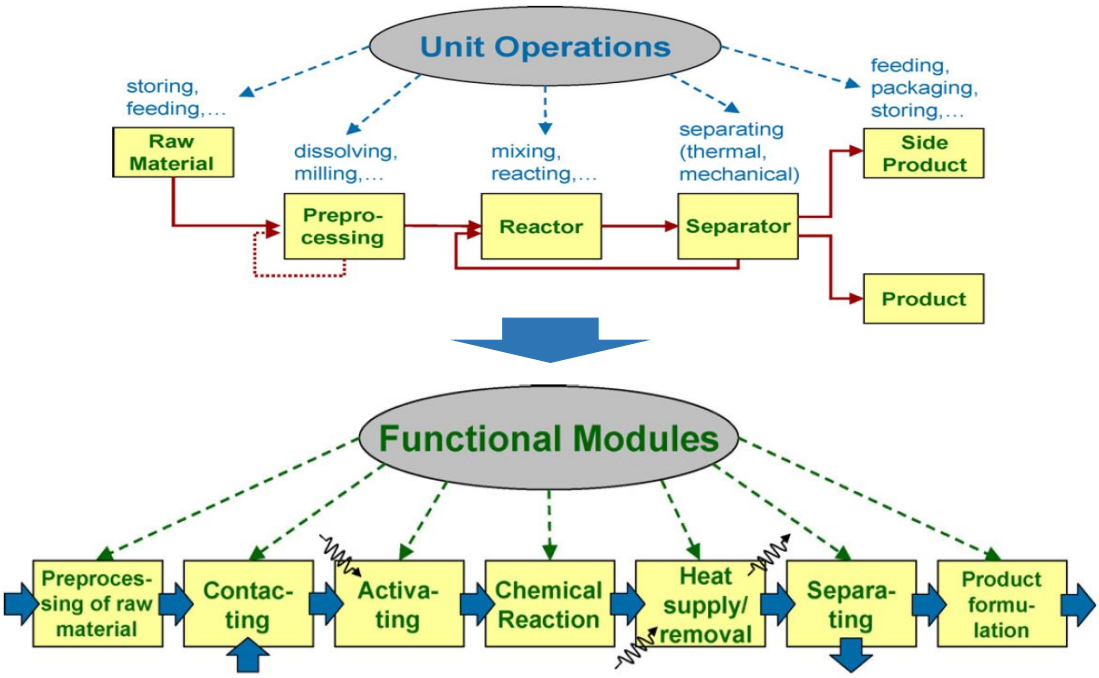

Figure 2.2: Paradigm shift for process design from *unit operations* towards *functional modules* (adapted from [3])

Optimal route of a fluid element in the thermodynamic state space

In contrast to state-of-the-art process design approaches, which either search for the best flow sheet configuration of unit operations from a predefined set or determine all attainable state configurations, the process design with the EPF methodology bases on a more intuitive notion. Its key idea is the Lagrangian tracking of a fluid element on its way through the chemical process. Starting from an initial point in the thermodynamic state space its states are manipulated by internal and external fluxes in order to follow an optimal path and aiming at the optimization of a given objective or attaining a predefined final point, see Fig. 2.3.

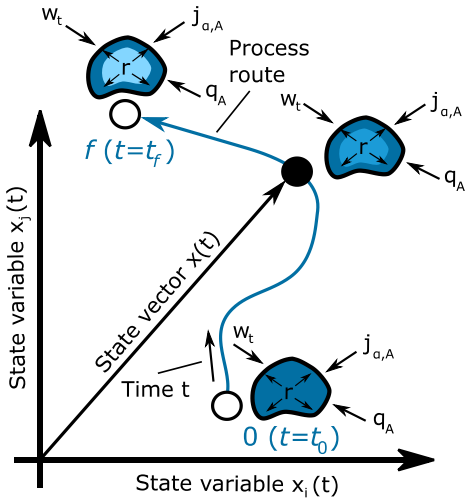

Figure 2.3: Path of fluid element in thermodynamic state space from starting point **0** to final point $\boldsymbol{f}$ under manipulation of heat flux $\boldsymbol{q_A}$, dosing fluxes $\boldsymbol{j_{\alpha,A}}$, technical work $\boldsymbol{w_t}$, and internal reaction flux $\boldsymbol{r}$

The manipulating or controlling fluxes and the corresponding evolution of states are determined by means of a dynamic optimization problem (DOP), which is solved for each functional module. The

evolution of states in the DOP is subject to equations of change, kinetic expressions, and thermodynamic relations, e.g. state equations.

In order to achieve a systematic mathematical framework for the modeling of the states of the fluid element and its manipulating fluxes, Sundmacher and Freund [15] suggested a vector-matrix notation that allows to subdivide the equations of change, i.e. the balance equations of the states, into a matrix of elementary process functions $\boldsymbol{E}(\boldsymbol{x})$ and a vector of internal and external fluxes $\boldsymbol{s}(\boldsymbol{x}, \boldsymbol{x_{eq}})$. As illustrated in Fig. 2.4, the matrix of elementary process functions itself is a composition of a capacity matrix $\boldsymbol{C}(\boldsymbol{x})$ and a flux weighting matrix $\boldsymbol{F}$, whereas the flux vector decomposes to a kinetic matrix $\boldsymbol{K}(\boldsymbol{x})$ and a vector of driving forces $\boldsymbol{f}(\boldsymbol{d}(\boldsymbol{x}, \boldsymbol{x_{eq}}))$. This classification of the deciding modeling entities allows for a systematic analysis of process design and intensification potentials, whereby the entries in each column in Fig. 2.4 give a hint, which options exist. For instance, changing an inert component in the process affects the sensitivities of densities and enthalpies in the capacity matrix; downsizing unit dimensions enables a higher surface to volume ratio in the flux-weighting matrix; the use of an improved catalyst system, or at least providing conditions which increase the amount of active catalyst species, influences the kinetic matrix; or changing the pressure level increases the driving force of a mass transfer rate.

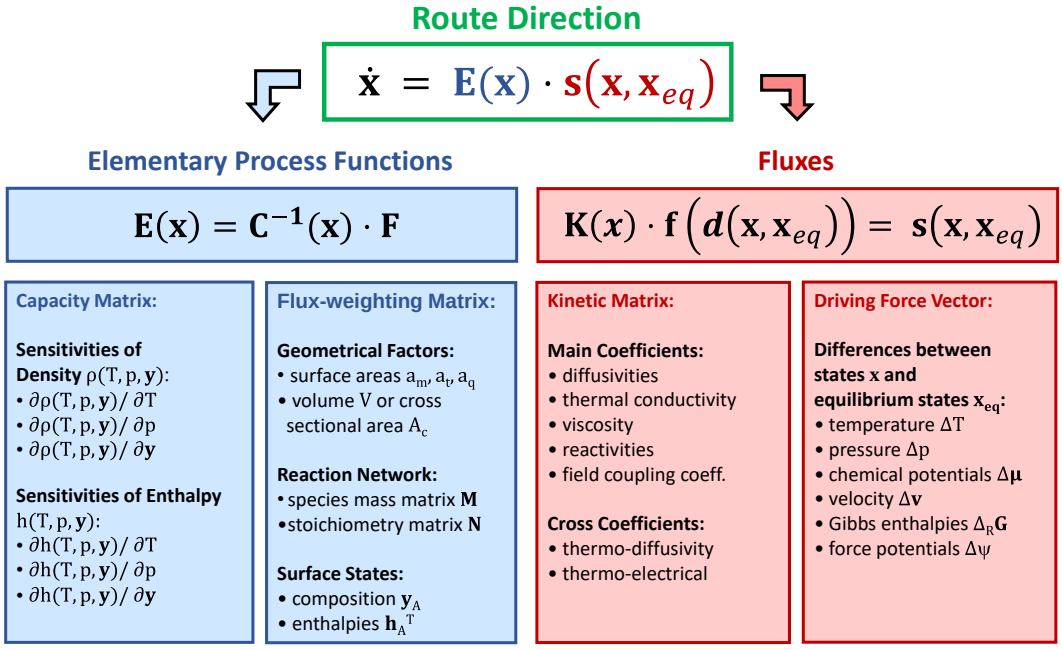

Figure 2.4: Vector-matrix notation of the EPF methodology for systematic process design and intensification (adapted from [15])

Hierarchical and sequential reactor design based on the EPF method

The methodology of *elementary process functions* was already used as basis for two systematic process/reactor design approaches. Peschel et al. [4] proposed a three level reactor design approach which focuses on a step by step increase of model details and accompanying limitations and intended to include possible process intensification options on the way. The levels are defined as following:

- Level 1: The dynamic optimization problem stated by the EPF method is solved for different enhancement concepts. Thereby, the fluxes are unlimited what gives rise to identifying the global optimal limit of the process performance.

- Level 2: Subsequently, the most promising enhancement concept is further investigated by choosing a set of suitable control variables to realize the fluxes. Therefore, transport kinetics are included, what requires knowledge about the specific dimensions of the system, and the fluxes are limited, what leads to a performance loss in comparison to the potential revealed in level 1.
- Level 3: Finally, the optimal trajectories of the control variables are approximated in a technical realization of the process. This induces additional limitations by the technically feasible designs. At this point, real apparatuses are chosen for the technical realization and the process parameters are determined.

Hentschel et al. (2014) carried out a process design study for a liquid multiphase process applying the first level of the 3-level reactor design approach of Peschel et al. (2010). In addition, they closed a global recycle of a separation section to the inlet of their optimal reactor. However, this was a case study, which was not accompanied by a systematic extension of the process design methodology. The separation section was predefined and a cost optimization of the overall process costs has been carried out in order to identify the reactor design which yields the best trade-off between utility costs, investment costs, and productivity.

Another approach was introduced by Karst et al. [16] which bases on the hierarchical multiscale concept shown in Fig. 2.1. Starting from the molecular level ending in an integrated plant, they propose crucial decisions, which have to be made on each level, and include the optimal process route determined by the EPF based dynamic optimization on the phase level. The levels are defined as following:

- Molecular level: The reaction is defined by choosing key components such as reactants, desired products and undesired side products, catalyst, solvents, and possible reaction routes. All following levels and design steps depend mainly on this definition of the reaction and its components.
- Phase level: The optimal route of the fluid element travelling through the process is determined solving the dynamic optimization problem stated by the EPF methodology. Again, the optimization results in unlimited fluxes and, thus, yields the maximum potential of the process.
- Process unit level: The translation of the optimal fluxes of the previous level into a control strategy of a technically realized apparatus is focused. Decisions about the operation mode, batch or continuous, are made. The translation concepts mainly corresponds to the second and third level of the approach of Peschel et al. [4].
- Plant level: Strategies for material and energy integration are considered around the optimal process unit of the previous level and the topology of the process structure is sought.

2.1.2 Methodical contribution of the presented work

The methodology of *elementary process functions* combines a very interesting intuitive notion of chemical processes and a solid mathematical basis for using it as framework for process design. Furthermore, the hierarchical concept of multiple levels differing with regard to time and length scales allows for a reasonable classification of occurring physico-chemical phenomena and modeling techniques. Although Peschel et al. [4] suggested a thoughtful and systematic approach for reactor design and intensification, which adopts the concept of optimizing the path of a fluid element in the thermodynamic state space from the EPF method, it tackles solely the phase level and the process unit level. Design information about the conceptual design of the plant, i.e. the topology or configuration

of the different process units, are not provided within their approach. Following this identification of missing aspects in the process design framework of the EPF methodology, the first main topic of the presented work is born: the synthesis or conceptual design of reactor-networks based on the methodology of *elementary process functions*. This endeavor contains the following aspects:

- Identification of back-mixing benefits of reaction sections to derive reactor-networks containing reactors with different mixing characteristics;
- Systematic investigation of recycling effects to identify reasonable recycle strategies;
- Assessing the process potentials under consideration of intermediate separations to decide about required number and position of separation sections in the topology of the network.

For this purpose, the optimal flux profiles resulting from the dynamic optimization of the fluid element are analyzed and process candidates of different complexity levels are derived, see chapter 3. For giving a better understanding of the methodical extension in the presented work, the breakdown of modeling entities and degrees of freedom for the synthesis and design in each hierarchical level are exemplarily illustrated in Fig. 2.5.

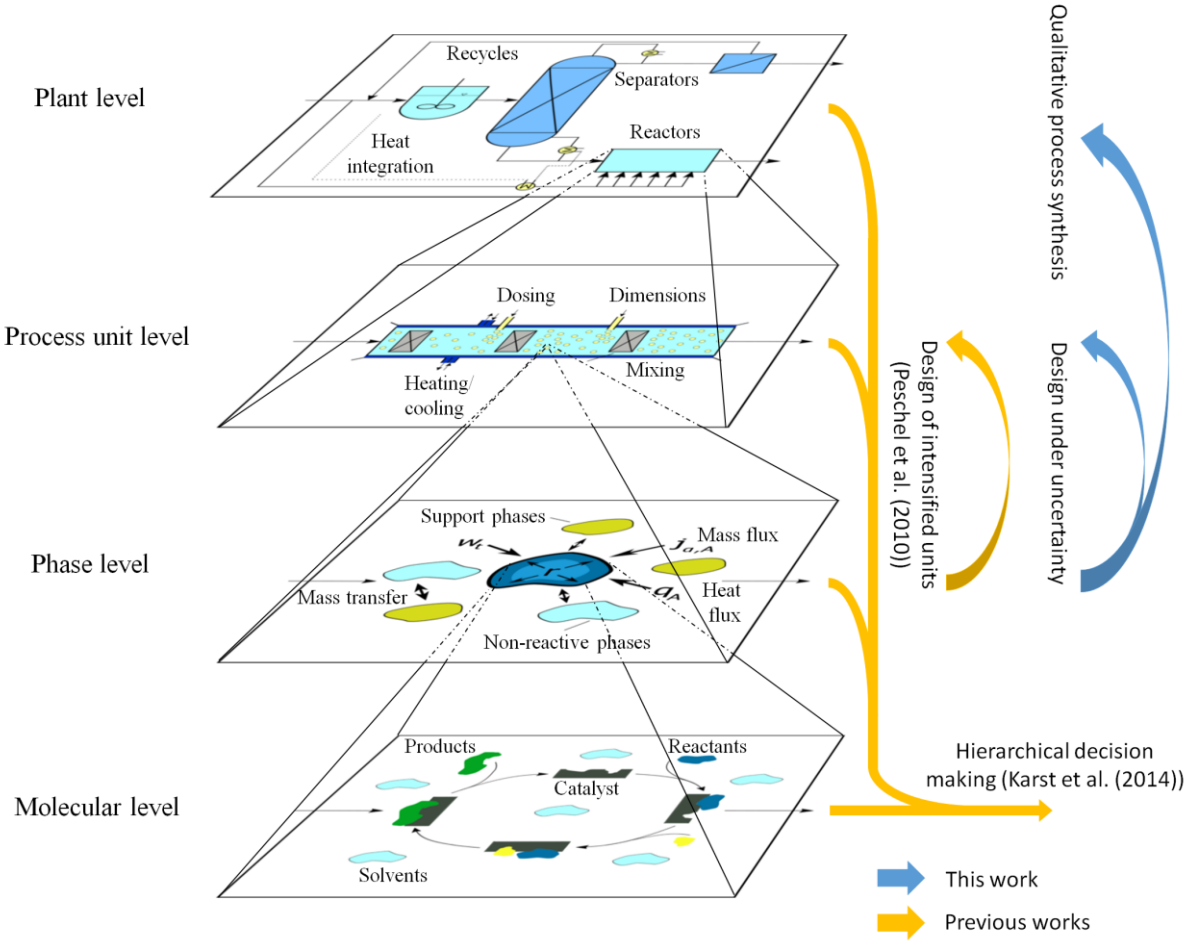

Figure 2.5: Hierarchical breakdown of EPF based process design and placement of previous works and presented approaches

The second main topic of the presented work and extension of the EPF based process design approach is independent of the hierarchical levels of the process. It refers to an inherent problem of all model-based design approaches: uncertainty quantification. Up to now, all design studies with the EPF method assumed deterministic models to predict optimal process conditions. However, mathematical models are always an approximate description of the real phenomena. They are subject to measurement errors of experiments, limitations of model and parameter accuracy, and simplifying

assumptions in the modeling itself. Due to the approximate nature of the model basis, the prediction of an optimal process will always deviate from the real behavior of the process. The uncertainty quantification aims at investigating the impact of those uncertainties to allow for a reliable or robust process design under uncertainty. The process design under uncertainty approach presented in this work includes the following aspects:

- Classification of uncertainty types arising within the EPF based process design;
- Selection of reasonable mathematical description of the uncertainty type;
- Identification of process/reactor designs which are robust against the considered uncertainties;
- Determining alternative process/reactor designs that provide higher predictive powers of the final process performance.

2.2 State-of-the-art methods for reactor synthesis and design under uncertainty

The two foci of this work – reactor synthesis and design under uncertainty – have been treated extensively in literature for process systems in the last decades and are still subject of ongoing research. In the following, an overview of the most important methods and corresponding publications is given, not striving for comprehensiveness, but allowing for a placement of the presented work inside the state-of-the-art knowledge.

2.2.1 Reactor-network synthesis

Approaches for the synthesis of reactor-networks focus on the identification of networks of ideal reactor units which provide different mixing characteristics, i.e. (i) plug flow reactors (PFR), which have no back-mixing, (i) continuous stirred tank reactors (CSTR), which are totally back-mixed, and (iii) distributed side stream reactors (DSR), which allow for a distributed dosing of reactant along the reaction coordinate and, thus, allow for the realization of mixing behavior between the PFR and the CSTR [17]. The state-of-the-art reactor-network synthesis approaches can be classified into heuristics, attainable region (AR) approaches, and rigorous optimization based approaches, see Fig. 2.6.

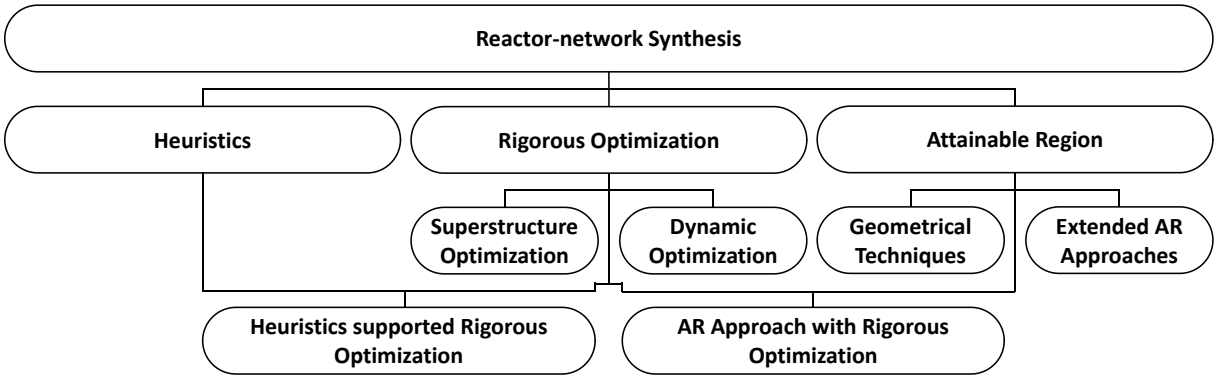

Figure 2.6: Classification of reactor-network synthesis approaches (adapted from [4])

Heuristics

In contrast to the other state-of-the-art methods, heuristical approaches do not base on simulation and optimization of mathematical models. They either derive reactor-network candidates based on experience, see e.g. [18] or [19], or use basic knowledge about the process to select and

reduce the search space for rigorous methods [20]. The advantages of these methods are their simple applicability and fast usability, and in general one achieves appropriate results. However, their application on complex systems, especially of uncommon characteristics, is limited. The heuristics do not enable the derivation of innovative or intensified units, since they choose from a predefined set of standard units.

Attainable region approaches

The fundamental idea of an attainable region, which contains all points in the concentration space of a chemical process being attainable by reaction and mixing only starting from a predefined feed point, was introduced by Horn [21]. This approach had its revival in the 1980s, when the idea of attainable regions was taken up again. Glasser et al. [22] suggested an approach which allows for graphical construction and interpretation of the attainable region of a process. This approach was further developed and generalized by Feinberg and Hildebrandt [17] who stated universal properties of the attainable region and emphasized the special meaning of the boundary of the AR. As the attainable region approach bases on a graphical analysis, it can only be applied to problems, which can be reduced to at most three dimensions. In order to overcome this limitation, computational techniques have been developed by Rooney et al. [23] and Abraham and Feinberg [24] to apply the AR to higher dimensional systems. Since the initial conditions for the composition and the temperature has to be known a priori, an additional drawback of the AR approach is, that its embedding in an overall process design procedure is very complicated. In this case a recalculation of the AR is required for every time the initial conditions of the composition change. Balakrishna and Biegler [25,26] developed a framework which combines rigorous optimization techniques with the AR approach to allow for solving higher dimensional problems and an embedding in overall process design procedures. As for higher dimensional problems the size of the problem with respect to number of equations and variables grows strongly, several authors worked on methods based on linear programming for determining the AR of higher dimensional problems, see e.g. [27], [28], [29]. To bridge the gap from the design of continuous reactor-networks to the design of optimal batch processes, Ming et al. [30] introduced the AR approach also for batch processes and described how the AR of a continuous process can be realized by batch reactors.

Rigorous optimization approaches

Optimization based approaches are subdivided into superstructure optimization and dynamic optimization. Superstructure optimization, originating from a work of Jackson [31], seeks the best reactor-network configuration within a pre-defined superstructure of possible units. The main advantages are that the objective function and the reactor-network are determined simultaneously, and that the formulation allows including constraints or changes in e.g. the objective function directly. Furthermore, the design problem can be extended easily by additional aspects of a process flow sheet simply adding the corresponding equations to the optimization problem, e.g. in case of additional units or streams. Main drawback is that the solution can only be part of the pre-defined superstructure. If the best process is not included in the candidate superstructure, it cannot be found. Moreover, the possible connections between the units must be specified a priori and the required connections of the optimal configuration are identified by the optimization what gives rise to integer decisions in the optimization problem. Due to nonlinear models in the optimization problem, e.g. reaction kinetics, mixed integer nonlinear programming (MINLP) problems arise that require powerful numerical tools still not guaranteeing to find global optimal solutions. Achenie and Biegler [32,33] used nonlinear programming (NLP) techniques, avoiding integer decisions, to optimize recycle reactors with indirect heat transfer options. Kokossis and Floudas [34] used general structures of PFRs and CSTRs, whereby

the PFRs were approximated by a cascade of CSTRs with same volumes, and enabled all possible recycling, (intermediate) feeding and by-passing strategies as well as intermediate cooling and heating what led to a large and complex MINLP problem. Further developments in this field are: incorporation of stochastic optimization, e.g. [35]; inclusion of differential side stream reactors [36]; use of optimal control techniques and optimization of cross flow reactors [37]; application of superstructures for attainable region construction using linear programming, e.g. [27]; and numerous applications of these methods for the design of different process examples. Although today's numerical solvers can handle most superstructure optimization problems, the modeling effort and the complexity of the optimization problem increases with the number of units within the initial configuration what makes the optimization complex and its convergence slow or even infeasible. Due to that, superstructure optimization approaches always require a trade-off between the solvability of the problem, the number of combinations included in the superstructure, and the uniqueness of the solution.

First approaches for dynamic optimization based reactor design came up in the middle of the 20th century. Bilous and Amundson [38,39] as well as Horn [40] and Aris [41] discussed the concept of optimizing the temperature and concentration profiles along the reaction coordinate. The latter already postulated the high potential of dynamic programming techniques as introduced by Bellman [42] for identifying optimal control scenarios for both batch reactors and continuous plug flow reactors. In the following decades several authors developed further approaches applying dynamic optimization techniques, especially for batch reactors. For instance, Soroush and Costas [43,44] created a framework taking into account aspects of flexibility, safety, and controllability, and applied their framework on a complex polymerization reaction. A similar reaction was tackled by Abel et al. [45] solving a problem on industrial scale under safety constraints. Other authors applied dynamic optimization techniques for designing optimal continuous reactors. For instance, Balakrishna and Biegler [25] introduced targeting strategies for optimizing side streams of so called cross flow reactors. Further approaches have been presented by Johannessen and Kjelstrup [46] and Hillestad [47,48]. Johannessen and Kjelstrup [46] used the minimum entropy production solving a dynamic optimization problem to identify optimal reactor designs, e.g. for the SO_2 oxidation. Hillestad developed an optimal control based framework to synthesize reactor-networks of ideal reactors and ideal feed streams added along the reactor path. His approach is not limited with regard of the number and reactions and components and has been applied for isothermal [47] and non-isothermal problems [48].

2.2.2 Reactor-separator-network synthesis

The synthesis of processes including units for reaction and separation, often accompanied by recycles and heat integration, is an unlike more complex task than the synthesis of reactor-networks already is. The developed approaches tackle the complexity of conceptual design with different tools, again starting from heuristic based approaches and ending in large scale MINLP problems including all possible topological alternatives.

Heuristics

The classical heuristical way, which is mostly still industrial practice, create the flow sheet configuration based on experience and knowledge of similar problems. Heuristics mostly start with the synthesis of a reactor-network and extend the flow sheet stepwise by separator, recycle, and heat exchangers, see e.g. [49], [12], [50]. The optimal process conditions are then determined by repetitive calculation of e.g. the process costs. The operation points and unit specifications of feasible alternatives are often determined by spreadsheet calculations and rules of thumb [51]. Evidently, the decomposition of a complex task such as the overall process synthesis has its advantage in the

reduction of its complexity and hence a better solvability. However, it might lead to suboptimal solutions, since the optimum of a system with recycles and, thus, interdependencies between the optimal operation points of the units cannot be identified when each unit is optimized individually. Hence, an integrated overall process synthesis is required to ensure that all synergy effects are identified and the finding of suboptimal solutions is avoided.

Optimization with generic units and short cut models

In order to achieve a fast synthesis, the number of promising concepts should be reduced in an early phase of the design procedure. Therefore, knowledge about possible performance bounds is of interest. Feinberg [52] as well as Feinberg and Ellison [53] applied the equivalence principle of continuous flow stirred tank reactors and sharp separation splits to identify the productivity and selectivity bounds of steady-state reactor-separator systems. Alternatively, Linke and Kokossis [54] suggested a superstructure optimization of generic synthesis units, i.e. mass exchanger and separator task units, aiming at the determination of performance targets and the identification of design options. With determining species-dependent residence time distributions, Balakrishna and Biegler [26] introduced a targeting approach for integrated reaction-separation tasks which was already used before for the purpose of reactor-network synthesis.

Several methods employ short-cut models in order to simplify the modeling and reduce the computational effort for the synthesis of integrated reaction-separation processes. This allows as well for a fast screening of performances of a plenty of possible configurations. Using Gibbs reactor models coupled with a thermodynamical rectification model Kossack et al. [55] estimated lower bounds for operating costs. McBride et al. [56] combined a CSTR cascade model with the Fenske-Underwood-Gilliland equations for distillation column modeling to determine plausible recycle conditions for a hydroformylation reaction including a Kriging model for the intermediate liquid-liquid phase separation. Alternatively, Ryll et al. [57] coupled the ∞/∞-method for distillation with equilibrium and conversion reactors to identify operating points with minimal recycle flows for all possible flow sheets.

Derivative-free and rigorous optimization

In order to enable the use of rigorous process unit models in the flow sheet, several authors proposed approaches which use derivative-free optimization algorithms, e.g. evolutionary algorithms, coupled with process simulators, see e.g. [58], [59]. The advantage of such procedures is the reduction of the numerically complex solving of the underlying optimization problem. However, since the optimization algorithm cannot distinguish between simulator errors due to violated process constraints or convergence failures, these procedures is often limited by the reliability of the process simulators. Furthermore, derivative-free optimization algorithms are mostly unable to find optimal solutions when the number of degrees of freedom exceeds ten, even in the absence of constraints and integer variables [60]. To increase the applicability of simulation-based optimization tools to larger problems, the model complexity can be reduced by use of surrogate models or reduced order models which are trained by rigorous simulations, see e.g. [61].

Superstructure optimization based approaches are also used for the synthesis of reactor-separator-networks. These methods correspond to the case that all variables and units are optimized simultaneously in one large optimization problem which generally involves integer decisions and, hence, the solving of MINLP problems, see e.g. [62], [63]. The advantages and disadvantages are similar as in case of reactor-network synthesis. However, for conceptual design the number of units and variables is unlike higher and, thus, its solvability even more complex. As the representation of the design space, i.e. the definition of a starting configuration including all possible solutions, is quite

complex and the solving of the resulting MINLP problems as well [64], the practicability of these approaches depends on the facilitation of their use by means of systematic procedures. Recently, new interesting methods have been proposed either facilitating the use of large scale optimization problems by providing an equation oriented framework which avoids integer decisions and introduces mathematical models of higher practicability [65], or introducing a systematic procedure in which generated process variants are first screened by means of short cut models to identify promising candidates for rigorous modeling [66].

Alternative perspectives on reactor synthesis

Further interesting approaches, which carry out reactor synthesis from other perspectives, are presented by Fox et al. [67] and Lutze et al. [68]. Fox et al. [67] suggested the use of GH-plots to facilitate the integrated design of reaction and separation. Enthalpy H and Gibbs free energy G representing the heat flow and work flow, respectively, are determined for all units and depicted graphically as vectors in the GH-space. This technique allows for determining the material, energy, and work balances of the units, which are rendered highly efficient, by manipulation of the vectors in the GH-space. Lutze et al. [68] proposed a framework for phenomena-based synthesis of processes including process intensification options. Therefore, the relevant phenomena of all units are identified to generate intensified units. These units are recombined to generate sustainable and intensified process flow sheets.

A discussion of the approaches introduced and used in this work in comparison to state-of-the-art methods will be carried out at the end of subchapters 3.2 and 3.3 for reactor-network synthesis and of subchapter 3.5 for reactor-separator-network synthesis.

2.2.3 Design under uncertainty

The synthesis and design approaches summarized in the previous two subchapters have successfully been used in a vast amount of applications and processes. However, their basic character includes a simplification that neglects a very important aspect for the design of real processes – the natural uncertainty of models and process conditions. Predictions based on mathematical models are inherently uncertain since (i) measurements of physical and chemical phenomena are subject to randomness and variability, and (ii) the discrimination of models and the identification of model parameters are accompanied by selection and estimation errors, respectively. To account for those uncertainties in the design of process systems, several branches of techniques have evolved in the last decades of process systems engineering (PSE) research. However, the uncertainty quantification (UQ) of model-based predictions has as well a long history in other research areas, especially in mechanical engineering and operational research, see [69] and [70] for comprehensive and recent reviews, respectively. The approaches developed in PSE can be structured into three main areas (Fig. 2.7) – stochastic programming, fuzzy programming, and robust optimization – whereby the first and the latter got most attention. In the following, the methods evolved in these areas are briefly reviewed, examples for their application are given, and their differences are elucidated. A discussion of the design under uncertainty approach presented in this work with regard to the state-of-the-art approaches can be found in subchapter 4.4.

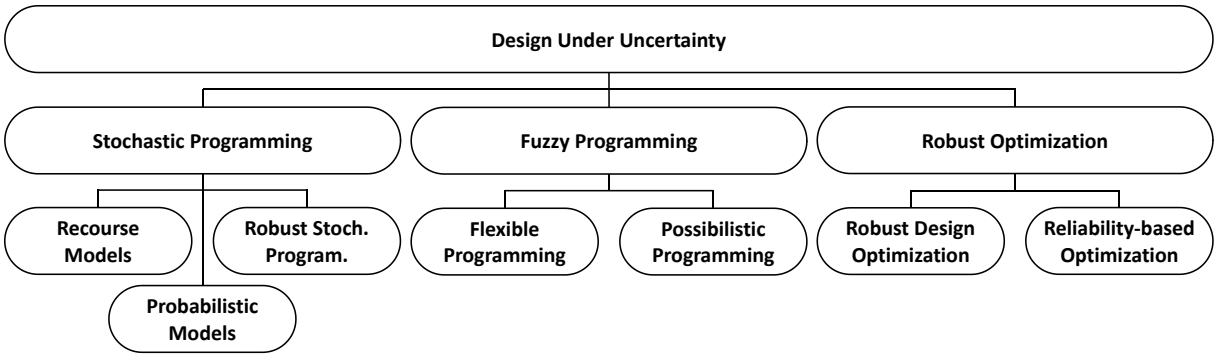

Figure 2.7: Classification of design under uncertainty approaches

Despite of clear methodical differences, all methods for design under uncertainty have in common that uncertainties have to be classified according to their origin and inclusion into the design procedure. The most popular classifications are (i) the distinction of exogenous and endogenous uncertainties (see e.g. [71]) and (ii) epistemic and aleatoric uncertainties (see e.g. [72]). The first classification focuses on the origin of the uncertainties. Exogenous uncertainties are decision independent, i.e. they affect the process from outside and cannot be reduced or certainly predicted in the process environment (e.g. feed quality, demands), whereas endogenous uncertainties are decision dependent, i.e. the choice of decision variables can affect the size or the effect of these uncertainties (e.g. control actions, design aspects). The second classification considers the presence and quantifiability of uncertainties. Aleatoric uncertainties are truly random stochastic quantities and processes and are referred to as statistical uncertainties, whereas epistemic uncertainties are of systematic or structural nature, i.e. they arise due to non-accurate measurements, parameter estimation errors, or simplifications in the model.

Stochastic programming

The first branch of design under uncertainty consists of stochastic programming approaches. These methods consider scenarios of uncertainty realizations and take recourse actions in two or multiple stages to impinge on uncertainty effects while optimizing a given design objective. The classical two-stage stochastic programming contains first-stage variables, which have to be optimized before the uncertainties are realized, and second-stage variables, so called recourses, which minimize at a certain cost the effect of uncertain events on the design or operation. The objective is, hence, to "choose the first-stage variables in a way that the sum of the first-stage costs and the expected value of the random second-stage costs is minimized" [73]. Due to the nature of the corrective recourse actions on the design optimization, stochastic programming approaches tend to be more appropriate for strategic design decisions and production planning, i.e. long-term decision-making, as the recourse decisions allow future (re-)actions to adapt in response of uncertainty effects [71]. Sahinidis [73] proposed a classification of stochastic programming approaches into the branches of recourse models, robust stochastic programming, and probabilistic programming.

The first was briefly introduced before and was applied for several types of optimization problems. For linear problems, for instance, solution strategies based on decomposition of the uncertainty set (e.g. [74]), sampling-based decomposition for continuous distributions (e.g. [75]) and gradient-based approaches (e.g. [76]) have been introduced. In stochastic integer programming, the uncertainty set contains integer restrictions. First works on these problems used heuristical analyses for two-stage integer programming (e.g. [77]). In the following, the algorithmic approaches improved and extensions of the decomposition-based solution strategies for linear problems have been developed (e.g. [78]). Caroe and coworkers [79,80] introduced branch-and-bound methods to cope

with integer restrictions in two-stage stochastic programming. More recently, stochastic programming approaches are applied for usually more challenging non-linear problems. For instance, Sakalauskas [81] presented a stochastic non-linear programming framework based on Monte Carlo estimators. Dealing with probability distributions and discrete intervals, Li and Huang [82] presented a well noticed framework for two-stage stochastic nonlinear programming applied on a water resource management problem. Shastri and Diwekar [83] extended the traditional L-shaped method for application on non-linear problems by incorporating a reweighting scheme that reduces the computational load of the second-stage evaluations. An application on conceptual design problems utilizing two-stage stochastic non-linear programming has been proposed recently by Steimel and Engell [84].

Robust stochastic programming extends the recourse model based approaches by an important aspect of design under uncertainty, the notion of risk. This allows weighting the objective and the risk to miss it, i.e. its predictive power. For instance, a sound application of robust stochastic programming for chemical process planning was published by Ahmed and Sahinidis [85], and quite recently, Guo et al. [86] presented the use of an interval two-stage robust stochastic programming approach for planning of carbon sink trading aiming at an improvement of the regional ecosystem sustainability.

In contrast to the robust stochastic programming approach the probabilistic programming focuses not only on the minimization of the expected recourse costs and its risk. Instead, the reliability of complying with the constraints is emphasized by introducing probabilities for the constraints, so called chance constraints. A recent application on a recurring topic was presented by Liu et al. [87]. They employed a multi-stage stochastic programming approach with embedded chance constraints for a water resource management problem and indicated the superior use of probabilistic constraints in the stochastic programming problem. Both robust stochastic programming and probabilistic programming have a counterpart in the area of robust optimization that will be discussed later.

Fuzzy programming

In contrast to stochastic programming and robust optimization, fuzzy programming is a non-probabilistic way to handle uncertainties in model-based design approaches. Instead of using discrete or continuous probability functions to model uncertainties, in fuzzy programming random variables are considered as fuzzy numbers and constraints as fuzzy sets. Thereby, a certain degree of constraint violation is accepted and a membership function is used to describe the degree of satisfying a constraint. The fuzzy sets can be of arbitrary form, whereby typically linear membership functions are used indicating a very good approximation of more complex non-linear functions [88]. The objective function is translated into a membership function giving an upper and lower bound of the expected objective value. The two general types of fuzzy programming problems account for fuzziness in different parts of the optimization problem. Flexible programming considers uncertainty regarding the exact values of coefficients, e.g. in model equations, inequality constraints, objective coefficients, and denotes them as fuzzy [89]. In case the optimization problem involves uncertainty in the constraint coefficients, those are denoted in fuzzy sets and a possibilistic programming problem arises [90]. A seminal, ground-breaking work about fuzzy programming was presented by Bellman and Zadeh [91]. For process systems engineering applications, several authors applied fuzzy programming techniques. For instance, Liu and Sahinidis [92] carried out chemical process planning under uncertainty using stochastic and fuzzy programming approaches. They indicated that the stochastic programming yields better results even in the absence of probabilistic uncertainty sets. For the synthesis of robust water reuse networks Tan and Cruz [93] applied fuzzy linear programming including formulations for mass exchange units and source/sink problems. In contrast to the previously mentioned comparison, they highlighted the simplicity and the computational efficiency compared to stochastic programming algorithms. Park et al. [94] considered fuzzy nonlinear programming for the optimization of a gas

production system and combined it for the sake of solvability with a derivative-free genetic optimization algorithm. Due to the feature that fuzzy programs reformulate the objective as constraints, the consideration of multiple objectives is clearly simplified. Therefore, several authors used fuzzy programming for multi-objective optimization problems, e.g. for the synthesis of a sustainable integrated biorefinery [95] or the supply chain optimization of distribution centers [96].

Robust optimization

The second branch of probabilistic approaches for design under uncertainty widely spread in PSE research is robust optimization. In contrast to the scenario-based procedure in stochastic programming, robust optimization seeks for an optimal objective value(s) guaranteeing feasibility over a specified set of uncertainties. This makes it more appropriate for short-term problems, either regarding operation, e.g. in scheduling problems, or for the design of processes under model uncertainties [71]. Since the optimal solution includes all possible realizations of an uncertainty set, the worst case scenario is included as well making it a highly conservative approach. To reduce the level of conservatism one can either include a reduced uncertainty set resulting in a feasibility of the solution of reduced probability, or introduce feasibility bounds for the constraint violations. Robust optimization approaches can be subdivided in classes of robust design optimization (RDO) and reliability-based optimization (RBO) [97]. The latter is strongly linked to flexibility analysis for chemical processes under uncertainty, which was earlier introduced by Grossmann and coworkers [98,99]. Recent insights on the relation between these two approaches are presented in [100].

Robust design optimization extends the concept of robust optimization by finding optimal solutions which are not only guaranteeing feasibility for all uncertainty realizations but increase the relative invariance of the solution to the considered uncertainties and, thus, its robustness. Therefore, measures for quantifying the robustness have to be included into the optimization problem. This is mostly done by use of statistical moments of the probability function of the objective, i.e. its expected value and its variance, giving rise to multiple criteria decision problems and Pareto optimal solutions. Therefore, RDO is often linked to multi-objective optimization techniques. One of the earliest attempts for RDO was presented by Taguchi [101]. He introduced uncertainties as performance variations due to noise factors beyond the control of the designer. Depending on the design objective, so-called signal-to-noise measures are proposed which are to be maximized with regard to the design variables. Beside of that, applications of the classical RDO approach can be found in several publications in process engineering research. For instance, Suh and Lee [102] used RDO for design and planning of chemical processes considering the worst-case scenario as robustness measure in the cost minimization problem. Introducing a general framework for robust optimal control of (bio-)chemical processes, Logist et al. [103] proposed approaches for robust design optimization using either scalarization based multi-objective optimization or solution techniques based on Lyapunov differential equations. In a recent work Majewski et al. [104] applied RDO for the sustainable design of distributed energy supply systems considering economic and ecologic objectives.

In contrast to robust design optimization, reliability-based optimization does not seek for higher robustness of optimal solutions. RBO intends to find the optimal solution under consideration of predefined reliability levels of constraints and, thus, identifies and quantifies trade-offs between profitability and reliability of a design [105]. By changing the confidence intervals of feasibilities of constraints, the RBO allows for adjusting the level of conservatism of an optimal solution. Due to the reliability setting of constraints, RBO is often used to incorporate exogenous uncertainties, i.e. variations of external variables such as feed composition or market conditions. In order to describe the reliability level of constraints, they are described by probability functions. Due to that they are often referred to as chance constraints. Different examples for the use of chance constraints in optimization can be found in PSE research. Li et al. [106] presented a model predictive control approach utilizing

chance constraints for the optimal control of a distillation column. Proposing an approach for translating chance constraints into deterministic constraints, Ostrovsky et al. [107] used chance constraints in a one-stage optimization approach. Leveraging this approach, an optimization framework for chemical processes with joint chance constraints was introduced recently, i.e. all or several probabilistic constraints of independent random parameters have to satisfy a joint pre-defined reliability level [108].

2.3 Example process: Hydroformylation of 1-dodecene

The reactor synthesis and design under uncertainty approaches presented in this work are exemplarily applied on a complex chemical multiphase process that is a relevant subject of research – the hydroformylation of 1-dodecene in a thermomorphic multicomponent solvent (TMS) system. In the following, the research motivation for this reaction and solvent class is derived from the state-of-the-art processes for hydroformylation and their drawbacks for the efficient use for long chain alkenes.

2.3.1 Hydroformylation process

During his research on the Fischer-Tropsch synthesis, the German chemist Otto Roelen identified the hydroformylation reaction in 1938 and developed the eponymous process, which became the first and one of the most important homogeneously catalyzed industrial processes. In the hydroformylation reaction alkenes react with carbon monoxide (CO) and hydrogen (H_2) to aldehydes. Thereby, hydrogen is added to one side of the double bond of the alkene and a formyl group to the other, see Fig. 2.8. Under atmospheric pressure, the aldehydes (>C3) are always liquid, whereas the alkenes are either gaseous (<C6) or liquid (>C5). Aldehydes are widely used in chemical processes, e.g. as intermediates for alcohols, carboxylic acids, and amines, and for the production of detergents, plasticizers, and surfactants. The aldehydes occur either in linear or branched form, in the following referred to as n- and iso-aldehydes, respectively. Linear aldehyde are desired as their higher biodegradability make them more valuable than the branched isomers [109]. The separation of linear and branched aldehydes is energetically highly demanding since their physical properties are very similar. Thus, due to the higher value of linear aldehydes and their demanding separation, the n/iso-ratio of aldehydes is supposed to be high.

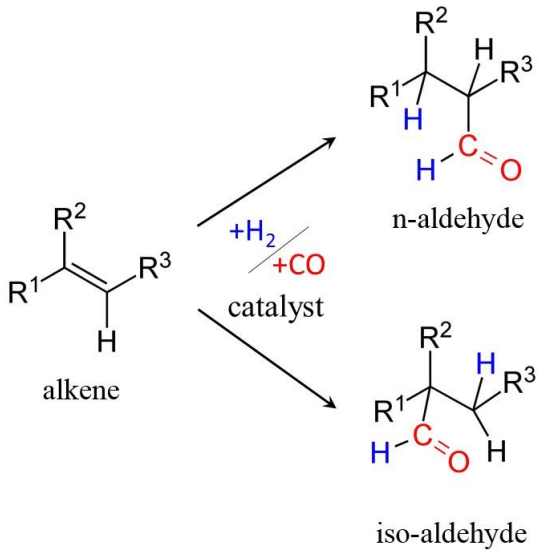

Figure 2.8: General hydroformylation reaction scheme

Beside the alkenes as substrate of the hydroformylation, other compounds with carbon double bonds are of interest, e.g. dienes, alkynes [110]. Moreover, the use of renewable and sustainable substrates such as terpenes and oleos are investigated as potential basis for alterative process structures allowing for the substitution of petrochemical feedstocks [111].

Homogeneous catalysts

The hydroformylation reaction is in general catalyzed by every transition metal whose central atom is able to form carbonyl groups. In practice, only cobalt and rhodium are used due to their sufficiently high activity. However, although rhodium shows a significantly higher activity than cobalt and its use allows for milder reaction conditions, its wider industrial application is hindered by its high expense [112].

Cobalt catalysts are almost completely substituted by rhodium catalysts for hydroformylation processes of short chain alkenes. For long chain alkene hydroformylation it is still mostly used since it is much cheaper than rhodium and, thus, more profitable. Main drawbacks of the cobalt-based processes are the high costs for product purification and catalyst regeneration as the catalyst is commonly destroyed in precipitation or distillation steps to remove it from the product phase [113]. The increased pressure and temperature conditions in comparison to the rhodium-based processes are required to compensate the low activity and prevent possible catalyst decomposition caused by low CO partial pressure.

In addition to the much higher activity, rhodium catalysts are more stable not requiring high CO partial pressure. Due to that, the rhodium-based processes have much lower catalyst concentrations and milder reaction conditions, still showing better selectivity than cobalt-based hydroformylation [112]. For short chain alkenes their low boiling point and high volatility allow for an efficient catalyst separation and recovery. For long chain alkenes these properties change unfavorably so that a separation of catalyst and products via distillation would destroy the catalyst. Thus, due to the high price of rhodium and its non-trivial recovery, still major research is necessary to develop economically profitable processes for rhodium-based hydroformylation of long chain alkenes (see subchapter 2.3.2).

In academia, alterative transition metals are investigated for the use as hydroformylation catalyst. For instance, a palladium based hydroformylation process showed high selectivity to the linear aldehyde when supported by low concentrations of acid [114], and van Duren et al. [115] used platinum-based catalysts with tin/diphosphine ligands for the hydroformylation of octene. For further insights about hydroformylation catalyzed by alternative transition metals, the interested reader is referred to [116].

For a high selectivity, especially the regioselectivity with respect to linear and branched aldehydes, the transition metal complexes require support of well-designed ligands [117]. These ligands affect the reaction via their steric and electronic properties. The position of the reactant and product around the transition metal can be manipulated by the steric properties of the ligand, which represents its form and orientation. The electronic properties of the ligand affect the electron density on the transition metal (see e.g. [110]). The expedient design of the ligand and its properties can, therefore, significantly affect the reaction performance. However, beside of the increased activity and selectivity, the design of the ligand has to take into account as well its solubility in the non-product phase to enable an efficient recovery and possible effects on the solubility of the metal complex. This property is of special importance in case the ligand is similarly expensive as rhodium. In case of rhodium-based hydroformylation phosphine ligands indicated the highest levels of activity and selectivity with respect to the linear aldehyde, e.g. TPP, TPPTS. In order to further increase the regioselectivity with respect to the linear aldehyde without loss of conversion, the phosphite ligand Biphephos seems promising for hydroformylation [118].

Existing process concepts

As mentioned before, for hydroformylation of long chain alkenes mainly cobalt-based processes are established. Most of them have been developed in large chemical companies, are well established, and used for decades. Famous processes are [112]:

- Shell Process: This process is used for C7 to C14 alkenes. Using a cobalt catalyst with phosphine modification the aldehyde is formed and directly reacts further to fatty alcohols in a one-pot reaction. The reaction takes place at 40 to 80 bar and 150 to 190 °C and the subsequent separation of catalyst and product is carried out in a distillation column whose catalyst rich bottom stream is recycled to the reactor inlet.
- Exxon/Kuhlmann Process: Here, C6 to C12 alkenes react under 300 bar and 160 to 180 °C catalyzed by an unmodified cobalt-carbonyl complex. The catalyst is extracted with fresh alkene and neutralized with sulfuric acid, as the product phase is beforehand mixed with caustic. Afterwards the catalyst is reformulated under high CO pressure, stripped with synthesis gas and recycled to the reactor. The reactor is designed as a vertical loop reactor or a series of loop reactors [119]. In the part of upwards moving liquid, the gas is injected and at the top both phases are partly withdrawn, whereby in the downwards part the heat of reaction is removed.
- BASF Oxo Process: A claimed advantage of this process is its use for all types of alkenes. Again, an unmodified cobalt complex is used at similar severe conditions as in the Exxon/Kuhlmann process. The separation of the catalyst is realized by precipitation through addition of aqueous acid and atmospheric oxygen, whereby the catalyst phase is separated in an aqueous phase. For reuse of the catalyst it is activated again with syngas and fresh cobalt and recycled to the reactor.

A critical disadvantage of the latter two processes is the formation of high boilers and alkanes due to high pressures and temperatures. To avoid this, the use of low pressure rhodium-based processes has been developed. For short chain alkenes the only industrially established processes are:

- Low Pressure Oxo Process [120,121]: This process exists in two configurations, i.e. as a gas recycle process and a liquid recycle process, and is also known as UCC Process.
  The gas recycle process works at low reaction temperature around 90 to 100 °C to avoid catalyst degradation. Therefore, it is only applied for short chain alkenes (<C5), since larger alkenes would require higher temperatures. It utilizes a rhodium triphenyl phosphine complex, which is dissolved in the reaction products serving as catalyst solvent. Hence, no additional solvent is required. The gaseous reactants are fed as bubbles at the bottom of the reactor and react on their way to the top, whereby the product is stripped from the catalyst solution which remains in the liquid bulk phase in the reactor. Subsequently, the product vapor phase is condensed to separate the product from remaining reactants, which are then recompressed and recycled to the reactor. Therefore, it is not necessary to reach a 100 % conversion per pass, rather around 30 % [122]. Due to possible forming of rhodium clusters, the deactivation of the catalyst is prevented by regeneration using special equipment. This process is limited by its fixed phase behavior, which is adjusted by the synthesis gas flow rate and reactor temperature. These two values are used to balance the vapor outlet flow with the aldehyde production. The reactor is realized as a stripper-reactor, as the synthesis gas acts as reactant and stripping medium for the product simultaneously [123]. Designed as a packed

column with counter-current flow of liquid and gas phase, two sections are formed, i.e. an upper stripping section and a lower reaction section.
In the liquid recycle process the liquid product phase and the catalyst leave the reactor and are separated outside the reactor. This decouples the reaction from the separation leading to a much smaller reactor volume and the possibility to optimize the reaction conditions. However, using the same catalyst a series of separation steps is required at whose end the catalyst is recycled to the reactor. This is avoided by a further development in the Mark IV Process, by use of a biphosphine-modified rhodium catalyst. Here, the reaction temperature is slightly decreased resulting in a better n/iso-ratio. This enables a single pass process either with a single CSTR or a cascade of CSTRs and a single flash separation of the product and the catalyst resulting in high conversions of 98.7 % [112].

- Ruhrchemie/Rhône-Poulenc Process [124]: This process uses a rhodium-carbonyl complex modified with a TPPTS ligand. Due to its sulfonate groups, the catalyst complex is hydrophilic. Thus, it can easily be separated from the product, as the catalyst stays in an aqueous phase and the product builds an organic phase. In the aqueous phase the gaseous reactants are dispersed and the reaction takes place at 110 to 130 °C and 3 to 5 bar in a CSTR with multi-blade stirrer and co-current flow of gas and liquid reactants [113]. The organic, low density product phase is removed from the top of the reactor and stripped to separate remaining reactants which is then recycled to the reactor. This simple and efficient process can only be used for the hydroformylation of propene. Ethylene hydroformylation fails at the solubility of the propanal product in water, and in case of longer-chain alkenes the reactants are not sufficiently soluble in water. The high efficiency of this process is achieved on the one hand by using the synthesis gas as reactant and stripping medium for remaining reactant separation from the product mixture, and on the other hand by heat integration of reactor and reboiler of the final distillation column via falling film evaporator [125].

A further process of this type is the new BASF Oxo Process. It has a similar structure as the Low Pressure Oxo Process with liquid recycle. Due to UCC patents, its reaction conditions are limited [124]. For long chain alkene (C6 – C14) hydroformylation using rhodium catalysts there exists only one commercial process, which is a further development of the UCC process.

- Adapted Low Pressure UCC Process: In this process a rhodium catalyst is modified by a polar TTPTS ligand and provided to the reaction dissolved in water. Together with a specific amount of N-Methyl-2-pyrrolidon (NMP) as mid-polar solvent, which depends on the length of the alkene and the amount of water, and the reactant it builds a homogeneous phase under reaction conditions (110 to 120 °C and 7 bar). Subsequent to the reaction, the reaction mixture is cooled down to 25 °C and water is added such that a phase split is induced resulting in a NMP/water phase, which contains the catalyst, and an organic product phase. After additional separation of catalyst traces and water, the NMP/catalyst mixture is returned to the reactor. For an efficient process operation, the water separated from the NMP/catalyst mixture is reused for the phase split.

Beside the industrially used processes, some research is conducted in academia seeking for interesting and intensified process or reactor concepts. For instance, Enache et al. [126] suggested a heat exchanger reactor for a solvent free hydroformylation of short chain alkenes. The heat exchanger reactor is chosen due to the required high mass and heat transfer rates caused by high catalyst loads. Although using this high amount of catalyst, no recovery strategy is provided. As well working with high catalyst loads, Wiese et al. [127] proposed the use of a long, thin tubular reactor with static

mixers for the hydroformylation of C3 to C8 alkenes. Due to the high catalyst loadings, the residence time in the reactor is only about a few seconds. The catalyst is recovered using an aqueous biphasic solvent system, which is separated after the reaction in a liquid-liquid phase separation.

2.3.2 Innovative concepts for homogeneously catalyzed multiphase processes

As the Adapted Low Pressure UCC process is currently the only industrially applied process for rhodium-based hydroformylation of long chain alkenes, academic and industrial research seeks for more profitable and flexible process alternatives. Several challenges are faced in course of this endeavor. In contrast to short chain alkenes, long chain alkenes are only barely miscible with water or other polar solvents, in which the catalyst is dissolved, due to their non-polarity what hinders the formation of a single phase under reaction conditions. Moreover, the biphasic separation fails due to the miscibility of the aldehyde products with their corresponding alkene reactants, as realized in the Ruhrchemie/Rhône-Poulenc Process. A separation via stripping or vaporization as in the Low Pressure Oxo Processes is as well not possible, since the high boiling points of the long chain alkenes would require high temperatures, which destroy the homogeneous catalyst. However, a quantitative recovery and recycle of the catalyst is indispensable due to the high expense of the rhodium metal and sophisticated ligands such as Biphephos. The most promising approaches for new process concepts utilizing innovative solvent systems are summarized in the following. Thereby, the focus is put on thermomorphic multicomponent solvent systems, as they are used in this work, and further concepts are briefly summarized.

Thermomorphic multicomponent solvent systems

Following the concept of adding a mid-polar solvent to a biphasic system as used in the Adapted Low Pressure UCC Process, to enable homogeneous phase conditions during reaction and a temperature controlled phase split for the separation of the catalyst from the product phase, the principles of thermomorphic multicomponent solvent systems become evident. They combine the features of the two-phasic separation approach and thermo-regulated phase transfer catalysis. Note, that TMS systems do not intend to require additional extraction with polar solvent and several subsequent separation steps to finally being able to recycle the catalyst. Behr et al. [128] suggested the use of these temperature-dependent, or thermomorphic, solvent systems for homogeneously catalyzed processes and distinguished three types of TMS systems. The first two types consider a particular third solvent and distinguish the form of the miscibility gap. The third type indicates the use of the reactant and the product as mid-polar solvent, or solubilizer, avoiding an additional solvent in the mixture.

The concept of this type III TMS system, illustrated in Fig. 2.9, is recapitulated as follows: Under reaction conditions, i.e. elevated temperature, the polar solvent, the nonpolar solvent, and the reactant form a homogeneous phase. Hence, the composition is located above the bimodal curve within the ternary triangle (left). After the reaction is terminated, cooling down the reaction mixture in a liquid-liquid phase separator induces a phase split. The miscibility gap in the ternary diagram of the polar solvent, the nonpolar solvent, and the product changes and the composition lies underneath the bimodal curve. The catalyst is dissolved in the polar solvent and recycled to the reactor, whereas the products and remaining reactant are located in the organic solvent and further processed downstream. The form of the miscibility gap is controlled by temperature and composition of the mixture. In case of type I or II TMS systems the mid-polar solvent affects it as well.

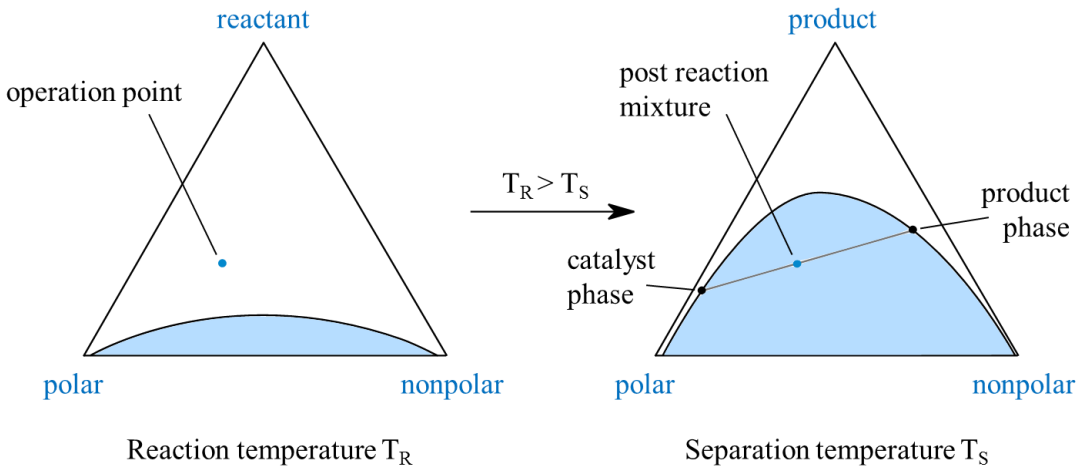

Figure 2.9: Scheme of TMS principle

Following this procedure, a TMS system has to fulfill two crucial requirements: (i) it has to form a single homogeneous phase under reaction conditions to avoid mass transfer resistances; and (ii) it has to allow for liquid-liquid phase splitting of a catalyst rich phase and a product phase induced by temperature shift. The challenges for the design of TMS systems arising out of these requirements are: (i) the solvents have to be chosen such that occurring products and side products during reaction do not show a heterogeneous phase behavior in the reactor; (ii) reactants, products, and side products should not hinder a clear phase separation by cooling; (iii) the solubility of the catalyst should be very high for the polar solvent and very low for the nonpolar solvent; and (iv) the solubilities of the products and reactants require the opposite behavior.

First, the selection of suitable solvents for TMS systems have been based on the phase separation behavior of two or three solvents [129], whereas their respective pure solvent parameters such as polarities are included using Hansen solubility parameters [130]. In a later work, Behr and Wintzer [131] proposed a comprehensive guide to solvent selection where the upper critical solution temperature of the solvent mixture and the solvents' respective Hansen solubility parameters are identified as most critical attributes. In addition, environmental factors and the compatibility with other compounds formed during the process are mentioned as decisive aspects. Based on these works, McBride et al. [132] presented recently a systematic computer-aided design procedure for TMS systems that bases on property predictions with COSMO-RS and model-based liquid-liquid phase behaviors. It has successfully been applied and experimentally validated for the TMS design for the hydroformylation of 1-dodecene.

Further promising process concepts

In most of the process concepts proposed in literature, the recovery of the homogeneous catalysts is emphasized. Additionally, some of the concepts intend to enhance the reaction potential. In the following, the innovative process concepts are classified within the areas of: (i) multiphase systems; (ii) immobilization techniques; (iii) phase enhancement; and (iv) filtration strategies. Thereby, the combination of concepts of different categories can indicate promising synergy effects.

The basic concept of multiphase systems is elucidated in the course of TMS systems and the bi-phasic industrial processes for hydroformylation. They differ mainly with respect to the handling of the catalyst phase and the liquid-liquid phase separation. Interesting multiphase concepts are:

- Perfluorinated solvents: The underlying concept is that a catalyst/ligand is tagged with fluorinated sections such that it dissolves in a perfluorinated solvent whose miscibility with

organic and aqueous phases can be controlled via temperature, similar to TMS systems. Depending on the solvent system, the fluorinated catalyst/ligand may build an individual phase without addition of a fluorinated solvent. Horvath et al. [133] reported a successful application for the hydroformylation of 1-decene indicating a very small catalyst leaching. Drawbacks of this concept are the high costs of the fluorinated solvents and ligands.

- Micellar solvent systems: Instead of mid-polar solvents surfactants are added leading to the formation of micelles, which increase the liquid-liquid surface area. Inside of the micelles one of the phases, mostly the catalyst and thus reaction phase, is enclosed. The solvent system, consisting of water, surfactant, and an organic phase, is composed such that a phase split is induced under lowered temperature conditions allowing for a recovery of the catalyst from the aqueous solvent phase. For the hydroformylation of 1-dodecene using a rhodium catalyst modified with a TPPTS ligand, Haumann et al. [134] developed an efficient micellar solvent system and indicated higher activities though less selectivity in the microemulsion in comparison to homogeneous systems.
- Ionic liquids: Similar to perfluorinated solvents, the idea of the use of ionic liquids is to provide a phase in which catalysts/ligands with ionic properties can be dissolved and thereby recovered. After the reaction is terminated, the products and remaining reactants are separated with organic solvents from the ionic liquid, which is recycled with the therein dissolved catalyst to the reactor. The decisive properties of the ionic liquid, i.e. solubilities of reactants and products, and activity and selectivity of the catalyst, can be adjusted by the type of its anions and cations [135]. Tan et al. [136] reported the use of a thermo-regulated ionic liquid for the rhodium catalyzed hydroformylation of 1-dodecene yielding very high conversions and selectivities around 99 % and 97 %, respectively. The drawbacks of ionic liquids are on the one hand their impact on process materials and on the other hand their high prices compared to organic solvents [137].
- Pickering emulsions: Here, instead of surfactants amphiphilic nanoparticles are added to the system of immiscible fluids, which are thereby kinetically stabilized. Similar to the micellar solvent systems, the catalyst is enclosed by the particles and the reactants and products diffuse through the interphase. Their advantages are that high interphase areas are formed, fast diffusion of reactants and products through the interphase is enabled, and the materials are environmentally friendly [138]. For the hydroformylation of 1-octene, Zhao et al. [139] reported the successful application of Pickering emulsions showing stable conversions and selectivities for several reaction cycles. The catalyst was recovered by centrifuging the reaction mixture leading to a precipitation of the particles and a separation of the water and organic phase.

With regard of immobilization techniques, the process concepts can be distinguished corresponding to the support phase containing or fixing the homogeneous catalyst. One can distinguish:

- Membrane/polymer support: This concept immobilizes the catalyst in the reactor on a solid support structure, e.g. membranes or silica, to avoid the effort of subsequent separation and recovery. For instance, Song et al. [140] attached the rhodium complex on mesoporous silica in the hydroformylation of 1-octene. They reported of very low levels of catalyst leaching, however, accompanied by poor regioselectivity.
- Aqueous support: Here, the catalyst is immobilized in a thin film of water on a solid surface such as silica or monoliths. Arhancet et al. [141] introduced this as a promising approach for hydroformylation reactions. However, this concept suffers from low solubilities of organic molecules and evaporation of water from the porous support.

- Ionic liquid support: An enhancement of the aforementioned concept is the use of ionic liquid instead of water, called supported ionic liquid phase (SILP) [142]. They outperform water due to their low vapor pressure and high viscosity. Riisager et al. [143] demonstrated successfully the use of SILP for the rhodium catalyzed gas and liquid phase hydroformylation of propene and 1-octene indicating no detectable catalyst leaching. An advantage of the use of SILP in comparison to the conventional bi-phasic process was the high dispersion of the ionic liquid catalyst solution, whereas an identified drawback was a poor solubility of synthesis gas probably caused by limited mass transfer.

As mentioned before, some concepts rather intend to enhance the reaction conditions than the efficient recovery of the homogeneous catalyst. Famous examples are:

- Supercritical fluids: By compressing gases above their critical temperature and pressure they become supercritical fluids, which have the ability to dissolve many organic molecules with low and medium polarity and gases [144]. By using them as solvents, mass transfer resistances are strongly decreased and reactions are enhanced. Koch and Leitner [145] showed how the choice of the right ligand enables hydroformylation catalysts to be dissolved in supercritical fluids such as $scCO_2$.
- Gas expanded liquids: The liquid volume of solvents is expanded using gases which show liquid like densities around their critical point. This leads to a change of phase properties of these so called gas expanded liquids, e.g. lower viscosity and higher diffusion coefficients [146]. Hence, they can be used to tune, e.g. the solubilities of gaseous reactants in the liquid reaction phase. Jin and Subramaniam [147] reported a significant increase of the turn over number for the hydroformylation of 1-octene using CO_2 as expanding gas due to higher solubilities of the synthesis gas.

In contrast to the use of solvent systems, a few approaches have been developed to recover the homogeneous catalyst by filtration methods. For instance, for the continuous hydroformylation of 1-octene Fang et al. [148] designed polymer catalysts such that they can efficiently be recovered by membrane filtration due to a reduced permeability caused by their bulky form. For the same reaction, Xie et al. [149] modified a rhodium catalyst with polydimethylsiloxane making it an inexpensive, nano-filterable homogeneous catalyst, whose successful recovery was experimentally tested in a 120 h run. As mentioned before, several approaches combined strategies to use arising synergy effects. For instance, Webb et al. [150] combined the use of supercritical CO_2 and an ionic liquid for the hydroformylation of 1-dodecene claiming that the solvent system can be operated continuously for several weeks without any catalyst degradation. Hintermair et al. [151] immobilized the catalyst in a supported ionic liquid phase and used CO_2 to form a gas expanded liquid. They state that due to the formation of a gas expanded liquid at higher pressures, the reaction rates have been increased and the catalyst leaching reduced. Due to the lower viscosity the gas expanded liquid enabled better transport of synthesis gas to the catalyst, and its reduced polarity made it less soluble for the ionic liquid.

2.3.3 Fundamentals of the example process

From the overview of potential homogeneous transition metal catalysts it became evident that rhodium catalysts are the most promising due to their very high activity. Moreover, the meaning of high performing ligands for the suitable control of chemo- and regioselectivity was pointed out. The indispensable requirement of a quantitative recovery of both metal complex and ligand for establishing an industrially applicable process was reasoned by their high prices. Several interesting process concepts for catalyst recovery and reaction enhancement indicate the high improvement potentials

which are still under research and high likely about to be exploited in the near future. Due to its similarities to the existing Adapted Low Pressure UCC Process, thermomorphic multicomponent solvent systems seem to be quite close to be used for a real process concept. In comparison to alternative concepts previously discussed, they do not require expensive solvents, surface active or solid additives, or energy demanding separation steps. Moreover, they provide a homogeneous reaction phase leading to reduced mass transfer resistances. Due to these features, the development of new process structures for the hydroformylation of long chain alkenes within the Collaborative Research Centre TR63 InPROMPT is carried out using TMS systems (beside others). The example process was chosen to be the hydroformylation of 1-dodecene aiming at the production of n-tridecanal. As indicated in literature [152], the use of a $Rh(acac)(CO)_2$ catalyst modified with a Biphephos ligand provides very high activity, chemo- and regioselectivity, and was, thus, used for the investigated hydroformylation process.

Behr et al. [153] suggested the use of a TMS system consisting of n-decane as nonpolar solvent and N-,N-dimethylformamide as polar solvent. Schäfer et al. [154] carried out thorough studies about the phase behavior, reaction performance, and the catalyst recycling in this TMS system. Based on these studies, they suggested an overall solvent fraction of at least $80\,\%$ to ensure homogeneous phase conditions under reaction conditions and a phase split at room temperature. Thereby, the catalyst recovery increases with decreasing separation temperature.

Considering this TMS system and the aforementioned catalyst complex, Markert et al. [155] and Kiedorf et al. [156] carried out extensive studies on the kinetic mechanisms of the hydroformylation process and identified a reaction network and corresponding reaction rates. In a subsequent study, Hentschel et al. [157] refined this network based on new experimental results of perturbation experiments intending to better quantify the impact of gaseous reactants. This resulted in the addition of a sixth reaction, i.e. the direct conversion of 1-dodecene (nC12en) to branched aldehydes (iC13al), and a new estimation of kinetic coefficients. The resulting reaction network (Fig. 2.10) consists of the hydroformylation of 1-dodecene to n-tridecanal (nC13al) r_1, the isomerization of 1-dodecene to its isomers (iC12en) r_2, the hydrogenation of 1-dodecene and the iso-dodecenes to n-dodecane (nC12an) r_3 and r_4, respectively, and the formation of branched aldehyde 2-methyl-dodecanal (iC13al) from 1-dodecene and iso-dodecenes r_5 and r_6, respectively.

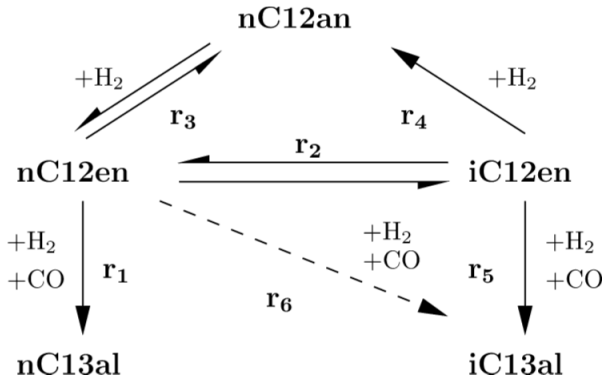

Figure 2.10: Reaction network according to [157]

Kiedorf et al. [156] suggested the inclusion of the side reactions to the catalytic cycle of the hydroformylation, as to their findings all reactions compete for the same active catalyst species. This active catalyst species is situated in a pre-equilibrium between the active resting state, its inactive states, and the precursor before the catalytic cycles start. The amount of active species, which is performing the catalytic cycle, depends on the amount of ligand, as well as the concentrations of

carbon monoxide and hydrogen. Therefore, they derived an equation to determine the amount of active catalyst species (Eq. (2.1)).

$$c_{cat} = \frac{c_{cat,tot}}{1+K_{cat,1}c_{CO}^{K_{cat,3}}+K_{cat,2}\frac{c_{CO}^{K_{cat,3}}}{c_{H2}}} \tag{2.1}$$

Based on these assumptions and the catalytic cycle including hydroformylation, isomerization, and hydrogenation reactions, they derived reaction rate equations (Eqs. (2.2)-(2.6)) for the reactions in the reaction network, which are valid for $10\,\text{bar} \leq p_{tot} \leq 20\,\text{bar}$ and $368.15\,\text{K} \leq T \leq 388.15\,\text{K}$. As mentioned before, a refinement study led to the addition of a sixth reaction and corresponding rate equation (Eq. (2.7)) not affecting the form of the other rates equations [157].

$$r_1 = \frac{k_{1,0}(T)c_{nC12en}c_{H2}c_{CO}}{1+K_{1,1}c_{nC12en}+K_{1,2}c_{nC13al}+K_{1,3}c_{H2}} \tag{2.2}$$

$$r_2 = \frac{k_{2,0}(T)\left(c_{nC12en}-\frac{c_{iC12en}}{K_{eq,2}}\right)}{1+K_{2,1}c_{nC12en}+K_{2,2}c_{iC12en}} \tag{2.3}$$

$$r_3 = \frac{k_{3,0}(T)\left(c_{nC12en}c_{H2}-\frac{c_{nC12an}}{K_{eq,3}}\right)}{1+K_{3,1}c_{nC12en}+K_{3,2}c_{nC12an}+K_{3,3}c_{H2}} \tag{2.4}$$

$$r_4 = k_{4,0}(T)c_{iC12en}c_{H_2} \tag{2.5}$$

$$r_5 = k_{5,0}(T)c_{iC12en}c_{H_2}c_{CO} \tag{2.6}$$

$$r_6 = k_{6,0}(T)c_{nC12en}c_{H_2}c_{CO} \tag{2.7}$$

The temperature dependencies of the reaction constants $k_{j,0}$ are modeled via an Arrhenius equation (Eq. (2.8)) with $T_{ref} = 378.15\,\text{K}$.

$$k_j(T) = k_{0,j}\,exp\left(\frac{-E_{A,j}}{R}\left(\frac{1}{T}-\frac{1}{T_{ref}}\right)\right) \quad , j \in RCT \tag{2.8}$$

The equilibrium constants $K_{eq,j}$ in r_2 and r_3 and the required Gibbs energies of formation $\Delta_R G_j$ are determined via Eq. (2.9) and (2.10), respectively.

$$K_{eq,j} = exp\left(\frac{-\Delta_R G_j}{RT}\right), \tag{2.9}$$

$$\Delta_R G_j = a_{0,j} + a_{1,j}T + a_{2,j}T^2,\ j \in \{2,3\}. \tag{2.10}$$

The parameters of the reaction constants and the catalyst equilibrium as well as the equilibrium constants are listed in Tab. A.1 and Tab. A.2, respectively.

Following the work of Hentschel et al. [157], the gas solubilities for carbon monoxide and hydrogen in the TMS system can be calculated via the use of Henry constants H_α (Eq. (2.11)), whereby the effect of product formation on the solubilities are neglected due to the excess of solvents. The Henry constants are determined with Eq. (2.12) whose parameters are given in Tab. A.3.

$$c_\alpha^* = \frac{p_\alpha}{H_\alpha} \quad , \alpha \in \{GAS\} \tag{2.11}$$

$$H_\alpha = H_\alpha^0\,exp\left(\frac{-\Delta_S H_\alpha}{RT}\right) \tag{2.12}$$

Note, that the reaction kinetics and gas solubilities are only valid for the applied mass fractions of solvents and molar amount of the catalyst, see Eq. (2.13) and Eq. (2.14), respectively.

$$w_{DMF} = w_{C10an} = 0.42, w_{nC12en} = 0.16 \tag{2.13}$$

$$c_{cat} = c_{nC12en} \cdot 2.5 \cdot 10^{-4} \tag{2.14}$$

3 Qualitative reactor synthesis

This chapter introduces the framework for the qualitative synthesis of chemical process networks, i.e. reactor-networks, reactor-recycle-networks, and reactor-separator-recycle-networks, based on the methodology of *elementary process functions*.

In subchapter 3.1 the main aspects of chemical reactor synthesis are summarized, and the targets of the presented synthesis framework are discussed. Originating from that, the synthesis approach is derived from the conception and the mathematical description of the EPF methodology. The use of the Lagrangian description of the fluid element and the search for optimal fluxes controlling it, lead to the formulation of a dynamic optimization problem whose components are discussed in detail. Based on that, the qualitative reactor synthesis via *flux profile analysis* (FPA) is introduced, which allows for generating candidates of optimal process networks from the results of the dynamic optimization of the process.

The first FPA application scenario, i.e. the synthesis of reactor-networks, is covered in subchapter 3.2. The mathematical basis and the resulting DOP are adapted for this purpose and two application examples are elaborated. First, a literature example is considered allowing for a comparison of the synthesis results with the attainable region approach. Second, reactor-network candidates are derived for the hydroformylation process introduced in subchapter 2.3. Several candidates are derived and their performances are compared in the selectivity-conversion space.

In subchapter 3.3 the focus lies on the synthesis of reactor-recycle-networks via FPA. Again, the mathematical basis and the DOP are adapted accordingly, and two examples are chosen to showcase the applicability of the presented reactor synthesis approach. As in subchapter 3.2, the first example is taken from literature and enables a comparison with superstructure optimization approaches on this synthesis level, and again, the second process example is the aforementioned hydroformylation process. Reactor-recycle-network candidates are derived using different reduction scenarios, and the resulting candidates are compared among each other and with the results from subchapter 3.2. In addition to the synthesis of reactor-networks via FPA, a sensitivity analysis is carried out in this subchapter to quantify the impact of storage tank filling levels on the synthesis.

The last application level is the synthesis of reactor-separator-recycle-networks in subchapter 3.4. After adapting the mathematical basis and the corresponding DOP, the FPA is carried out for the hydroformylation process and a promising reactor-network candidate is derived. Its performance is determined in the selectivity-conversion space and compared to selected results from the previous two synthesis levels. Additionally, a sensitivity analysis for the number of separations in the reactor-network is conducted.

Finally, the presented qualitative reactor synthesis approach and the results of the applications on the three synthesis levels are discussed in subchapter 3.5.

3.1 Methodical framework

3.1.1 Aims of the presented qualitative reactor synthesis approach

The synthesis of process networks, sometimes called conceptual design or flow sheet optimization, focuses on finding the optimal configuration of different process units within the overall structure of the process. In contrast to process design methods aiming at a detailed shaping of the units within the process, the abstraction level is higher and, hence, the level of detail of the considered models is lower for reactor synthesis purposes. Regarding the hierarchical classification introduced in the EPF concept, see subchapter 2.1, the synthesis is located on the plant level taking only major characteristic information about the units into account, whereby the more detailed process design acts

on the process unit level. Due to the broader view on the process on the plant level, multiple different aspects are considered in the overall structure of the process simultaneously, e.g. chemical reaction, recycling, separation, heat supply/removal, etc. Depending on the system bounds chosen for the synthesis, the functions that are considered become manifold and the resulting synthesis very complex. Therefore, every synthesis has to state in advance which main functions are supposed to be included and the approach used for the synthesis is classified according to the included process functions. Typical examples for different kinds of synthesis approaches in process engineering are discussed in chapter 2.2, see Fig. 2.6.

The synthesis framework for chemical processes introduced in the following is built on the assumption that the core of a chemical process is the step of transformation of chemical components into higher valuable products. Although the complete process includes preliminary steps such as preprocessing of raw materials, contacting of phases, and activating of e.g. catalysts, and post processing steps such as heat supply/removal, separating, and product formulation, those steps have a supporting character for the chemical reaction step. In the preprocessing steps the (initial) conditions required for an optimal reaction are achieved. The postprocessing has two crucial aspects: (i) it separates, purifies, and formulates the desired product up to a desired quality for the market, and (ii) it makes the side and couple products coming along the reaction available for either further use in other processes or recycling, which might support again achieving the best (initial) conditions for the actual chemical reaction. Self-evidently, these different steps in a chemical process are not necessarily separated. There exist intensified and/or multifunctional units, which combine several steps such as reactive separations or heat-integrated reactors. In other cases, specific steps might even be simply unnecessary. Common to all cases is, that the reaction step is not negligible, which highlights its meaning as core of a chemical process. This assumption is included in several synthesis and design approaches, e.g. the onion model by Smith and Linnhoff [12] or the hierarchical decision procedure by Douglas [11]. Although the chemical reaction is treated as core of the process, other functions are included in the presented synthesis approach as well:

- The *contacting/mixing* of components, which is realized by dosing along the reaction coordinate and which, moreover, includes the realization of the optimal compositions by back-mixing and recycling.
- The *heat supply/removal*, which is adjusted already during reaction to steer the reactions within the thermodynamic state space.
- The *separation* of either valuable products or useful side products, which are supposed to be used for dosing along the reaction coordinate, or useless components, which need to be removed to achieve a specified or improved product purity.

The inclusion of these process functions takes place in the context of their effects on the optimal control of the chemical reaction. They are not analyzed individually. Furthermore, these aspects are only treated on an abstract, idealized level and require more detailed design in later steps of the process design procedure.

In addition to the process functions, which are supposed to be included in the synthesized process, the question of operational mode comes into play. Generally, one can distinguish between discontinuous and continuous processes. The former are often associated with smaller scale productions like for pharmaceuticals and fine chemicals, while the latter with large-scale productions of bulk chemicals. Classical synthesis approaches are derived and used for continuous processes, whereby discontinuous processes are mostly a subject of scheduling or finding optimal recipes. The presented synthesis approach intends to synthesize the process independently of the operational mode of single units. The decision-making about it is treated as question of best technical realization and,

thus, of quantitative economic evaluation at a later stage of process design. The mainly qualitative information gathered by the presented reactor synthesis approach allow for generating also candidates of hybrid batch-continuous reactor-networks, since the dynamic control of reactor units, which might be replaced by batch reactors, is available from the dynamic optimization anyway. For possible separation steps this is valid as well, but out of the scope of this work. Note, that the resulting process can remain of continuous operation, since possible replacements by batch units are simply integrated in the continuous overall process.

Main target of the presented reactor synthesis approach is the rational derivation of reactor-network candidates by analyzing reaction, mixing, and separation functions accompanied by heating/cooling along the reaction coordinate. The analysis is based on fundamental reaction engineering knowledge. Its results are qualitative process structures. Due to the aspired simplicity of the underlying dynamic optimization, the framework can be used for fast synthesis of reactor-network candidates and shrinking of the potential search space for more detailed and, thus, time-consuming approaches.

3.1.2 Placement of the qualitative reactor synthesis approach within the EPF framework

The original EPF method was established for the purpose of shifting the consideration of a process in terms of unit operations towards the consideration of functional modules within process analysis and design, which allows for optimizing these modules individually and identifying process intensification potentials. The mathematical formulation of the EPF method intends to be comprehensive with regard to physico-chemical phenomena, which affect process design and its intensification and, thus, has to be included in a general framework. The formulation considers mechanical as well as thermodynamic states of the fluid element, volume-related and surface-related mass, momentum, and energy fluxes and the corresponding balance equations, as well as state-dependent capacities and state-independent weights of acting fluxes, and unifies all within a matrix-vector notation, see subchapter 2.1.1. The resulting general dynamic optimization problem of the EPF concept reads:

$$\min_{\boldsymbol{u}(t),\boldsymbol{\xi}} \left(\int_0^{t_f} L(t)dt + I(\boldsymbol{x}_0) + W(\boldsymbol{x}_f) \right) \tag{3.1}$$

$$\text{s.t. } \boldsymbol{C}(\boldsymbol{x}) \cdot \frac{d\boldsymbol{x}}{dt} = \boldsymbol{F} \cdot \boldsymbol{j}(\boldsymbol{x}) \tag{3.2}$$

$$\boldsymbol{g}(\boldsymbol{x}) = 0, \boldsymbol{h}(\boldsymbol{x}) \leq 0 \tag{3.3}$$

$$\boldsymbol{u}^L \leq \boldsymbol{u}(t) \leq \boldsymbol{u}^U \tag{3.4}$$

$$\boldsymbol{\xi}^L \leq \boldsymbol{\xi} \leq \boldsymbol{\xi}^U \tag{3.5}$$

$$\boldsymbol{x}(t_0) = \boldsymbol{x}_0, \boldsymbol{x}(t_f) = \boldsymbol{x}_f \tag{3.6}$$

The objective function (Eq. (3.1)) consists of the stage cost $L(t)$, an initial cost $I(\boldsymbol{x}_0)$, and a final cost $W(\boldsymbol{x}_f)$. The first represents a Lagrangian type objective function, the two others are of Mayer type, and all together are called a Bolza type problem. The control vector $\boldsymbol{u}(t)$ contains time-dependent decision variables, which are chosen to manipulate the fluid element along the reaction coordinate, both external fluxes, such as heat and mass flux, and internal properties such as the catalyst density. They are bounded by lower limits $\boldsymbol{u}^L$ and upper limits $\boldsymbol{u}^U$ (Eq. (3.4)). In addition, there are time-independent decision variables collated in the parameter vector $\boldsymbol{\xi}$ such as the final reaction time t_f. Again, accompanied by lower bounds $\boldsymbol{\xi}^L$ and upper bounds $\boldsymbol{\xi}^U$ (Eq. (3.5)). Within the general dynamic optimization problem the vector $\boldsymbol{g}$ contains equality constraints and $\boldsymbol{h}$ collates inequality constraints

(Eq. (3.3)). Finally, the initial state vector and the final state vector are defined by $\boldsymbol{x}_0$ and $\boldsymbol{x}_f$, respectively (Eq. (3.6)). The EPF concept is a rigorous model-based approach and complies with the equations of change, i.e. the total mass balance (Eq. (A.1)), the component mass balance (Eq. (A.2)), the momentum balance (Eq. (A.3)), the total energy balance (Eq. (A.4)), and in addition an evolution equation for the geometry (Eq. (A.5)), which are collated in Eq. (3.2). From this notation follows the state vector [15]:

$$\boldsymbol{x}^{\mathrm{T}}(t) = \big(T(t), p(t), \boldsymbol{w}^{T}(t), v(t), G(t)\big). \tag{3.7}$$

According to Eq. (3.7) the state vector is defined by the temperature T, the pressure p, the mass fraction vector $\boldsymbol{w}^{T}$, the velocity v, and the geometrical state G. Depending on the operational mode of the process, the geometrical state is the volume of the fluid element $G = V$ in a batch process or the volumetric mass flux $G = vA_c$ in a continuous process, respectively, with A_c being the cross sectional area of the matter element. The volume of the fluid element is assumed to be ideally mixed, i.e. no gradients with respect to mass, energy, or momentum occur inside the fluid element. The state dependent capacity matrix $\boldsymbol{C}$ and the state independent matrix $\boldsymbol{F}$ are derived from the aforementioned equations of state, see Eqs. (A.1)-(A.5). The matrix $\boldsymbol{F}$ contains the weighting factors of the flux vector [15]:

$$\boldsymbol{j}^{\mathrm{T}}(t) = (m_A, j_A^{T}, r_V^{T}, \tau_A, f_V, q_A, w, g). \tag{3.8}$$

In Eq. (3.8), m_A is the total mass flux density, $j_A \in \mathbb{R}^{N-1}$ corresponds to the diffusion flux densities of the chemical components, $r_V \in \mathbb{R}^{M}$ defines the rate vector of M chemical reactions, τ_A stands for the surface stress, f_V is the body force in direction of the main flow, q_A is the heat flux, w is the work, and g quantifies the rate of the geometry variation of the fluid element.

Although this general formulation is reasonable for the purpose of comprehensive process design and inclusion of process intensification potentials, one can neglect several aspects within this formulation when focusing only on reactor synthesis. The main requirement of model-based reactor synthesis and design procedures is a fundamental knowledge about the underlying reaction network, the corresponding reaction rates, and/or the chemical equilibria of the attending reactions. As the reaction network included in Fig 3.1 exemplarily illustrates, a reaction network consists of chemical species and reactions transforming them into each other, either in single, parallel, or consecutive reaction steps.

In terms of graph theory, one can imagine the chemical species to be the nodes and the reactions to be the edges. Thus, finding the optimal reaction route and designing a process for a given reaction network can be seen as optimally manipulating the edges and nodes of the corresponding reaction network. This is the fundamental idea the EPF framework bases on. The thermodynamic states, e.g. mass fractions of the chemical species, temperature, pressure, etc. of the fluid element are manipulated by external and internal fluxes while evolving over time, i.e. travelling through the process, see Fig. 3.1. The manipulation of these states leads to a change of the edges and nodes, i.e. the reaction rates and amount of chemical species, of the reaction network inside the fluid element. Following this train of thought, the main states of interest for reactor synthesis are the temperature T and the component masses $\boldsymbol{m}^{T}$, which are controlled by external heat flux q_A and mass flux m_A, respectively. They are used to steer the reaction rate fluxes $\boldsymbol{r}_V$. This conception is corroborated by the state-of-the-art methods for reactor synthesis described in subchapter 2.2.1, according to which the reactor-network is found by analyzing only reaction and mixing. When generalizing the synthesis on processes including separations, this is extended by removal, i.e. negative mass fluxes.

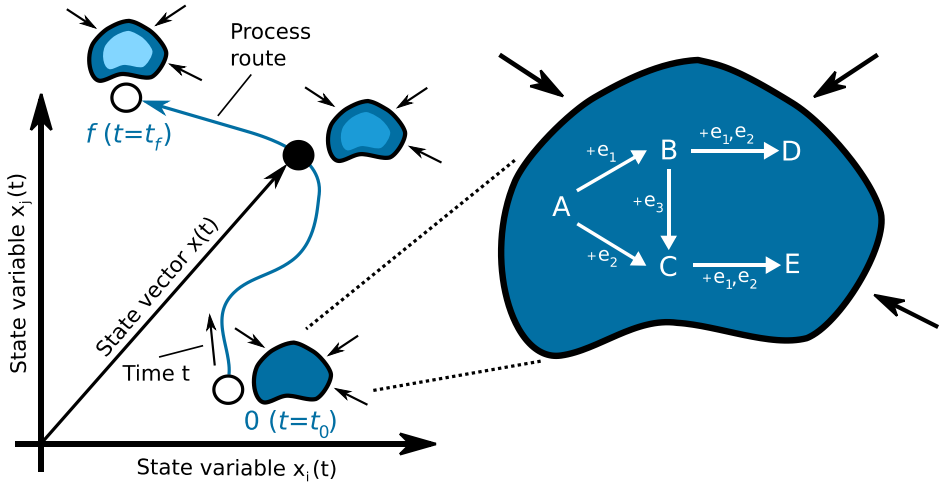

Figure 3.1: Fluid element in thermodynamic state space containing reaction information of the process [158]

To reduce the mathematical formulation of the EPF method aiming at the necessary equations for reactor synthesis, the following assumptions are made:

- The total mass (Eq. (A.1)) is linearly dependent on the component masses (Eq. (A.2)) and, hence, does not have to be considered individually. Instead, the component mass balance and all corresponding fluxes and matrices are defined in $\mathbb{R}^N$ in the following.
- The velocity v is assumed not to affect the optimal reaction control and, hence, the momentum balance (Eq. (A.3)) is neglected, see e.g. [14].
- The temperature T can be manipulated ideally due to the negligence of possible heat transport limitations. Hence, the total energy balance (Eq. (A.4)) is skipped and T is treated directly as decision variable, see e.g. [37].
- The geometrical state G (Eq. (A.5)), i.e. the volume of the fluid element, is of minor importance and, thus, does not have to be balanced. In case of need the volume V as well as the pressure p can be determined by constitutive equations, see e.g. [159].

Taking these assumptions into account, only the component mass balance (Eq. (3.9)) has to be considered to describe the deciding state changes in the fluid element for reactor synthesis.

$$\frac{d\boldsymbol{\rho}}{dt} = a_m \cdot (\boldsymbol{j}_A + \boldsymbol{w} \cdot m_A) + \boldsymbol{M} \cdot \boldsymbol{N} \cdot \boldsymbol{r}_V \tag{3.9}$$

The time evolution of the partial densities vector $\boldsymbol{\rho}$ is defined by the specific surface area a_m of the fluid element, the aforementioned diffusion flux densities of the species $\boldsymbol{j}_A \in \mathbb{R}^N$, the component mass fraction vector $\boldsymbol{w}$, the total mass flux density m_A, the diagonal matrix of molar masses of chemical components $\boldsymbol{M} \in \mathbb{R}^{N\times N}$, the stoichiometric coefficient matrix $\boldsymbol{N} \in \mathbb{R}^{N\times M}$, and the aforementioned reaction flux vector $\boldsymbol{r}_V \in \mathbb{R}^M$. The diffusion flux densities $\boldsymbol{j}_A$ are assumed to come into play only in case of multiphase processes in which species from other phases enter the fluid element. Since the fluid element is ideally mixed, the only case where concentration gradients lead to diffusion fluxes are mass transfer phenomena at interphases. For the sake of simplicity, the flux densities and the specific surface area are not optimized individually. Thus, they are lumped to a component diffusion flux density vector $\boldsymbol{j} = a_m \cdot \boldsymbol{j}_A$ and a component mass flux density vector $\boldsymbol{y} = a_m \cdot \boldsymbol{w} \cdot m_A$. The resulting component mass balance reads:

$$\frac{d\boldsymbol{\rho}}{dt} = \boldsymbol{j} + \boldsymbol{y} + \boldsymbol{M} \cdot \boldsymbol{N} \cdot \boldsymbol{r}_V. \tag{3.10}$$

As discussed before, the remaining fluxes are the component mass flux densities y_α into and out of the fluid element and the heat flux q_A which is substituted by the temperature T due to aforementioned assumptions. It affects the mass balance due to the temperature dependence of the reaction fluxes $\boldsymbol{r}_V$. Depending on the sign of the component mass flux density vector it is either referred to as dosing flux density vector $\boldsymbol{y}$ (positive) or removal flux density vector $\boldsymbol{z}$ (negative).

3.1.3 Flux profile analysis

The presented approach for qualitative synthesis of reactor-networks bases on the analysis of the flux profiles of the mass fluxes and the temperature, which are a result of solving a dynamic optimization problem, and is named *flux profile analysis*. It aims at identifying sections of (i) benefits from either back-mixing or plug flow, (ii) distributed or constant heating/cooling strategies, (iii) initial or distributed reactant dosing, (iv) optimal reaction control by initial or distributed recycling of (by)products, and (v) the removal of components which are adverse to the reaction progress or the objective, respectively. The general procedure is subdivided in three steps that are discussed in detail below.

Step 1: Dynamic optimization of mass and energy control fluxes

Main target in step 1 is the formulation and solving of the dynamic optimization problem, which corresponds to the state evolution in time of the fluid element tracked on its way through the process. The reasonable formulation of the dynamic optimization problem, providing optimal dosing fluxes, removal fluxes, and temperature profile, depends on intrinsic limitations of the process, the suitable choice of decision variables, and the objective of the process design. The impact of the objective is discussed in more detail in subchapter 3.5. The decision variables have to be chosen according to the characteristics of the process. In a multiphase process, for instance, the compositions of the non-reactive phases, which can be treated as support phases, are additional degrees of freedom. This is further discussed in the subchapter 3.2. Depending on the type of process, it might also be possible to change the catalyst density along the reaction coordinate, e.g. in heterogeneous gas phase processes, in contrast to having a constant predefined catalyst density [4]. As elucidated in subchapter 3.1.2, the dynamic optimization problem is constrained by equations of change, and additional inequality and equality constraints. The latter are model equations which are, beside of the balance equations, indispensable for a comprehensive physico-chemical model of the reaction progress, i.e. reaction kinetics and thermodynamic relationships e.g. in form of equations of state. The intrinsic bounds on the decision variables normally arise by the validity bounds of these models or material properties, e.g. maximum temperature in order to prevent catalyst damage. However, the limitations should be hold as small as possible, since all bounds or predefinitions reduce the search space and, thus, the possible maximum potential of the process, which is sought in this procedure.

For the dynamic optimization in step 1 the system bounds for the striven synthesis, i.e. the process functions that are supposed to be included, have to be defined. Within the presented approach three types of synthesis are discussed: (i) the reactor-network synthesis, (ii) the reactor-recycle-network synthesis, and (iii) the reactor-separator-recycle-network synthesis. In context of the optimization of the external fluxes of the fluid element along the reaction coordinate, they simply differ in the considered mass flux properties. In (i) only the dosing of reactant(s) is investigated; (ii) includes additionally the dosing of products, which are provided by the recycle streams from an ideal

separation subsequently to the reaction; in the last step (iii) the removal of all components along the reaction coordinate is included as well, which allows for positioning of separation steps.

In addition to the external mass and energy fluxes, a measure for the analysis of the internal reaction fluxes - the *differential selectivity* – is introduced (Eq. (3.11)). It enables the identification of reaction sections of beneficial back-mixing without taking the product dosing necessarily into account.

$$\varphi = \frac{moles\ of\ desired\ product\ formed}{moles\ of\ main\ reactant\ consumed} \tag{3.11}$$

It is a measure that brings the formation rate of the desired product in relation to the consumption rate of the reactant. This allows for identifying changes of the reaction orders of the deciding reactions for the formation of the desired product and, hence, its selectivity. The change of the differential selectivity over conversion of the main reactant or the reaction time indicates thereby whether back-mixing is beneficial for the production of the desired product or not [160]. Within the EPF concept this measure can be seen as an analysis of the internal differential reaction flux r_V of the fluid element. In case of recycling, sections of beneficial back-mixing might be also identifiable by product dosing and, thus, both indicators can be used and taken as validation.

At the end of step 1, one has determined the optimal dosing and removal fluxes, an optimal temperature profile, the profile of the differential reaction flux, and the evolution of the chemical component concentrations along the reaction coordinate.

Step 2: Sectioning of optimal flux profiles in characteristic sections

Once the dynamic optimization is carried out and the aforementioned optimal fluxes are determined, one has to subdivide the reaction coordinate of the process into specific sections of characteristic behavior. The following rules have to be complied with:

- The first section starts at $t = t_0$ and the last section ends at $t = t_f$. The sectioning should be carried out sequentially along the reaction coordinate from t_0 to t_f.
- At the beginning of the reaction coordinate an initial dosing takes place to adjust the optimal initial concentrations; since no reaction can take place without any reactant, this initialization section always appears, dosing either a reactant or a reversible product.
- Every new dosing of either reactant or product indicates a new section, both for initial dosing or distributed dosing.
- Removal fluxes are treated identically to dosing fluxes regarding the sectioning.
- A change of temperature between dynamic and constant behavior, and a discontinuity in the temperature profile indicate a new section. Temperature changes can indicate impacts of different phenomena, e.g. activation energies, chemical equilibria, solubilities, densities, etc.
- The differential selectivity is analyzed in form of its gradient over the reaction coordinate and should be intersected only at points of changing sign of its gradient.
- The concentration profiles of the chemical components are not subdivided individually. They should be used as assistance in case the other flux profiles are not unambiguous.
- A new section can start without new dosing of any component. It simply implies, that the reaction mixture from the previous section is the inlet mixture for the next section.

Following these rules for sectioning the flux profiles, one ends up with the maximum amount of possible reaction sections, since each characteristic change is considered. Translating these directly into a reactor-network might lead to very large network candidates. Thus, there is already a reduction potential in step two of the approach. By engineer's knowledge a reasonable negligence or merger of

reaction sections should be conducted, which leads to additional reactor-network candidates of less complexity.

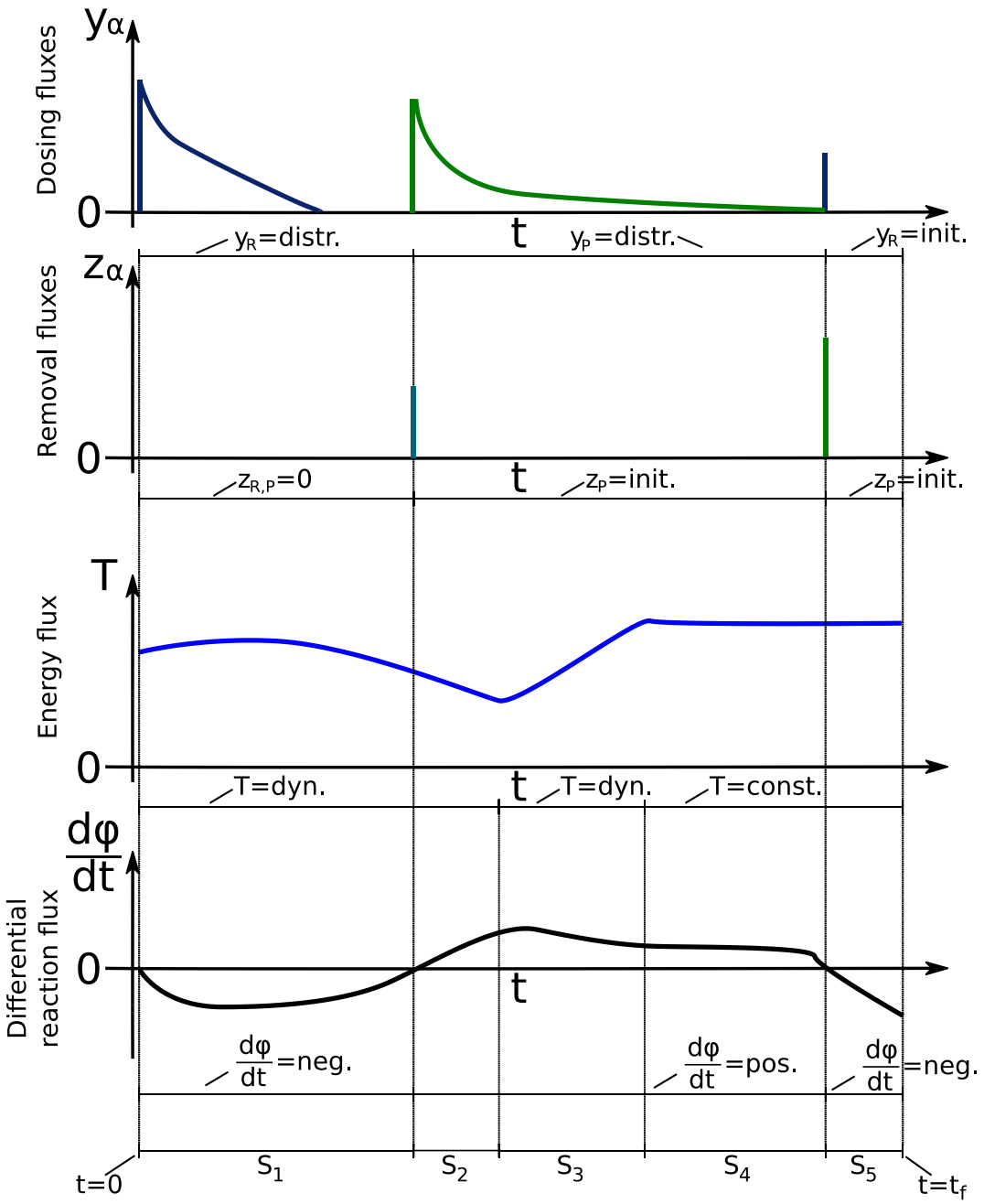

Figure 3.2: Exemplary illustration of sectioning of the time horizon of flux profiles. **y** – dosing flux density; **z** – removal flux density; **φ** – differential selectivity (see Eq. (3.11)); **R** – reactant (dark blue); **P** – product (green); distr. – distributed; init. – initial; dyn. – dynamic; const. – constant; neg – negative; pos – positive; S – section; t – time; t_f – final time.

Those might later be compared to the largest candidate to identify the impacts of the reductions. Potentials for these reductions arise, for instance, from:

- Simultaneous distributed dosing of different components, even when they are of different length or there starting points are slightly different, which can nevertheless be realized within one section of distributed dosing;
- Initial dosing of different components and simultaneous distributed dosing of one or more components, which again can be realized in one section of distributed dosing including an initial dosing;

- Initial dosing and removal of components, which can be realized in one section;
- Similar temperature control profiles of neighboring sections, which might be approximated by one control section; this is of special interest in case the differential selectivity change has the same sign in these sections;
- Several sections having distributed control profiles only intersected by small sections of constant temperature control, which can as well be realized within a larger distributed temperature control section;
- etc.

Depending on the specific process example further reductions might occur, e.g. in case a multiphase process provides additional degrees of freedom by supporting phases. Due to analyzing several fluxes simultaneously, numerous cases are possible. Thereby, certain characteristics might occur more often because they represent typical features of a certain problem class. For instance, dosing of side products at the beginning of a reaction occurs in case of a selectivity problem with chemical equilibrium limitations, or an almost constant temperature profile is accompanied by a positive change of the differential selectivity pointing on a realization in a continuous stirred tank reactor. An example of the sectioning of flux profiles is illustrated in Fig. 3.2 for arbitrary trajectories. Therein, the notation for the *flux profile analysis* is introduced.

Step 3: Association of characteristic flux profile sections to ideal reactor types as well as recycling and separation strategies

The subdivided sections of step 2, either of one or several different sectionings, are analyzed in step 3 regarding their characteristics. Subsequently, they are associated to generic ideal reactor types, recycling strategies, and separation strategies.

- Ideal reactor types: The dosing strategies of the reactants as well as the profile of the differential selectivity indicate the choice of a suitable ideal reactor type for a specific section. These are a plug flow reactor (PFR), a differential sidestream reactor (DSR), and a continuous stirred tank reactor (CSTR), which are discussed in detail in subchapter 3.2. The dosing of products gives additional hints on a possible benefit of back-mixing for the choice of an appropriate reactor.
- Recycling strategies: The dosing strategies of products indicate the best recycling strategy of those components from the separation subsequent to the reaction. The aforementioned ideal reactor types are therefore augmented by the possibilities of either initial recycling or distributed recycling. For the qualitative analysis of the process potential and the derivation of possible reactor-network candidates, the separation at the end of the process is assumed to work ideally, i.e. it has ideal, sharp split factors. How this is realized and how the size of the recycle streams might affect the synthesis result is discussed in subchapter 3.3.
- Separation strategies: The removal flux is analyzed to identify the best separation strategy. Again, ideal separations are assumed, which allow using any desired removal flux quality. The analysis of the removal flux includes two aspects: (i) the optimal number of removals within the reactor-network, and (ii) their location. How the removal streams are translated for the synthesis and how the number and the location of the removals are determined based on the dynamic optimization of the process is covered in subchapter 3.4.

In addition to the analysis of the dosing and removal fluxes as well as the differential selectivity as reaction flux, the temperature profile indicates the match to either a distributed or concentrated reactor

type. The spatially distributed reactors, PFR and DSR, can realize both kinds of temperature profile, whereby the concentrated CSTR is only able to realize a constant temperature profile.

Moreover, it has to be noted, that in case of reactant dosing the DSR can be approximated by a cascade of PFRs. In case of product recycling both the DSR and the PFR have the possibility to be approximated by a cascade of PFRs, and in addition by a cascade of CSTRs, which might enhance the beneficial impact of back-mixing. The decision-making depends strongly on the complexity of the dosing profiles of reactants and products. Anyway, these options should be included to generate additional reactor-network candidates. The actual decision can then be made depending on the final detailed process design and the corresponding objective.

The qualitative reactor synthesis approach is described in three successive levels starting from the case of synthesizing only reactor-networks up to the case of additional consideration of recycling and separation. On each level the generic ideal reactor types are extended according to the additional degrees of freedom in the reactor synthesis.

3.2 Reactor-network synthesis

In this subchapter the *flux profile analysis* approach is reduced for the application of reactor-network synthesis. Therefore, the generic ideal reactor types are discussed, which are used as basis for the subsequent subchapters, and the dynamic optimization problem is adapted. Aiming at a clearer understanding of the fluid element travelling through the process in terms of process engineering, a batch process scheme is derived as more intuitive substitute. It is stepwise augmented for the subsequent reactor synthesis levels. After laying the fundamentals, the qualitative reactor-network synthesis approach is applied first on a well-known literature example aiming at an evaluation of the presented approach by comparison with the attainable region approach, and second on the hydroformylation of 1-dodecene, which acts as main process example in this thesis as introduced in subchapter 2.3.

3.2.1 Fundamentals

The most fundamental kind of conceptual design of a chemical process is the synthesis of reactor-networks, since, as stated in the previous subchapter, the chemical reaction is the core of a chemical process. The different types of reactors included and combined in classical reactor-network synthesis approaches, such as attainable region approach and superstructure optimization (compare subchapter 2.2.1), are ideal reactors of which each represents certain important characteristic of mixing, see Fig. 3.3.

- Plug Flow Reactor (PFR): The PFR is free of back-mixing due to the plug flow characteristics. The reactants are fed only at the beginning of the reaction, i.e. the entry of the reactor, and no distributed reactant and product dosing is possible. The reaction progress takes place along the length of the PFR. Due to its spatial distribution the PFR is able to have a distributed control of e.g. temperature. A PFR is analogous to a standard batch reactor without dosing whereby the feed concentration of the PFR $\boldsymbol{c}_{feed}^{PFR}$ corresponds to the initial concentration of the batch $\boldsymbol{c}_{batch}(t = 0)$. Note, that the residence time τ_f in a PFR corresponds to the reaction time t_f in a batch reactor.
- Differential Sidestream Reactor (DSR): The DSR is similar to the PFR including the possibility to dose reactant along the reactor length, i.e. the reaction time in a batch process.
- Continuous Stirred Tank Reactor (CSTR): As opposite to the spatially distributed PFR and DSR, the CSTR is a concentrated system with total back-mixing and, thus, the reactor states are equal to its output states. Since it operates in steady-state, it has no transient behavior and

constant control inputs. Regarding the analogous batch process concept, one can imagine a fed-batch process with constant feed composition corresponding to the feed composition of the CSTR $\boldsymbol{c}_{feed}^{CSTR}$. The initial batch composition has to be sufficiently close to the outlet concentration of the CSTR $\boldsymbol{c}_{final}^{CSTR}$. Depending on the volumetric feed rate F_{batch} and the reactor volume V_{batch} a certain equilibrium composition will result corresponding to the steady-state CSTR composition for a certain residence time τ_{CSTR} [30].

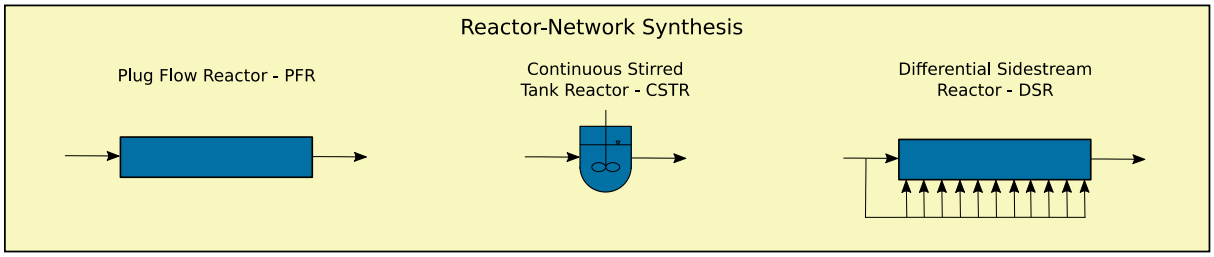

Figure 3.3: Generic ideal reactor types for reactor-network synthesis within the FPA approach

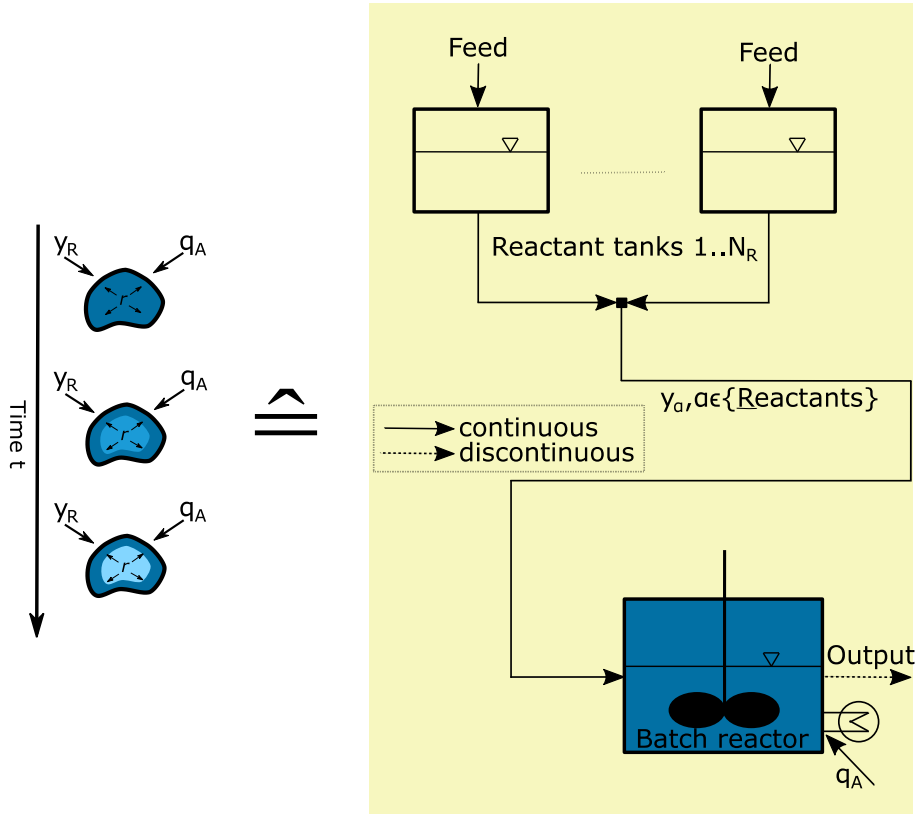

Figure 3.4: Translation of EPF fluid element into analogous batch process scheme in case of reactor-network synthesis

In reactor-network synthesis the CSTR has a special role due to its ability of back-mixing. On this level of synthesis, where no separating and recycling of products is considered, back-mixing is the only way to change the product amounts along the reaction coordinate. Albeit there exist numerous other special reactor types, the ideal reactors are sufficient to describe the main necessary reaction and mixing characteristics, which are important to identify the maximum potentials of a reaction in a continuous reactor-network. Other special reactor types either try to approximate their ideal features or focus with their special features on other phenomena, which are of minor importance for the conceptual process design and rather of interest for detailed design.

For a more intuitive understanding and as basis for the modeling of the fluid element and its fluxes, a process scheme is derived which collates all aforementioned features. The fluid element can be translated into a semi-batch reactor which is optimally controlled in time by (i) dosing of reactants and products, (ii) removal of chemical species, and (iii) a temperature profile. To realize the dosing streams, storage tanks for all chemical species are added to the process scheme. The removal streams, both intermediate and final, are realized in form of ideal separations, and the temperature control simply by adding a cooling/heating jacket to the semi-batch reactor unit. For reactor-network synthesis recycling or separating of products and side products are not considered and, thus, the aforementioned optimization framework is reduced by dosing fluxes of non-reactant components and by all removal fluxes. As a result, only the dosing of reactants and the temperature control are considered. The resulting batch process scheme for reactor-network synthesis is given in Fig. 3.4.

For the purpose of reactor-network synthesis combining the three generic ideal reactor types PFR, DSR, and CSTR, the resulting dynamic optimization problem reads:

$$\min_{\boldsymbol{u}(t),\boldsymbol{\xi}} \left(\int_0^{t_f} L(t)dt + I(\boldsymbol{\rho}_0) + W\left(\boldsymbol{\rho}_f\right) \right) \tag{3.12}$$

$$\text{s.t. } \frac{d\boldsymbol{\rho}}{dt} = \boldsymbol{j} + \boldsymbol{y} + \boldsymbol{M} \cdot \boldsymbol{N} \cdot \boldsymbol{r}_V \tag{3.13}$$

$$\frac{d\boldsymbol{\rho}_{st}}{dt} = -\boldsymbol{y} \tag{3.14}$$

$$\boldsymbol{g}(\boldsymbol{\rho}) = 0, \boldsymbol{h}(\boldsymbol{\rho}) \leq 0 \tag{3.15}$$

$$\boldsymbol{u}^L \leq \boldsymbol{u}(t) \leq \boldsymbol{u}^U \tag{3.16}$$

$$\boldsymbol{\xi}^L \leq \boldsymbol{\xi} \leq \boldsymbol{\xi}^U \tag{3.17}$$

$$\boldsymbol{u}(t) = [\boldsymbol{j}(t), \boldsymbol{y}(t), T(t)] \tag{3.18}$$

$$\boldsymbol{\xi} = [t_f] \tag{3.19}$$

$$\boldsymbol{y}(t) \geq 0, \quad \alpha \in \{reactants\} \tag{3.20}$$

$$\boldsymbol{y}(t) = 0, \quad \alpha \in \{products\} \tag{3.21}$$

$$\boldsymbol{\rho}(t=0) = \boldsymbol{\rho}_0 = \boldsymbol{0}, \boldsymbol{\rho}\left(t=t_f\right) = \boldsymbol{\rho}_f, \boldsymbol{\rho}_{st}\left(t=t_f\right) = \boldsymbol{\rho}_{st}^f \tag{3.22}$$

$$\boldsymbol{\rho}_{st}(t=0) = \boldsymbol{\rho}_{st}^0 = \begin{cases} \rho_{\alpha,st}^0, & \alpha \in \{reactants\} \\ 0, & \alpha \in \{products\} \end{cases} \tag{3.23}$$

$$\int_0^{t_f} \boldsymbol{y}(t)\, dt \geq \rho_\alpha^{min}, \quad \alpha \in \{reactants\}. \tag{3.24}$$

The modeling of this batch process, which replaces the fluid element concept, requires a balancing of the storage tanks (Eq. (3.14)), initial conditions of the storage tanks (Eq. (3.23)), and a constraint in the resulting dynamic optimization problem to ensure that a minimum amount of main reactant is dosed (Eq. (3.24)). As a result of this dynamic optimization problem, one obtains the optimal temperature profile, the optimal dosing of reactants along the reaction coordinate, and the optimal final reaction time. The latter is always optimized in addition to the dosing fluxes and temperature. It is either bounded reasonably taking the general speed of reaction into account or bounded intrinsically by the objective, e.g. choosing the space-time yield.

3.2.2 Comparison to attainable region approach for the modified van-de-Vusse reaction

Following the previously described procedure, one obtains a rational selection of reactor-network candidates for the investigated process. To evaluate the results gained by the presented qualitative reactor synthesis approach on the stage of reactor-network synthesis, a comparison with the results of the attainable region approach for a well-known literature example, namely the modified

van-de-Vusse reaction, is carried out. Therefore, the FPA is applied to generate optimal reactor-network candidates and it is shown, how it can be used to construct the AR of the process.

The classical van-de-Vusse reaction combines a parallel and a consecutive reaction in one scheme implying a selectivity problem for the intermediate species. The modified reaction contains an additional reverse reaction from this intermediate species back to the main reactant. The resulting reaction scheme is:

$$A \underset{r_2}{\overset{r_1}{\rightleftharpoons}} B \overset{r_3}{\rightarrow} C$$

$$2A \overset{r_4}{\rightarrow} D$$

Scheme 3.1: Modified van-de-Vusse reaction

This process was considered for attainable region analysis in literature by e.g. Metzger et al. [161] and Burri et al. [162]. Metzger et al. [161] chose the classical way of simulating the ideal reactor types from the starting point to first compare the performances and then construct the AR step by step by further simulations from suitable chosen points of the best performing reactor type. This is closely related to the classical AR idea of graphical analysis and construction of the AR, which is, however, limited to low-dimensional examples. Burri et al. [162] applied the IDEAS framework using Linear Programming to determine the AR. Both achieved the same attainable region for the given process. For the sake of comparability, the same model equations and model parameter as given in the two aforementioned literature sources are used in the following analysis.

Model formulation and optimization problem

In light of the presented synthesis approach only the balance equations of the batch reactor are used corresponding to those of the PFR in the literature sources. The algebraic equations for the CSTR in the literature model are dispensable due to the consideration of a Lagrangian fluid element in the EPF framework. The generic formulation in the previous subchapter is reduced by the degree of freedom of distributed reactant dosing, as it is in the literature example. In AR construction the distributed dosing of components is not beneficial for 2-dimensional problems, i.e. the number of independent reactions is smaller than three [163]. Based on this reduction, the storage tanks are neglected. Furthermore, the amounts of moles and the reactor volume are combined to concentrations, because the example gives no option to calculate the volumetric changes from molar changes. The reaction kinetics is based on simple power laws. The model equations read:

$$\frac{dc_A}{dt} = -k_1 c_A + k_2 c_B - k_4 c_A^2 \tag{3.25}$$

$$\frac{dc_B}{dt} = k_1 c_A - k_2 c_B - k_3 c_B \tag{3.26}$$

$$\frac{dc_C}{dt} = k_3 c_B \tag{3.27}$$

$$\frac{dc_D}{dt} = k_4 c_A^2 \tag{3.28}$$

with $k_i, i \in \{reactions\}$ as reaction coefficients and $c_\alpha, \alpha \in \{components\}$ are the component concentrations. Parameters and initial conditions are adopted from the aforementioned literature

sources with $k_1 = 0.01\ \mathrm{s}^{-1}$, $k_2 = 5\ \mathrm{s}^{-1}$, $k_3 = 10\ \mathrm{s}^{-1}$, $k_4 = 0.01\ \mathrm{m^3 kmol^{-1} s^{-1}}$ and $c_A^0 = 1$, $c_B^0 = c_C^0 = c_D^0 = 0$, respectively [161,162]. The resulting optimization problem for the *flux profile analysis* is stated as follows:

$$\max_{t_f} \ c_B(t_f) \tag{3.29}$$

s.t. Component mass balances: Eqs. (3.25)-(3.28) (3.30)

Path constraints: $\boldsymbol{c}(t) \geq 0$ (3.31)

Initial conditions: $\boldsymbol{c}(0) = [1, 0, 0, 0]$ (3.32)

Differential selectivity: $\varphi = \frac{r_1 - r_2 - r_3}{r_1 + r_4}$. (3.33)

Results of flux profile analysis

The dynamic optimization aims at maximizing the concentration of the intermediate component B. The example does not consider a temperature dependence and, thus, the temperature profile is not part of its analysis. As mentioned before, the distributed reactant dosing is neglected, too. Hence, the focus lies on the differential reaction flux $d\varphi/dt$. The result of the corresponding dynamic optimization (Eqs. (3.29)-(3.33)) is depicted in Fig. 3.5.

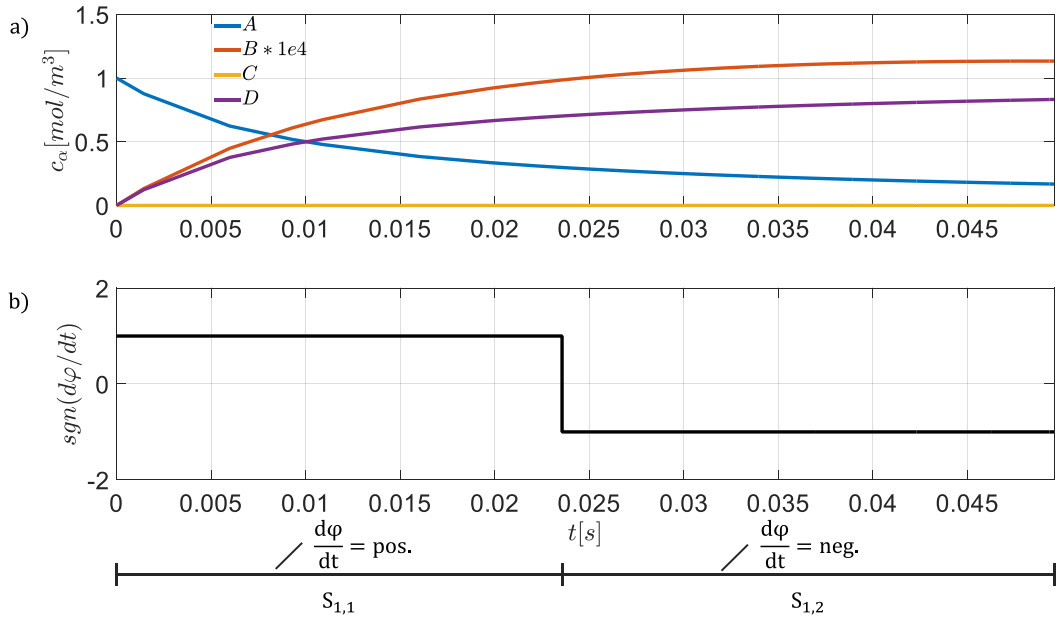

Figure 3.5: Results of the dynamic optimization of the modified van-de-Vusse reaction: a) Reaction progress; b) Differential reaction flux

The resulting flux profile is subdivided in two sections:

- The first section $S_{1,1}$ has a positive differential reaction flux indicating a back-mixing benefit and, thus, is associated with a CSTR.
- The second section $S_{1,2}$ has a negative differential reaction flux indicating a benefit by plug flow behavior. As there is no further dosing and temperature control, the best association for this section is a PFR.

The optimal concentration of B achieved in the optimization is $c_B^* = 1.13 \cdot 10^{-4}\ \mathrm{kmol/m^3}$. Note, that this is the optimum using only a PFR, which corresponds to the Lagrangian description used for the optimization. The mixing benefit from the use of a CSTR in the first reaction section takes effect when optimizing the derived optimal reactor-network consisting of a CSTR and a PFR. This leads to an optimum at $c_B^* = 1.24 \cdot 10^{-4}\ \mathrm{kmol/m^3}$, which is in accordance to literature [161,162].

In a second step, the same approach is used to construct the AR of the process. For this purpose, the differential reaction flux is included in the dynamic optimization to switch between the balance equation for the PFR and the CSTR, see Eq. (3.34). This is possible since a simultaneous optimization framework on a discretized time horizon is used (see subchapter A.7). Therein, the numerical solver can choose between the balance equation of the PFR and the back-mixed CSTR depending on the calculated differential reaction flux on every discretized element in each iteration of the dynamic optimization. This can be seen as a kind of automation of the analysis of the differential reaction flux, instead of the graphical analysis introduced before. The dosing, removal, and temperature control are independent of this.

$$\boldsymbol{c}(t_i) = \begin{cases} \boldsymbol{c}(t_{i-1}) + \frac{d\boldsymbol{c}}{dt_i}\ ,\ if\ \frac{d\varphi}{dt_i} < 0 \\ \boldsymbol{c}(t_{i-1}) + \tau \cdot \boldsymbol{N} \cdot \boldsymbol{r}(\boldsymbol{c}(t_i)),\ if\ \frac{d\varphi}{dt_i} > 0 \end{cases} \quad \forall i \in \{discretized\ elements\} \tag{3.34}$$

The AR of this example is constructed in the $[c_A, c_B]$-space, such as introduced in literature [161,162]. To use the presented dynamic optimization framework for AR construction, the optimization aiming at maximum c_B is carried out for different specified final values c_A^f. The resulting dynamic optimization problem is therefore extended by the terminal constraint $c_A(t_f) = c_A^f$, and the switching condition (Eq. (3.34)). The results of several runs of this optimization for scanning c_A^f from 0 to 1 are shown in Fig. 3.6 (red, dashed line). The dynamic optimization based results indicate as shown before the use of a CSTR and a subsequent PFR as optimal reactor-network to reach the optimal point with highest concentration c_B^f. However, the hull of the AR is not convex in the range of $0.4 \leq c_A \leq 1$. In the classical AR approach those concave regions can be closed by mixing of streams from different points of the AR. In the here developed FPA approach it can be identified by optimal dosing of components, e.g. inlet stream along the reaction coordinate. Since this was neglected, the concept of dosing has to be reduced to bypassing only, to find at least benefits from mixing reactor inlet and outlet streams. This is realized by changing the definition of the final values of the concentrations in the dynamic optimization problem (Eqs. (3.35)-(3.36)). The objective function is changed to:

$$\max_{t_f, \varepsilon} c_B^f = \varepsilon c_B(t_f) + (1 - \varepsilon) c_B(0), \tag{3.35}$$

and the terminal constraint defining the final value of A is replaced by:

$$c_A^f = \varepsilon c_A(t_f) + (1 - \varepsilon) c_A(0), \tag{3.36}$$

whereby $\varepsilon\ \epsilon\ [0,1]$ is a mixing factor deciding about the mixing fractions of inlet and outlet stream. The calculation of the AR, considering these modifications and the same procedure as stated before, leads to the blue, solid line in Fig. 3.6 which matches exactly the results from literature [161,162].

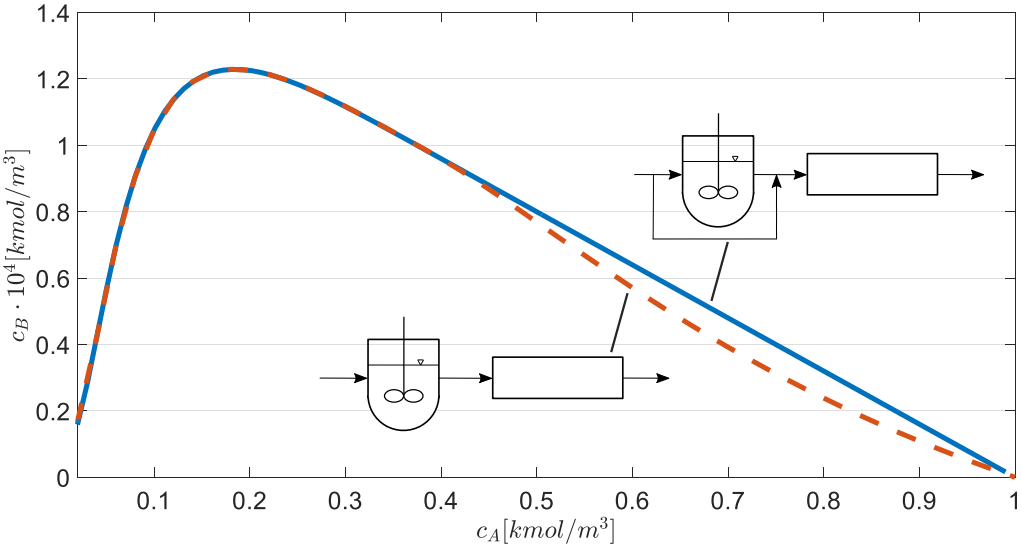

Figure 3.6: Attainable region constructed by the presented reactor-network synthesis approach without bypass mixing (red, dashed line) and with by-pass mixing (blue, solid line)

Discussion

The comparison of the *flux profile analysis* and the attainable region approach for reactor-network synthesis revealed that the main difference and possible advantage of a dynamic optimization approach is the direct determining of an optimal process design. While the AR approach determines the whole region of attainable states, i.e. concentrations, the FPA seeks for a particular optimal design consisting of the optimal reactor-network and its control by heat and mass fluxes. This allows on the one hand for a direct translation into candidates for optimal continuous reactor-networks and on the other hand for a direct adaptation of the results for an optimal control strategy of a batch process. Since the FPA is not tailored to construct the AR of a process, several adaptations have to be made to use it for this purpose, e.g. the transformation to the concentration space. The construction of an attainable region with the *flux profile analysis* is possible by solving a series of dynamic optimizations to determine the convex hull of the corresponding AR. The simultaneous inclusion of the proposed bypass modification is used for the case that the concave part of the AR is already identified and is supposed to be closed. Theoretically, this degree of freedom can be included for all finite elements within the discretized dynamic optimization, but the computational cost increases significantly for high number of elements. It is rather recommended to conduct this part of the AR construction either when the knowledge of the concave regions is already available, or by reaching the points of the convex hull by mixing of available streams within the AR corresponding to the classical graphical construction. For higher dimensional problems ($n \geq 3$), the computational effort for constructing the AR with the presented dynamic optimization based approach might be larger in comparison to state-of-the-art approaches, which are tailored for this purpose. For these cases, Feinberg [163] and Hillestad [47,48] demonstrated how the distributed dosing in a DSR can be introduced to the construction of an AR and a corresponding dynamic optimization problem, respectively.

The systematic generation approach of Hillestad [47,48] derives ideal reactor-networks as well from analyzing the results of optimal control calculations. The beneficial mixing for each reaction section is evaluated using a dimensionless dispersion coefficient, which is calculated along the reaction path, similar to the differential selectivity used in the presented approach. The differences of the FPA originate from the notion and description of the fluid element and the formulation within the EPF framework. Since the systematic generation approach of Hillestad [47,48] is derived within the

same clear mathematical description as the AR approach, it is assumed that the presented results would be in accordance with results achieved by applying this procedure.

3.2.3 Reactor-network synthesis for hydroformylation of 1-dodecene

In the previous section it was demonstrated, how the *flux profile analysis* is linked to the attainable region approach, and it was successfully applied to a reaction network which stands exemplarily for numerous real processes. For the sake of comparability, no temperature control and distributed reactant dosing was enabled. In the following, the *flux profile analysis* is applied on the hydroformylation of 1-dodecene aiming at the synthesis of reactor-network candidates, whereby both the temperature control and the distributed dosing of reactant 1-dodecene are enabled. Furthermore, the optimal distributed control of syngas partial pressures is activated, since the hydroformylation is a gas-liquid multiphase process, which requires gaseous components for the desired reaction to take place.

Model formulation and optimization problem

The hydroformylation reaction network is illustrated in Fig. 2.10 and the corresponding reaction rates are given in Eqs. (2.1)-(2.7). It is assumed that the mass transfer from gas to liquid is not limiting and, thus, the gas concentrations in the liquid phase are always at their equilibrium concentrations, which are calculated based on the corresponding partial pressures of the gaseous reactants, H_2 and CO, according to Eq. (2.11). Based on this assumption, the partial pressures of H_2 and CO are not balanced individually and instead directly optimized as decision variables. The component mass balance for the liquid phase components (Eq. (3.37)), i.e. the hydrocarbons (CH), is derived in terms of moles from the generic mass balance in Eq. (3.13). In such a case that the balanced states are extensive, e.g. amount of moles or masses, it is reasonable to directly optimize the corresponding flux instead of its flux density, because then the volumes can be determined independently. Therefore, the molar flux density vector $\boldsymbol{y}^m$ is replaced by the molar flux vector $\boldsymbol{y}_V^m = \boldsymbol{y}^m \cdot V_{flux}$. This adaptation will be used for all following modeling within the FPA approach throughout the work. The solvents (SOL) and gases (GAS) in the liquid phase are not balanced, since they are treated as inert for the reaction.

$$\frac{dn_\alpha}{dt} = V_{liq}\left(j_\alpha^m + c_{cat} M_{cat}\left(\sum_{m=1}^{M} \nu_{\alpha,m} r_m\right)\right) + y_{V,\alpha}^m, \quad \alpha \in CH \tag{3.37}$$

The changes of amount of moles n_α in Eq. (3.37) are defined by the volume of the liquid phase V_{liq} calculated via Eq. (3.38), the molar diffusion fluxes j_α^m which are zero due to the assumption that no hydrocarbons can move across the border of the fluid element, the molar mass fluxes y_α^m which are degrees of freedom according to the chosen synthesis purpose, the stoichiometric coefficients $\nu_{\alpha,m}$ of the hydroformylation reaction, and the reaction rates r_m. Because the latter are defined in dimensions $\mathrm{mol\,ml^{-1}g_{cat}^{-1}}$, the reaction rates are multiplied with the concentration c_{cat} and molar mass M_{cat} of the homogeneous catalyst.

$$V_{liq} = \sum_{\alpha \in COM} \frac{n_\alpha M_\alpha}{\rho_\alpha} \tag{3.38}$$

For the calculation of V_{liq} in Eq. (3.38) the molar masses M_α (Tab. A.4) and the mass densities ρ_α (Eq. (3.39)) of all chemical components (COM) are included. The coefficients in Eq. (3.39) are given in Tab. A.4.

$$\rho_\alpha = a_{\rho,0,\alpha} + a_{\rho,1,\alpha} T, \quad \alpha \in COM \tag{3.39}$$

In addition, the storage tanks introduced in Fig. 3.4 are balanced according to Eq. (3.40).

$$\frac{dn_{a,st}}{dt} = \begin{cases} -y_{V,a}^{m}(t), & \alpha \in \{nC12en\} \\ 0, & \alpha \in \{CH/nC12en\} \end{cases} \tag{3.40}$$

Based on this model formulation and the corresponding assumptions, the dynamic optimization problem can be derived. Because of the arising selectivity problem with respect to the desired linear aldehyde, the objective for the reactor-network synthesis is chosen to be the selectivity with respect to n-tridecanal (nC13al). The synthesis is exemplarily carried out for a predefined conversion of the main reactant 1-dodecene (nC12en) of 99 % (Eq. (3.54)) and a constraint is added which ensures a high ratio of linear to branched aldehydes (n/iso) (Eq. (3.56)). The first is chosen in order to find the best performance at high use of reactant and the latter to avoid high formation of branched aldehydes, which are very hard to separate from the preferred linear product. The final time is exemplarily set an upper limit of 100 min. Together with the aforementioned degrees of freedom, the resulting dynamic optimization problem reads:

$$\max_{T(t),y_{V,nC12en}^{m}(t),p_{CO}(t),p_{H_2}(t),t_f} \quad S_{nC13al}(t_f) \tag{3.41}$$

s.t.	Component mass balances:	Eq. (3.37)	(3.42)
	Storage mass balances:	Eq. (3.40)	(3.43)
	Reaction kinetics:	Eqs. (2.2)-(2.7)	(3.44)
	Catalyst equilibrium:	Eq. (2.1)	(3.45)
	Constitutive equations:	Eqs. (3.38)-(3.39)	(3.46)
	Gas solubilities:	Eq. (2.11)	(3.47)
	Catalyst and solvent ratios:	Eqs. (2.13)-(2.14)	(3.48)
	Dosing constraint:	$\int_0^{t_f} y_{V,nC12en}^{m}(t)\,dt \geq n_{nC12en}^{min}$	(3.49)
	Path constraints:	$\boldsymbol{n}(t) \geq 0, \boldsymbol{n}_{st}(t) \geq 0$	(3.50)
		$y_{V,\alpha}^{m}(t) = 0, \alpha \in \{CH/nC12en\}$	(3.51)
		$y_{V,nC12en}^{m}(t) \geq 0$	(3.52)
		$10\ \text{bar} \leq p_{tot}(t) = p_{CO}(t) + p_{H_2}(t) \leq 20\ \text{bar}$	(3.53)
		$363.15\ \text{K} \leq T(t) \leq 388.15\ \text{K}$	(3.54)
	Terminal constraints:	$t_f \leq 100\ \text{min}$	(3.55)
		$X_{nC12en} = \frac{n_{nC12en}(0) - n_{nC12en}(t_f)}{n_{nC12en}(0)} = 99\ \%$	(3.56)
		$S_{nC13al} = \frac{n_{nC13al}(t_f) - n_{nC13al}(0)}{n_{nC12en}(0) - n_{nC12en}(t_f)}$	(3.57)
		$n/iso = \frac{n_{nC13al}(t_f)}{n_{nC13al}(t_f) + n_{iC13al}(t_f)} \geq 95\ \%$	(3.58)
	Initial conditions:	$\boldsymbol{n}(t=0) = \boldsymbol{n}_0 = \boldsymbol{0}$	(3.59)
		$\boldsymbol{n}_{st}(t=0) = \boldsymbol{n}_{st,0} = \boldsymbol{1}$	(3.60)
	Differential selectivity:	$\varphi = \frac{r_1}{r_1 + r_2 + r_3 + r_6}$.	(3.61)

Results of flux profile analysis

The first step of the FPA is to solve the dynamic optimization problem above aiming at the flux profiles for the reactant dosing, the temperature, and the differential reaction flux. In addition, the

control of the gas partial pressures of H_2 and CO arise, which are treated similar to the temperature as a control variable and not as an individual reactant dosing, because their characteristics are not informative regarding the beneficial mixing behavior but for decision-making about distributed, initial, or constant control of the corresponding reaction section.

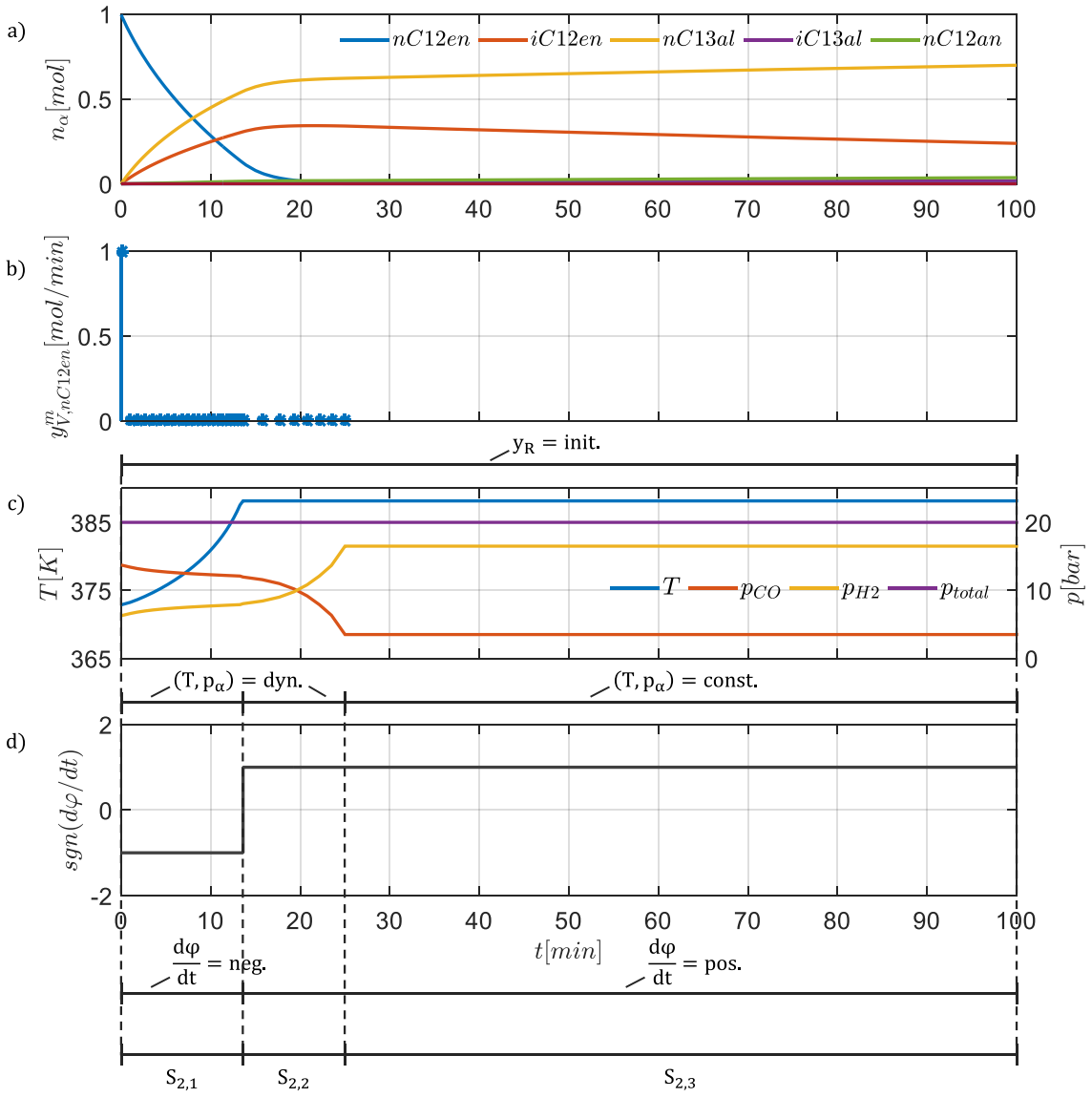

Figure 3.7: Results of the dynamic optimization of the hydroformylation of 1-dodecene for reactor-network synthesis: a) Reaction progress in moles; b) Reactant dosing flux profile; c) Control flux profiles; d) Differential reaction flux

Therefore, the partial pressure profiles are drawn together with the temperature profile in one plot. The results of the dynamic optimization problem in Eqs. (3.41)-(3.61) are shown in Fig. 3.7. Analyzing the course of the flux profiles and subdividing them into characteristic sections is step two of the FPA. Following the rules introduced in subchapter 3.1.3, one obtains a maximum of three sections as illustrated in Fig. 3.7. They are analyzed and associated with appropriate reactor types in the following:

- In the first section $S_{2,1}$ an initial dosing of the reactant takes place, the temperature shows an increasing and, thus, dynamic characteristic, the partial pressure indicates a dynamic profile as well, and the differential reaction flux is negative. Due to its dynamic control and negative

differential reaction flux it is best realized with a PFR. Although the liquid reactant dosing is only initial, the dynamic partial pressures require a distributed dosing of gaseous reactants.

- In the subsequent section $S_{2,2}$ no dosing appears, the temperature profile is constant, the partial pressures are still dynamic, and the differential reaction flux has changed to positive. The latter indicates a benefit from back-mixing and, thus, a CSTR, in which also the constant temperature profile can be realized. But the dynamic partial pressure profiles need a distributed dosing or a cascade of reactors, which allows to approximate the dynamic profiles. Therefore, this section can be approximated by a cascade of CSTRs.
- Finally, the last section $S_{2,3}$ has no dosing, constant temperature and partial pressure profiles, and a positive differential reaction flux. With these characteristics it is predestined to be realized in a single CSTR.

This leads to an optimal reactor-network of a PFR with distributed gas dosing followed by a cascade of CSTRs. As discussed in subchapter 3.1.3 it is worthwhile to analyze the network for possible reduction potentials. One can see, that the second section might also be merged either with the first section neglecting the back-mixing benefit, or with the third section neglecting its dynamic partial pressure profiles. Both mergers would lead to an alternative reactor-network of only two units, a PFR with distributed gas dosing and a CSTR. The maximal reactor-network, in which the number of CSTRs in the cascade is set to three, and the reduced reactor-network are illustrated in Fig. 3.8 c) and b), respectively. To quantify the potentials of both candidates, they are evaluated in the $[S_{nC13al}, X_{nC12en}]$-space. With this analysis, the potentials of the derived reactor-network candidates are quantified for other conversions, too. As reference case, a single DSR (Fig. 3.8 a)) is investigated, since it is the direct continuous analog to the underlying semi-batch reactor process and, thus, the EPF fluid element.

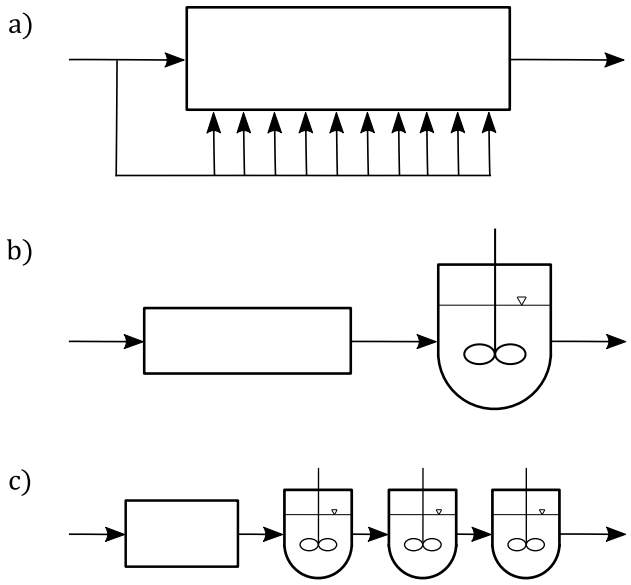

Figure 3.8: Reactor-network candidates for the hydroformylation of 1-dodecene

The results of the evaluation of the three derived reactor-network candidates in Fig. 3.9 indicate that the addition of a back-mixed reaction section in form of a CSTR to the PFR with distributed gas dosing is beneficial, especially for conversions between 90 % and 99 % (red line). At the conversion point chosen for the *flux profile analysis* ($X_{nC12en} = 99\,\%$) a selectivity enhancement of 3 % is achieved in comparison to the single DSR (blue line). The further addition of CSTRs in form of a

cascade (yellow line) has no significant benefit. The PFR+CSTR network is, thus, the most promising candidate for a further detailed design showing the best performance in the $[S_{nC13al}, X_{nC12en}]$-space.

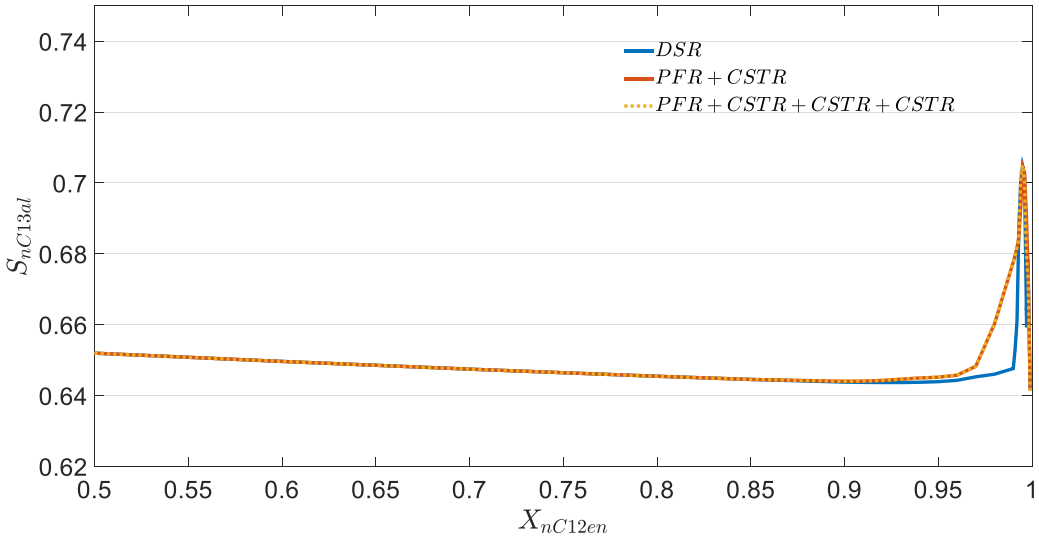

Figure 3.9: Evaluation of the reactor-network candidates from Fig. 3.8 in the $[S_{nC13al}, X_{nC12en}]$-space

3.3 Reactor-recycle-network synthesis

The next level of synthesis is the reactor-network synthesis with recycling. It corresponds to the flux profile analysis enabling the dosing of reactants and products, whereby recycling provides the latter. Therefore, a separation has to be assumed after the reaction takes place. To allow for recycling of pure species the separation has to have ideal splits. The fundamentals of the FPA in subchapter 3.2.1 are extended for the case of additional product dosing with respect to the dynamic optimization problem, the underlying batch process scheme, and the ideal units, which are supposed to be associated to the characteristic flux profile sections. In the first step, the FPA for reactor-recycle-network synthesis is applied again on a literature example. This time the focus lies on its comparison to typical superstructure optimization approaches as second state-of-the-art method for reactor synthesis. Subsequently, the hydroformylation process of 1-dodecene in a TMS system is considered and optimal candidates for reactor-recycle-networks are derived via FPA.

3.3.1 Fundamentals

The additionally considered recycling of components allows for including product dosing into the optimization and its corresponding batch process scheme. The previous scheme for reactor-network synthesis (Fig. 3.4) is extended by an ideal separation and storage tanks for products, see Fig. 3.10. The ideal separation is assumed to work instantaneously and refills the product storage tanks to the same level as they were before the reaction started. This extension intends to ensure, that the amounts of products that are considered to evaluate the process performance are not originated from the storage tanks but only from the reaction progress. Furthermore, it ensures that the amounts of products dosed to the process are collected after the process and are - virtually - available for the next batch run. Hence, the products are only added in order to analyze the reaction characteristics. The resulting dynamic optimization problem is stated in Eqs. (3.62)-(3.74).

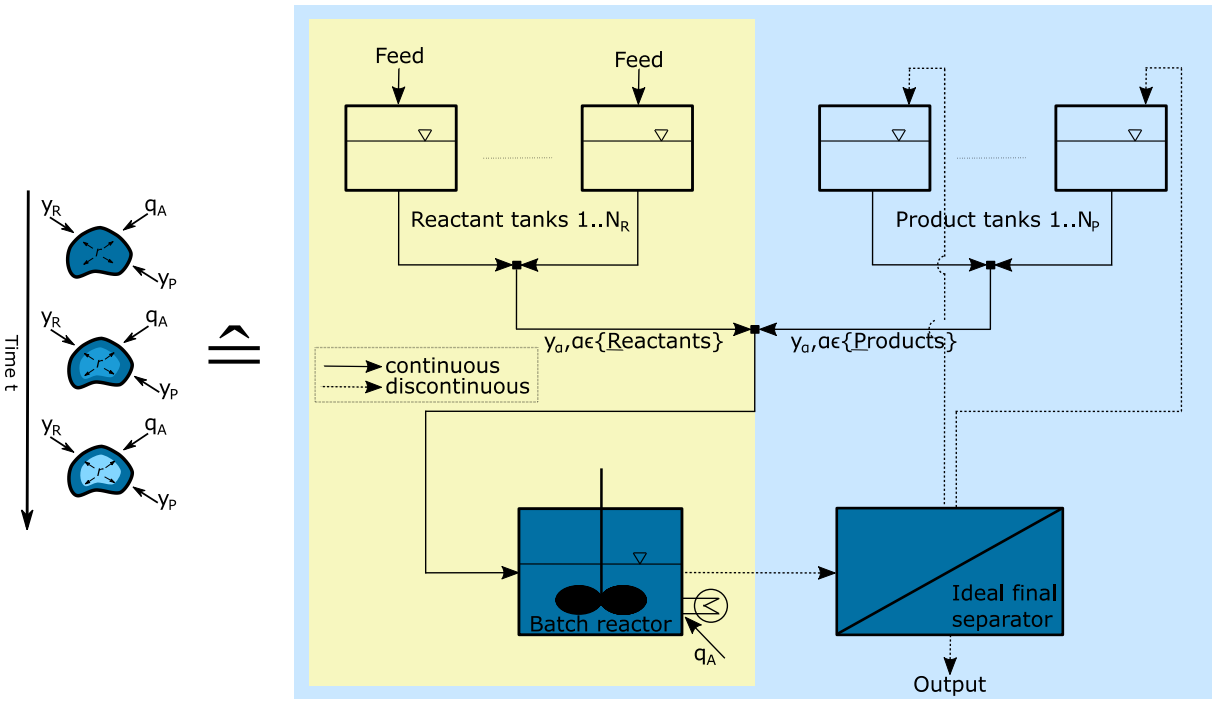

Figure 3.10: Translation of EPF fluid element into analogous batch process scheme in case of reactor-recycle-network synthesis

$$\min_{\boldsymbol{u}(t),\boldsymbol{\xi}} \left(\int_0^{t_f} L(t)dt + I(\boldsymbol{\rho}_0) + E(\boldsymbol{\rho}_f) \right) \tag{3.62}$$

$$\text{s.t.} \quad \frac{d\boldsymbol{\rho}}{dt} = \boldsymbol{j} + \boldsymbol{y} + \boldsymbol{M} \cdot \boldsymbol{N} \cdot \boldsymbol{r}_V \tag{3.63}$$

$$\frac{d\boldsymbol{\rho}_{st}}{dt} = -\boldsymbol{y} \tag{3.64}$$

$$\boldsymbol{g}(\boldsymbol{\rho}) = 0, \boldsymbol{h}(\boldsymbol{\rho}) \leq 0 \tag{3.65}$$

$$\boldsymbol{u}^L \leq \boldsymbol{u}(t) \leq \boldsymbol{u}^U \tag{3.66}$$

$$\boldsymbol{\xi}^L \leq \boldsymbol{\xi} \leq \boldsymbol{\xi}^U \tag{3.67}$$

$$\boldsymbol{u}(t) = [\boldsymbol{j}(t), \boldsymbol{y}(t), T(t)] \tag{3.68}$$

$$\boldsymbol{\xi} = [t_f] \tag{3.69}$$

$$\boldsymbol{y}(t) \geq 0 \tag{3.70}$$

$$\boldsymbol{\rho}(t=0) = \boldsymbol{\rho}_0 = \boldsymbol{0} \tag{3.71}$$

$$\boldsymbol{\rho}_f = \begin{cases} \rho_\alpha(t_f), & \alpha \in \{reactants\} \\ \rho_\alpha(t_f) - \int_0^{t_f} y_\alpha(t)\, dt, & \alpha \in \{products\} \end{cases} \tag{3.72}$$

$$\boldsymbol{\rho}_{st}(t=0) = \boldsymbol{\rho}_{st}^0, \boldsymbol{\rho}_{st}(t=t_f) = \boldsymbol{\rho}_{st}^f \tag{3.73}$$

$$\int_0^{t_f} \boldsymbol{y}(t)\, dt \geq \begin{cases} \rho_\alpha^{min}, & \alpha \in \{reactants\} \\ 0, & \alpha \in \{products\} \end{cases}. \tag{3.74}$$

In comparison to the DOP in subchapter 3.2.1 it is augmented by constraints for handling the additional product streams. With Eq. (3.72) the correct product streams for performance evaluation are determined and Eq. (3.73) defines the filling levels of the product storage tanks. In addition, the dosing fluxes are enabled for products in Eq. (3.70) and Eq. (3.74) as well. The filling levels have an important role in carrying out the analysis, since depending on their predefined values the reactor synthesis obtains different results. Thereby, the resulting maximum possible ratios of particular products to the main reactant are crucial. They decide about the possible scale of the recycle streams

and the possible dilution of reactants. To evaluate the impact of these filling levels, a sensitivity analysis is recommended. Especially in the case that a component is completely dosed along the reaction coordinate and, thus, limited by its predefined filling level. In the following examples (subchapters 3.3.2 and 3.3.3) it is demonstrated exemplarily, how such an analysis might be conducted.

In contrast to the reactor-network synthesis, the additional product dosing on this level allows for attaining a significantly larger part of the composition space at each point along the reaction coordinate. On the former level only back-mixing as a form of internal recycling is available. On the level of reactor-recycle-network synthesis the recycling of products allows for adjusting the optimal composition along the reaction coordinate more accurately. Thereby, the recycling can be of two different kinds: (i) a recycle from the end of the reaction to the beginning of a section which is called *initial recycling* (IR) and (ii) an intermediate recycle along the reaction coordinate which is called *distributed recycling* (DR). In case scenario (i) occurs in the first reaction section it is called a global recycle. The set of ideal process units introduced in Fig. 3.3 in subchapter 3.2.1 is, therefore, augmented by generic ideal process units with recycling, see Fig. 3.11.

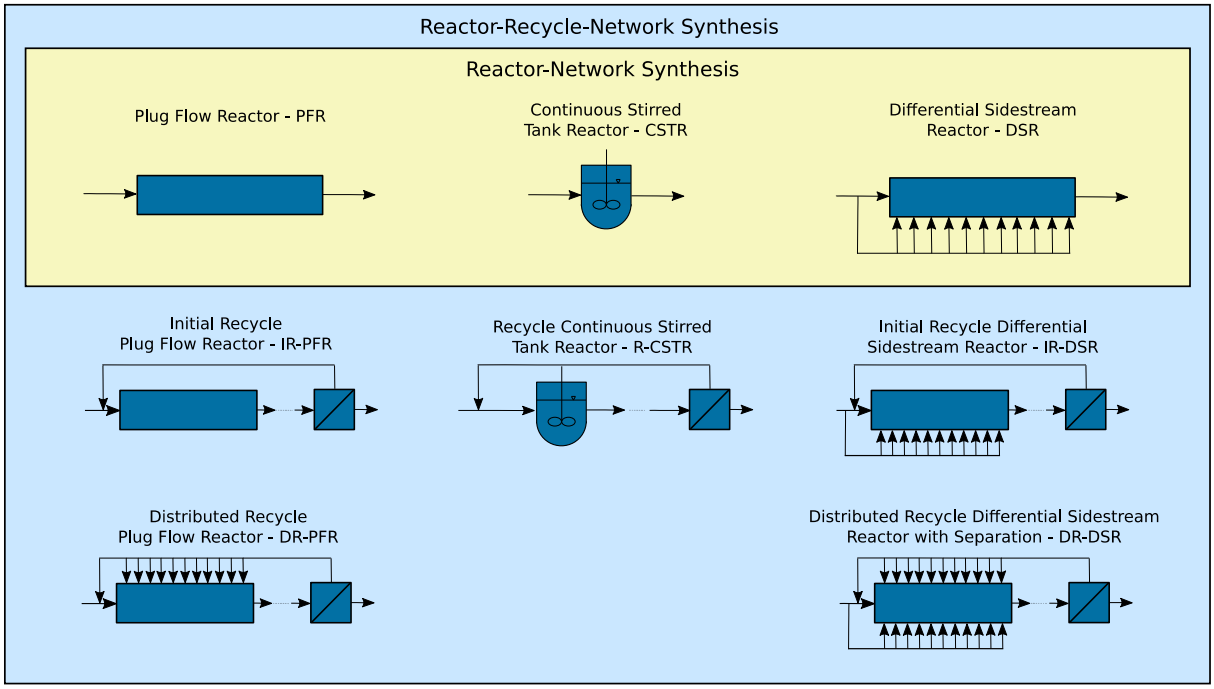

Figure 3.11: Generic ideal process units for reactor-recycle-network synthesis within the FPA framework

Due to the potential gained by the additional product dosing, the result of the dynamic optimization cannot be enhanced by sectioning in back-mixed and plug flow sections. It represents already the maximum potential of the reaction by dosing of reactants and products and can be realized in a DR-DSR. The only limitation might arise by the amount of species provided for dosing, i.e. the filling levels of the product storage tanks. However, this is considered within a sensitivity analysis as mentioned above. The target of the FPA on the level of reactor-recycle-network synthesis is, thus, not to find a reactor-network which is better than a single unit with distributed control. Instead, the maximum potential of the optimal DR-DSR is identified and the corresponding fluxes are determined, in order to approximate it with reactor-recycle-network candidates of less complexity, i.e. less amount of required recycle streams, or simpler control trajectories. The distributed dosing of all chemical components, especially the products, of any arbitrary composition is only possible assuming ideal splits in the separation unit. In case of non-ideal splits, the realizability of these recycling fluxes is limited and it would be reasonable to find reactor-networks, which approximate the optimal solution

with fewer amount of different recycling fluxes. Therefore, the FPA provides the necessary tools. As introduced in the previous subchapters, the fluxes are determined and subdivided in characteristic sections. Analyzing these fluxes and their sections carefully allows for revealing reduction potentials. The main difference to the reactor-network synthesis is the target of the reduction process. Instead of reducing only the amount of sections and, thus, of corresponding reactor units, in addition the amount of required recycling fluxes is reduced, and sections of beneficial recycling are e.g. approximated by a back-mixed reactor or neglected when the section is of minor importance. A subsequent evaluation of the resulting candidates, e.g. in the selectivity-conversion-space, allows for quantifying the impact of the recycling fluxes and identifying the approximation with the best trade-off between recycling effort and reaction performance. A lucid way to illustrate the reduction steps and the corresponding is a tree diagram where every further branch leads to an additional reactor-recycle-network candidate. This will be demonstrated on the reactor-recycle-synthesis for the literature example in subchapter 3.3.2 and the hydroformylation process in subchapter 3.3.3.

3.3.2 Comparison to superstructure optimization approaches for the van-de-Vusse reaction

The synthesis of reactor-networks of any kind is often done by means of superstructure (SS) optimization. The available methods in literature and prominent application examples have been discussed in subchapter 2.2. One of these examples is the classical van-de-Vusse reaction combining a consecutive and a parallel reaction of different order while favoring the intermediate product. This process example is optimized using SS optimization in several publications, see e.g. [34], [37]. In contrast to the modified van-de-Vusse reaction introduced in subchapter 3.2.2, the classical reaction network has no reverse reaction. In addition, the temperature dependence is considered allowing for optimizing the temperature profile. The application on this process example and the comparison to the literature results intends to demonstrate, how the presented reactor synthesis is able to provide candidates for further detailed design and to reduce the search space for a subsequent use of SS optimization approaches. The reaction network for the classical van-de-Vusse process is illustrated in Scheme 3.2.

$$A \overset{r_1}{\rightarrow} B \overset{r_2}{\rightarrow} C$$
$$2A \overset{r_3}{\rightarrow} D$$

Scheme 3.2: Classical van-de-Vusse reaction

Model formulation and optimization problem

The aforementioned temperature dependence is taken into account by adding a standard Arrhenius term to the reaction rates (Eq. (3.75)).

$$k_i = k_{0,i}\, exp\left(\frac{-E_{A,i}}{RT}\right), \forall i \in \{reactions\} \tag{3.75}$$

The rate coefficients k_i in Eq. (3.75) are defined by the rate constants $k_{0,i}$, the activation energies $E_{A,i}$, the universal gas constant R, and the temperature T. According to literature, the rate constants are defined with $k_{0,1} = 1.5 \cdot 10^6\ \mathrm{s}^{-1}$, $k_{0,2} = 4.4 \cdot 10^8\ \mathrm{s}^{-1}$, and $k_{0,3} = 100\ \mathrm{L\,mol}^{-1}\,\mathrm{s}^{-1}$, and the activation energies with $E_{A,1} = 6.6274 \cdot 10^4\ \mathrm{J\,mol}^{-1}$, $E_{A,2} = 9.9411 \cdot 10^5\ \mathrm{J\,mol}^{-1}$, and $E_{A,3} = 3.3137 \cdot 10^4\ \mathrm{J\,mol}^{-1}$. The mass balances are derived in terms of moles (Eqs. (3.76)-(3.80)).

$$\frac{dn_A}{dt} = V_R(-k_1 c_A - k_3 c_A^2) + y_{V,A}^m, \tag{3.76}$$
$$\frac{dn_B}{dt} = V_R(k_1 c_A - k_2 c_B) + y_{V,B}^m, \tag{3.77}$$
$$\frac{dn_C}{dt} = V_R(k_2 c_B) + y_{V,C}^m, \tag{3.78}$$
$$\frac{dn_D}{dt} = V_R(k_3 c_A^2) + y_{V,D}^m, \tag{3.79}$$

$$V_R = \frac{n_{tot}}{c_{tot}} = \frac{\sum_{\alpha=1}^{N} n_\alpha}{\sum_{\alpha=1}^{N} c_\alpha}, \tag{3.80}$$

The therein explicitly occurring reactor volume V_R is determined via Eq. (3.80) assuming a constant total concentration of $c_{tot} = 1\,\mathrm{mol/L}$ according to literature [34,37]. The initial filling level of reactant A in the storage tank is equal to the initial condition in the literature sources ($n_{A,st}^0 = 1\,\mathrm{mol}$), whereas the initial filling levels of the product tanks are not put to zero as the initial conditions in the literature sources. Instead, they are set to $n_{B,st}^0 = n_{C,st}^0 = n_{D,st}^0 = 1\,\mathrm{mol}$ to identify the benefits of product dosing, i.e. recycling of products. Due to the considered dosing of chemical components from the storage tanks, balances for storage tanks are added (Eq. (3.81)).

$$\frac{d\boldsymbol{n}_{st}}{dt} = -\boldsymbol{y}_V^m \tag{3.81}$$

The resulting optimization problem is stated as:

$$\max_{\boldsymbol{y}_V^m(t), T(t), t_f} n_B^f \tag{3.82}$$

s.t.	Component mass balances:	Eqs. (3.76)-(3.79)	(3.83)
	Storage mass balances:	Eq. (3.81)	(3.84)
	Constitutive equations:	Eqs. (3.75), (3.80)	(3.85)
	Dosing constraints:	$\int_0^{t_f} \boldsymbol{y}_V^m(t)\,dt \geq \begin{cases} n_\alpha^{min}, & \alpha \in \{A\} \\ 0, & \alpha \in \{B,C,D\} \end{cases}$	(3.86)
	Path constraints:	$\boldsymbol{y}(t) \geq 0, \boldsymbol{n}(t) \geq 0, \boldsymbol{n}_{st}(t) \geq 0$	(3.87)
		$300\,\mathrm{K} \leq T(t) \leq 800\,\mathrm{K}$	(3.88)
	Initial conditions:	$\boldsymbol{n}_0 = 0,\ \boldsymbol{n}_{0,st} = 1$	(3.89)
	Terminal constraints:	$t_f \leq 100\,\mathrm{s}$	(3.90)
		$\boldsymbol{n}_f = \begin{cases} n_\alpha(t_f), & \alpha \in \{A\} \\ n_\alpha(t_f) - \int_0^{t_f} y_{V,\alpha}^m(t)\,dt, & \alpha \in \{B,C,D\} \end{cases}$	(3.91)
		$\boldsymbol{n}_{st}^f = \boldsymbol{n}_{st}(t = t_f)$	(3.92)
	Differential selectivity:	$\varphi = \frac{r_1 - r_2}{r_1 + r_3}$.	(3.93)

Results of flux profile analysis

The results of the EPF optimization of the non-isothermal, classical van-de-Vusse reaction are shown in Fig. 3.12. The maximum objective is reached with $n_B^f = 0.8134\,\mathrm{mol}$. This value is in the same range as documented in literature [34,37]. The optimal dosing fluxes indicate that it is beneficial to dose reactant and side products at the very beginning of the process. The reason for the side product dosing is not the dilution of the reactant, instead the product B is supposed to be diluted. This is owed to the very high temperatures and corresponding high reaction rates at the beginning of the reaction. The solver chooses a trade-off between (i) high temperature at the beginning, which supports the undesired reaction r_2 due to its high activation energy, and (ii) the best ratio of concentrations of

components A and B. In order to support the main reaction from A to B, reactant A is completely dosed at the beginning. Simultaneously, the consecutive reaction r_2 is inhibited as well by diluting B via side product dosing. Subdividing the dosing flux, the temperature profile, and the differential reaction flux into characteristic sections, such as introduced in Section 3.1.3, one ends up with the following sections:

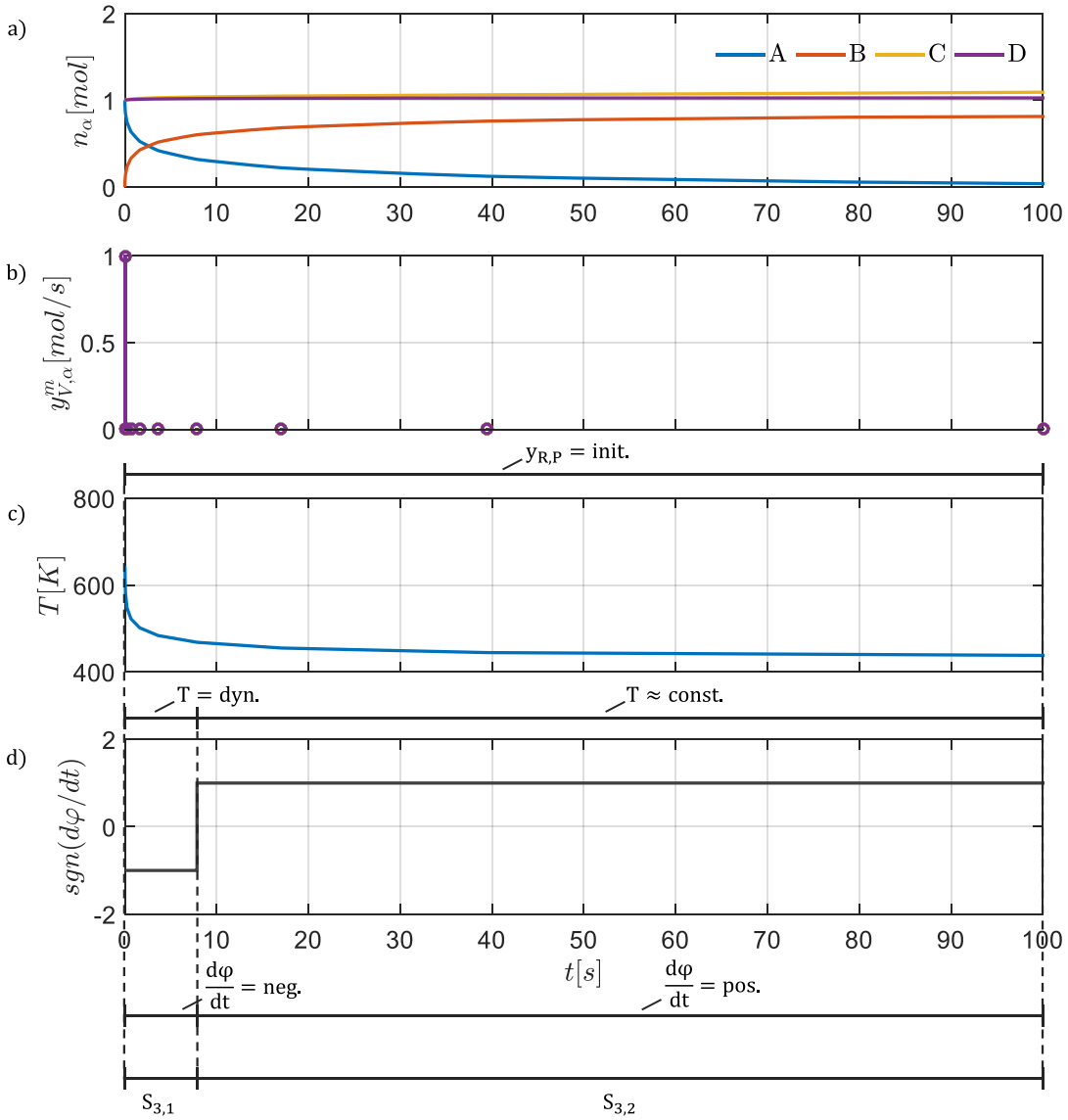

Figure 3.12: Results of the dynamic optimization of the classical van-de-Vusse reaction: a) Reaction progress; b) Dosing flux profiles; c) Temperature control profile; d) Differential reaction flux

- The first reaction section $S_{3,1}$ has an initial dosing of reactant and side products, a dynamic temperature profile and a negative differential reaction flux. According to the generic ideal process units given in Fig. 3.11, an IR-PFR is most suitable allowing for realization of the global recycling.
- The subsequent second reaction section $S_{3,2}$ is much longer and indicates no individual dosing, an almost constant temperature profile and a positive differential reaction flux. Due to these characteristics, only an internal recycling in form of back-mixing is necessary in this section, which points to the use of a CSTR. In case the temperature profile is not

approximated to be constant, the CSTR might be replaced by a DR-PFR with a slightly dynamic temperature profile.

The results indicate benefits from internal recycling (back-mixing) in the second reaction section and global recycling to the inlet of the reactor-network. A further important aspect is the realization of the sharp temperature profile in the first reaction section. A strict realization of these flux profiles ends up in a DR-DSR, as it was discussed in the previous subchapter. When the identified reaction sections from Fig. 3.12 are translated according to the FPA, the realization of an IR-PFR with either a subsequent CSTR or a DR-PFR is recommended. Depending whether the focus is put on the back-mixing benefit or the exact realization of the temperature profile in the second reaction zone, respectively. For a detailed quantitative analysis, it is reasonable to augment the set of reactor-network candidates by simpler reactor-networks neglecting e.g. the global recycle or approximating the sharp temperature control by a simpler profile. In this way the impact of these aspects on the performance can be identified and a better decision-making is possible, e.g. when it comes to an economic evaluation. Neglecting for instance the global recycling of side products, one obtains a simple PFR+CSTR network, which is in good accordance to the superstructure optimization results of Schweiger and Floudas [37] who proposed a network of a PFR with optimal temperature control and a subsequent CSTR. Note, that in their results the CSTR has a much higher residence time than the PFR and, thus, the back-mixing takes place almost over the entire reaction time, which might indicate also a benefit of a global recycling and is as well evident in the here determined residence times. An additional reduction option targets on the sharp temperature profile, which might be approximated by several small sections of constant temperature. Including the obvious benefit from side product recycling and the back-mixing benefit indicated by the differential reaction flux, a cascade of CSTRs seems to be a promising reduced reactor-network. The same result was achieved by Kokossis and Floudas [34], who optimized a PFR approximated by a cascade of CSTRs with intermediate cooling, indicating a similar temperature characteristic as shown in Fig. 3.12 b). Their results indicate a first section as well where no recycling takes place and a second section where recycling takes place. But these recycling streams are supposed to act as cooling medium, and a possible global recycle is again not included. The reduction scenarios and the resulting reactor-recycle-network candidates are summarized within a tree diagram (Fig. 3.13).

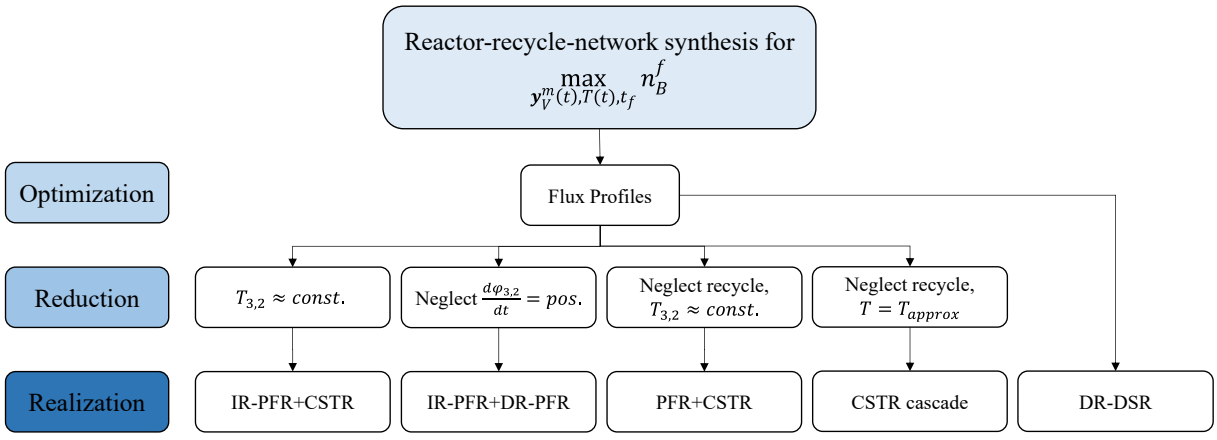

Figure 3.13: Tree diagram for the synthesis of reactor-recycle-network candidates for the classical van-de-Vusse reaction

Sensitivity analysis for the storage tank filling levels

As mentioned in the fundamentals for the reactor-recycle-network synthesis via FPA (subchapter 3.3.1), the filling levels of the product storage tanks play a crucial role when evaluating the maximum potential of a process on this level of synthesis. Therefore, a sensitivity analysis is carried out to quantify their impact on the previous synthesis procedure. The dynamic optimization problem is solved for different $n^0_{\alpha,st}$, $\alpha \in \{B, C, D\}$ in the range of $1..50$ mol. The resulting final values of component B are shown in Fig. 3.14.

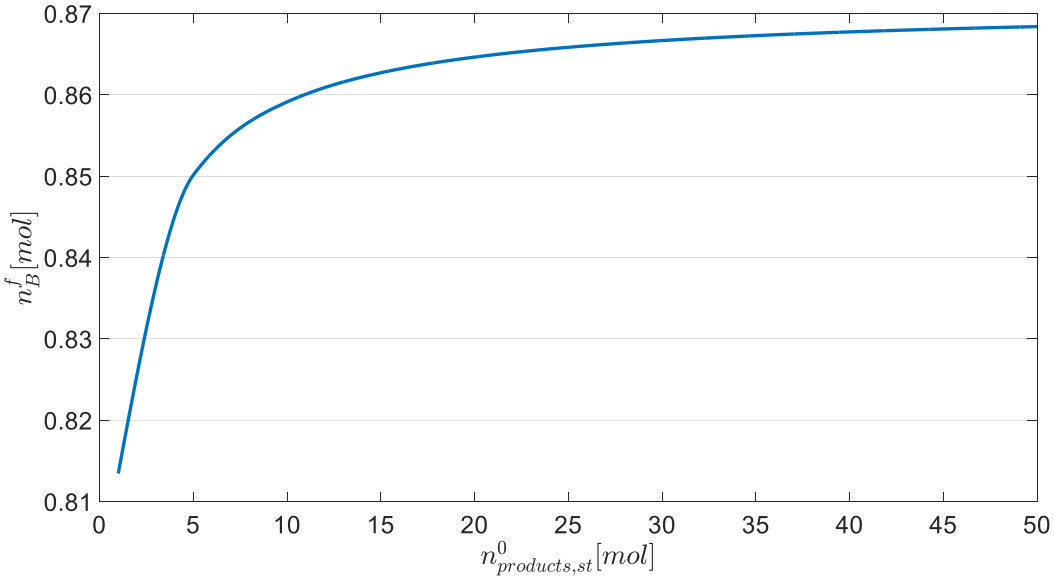

Figure 3.14: Sensitivity analysis of the final amount of product B for different storage tank filling levels within the dynamic optimization

Evidently, the initial filling levels of the product storage tanks influence the optimization results significantly. Several percent of product B can be gained by increasing the recycled amount of products by factors of two to five. With further increase of the filling levels this effect reduces clearly. An interesting aspect of this process is revealed when analyzing the flux profiles of the cases of higher storage tank filling levels. In Fig. 3.15 the case of $n^0_{\alpha,st} = 5$ mol, $\alpha \in \{B, C, D\}$ is illustrated. The characteristics of the dosing fluxes and the differential reaction flux are qualitatively the same as in the case of smaller filling levels, but the temperature profile is much less sharp at the beginning and the thereby arising maximum temperature is significantly smaller. Thus, the increase of the recycling streams is accompanied by a potentially simpler realizable temperature control. For a further detailed design, which might consider an economic evaluation, this aspect has to be paid attention. Moreover, it might be reasonable to carry out this sensitivity analysis first, in order to identify reasonable ranges for the filling levels, and afterwards conduct the FPA to derive suitable reactor-network candidates.

Although the product dosing should be able to identify back-mixing benefits, this example reveals a possibly arising problem. When the product dosing at the beginning of the reaction has a clear benefit, it is not increased individually at a section of back-mixing benefit, since the increased product amounts are still present from the initial dosing of products. This makes the analysis of the differential reaction flux indispensable for the presented approach.

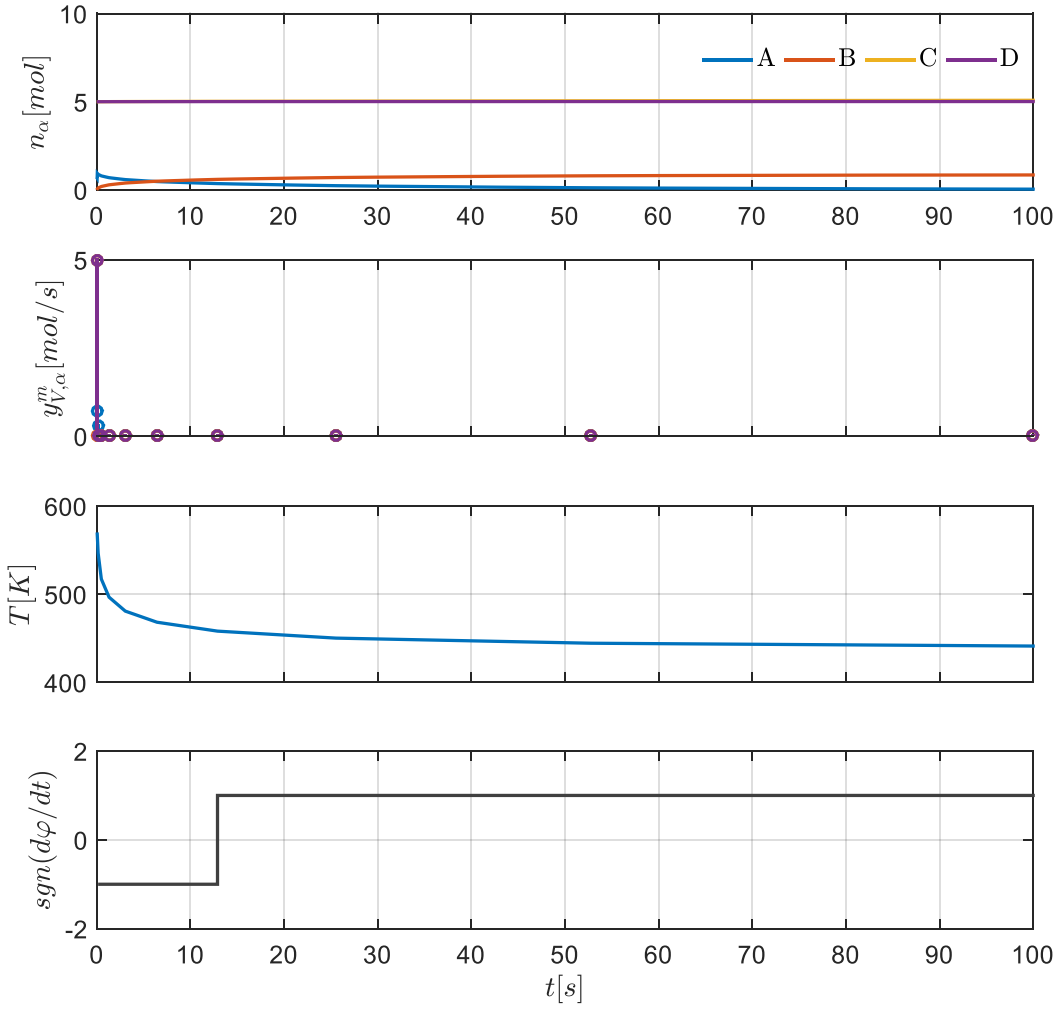

Figure 3.15: Results of the dynamic optimization of the classical van-de-Vusse reaction for storage tank filling levels at $\boldsymbol{n^0_{\alpha,st} = 5\ mol}$, $\boldsymbol{\alpha \in \{B, C, D\}}$: a) Reaction progress; b) Dosing flux profiles; c) Temperature control profile; d) Differential reaction flux

Discussion

Superstructure optimization is often used for process design purposes, especially for reactor-network synthesis. With nowadays computational power even very large-scale NLPs and MINLPs can be solved to find the optimal process configuration. Hence, the optimization of flow sheets of different kinds with superstructure optimization approaches is very powerful. However, as already Achenie and Biegler [32] stated in one of the fundamental articles about superstructure optimization, one of the main challenges for these approaches is the identification of suitable candidates. The *flux profile analysis* is a tool which is able to provide a rational selection procedure for promising reactor-network candidates, which are further designed and evaluated in detail. A special feature of the synthesis of candidates with the FPA approach is that it bases on reaction engineering fundamentals. The detailed process design based on the pre-selected reactor-networks with a superstructure optimization approach would result in exact values concerning residence times and the corresponding reactor volumes, the feed and recycle stream compositions, and the sizing of possible auxiliary units such as heat exchangers. This detailed process design is indispensable to compare different reactor-network candidates, their benefits in an overall process, and resulting costs. The pre-selection only provides

qualitative information. Note, that the presented synthesis procedure is able to provide quantitative information for the subsequent detailed process design. For instance, the initialization phase of the dosing policy indicates in which bounds the concentrations of different components in the recycle streams might be. In general, the values of states and controls of the dynamic optimization point out suitable bounds on states and controls of the detailed process design. This restricts the search space for optimization on a rational basis leading to reduced computational effort.

3.3.3 Reactor-recycle-network synthesis for hydroformylation of 1-dodecene

The impact of product recycling on the process performance is as well investigated for the hydroformylation of 1-dodecene in a TMS system. The corresponding DOP is extended for product dosing and solved. The resulting fluxes are analyzed via FPA to obtain reactor-recycle-network candidates. In accordance to subchapter 3.2.3 the resulting candidates are again evaluated in the $[S_{nC13al}, X_{nC12en}]$-space and compared to the performance of the previous level without recycling options. Finally, the impacts of the storage tank filling levels are quantified in the previously established way.

Model formulation and optimization problem

Since only the degree of freedom for the dosing of products is added in the dynamic optimization of the process, the model formulation is not changed and, thus, adopted completely from subchapter 3.2.3. The resulting DOP reads:

$$\max_{T(t),\boldsymbol{y}_V^m(t),p_{CO}(t),p_{H_2}(t),t_f} \; S_{nC13al}(t_f) \tag{3.94}$$

s.t. Component mass balances: Eq. (3.37) (3.95)

Storage mass balances: Eq. (3.40) (3.96)

Reaction kinetics: Eqs. (2.2)-(2.7) (3.97)

Catalyst equilibrium: Eq. (2.1) (3.98)

Constitutive equations: Eqs. (3.38)-(3.39) (3.99)

Gas solubilities: Eq. (2.11) (3.100)

Catalyst and solvent ratios: Eqs. (2.13)-(2.14) (3.101)

Dosing constraint: $\int_0^{t_f} y_{V,nC12en}^m(t)\,dt \geq n_{nC12en}^{min}$ (3.102)

Path constraints: $\boldsymbol{n}(t) \geq 0, \boldsymbol{n}_{st}(t) \geq 0$ (3.103)

$\boldsymbol{y}_V^m(t) \geq 0$ (3.104)

$10 \text{ bar} \leq p_t(t) = p_{CO}(t) + p_{H_2}(t) \leq 20 \text{ bar}$ (3.105)

$363.15 \text{ K} \leq T(t) \leq 388.15 \text{ K}$ (3.106)

Terminal constraints: $t_f \leq 100 \text{ min}$ (3.107)

$$X_{nC12en} = \frac{n_{nC12en}(0) - n_{nC12en}(t_f)}{n_{nC12en}(0)} = 99\ \% \tag{3.108}$$

$$S_{nC13al} = \frac{n_{nC13al}(t_f) - n_{nC13al}(0)}{n_{nC12en}(0) - n_{nC12en}(t_f)} \tag{3.109}$$

$$n/iso = \frac{n_{nC13al}(t_f)}{n_{nC13al}(t_f) + n_{iC13al}(t_f)} \geq 95\ \% \tag{3.110}$$

$$\boldsymbol{n}_f = \begin{cases} n_\alpha(t_f) - \int_0^{t_f} y_{V,\alpha}^m(t)\,dt, & \alpha \in \{CH/nC12en\} \\ n_\alpha(t_f), & \alpha \in \{nC12en\} \end{cases} \tag{3.111}$$

Initial conditions: $\boldsymbol{n}(t=0) = \boldsymbol{n}_0 = \boldsymbol{0}$ (3.112)

$\boldsymbol{n}_{st}(t=0) = \boldsymbol{n}_{st,0} = \boldsymbol{1}$ (3.113)

Differential selectivity: $\varphi = \frac{r_1}{r_1+r_2+r_3+r_6}$. (3.114)

As introduced in the previous section, it is necessary to extend the dynamic optimization problem for the purpose of product dosing by constraints for the product storage tank filling levels (Eq. (3.113)) and the corrected determination of the final product amounts (Eq. (3.111)). Again, the synthesis is carried out for a predefined conversion (Eq. (3.108)).

Results of flux profile analysis

In subchapter 3.2.3 it is already elucidated, how the control of the partial pressures as decision variables in this multiphase example are handled within the FPA. Together with the corresponding profiles of the amounts of moles, the temperature profile, the dosing fluxes for reactant and products, and the differential reaction flux they are shown in Fig. 3.16 as result of the dynamic optimization problem stated above (Eqs. (3.94)-(3.114)). The sectioning of these profiles leads to three characteristic reaction sections:

- The first section $S_{4,1}$ is defined by an initial dosing of the side products n-dodecane and iso-dodecenes. The temperature profile and the partial pressures show a constant behavior and the differential reaction flux is positive. Following the table of possible generic ideal process units in this level of synthesis, an IR-CSTR turns out to be most suitable. Instead of the main reactant, the iso-dodecenes are reacting in this section to tridecanal. But this reaction is rather slow and, thus, this section is quite long and has no large impact on the reaction. Hence, it might be reasonable to neglect this section. Furthermore, the beneficial back-mixing effect might be already satisfied by the initially recycled side products.
- The second section $S_{4,2}$ shows a distributed dosing of reactants and an initial dosing of products. It indicates dynamic control profiles and a negative differential reaction flux. Due to the distributed dosing characteristics for the reactant and the initial dosing for the side product, an IR-DSR is the best choice, which is also capable to realize the dynamic control profiles. This section should not be reduced, since it shows the main reaction performance. The reactant is converted to tridecanal, iso-dodecenes, and 2-methyl-dodecanal.
- In the subsequent third section $S_{4,3}$ no dosing appears, the temperature and partial pressure profiles are almost constant, and a positive differential reaction flux indicate the use of a back-mixed reactor unit, i.e. a CSTR. In contrast to the first section $S_{4,1}$, the last section indicates a benefit from back-mixing, but no products are dosed. The reason might be, that the products are already on a sufficiently high level from the previous sections; or the limited amount of products in the storage tanks is preferably dosed at the beginning of the process and would only be dosed in this section additionally when more product amounts for dosing are available.

The resulting reactor-recycle-network candidate is an IR-CSTR+IR-DSR+CSTR network (Fig. 3.17 a)) containing the reduction assumption that the control in the last section can be approximated to be constant. Reducing the FPA result with respect to the number of recycle streams, it seems to be reasonable to neglect the first reaction section together with its recycle, since the reaction progress in this section is very small though it is rather long, and to add the initial side product recycle to the initial recycle of the second section. Adding this reduction to the previous assumption, the resulting network consist of an IR-DSR and a CSTR (Fig. 3.17 b)).

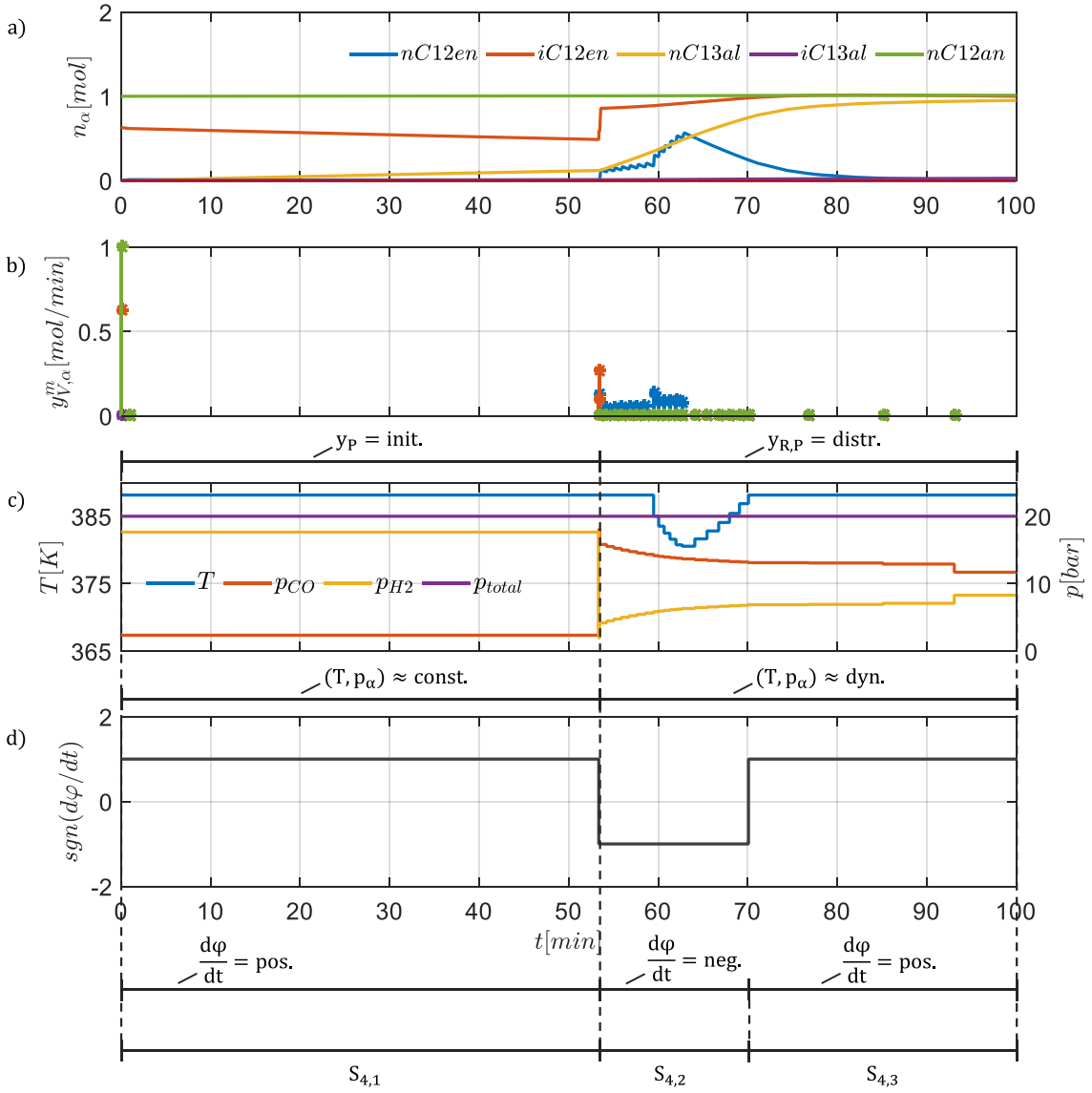

Figure 3.16: Results of the dynamic optimization of the hydroformylation of 1-dodecene for reactor-recycle-network synthesis: a) Reaction progress in moles; b) Dosing flux profiles; c) Control flux profiles; d) Differential reaction flux

A further reduction of the number of recycles is not expedient as its result is similar to the result of the previous synthesis level in subchapter 3.2.3. Instead, the first assumption of constant control in the last reaction section can be substituted by the negligence of the positive differential reaction flux in this reaction section, since the side product concentration is already high from the recycling in the second section. This assumption together with the negligence of the first reaction section is the third reduction scenario and results in a single IR-DSR (Fig. 3.17 c)). Again, the DR-DSR realization (Fig. 3.17 d)) will serve as maximum reference. All scenarios are summarized in a tree diagram for clarity (Fig. 3.18). Note, that the reactor units indicating a complex distributed control might also be realized technically with a semi-batch reactor, since the complex control profiles are easier to realize in a concentrated unit. However, those hybrid batch-continuous networks are not added as reactor-network candidates, since on this level of abstraction a substitution makes no difference for the achieved performance result.

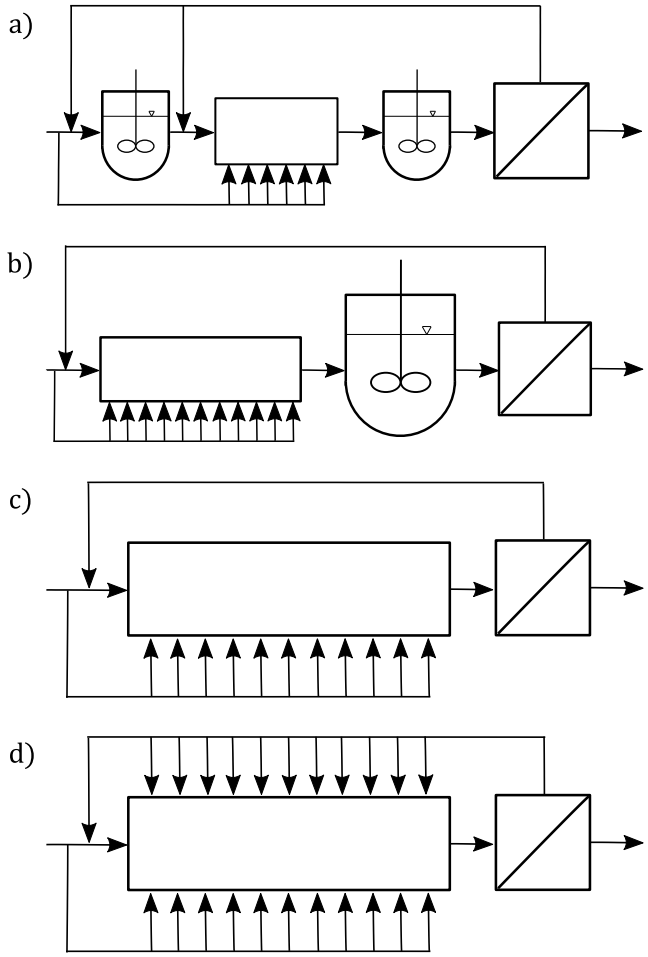

Figure 3.17: Reactor-recycle-network candidates for the hydroformylation of 1-dodecene: a) IR-CSTR+IR-DSR+CSTR; b) IR-DSR+CSTR; c) IR-DSR; d) DR-DSR

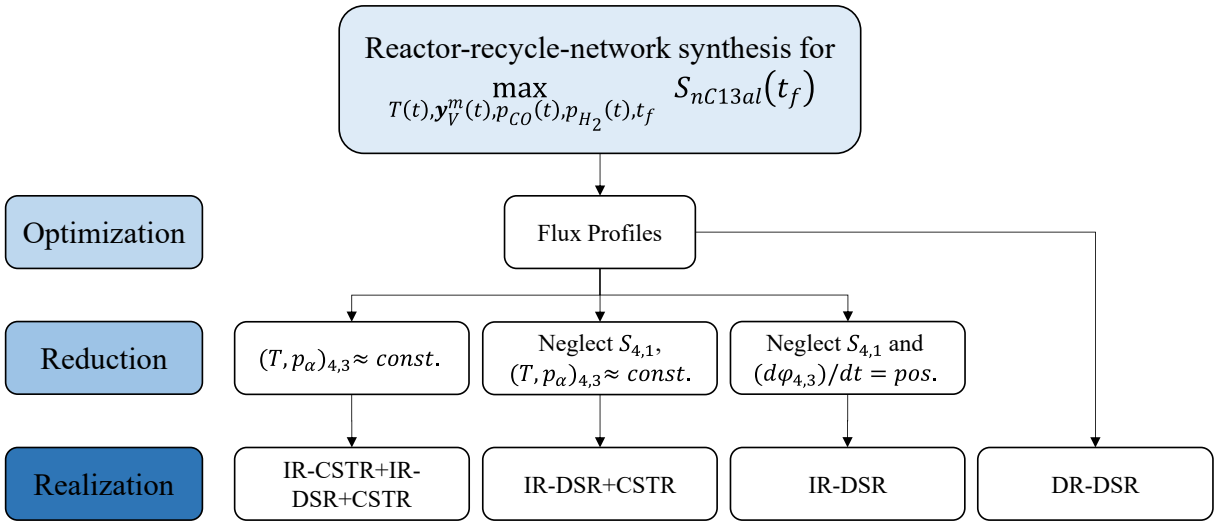

Figure 3.18: Tree diagram for the synthesis of reactor-recycle-network candidates for the hydroformylation of 1-dodecene

For quantification of the potentials of these reactor-recycle-network candidates, their performance is analyzed once again in the $[S_{nC13al}, X_{nC12en}]$-space. The corresponding results are shown in Fig. 3.19. One can see that the DR-DSR (green) constitutes, in fact, the upper performance limit. However, the other reactor-recycle-network candidates show a very similar performance with

only small deviations. This clearly indicates that the distributed product dosing and the additional effect of back-mixing units in the reduced networks have only a minor impact. This is demonstrated in more detail in the zoomed in figure for high conversions. Although the IR-DSR (red), which has neither distributed product dosing nor back-mixing sections, constitutes the lower performance limit, the other candidates show only a very slight better performance. Analyzing the fluctuations in the curves, these results might also suffer from numerical issues such as suboptimal local solutions. Note that, although the impact of distributed product dosing is negligible, the performance enhancement by the initial recycling is tremendously large. Compared to the reaction performance from the reactor-network synthesis in subchapter 3.2.3 without recycle option (blue) the selectivity with respect to the linear aldehyde is increased by 20..25 %.

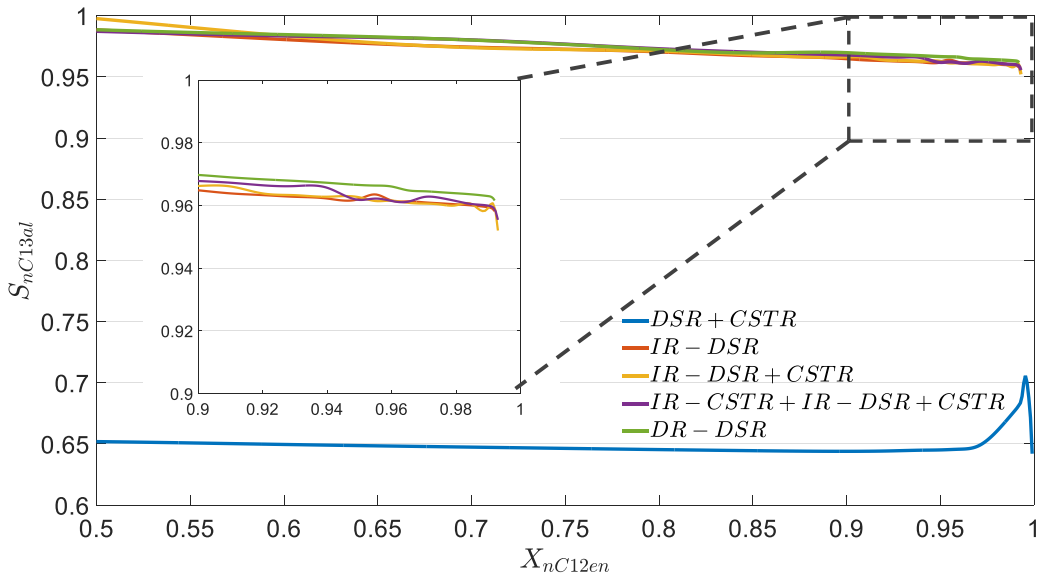

Figure 3.19: Evaluation of the reactor-recycle-network candidates from Fig. 3.17 in the $[\boldsymbol{S_{nC13al}, X_{nC12en}}]$-space and comparison to best result from the reactor-network synthesis in subchapter 3.2.3

Sensitivity analysis for the storage tank filling levels

Similar to the sensitivity analysis for the literature example in subchapter 3.3.2, the impact of the product storage tank filling levels on the optimization result is evaluated for the synthesis of an optimal reactor-recycle-network for the hydroformylation process. The initial product storage tank filling levels are varied from 0.5..10. The results in Fig. 3.20 demonstrate the importance of this analysis. For filling levels smaller than the initially chosen 1 mol the selectivity with respect to the desired tridecanal decreases significantly. For higher filling levels the performance increases up to a maximum of $S_{nC13al} \approx 98$ %.

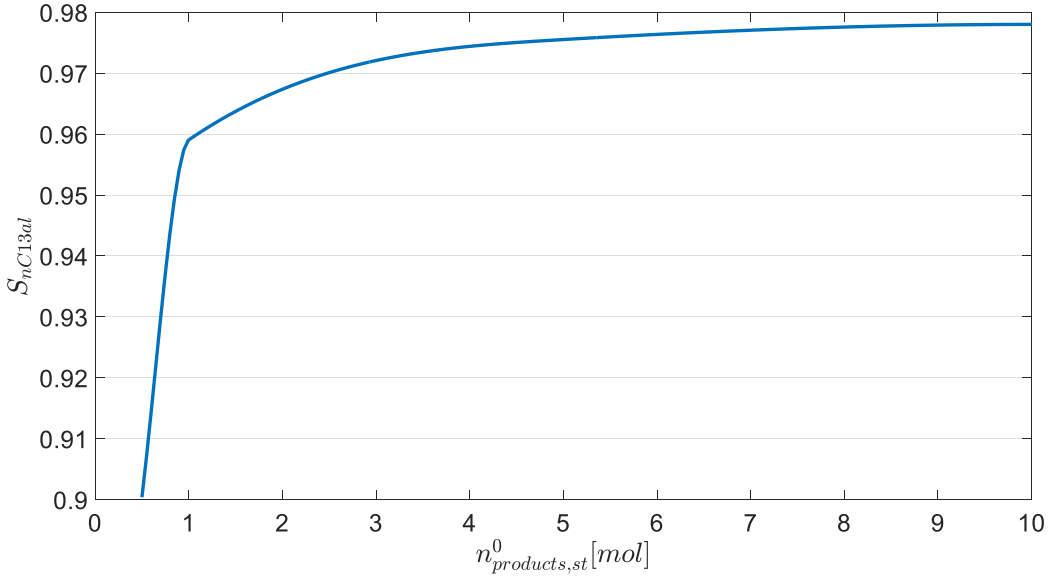

Figure 3.20: Sensitivity analysis of the final amount of product n-tridecanal for different storage tank filling levels within the dynamic optimization

3.4 Reactor-separator-recycle-network synthesis

The third and last level of synthesis, which is considered in this work, is the synthesis of reactor-separator-recycle-networks. Separators along the reaction coordinate allow for simultaneous removal of pure species and, thus, it reveals, together with the optional distributed reactant and product dosing of the last two subchapters, the maximum potential of a process. At first the fundamentals of the substitute batch process scheme and the resulting dynamic optimization problem are adapted to this additional degree of freedom and the list of generic ideal process units is augmented accordingly. Secondly, the reactor-separator-recycle-network synthesis approach will be applied to the same hydroformylation process, which was already treated in the previous subchapters.

3.4.1 Fundamentals

The addition of separators into the synthesis is mathematically simply realized by the permission of negative dosing fluxes, i.e. removal fluxes. Introducing this option to the batch process scheme leads to an extension by an ideal separator, which works intermediately to the batch reaction, and a product collector tank, see Fig. 3.21. A certain amount of reaction mixture is removed from the batch reactor and instantaneously split into two fractions. The first contains the pure species, which are supposed to be removed from the reaction mixture. They are led to the final product tank, to which at the end of the process also the final product stream from the ideal final separator is added. The second fraction is the remaining reaction mixture, which is directly returned to the batch reactor. This concept bases on the assumption that all these steps work instantaneously, such that the reaction is not lacking the removed and recycled reaction mixture. In contrast to the products, which are separated in the ideal final separator introduced in the subchapter of reactor-recycle-network synthesis, the products removed in the ideal intermediate separator are not fed to the product storage tanks. This is simply reasoned with their different meaning within this batch process concept. The products from the ideal final separator are only returned to their respective storage tanks up to the amount those storage tanks were filled with at the beginning of the process.

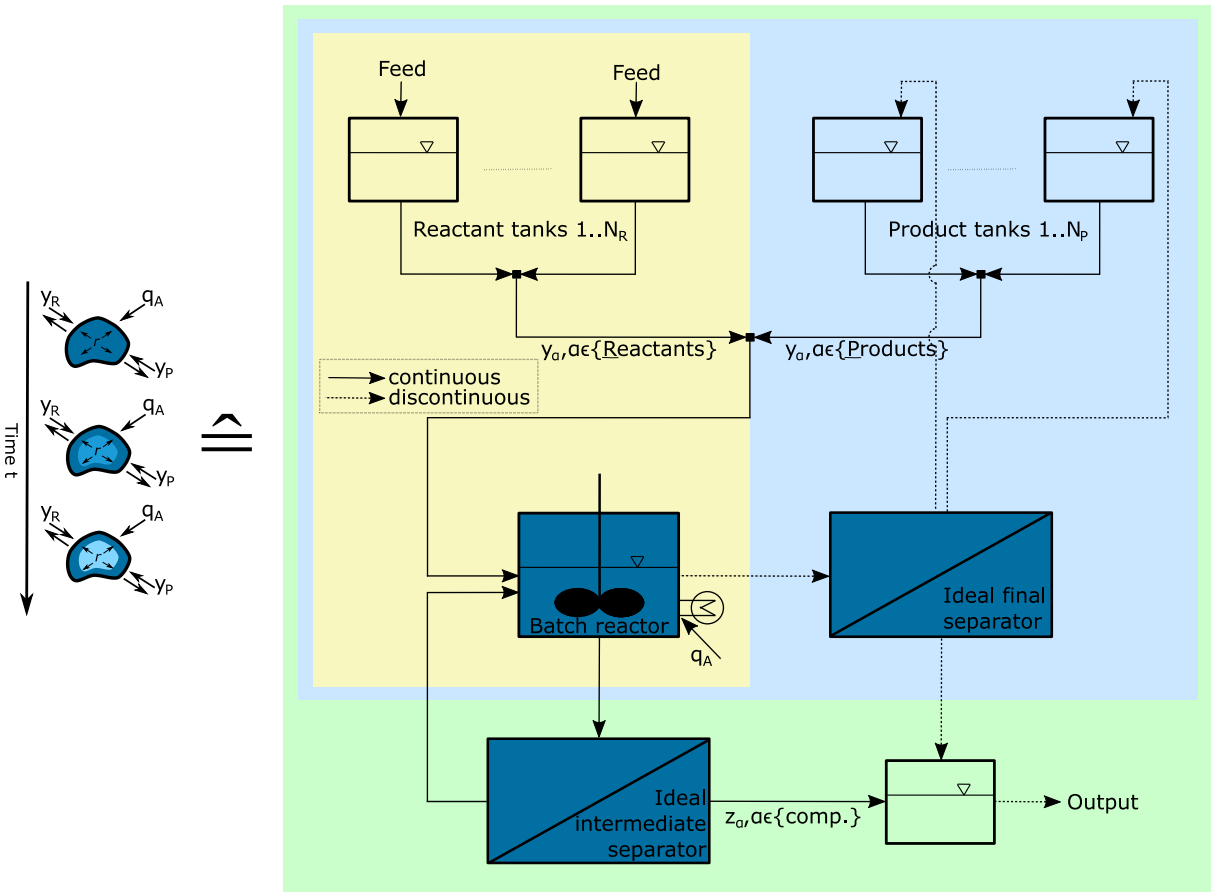

Figure 3.21: Translation of EPF fluid element into analogous batch process scheme in case of reactor-separator-recycle-network synthesis

This constraint intended to ensure, that no product is dosed just to improve the process performance and was used to analyze possible product dosing or back-mixing benefits. Whereas the products and also reactants, which are removed in the ideal intermediate separator, are clearly an output of the process and have to be counted at the very end of the process to evaluate its performance. For the sake of clear distinction of the removal streams and the dosing streams within the notation of the dynamic optimization problem and the graphical analysis, the removal streams are denoted in the following with $\boldsymbol{z}(t)$.

The reactor-separator-recycle-network synthesis has in common with the reactor-recycle-network synthesis that the optimal reactor for the realization of the optimal flux profiles will always be the distributed reactor unit with dosing and removal of all components of any arbitrary amount. In case of the reactor-recycle-network synthesis this unit, namely the DR-DSR, is realizable. However, in case of reactor-separator-recycle-network synthesis this not unequivocally possible. A removal of pure species simultaneous to reaction (and dosing) might be an option in some special cases, but normally this is accompanied by a lot of complications. Furthermore, this is rather a task for an advanced process intensification procedure and would not lead to a qualitative reactor-network. Hence, this is out of scope of this work. Instead, the removal is shifted outside the reaction or rather between the reaction sections using extra separation units. Thus, in every derived reaction section, which indicates a requirement for a removal of components, a separator is added, whose split mass fractions are led to the end of the process, where it is finally add to the output of the process, compare Fig. 3.21. The generic ideal process units resulting from this approach are simply all ideal process units from the previous two synthesis levels extended by a preceding separation unit (S), see Fig. 3.22. Finally, one has sixteen generic ideal process units out of which the optimal reactor-network can be constructed.

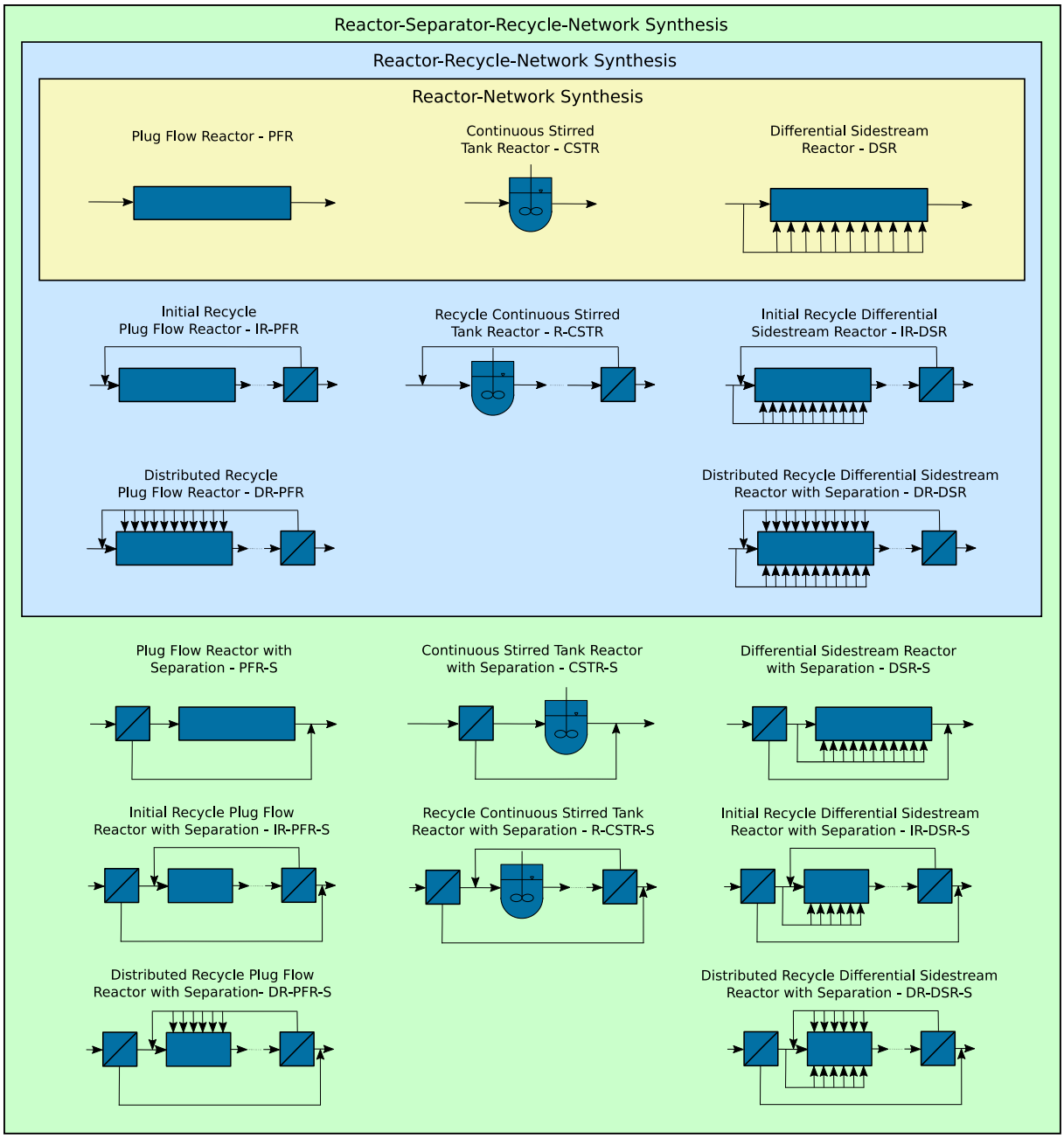

Figure 3.22: Generic ideal process units for reactor-separator-recycle-network synthesis within the FPA framework

The synthesis of reactor-network candidates from the flux profiles, which one obtains from solving the DOP (Eqs. (117)-(133)), is again a question of smart reduction of the maximum network based on reaction engineering knowledge. As described in subchapter 3.3.1 for the case of recycling, promising reactor-network candidates arise by reasonable reduction of the complexity of the maximum network resulting in different reduction cases, which are subsequently compared and analyzed. With regard to the separation effort within the network the task is similar, whereby the focus is put on the number of required separators Z instead of required recycles. In contrast to the previous level, the removal streams and the respective separators cannot be substituted by an alternative realization, as it was the case for the product recycling by internal back-mixing within a CSTR. Thus, it is only of interest to quantify the impact of the number of separators Z on the process performance. When Z is supposed to be reduced or set to a predefined value the solver still has to choose the size of the removal streams for each component and, even more challenging, their optimal position along the reaction coordinate. This optimal positioning is a kind of integer decision, which would change the

underlying optimization problem into mixed integer dynamic optimization (MIDO) problem. These systems are harder to solve and require special advanced solvers. To avoid the solving of a complex MIDO problem, an approach is used which intends to relax the integer decision by use of a sigmoidal function

$$\omega = \frac{\lambda^{\phi}}{\varepsilon_{set}^{\phi} + \lambda^{\phi}}. \tag{3.115}$$

In Eq. (3.115) the exponent n decides about the steepness of the sigmoidal function and has to be defined in advance (e.g. $n \approx 100$). The parameter ε_{set} is predefined as well, reasonably in a range of $\varepsilon_{set} \approx 1/Z_{max}$, and λ is the decision variable which the solver can choose to switch the sigmoidal function to either 0 or 1. The conceptual use of this sigmoidal function is illustrated in Fig. 3.23.

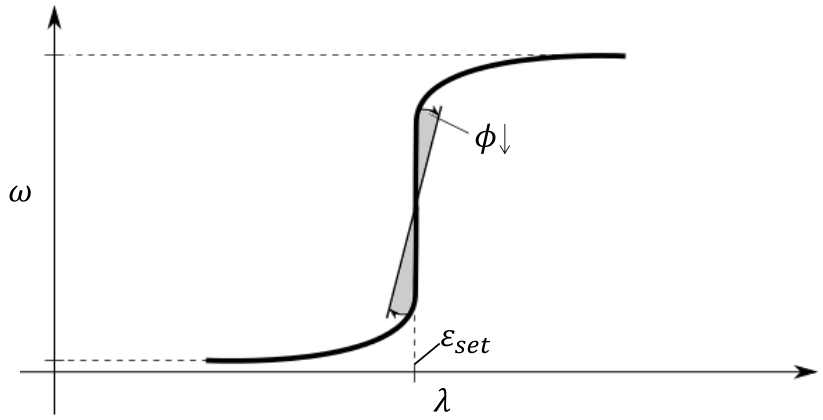

Figure 3.23: Scheme of the sigmoidal function and the decision variables for its shape

Every removal stream $z_{\alpha}(t)$ along the reaction coordinate is then multiplied by the corresponding sigmoidal function value $\omega = \omega(t)$ to achieve the effective removal stream, see Eq. (3.116).

$$\boldsymbol{z}_{eff}(t) = \boldsymbol{z}(t) \cdot \omega(t) \tag{3.116}$$

Within the DOP these effective removal streams are added to the mass balance (Eq. (3.118)), and the sum of removal streams of each component is added as term for the calculations of the final output of the process (Eq. (3.128)). The control vector (Eq. (3.123)) is extended by the removal streams $\boldsymbol{z}(t)$ and the decision variable $\lambda(t)$ of the sigmoidal function, whereby the effective removal stream is defined by Eq. (3.131). Furthermore, a non-negativity constraint for the removal streams is defined (Eq. (3.126)). The sigmoidal function is added (Eq. (3.132)) and its sum over the entire reaction time is supposed to be equal to the defined number of effective removal streams (Eq. (3.133)). The remaining DOP is the same as solved for the reactor-recycle-network synthesis in the previous subchapter.

$$\min_{\boldsymbol{u}(t),\boldsymbol{\xi}} \left(\int_0^{t_f} L(t)dt + I(\boldsymbol{x}_0) + W(\boldsymbol{x}_f) \right) \tag{3.117}$$

$$\text{s.t. } \frac{d\boldsymbol{\rho}}{dt} = \boldsymbol{j} + \boldsymbol{y} - \boldsymbol{z}_{eff} + \boldsymbol{M} \cdot \boldsymbol{N} \cdot \boldsymbol{r}_V \tag{3.118}$$

$$\frac{d\boldsymbol{\rho}_{st}}{dt} = -\boldsymbol{y} \tag{3.119}$$

$$\boldsymbol{g}(\boldsymbol{\rho}) = 0, \boldsymbol{h}(\boldsymbol{\rho}) \leq 0 \tag{3.120}$$

$$\boldsymbol{u}^L \leq \boldsymbol{u}(t) \leq \boldsymbol{u}^U \tag{3.121}$$

$$\boldsymbol{\xi}^L \leq \boldsymbol{\xi} \leq \boldsymbol{\xi}^U \tag{3.122}$$

$$\boldsymbol{u}(t) = [\boldsymbol{j}(t), \boldsymbol{y}(t), \boldsymbol{z}(t), T(t), \lambda(t)] \tag{3.123}$$

$$\boldsymbol{\xi} = [t_f] \tag{3.124}$$

$$\boldsymbol{y}(t) \geq 0 \tag{3.125}$$

$$\boldsymbol{z}(t), \boldsymbol{z}_{eff}(t) \geq 0 \tag{3.126}$$

$$\boldsymbol{\rho}(t=0) = \boldsymbol{\rho}_0 = \boldsymbol{0} \tag{3.127}$$

$$\boldsymbol{\rho}_f = \begin{cases} \rho_\alpha(t_f) + \int_0^{t_f} z_\alpha^{eff}(t)\, dt, & \alpha \in \{reactants\} \\ \rho_\alpha(t_f) - \int_0^{t_f} y_\alpha(t)\, dt + \int_0^{t_f} z_\alpha^{eff}(t)\, dt, & \alpha \in \{products\} \end{cases} \tag{3.128}$$

$$\boldsymbol{\rho}_{st}(t=0) = \boldsymbol{\rho}_{st}^0, \boldsymbol{\rho}_{st}(t=t_f) = \boldsymbol{\rho}_{st}^f \tag{3.129}$$

$$\int_0^{t_f} \boldsymbol{y}(t)\, dt \geq \begin{cases} \rho_\alpha^{min}, & \alpha \in \{reactants\} \\ 0, & \alpha \in \{products\} \end{cases} \tag{3.130}$$

$$\boldsymbol{z}_{eff}(t) = \boldsymbol{z}(t) \cdot \omega(t) \tag{3.131}$$

$$\omega(t) = \frac{\lambda(t)^n}{\varepsilon_{set}^n + \lambda(t)^n} \tag{3.132}$$

$$\int_0^{t_f} \omega(t) = Z_{set}. \tag{3.133}$$

This DOP has to be solved for every defined value of Z_{set}, i.e. number of separators in the resulting reactor-network. Thus, the tree of reduction cases, introduced in subchapter 3.3.1, has to be created for every number of separators, since they have a clear impact on the other control or decision variables. It is hence recommended to carry out the analysis of the separator impact on the performance first and then decide about possible reduction cases for the realization of the optimal flux profiles.

3.4.2 Reactor-separator-recycle-network synthesis for hydroformylation of 1-dodecene

In the following the reactor-separator-recycle-network synthesis is carried out exemplarily for the hydroformylation process using the FPA. The optimal flux profiles are determined for a predefined number of separators and optimal reactor-network candidates are derived. Subsequently, the impact of the number of separators on the process performance is analyzed.

Model formulation and optimization problem

The model formulation is only changed by adding the effective removal streams to the component mass balances (Eq. (3.134)) compared to the two previous synthesis levels, see subchapters 3.2.3 and 3.3.3.

$$\frac{dn_\alpha}{dt} = V_{liq}\left(j_\alpha^m + c_{cat} M_{cat}\left(\sum_{m=1}^{M} \nu_{\alpha,m} r_m\right)\right) + y_{V,\alpha}^m - z_{V,\alpha}^{m,eff}, \quad \alpha \in CH \tag{3.134}$$

The changes within the resulting DOP refer to the abovementioned extension for the removal streams in Eqs. (3.135), (3.136), (3.146), (3.153) and the addition of side calculations for the sigmoidal function Eqs. (3.157), (3.158), (3.159). The final DOP reads:

$$\max_{T(t), \boldsymbol{y}_V^m(t), \boldsymbol{z}_V^m(t), \lambda(t), p_{CO}(t), p_{H_2}(t), t_f} \; S_{nC13al}(t_f) \tag{3.135}$$

s.t. Component mass balances: Eq. (3.130) (3.136)

Storage mass balances:	Eq. (3.40)	(3.137)
Reaction kinetics:	Eqs. (2.2)-(2.7)	(3.138)
Catalyst equilibrium:	Eq. (2.1)	(3.139)
Constitutive equations:	Eqs. (3.38)-(3.39)	(3.140)
Gas solubilities:	Eq. (2.11)	(3.141)
Catalyst and solvent ratios:	Eqs. (2.13)-(2.14)	(3.142)
Dosing constraint:	$\int_0^{t_f} y_{V,nC12en}^m(t)\,dt \geq n_{nC12en}^{min}$	(3.143)
Path constraints:	$\boldsymbol{n}(t) \geq 0, \boldsymbol{n}_{st}(t) \geq 0$	(3.144)
	$\boldsymbol{y}_V^m(t) \geq 0$	(3.145)
	$\boldsymbol{z}_V^m(t) \geq 0, \boldsymbol{z}_V^{m,eff}(t) \geq 0$	(3.146)
	$10\text{ bar} \leq p_t(t) = p_{CO}(t) + p_{H_2}(t) \leq 20\text{ bar}$	(3.147)
	$363.15\text{ K} \leq T(t) \leq 388.15\text{ K}$	(3.148)
Terminal constraints:	$t_f \leq 100\text{ min}$	(3.149)
	$X_{nC12en} = \frac{n_{nC12en}(0) - n_{nC12en}(t_f)}{n_{nC12en}(0)} = 99\,\%$	(3.150)
	$S_{nC13al} = \frac{n_{nC13al}(t_f) - n_{nC13al}(0)}{n_{nC12en}(0) - n_{nC12en}(t_f)}$	(3.151)
	$n/iso = \frac{n_{nC13al}(t_f)}{n_{nC13al}(t_f) + n_{iC13al}(t_f)} \geq 95\,\%$	(3.152)
	$\boldsymbol{n}_f = \begin{cases} n_\alpha(t_f) - \int_0^{t_f} y_{V,\alpha}^m(t)\,dt + \int_0^{t_f} z_{V,\alpha}^{m,eff}(t)\,dt, & \alpha \in \{CH/nC12en\} \\ n_\alpha(t_f) + \int_0^{t_f} z_{V,\alpha}^{m,eff}(t)\,dt, & \alpha \in \{nC12en\} \end{cases}$	(3.153)
Initial conditions:	$\boldsymbol{n}(t=0) = \boldsymbol{n}_0 = \boldsymbol{0}$	(3.154)
	$\boldsymbol{n}_{st}(t=0) = \boldsymbol{n}_{st,0} = \boldsymbol{1}$	(3.155)
Differential selectivity:	$\varphi = \frac{r_1}{r_1 + r_2 + r_3 + r_6}$	(3.156)
Side calculations:	$\boldsymbol{z}_{eff}(t) = \boldsymbol{z}(t) \cdot \omega(t)$	(3.157)
	$\omega(t) = \frac{\lambda(t)^n}{\varepsilon_{set}^n + \lambda(t)^n}$	(3.158)
	$\int_0^{t_f} \omega(t) = Z_{set}.$	(3.159)

Results of flux profile analysis

The DOP is solved exemplarily for $Z_{set} = 2$ resulting in optimal flux profiles for a reactor-separator-recycle-network with two separators. The dosing flux, the differential reaction flux, and the control variables, temperature and gas partial pressures, are analyzed the same way as on the previous two synthesis levels. The FPA figure is extended by a subplot of the additionally optimized removal fluxes indicating their characteristics, see Fig. 3.24.

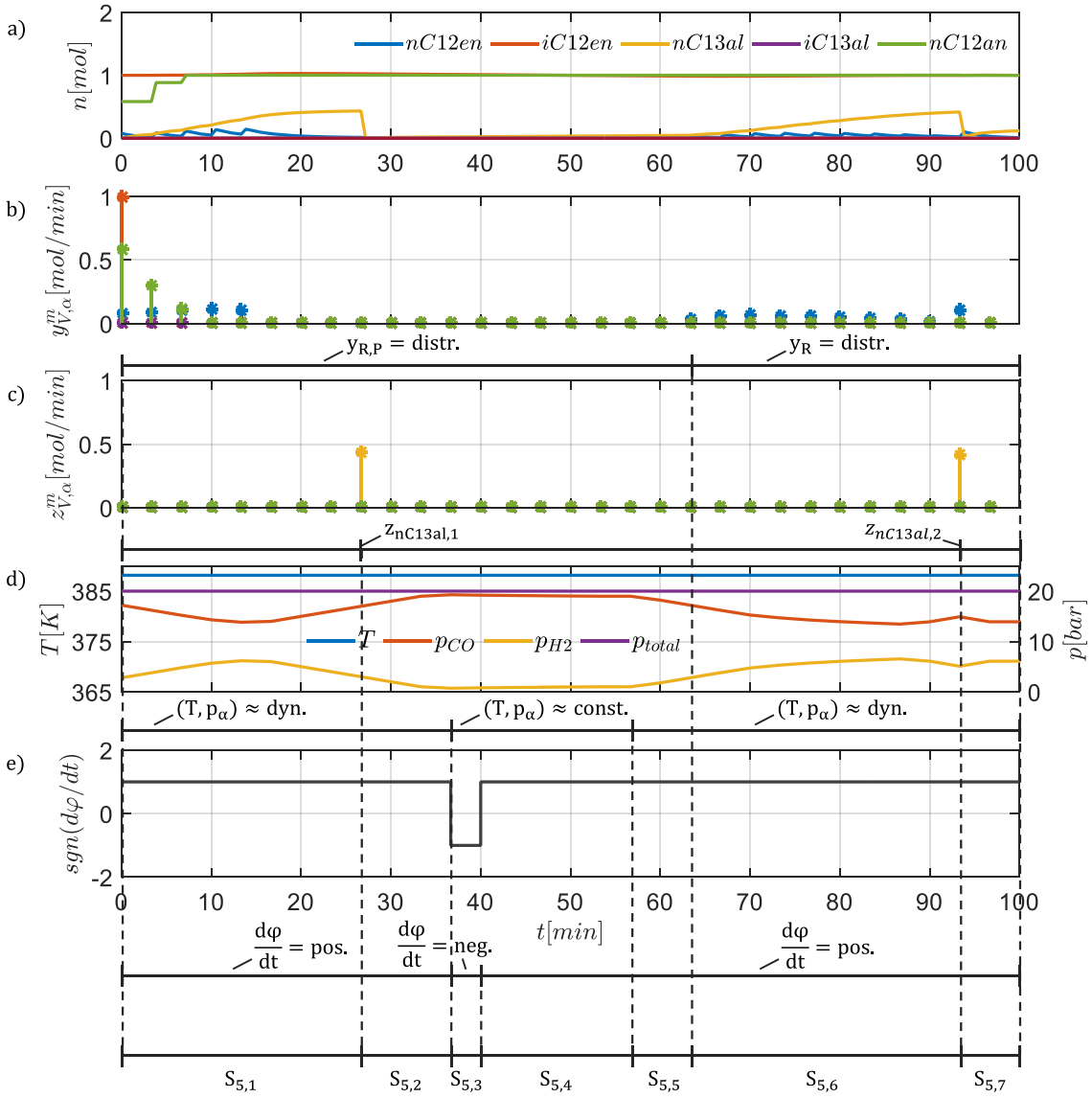

Figure 3.24: Results of the dynamic optimization of the hydroformylation of 1-dodecene for reactor-separator-recycle-network synthesis: a) Reaction progress in moles; b) Dosing flux profiles; c) Removal flux profiles/spots; d) Control flux profiles; e) Differential reaction flux

The sectioning indicates seven characteristic reaction sections:

- The first reaction section $S_{5,1}$ is defined by a distributed dosing of reactant and side products. The temperature control is constant, but the partial pressures are not. This and the distributed dosing of reactant indicate a need of a distributed reactor with dosing of liquid and gaseous reactants, although the differential reaction flux is positive. The latter is neglected, since with the initial dosing of side products, pointing on a global recycle, the back-mixing effect, i.e. an increased product concentration, is already satisfied. Hence, the first section is best realized with a DR-DSR.
- The second reaction section $S_{5,2}$ starts with the removal of the main product, has no dosing profile, and both the same control characteristics and differential reaction flux as the first section. This leads either to a CSTR-S or a PFR-S depending on the realization focus on either the positive differential reaction flux or the dynamic control profiles, respectively.

- The subsequent third reaction section $S_{5,3}$ is quite short, has neither dosing or removal streams, constant control profiles, and a negative differential reaction flux. The latter is the only indication for a PFR.
- The fourth reaction section $S_{5,4}$ has the same characteristics as the previous one, except of the again positive differential reaction flux. Thus, a CSTR seems appropriate.
- The fifth reaction section $S_{5,5}$ is very similar to the previous, except of a slightly dynamic partial pressure control. This section has an obvious reduction potential, since the approximation of the partial pressure controls with constant profiles allows for a merger with the previous reaction section.
- Indicating a distributed dosing of reactant and a dynamic partial pressure control, the sixth reaction section $S_{5,6}$ has to be realized with a DSR, although again the differential reaction flux is positive. With the same reasoning as for the first reaction section, this is neglected, since the product concentration is already high from initial side product dosing.
- The seventh and last reaction section $S_{5,7}$ shows an initial dosing of reactant and a removal of main product. The temperature control is constant, and the partial pressures can be approximated to be constant, too. The differential reaction flux is again positive and, thus, the optimal realization is chosen to be a CSTR-S.

The initial side product dosing being at its bound and the differential reaction flux being positive in all sections except of the third allows for the conclusion, that larger streams of recycled side products are beneficial for the reaction performance, as the sensitivity analysis in subchapter 3.3.3 already revealed. The aforementioned seven reaction sections still show potential for reasonable reduction. For instance, the negative differential reaction flux in section $S_{5,3}$ could be neglected and the slightly dynamic partial pressure profiles of section $S_{5,5}$ could be approximated to be constant on the same level as in the preceding section. Thus, these two reaction sections can be merged with sections $S_{5,2}$ and $S_{5,4}$ to one CSTR-S. This leads to an optimal reactor-separator-recycle-network candidate consisting of a DR-DSR, a CSTR-S, a DSR, and a CSTR-S (Fig. 3.25), which reflects the qualitative flux profiles characteristics very properly. As the reduction procedure and the corresponding derivation of several reactor-network candidates are already demonstrated in detail in subchapter 3.3.2 and 3.3.3, it is foregone here.

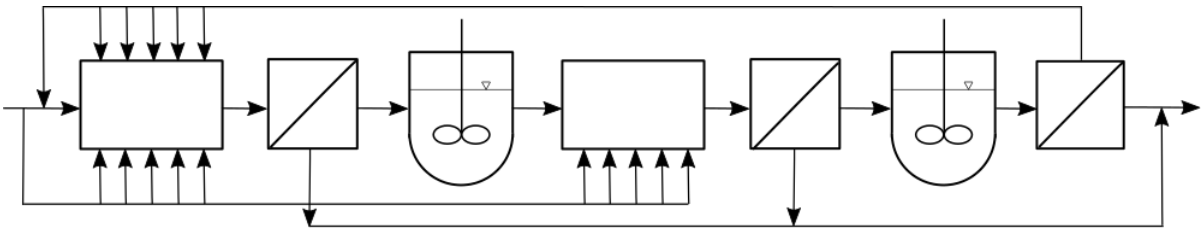

Figure 3.25: Reactor-separator-recycle-network candidate for the hydroformylation of 1-dodecene

To quantify the performance of this optimal reactor-network candidate, it is evaluated again in the $[S_{nC13al}, X_{nC12en}]$-space and compared to the results of the two previous synthesis levels, see Fig. 3.26. Evidently, the performance of the above process candidate (blue) is slightly better than the performance of the IR-DSR synthesized on the level of reactor-recycle-network synthesis (red). At the original design point $X_{nC12en} = 99\ \%$ the first provides a selectivity of $S_{nC13al} \approx 98\ \%$ and the latter of $S_{nC13al} \approx 95.9\ \%$. Nevertheless, the comparison of the network candidates of all three synthesis levels indicate clearly that the main performance gain is based on the globally recycled side products. The optimal candidate derived on the level of reactor-network synthesis (yellow) harness the beneficial product recycling only by use of an internal back-mixing with a CSTR at the end of the

reactor-network. However, with the degree of freedom of recycling the performance is increased tremendously and can only be slightly enhanced by the inclusion of separators along the reaction coordinate.

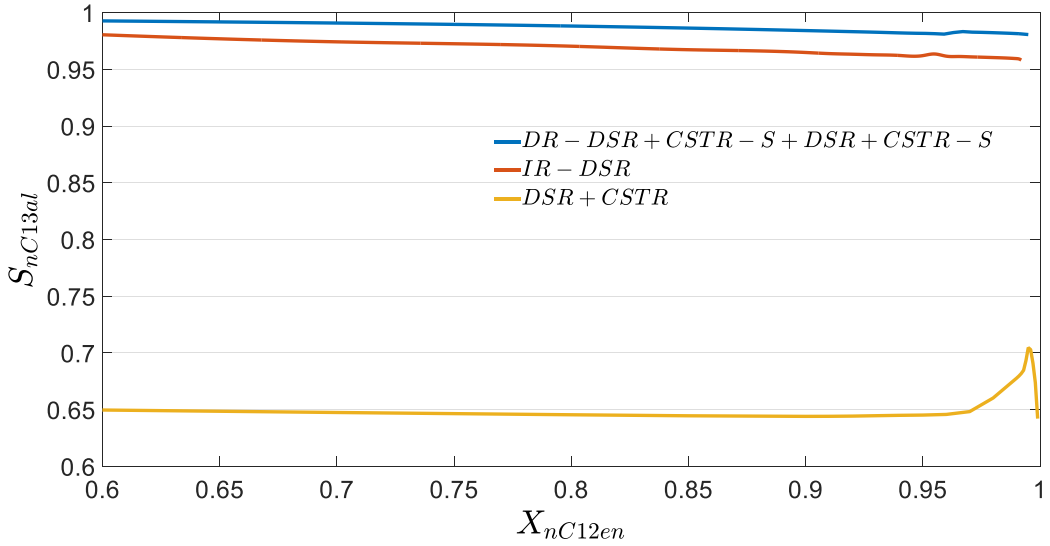

Figure 3.26: Evaluation of the reactor-separator-recycle-network candidate from Fig. 3.25 in the $[\boldsymbol{S_{nC13al}, X_{nC12en}}]$-space and comparison to results from the reactor-network synthesis in subchapter 3.2.3 and the reactor-recycle-network synthesis in subchapter 3.3.3

Performance screening for different numbers of separators

As mentioned before, it is analyzed how the predefined number of effective removal streams affects the selectivity performance of the hydroformylation process when carrying out the reactor-separator-recycle-network synthesis. Therefore, the DOP (Eqs. (3.135)-(3.159)) is solved for Z_{set} between $0 \ldots 30$, whereby the largest number corresponds to the number of finite elements within the discretization of the DOP (see subchapter A.7 for details). The resulting relation of the maximum selectivity with respect to n-tridecanal and the number of separators is drawn in Fig. 3.27.

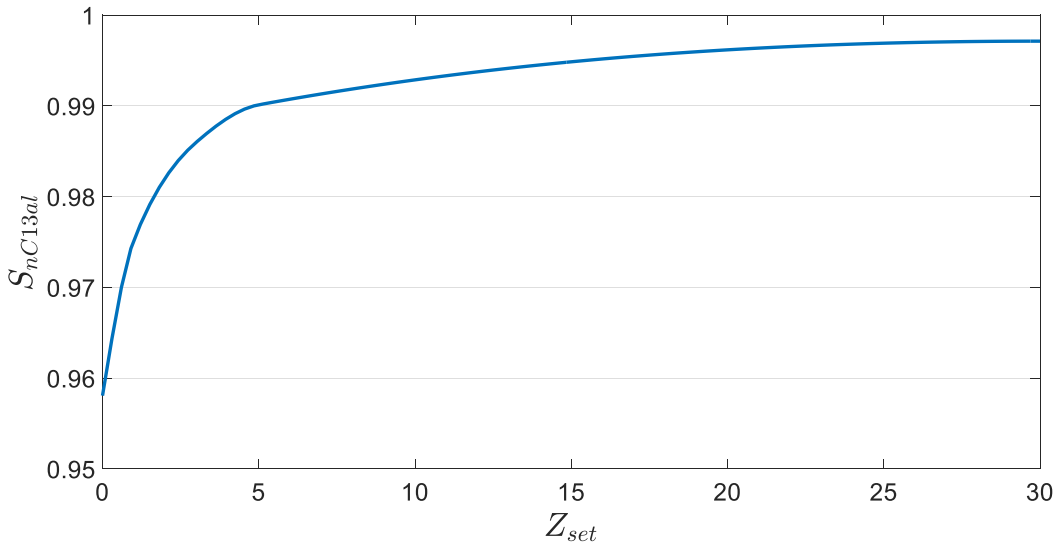

Figure 3.27: The maximum selectivity with respect to n-tridecanal for different predefined numbers of ideal separators within the reactor-separator-recycle-network synthesis

With increasing number of separators, the selectivity of the process approximates almost 100 %. Note, that this would imply a realization with either numerous ideal separations along the reaction coordinate or even an integrated reactor with continuous, ideal withdrawal of pure product. As this is not a realistic scenario, one can use this analysis to quantify the gain of every ideal separator, which is added to the network.

3.5 Discussion

Basing on a simple dynamic optimization problem only taking the chemical reaction into account, the *flux profile analysis* allows for a fast synthesis of reactor-network candidates on different synthesis levels. Since the analysis is based on fundamental reaction engineering knowledge it is not restricted to a certain kind of reaction and can be extended for different kind of processes, e.g. homogeneously catalyzed gas-liquid processes (as shown in the previous sections) or heterogeneously catalyzed reactions. It generates only qualitative candidates of possible conceptual designs, which serve as a basis for a further detailed process design, but reveals already the maximum potential of a reaction, since other phenomena such as mass or heat transfer resistances, flow fields, energy dissipation, etc. are neglected, keeping in mind that these non-idealities are decreasing the performance. Although the target of the FPA is the identification of an optimal reactor-network and not the determination of all attainable points in state space, the search space for the optimal configuration and, thus, the attainable region is rationally restricted.

For the synthesis of reactor-separator-recycle-networks the same advantages and disadvantages in comparison to state-of-the-art methods hold, as for the other synthesis levels. The FPA does not intend to surpass the state-of-the-art methods for process design. It tries to augment their features by analysis of the reaction engineering characteristics of the process and overcomes typical weaknesses of AR approaches and SS optimization as discussed in Section 3.2.2 and 3.3.2, respectively. It can be seen as extension of the portfolio of synthesis methods providing information about the process potentials and promising reactor-network candidates. Moreover, the developed batch process scheme allows on all synthesis levels for optimization with every available or future optimization approach simply optimizing the fluxes in the schemes such as it is done by dynamic optimization in this work. Furthermore, it allows for the synthesis of optimal continuous reactor-networks with discontinuous parts whose optimal control policy is provided directly by the results of the dynamic optimization. In this way, optimal hybrid batch-continuous reactor-networks can be derived. Parallel reactor structures are not required in an optimal reactor-network structure, since the optimal path of the fluid element in the thermodynamic state space is per definition not branched. Parallel structures are only one of several options to provide dosing streams of required compositions along the reaction coordinate.

Influence of objective and process conditions on the synthesis results

In the introduction of the FPA the functional module of chemical reaction is put in the focus of reactor synthesis and design, and the objective is chosen to be the selectivity of the desired product, accordingly. This does not dispute that every step in a chemical process can have a high impact on the reactor synthesis and design procedure, but only the step of chemical reaction. For instance, there exist processes in which the overall process costs are mainly affected by the quantitative separation and recycling, i.e. recovery, of expensive catalysts [164]. Other processes are mainly affected by the heat removal and its control, e.g. in start-up procedures of highly exothermic processes, maintaining a long-term stability of a catalyst [165]. Crucial for the impact of the different process steps on the reactor synthesis and design is the choice of the objective. In the aforementioned very up-to-date examples, the objectives are the overall process costs and the long-term catalyst stability, respectively. The latter

might be chosen due to economic considerations, too. However, the process cost as economic objective is simply a scalar value combining several different objectives weighting them with prices. This might lead to trivial or hardly analyzable results, when certain part is overwhelming all others. Finally, any kind of process design has to be evaluated by this kind of objective to check for or improve the profitability of the process. Nevertheless, it is of primary interest of an engineer to understand the intrinsic nature of a process and to classify its characteristics in well-known categories, which allows using established models or available apparatuses in the further design procedure. Chemical engineers would, therefore, probably use objectives such as high selectivity of a desired product, space-time-yields, long-term catalyst stability, etc., whereas other engineers rather consider objectives such as minimal fuel consumption, energy efficiency, or simply smaller failure rates. Summarizing, the result of a design procedure is strongly driven by the choice of its objective. Since the presented framework is supposed to identify candidates for optimal process networks focusing on the chemical reaction as core of the process, the chosen objectives underlying the synthesis and design procedure aim at quantifying the quality of the chemical reaction. These objectives are hence selectivities, conversions, and space-time-yields.

In addition to the decision about a suitable objective function, the dynamic optimization is in need of a predefinition of process conditions for which an optimal process is sought, e.g. conversion point, purity levels, restricted inlet conditions, etc. The consideration and/or change of these conditions within the dynamic optimization is thereby straightforward. To quantify the sensitivity of the optimal performance with respect to those predefined conditions or limitations, one can either carry out a multi-objective optimization defining one or more of the conditions as additional objective or evaluate the optimal performance for different values of those conditions to figure out how the optimal reactor-network would change. These changed process conditions might have a significant impact on the resulting reactor-network. However, process conditions in a certain neighborhood show often only small quantitative changes in the result, whereby the qualitative character of the optimal control stays the same as the deciding phenomena stay the same, see e.g. subchapter 3.3.2.

Hydroformylation process

In this work the evaluation within the selectivity-conversion-space is chosen to compare the performance of different reactor-network candidates and to quantify their selectivity potential for different conversions. This evaluation gives rise to the most promising candidate for further detailed process design. Although the candidate, which is coming closest to the dream point of the reaction at full conversion and maximum selectivity, is obviously the highest performing, reactor-network candidates resulting from a rational reduction procedure might show a better trade-off between performance and realizability and, thus, might be more promising. The results of the reactor synthesis for the proposed hydroformylation process indicate that the highest gain of the selectivity with respect to the tridecanal is achieved with recycling of the reversible side products. Other changes within the reactor-network, e.g. addition of separators or realization of sections with back-mixed reactors, have only a minor effect and could be neglected. Especially the intermediate separation of pure species is almost impossible to realize in a technical process. On the one hand the process costs would suffer tremendously from the possible catalyst loss, and on the other hand the separation of pure product would require a complex and large structure of separators. Furthermore, the results have to be assessed carefully, since several process conditions are added for the proof of concept of the presented approach for this process, which might have a significant impact on the resulting process. For instance, higher reaction time, lower conversion points, or different n/iso ratios would certainly change the outcome of the synthesis and, thus, the presented results are not of general value.

Challenging open tasks

Although the presented procedure of the FPA was successfully applied for several process examples and synthesis levels, it still points out improvement potentials with respect to its practicability. For instance, the graphical analysis suffers, obviously, from the illustration of the fluxes. In case the fluxes are not illustrated in a reasonable scale, the engineer might be misled in his decision-making. In course of the illustration and analysis of the fluxes, it might, moreover, be of advantage to consider the differential flux to be analyzed not only with regard to its sign, but also for its exact value. The size of its change at each point might give a hint about the sensitivity of the differential reaction flux for the choice of the best reactor. For future applications, it is recommended to investigate this deeper. A further aspect, which requires more attention, is the sensitivity of the control arcs of each flux. Since the decision-making strongly relies on the meaning of the control fluxes and their characteristic sections, the relevance of these characteristics for the final performance has to be quantified, which might lead to simpler control profiles and resulting reactor-networks.

In subchapter 3.4 the addition of removal streams is introduced to the FPA allowing for the synthesis of reactor-networks including different numbers of separators. However, the result of the dynamic optimization within the EPF framework can also be used to design integrated reaction-separation units. Therefore, a higher number of removal streams is activated or even a continuous removal flux profile is determined. The resulting simultaneous removal of chemical components during reaction is very complex and requires the consideration of additional phenomena within a sophisticated design and intensification framework, e.g. mass transfer, phase equilibria, etc. Nevertheless, it is an interesting task for the future to utilize this framework for this purpose. On the same level the FPA provides, so far, information about the qualitative process structure, the impact of position and number of recycle and removal streams, and possible sizes of those, which reduces the search space and the computational effort for further flow sheet optimization with e.g. SS optimization. The next step is the synthesis of integrated processes, in which dosing, recycling and removal streams within the flow sheet are connected. This is very challenging because the optimization of those streams would be interdependent and, furthermore, it would be necessary to consider more detailed separator models to ensure that the streams can be connected.

As hinted already in subchapter 3.2.2, it might be possible to automate the synthesis via FPA by inclusion of certain features directly to the dynamic optimization problem, or by carrying out the optimization within a loop extended by decision algorithms which choose promising candidates based on predefined performance limits. Therefore, heuristics have to be implemented based on reaction engineering knowledge. However, this would counteract the clear benefit of the presented approach that the engineer can either analyze results on different synthesis levels to steer the synthesis procedure or intervene within the synthesis procedure to add options such as intensifications, realization with special units, further constraints, etc. A further interesting potential lies in the preliminary reduction of the possible reactor-network by e.g. parameterization of the control fluxes. A parsimonious parameterization of the control fluxes to predefined numbers of input actions would result in reactor-networks of a maximum size equal to these numbers of input actions. In case, the forms of the control arcs are restricted as well, the procedure would be simplified significantly, and an automation of the synthesis is realistic as the requirement of engineering knowledge is reduced.

Furthermore, it might reveal interesting synergy effects when including the systematic generation approach of Hillestad [47,48] for reactor-network synthesis within the FPA, since it as well based on optimal control calculations. In contrast to the first synthesis level of the FPA, where the analysis of dosing fluxes and differential selectivity leads to information about beneficial mixing characteristics, the decision about the latter is done by the solver and, thus, does not require additional action by a decision-maker. Therefore, a thorough comparison of these two methods is still required, which was out of scope of this work.

Last but not least, the entire approach bases on solving dynamic optimization problems that, in case of high complexity, suffer from finding local solutions or no solutions at all due to numerical issues. A simple example for such an issue is the size of the numerical grid for the discretization of the time horizon, i.e. the number of finite elements (see A.7 for details), which might influence the result. Thus, either the automated software or the design engineer has to take this into account when analyzing the flux profiles.

4 Reactor design under uncertainty

In this chapter a systematic framework for the design of chemical reactors under uncertainty is introduced. Within the EPF methodology the dynamic optimization based reactor design approach is extended to account for the impact of different types of uncertainties, which arise during the design procedure, on the optimal reactor performance. This includes three aspects classifying this approach clearly within the branch of robust design optimization:

- Finding a design which is feasible for all possible occurring uncertainty scenarios, i.e. identifying a robust design.
- Identifying reactor designs with small deviation from the expected performance, i.e. maximizing its predictive power.
- Quantifying the impact of uncertain variables on the reactor performance, i.e. its sensitivity with respect to the uncertainties.

At first, the crucial types of uncertainties are identified and their role within the design procedure is analyzed. To include the uncertainties into the dynamic optimization problem, the *unscented transformation* (UT) is used allowing a rapid and easy to implement propagation of the moments of probability density functions (PDF), which describe the uncertainties, through the nonlinear process model. Therefore, the theory of the sigma point approach is elucidated and the mathematical formulation of the dynamic optimization problem with embedded sigma point approach is shown. Subsequently, the framework is applied to the hydroformylation process example introduced in subchapter 2.3.

The first application of this approach is demonstrated in subchapter 4.2, where a robust reactor design is determined accounting for model parameter uncertainties in the kinetic model and the gas-liquid solubilities. The result is then used to identify the most relevant model parameters via a global sensitivity analysis with Sobol indices. For the sake of validation, the results of the uncertainty quantification of the model parameters are compared to Monte-Carlo simulations applying the same optimal control profiles to the process.

In a second step, imperfect realizations of the distributed control profiles are treated as a kind of process noise influencing the performance of the process in subchapter 4.3. As an example, the impact of deviations from the optimal temperature control on the hydroformylation reaction performance is quantified. Subsequently, the interdependencies between temperature control deviations and model parameter uncertainties are identified by consideration of both types of uncertainties simultaneously. This is carried out for two different possible reactor realizations for the hydroformylation reaction to analyze and compare their robustness properties.

Finally, the advantages and disadvantages of the presented framework are discussed in subchapter 4.4, and it is classified within existing state-of-the-art methods. In addition, an outlook for future scientific work in this area is given.

4.1 Methodical framework

In subchapter 2.2 it was already discussed, how uncertainties are classified typically in literature and which different kind of strategies exist to cope with uncertainties within process design approaches. The presented framework for reactor design under uncertainty does not follow these classical ways. Instead, it is derived from the basic concept of the EPF methodology, namely the travelling fluid element. Starting from this notion it is discussed: (i) which types of uncertainty arise in the design procedure and in which step they might be included (4.1.1); (ii) how the uncertainties can

be propagated through the chemical process and which information about their distribution characteristics have to exist, e.g. real data is available, a standard distribution is a reasonable assumption, or only upper and lower bounds are known (4.1.2); and (iii) how the dynamic optimization problem is extended including the uncertainties intending to create an approach for reactor design under uncertainty, both considering static or dynamic uncertainties.

4.1.1 Types of uncertainty within the EPF reactor design procedure

A reactor design approach within the EPF framework was already developed by Peschel et al. [4], see subchapter 2.1.1. Their 3-level procedure aims at a stepwise design starting from the dynamic optimization of the fluid element and its control fluxes, continuing by translation into a distributed reactor and choosing suitable control variables, and finalizing by deriving a technical realization of the optimal control profiles in an intensified reactor unit. Both this approach and the design of optimal reactor networks via *flux profile analysis*, see chapter 3, base in the first step on the dynamic optimization of external and internal fluxes, which manipulate the ideally mixed fluid element on its way through the process, only taking into account fundamental phenomena, i.e. chemical reaction and, in case of multiphase processes, phase equilibria, which provide information about bounds of corresponding state variables. Although the presented approach for reactor design under uncertainty is not following the same 3-level route and, moreover, does not intend to put an emphasis on process intensification, the following identified types of uncertainties are associated with these three design levels. This allows for a straightforward extension of the 3-level design approach by uncertainties and enables the analysis of critical uncertain phenomena at different stages of the design procedure. Three essential types of uncertainties are identified and their occurrence during the design procedure is discussed:

- Model uncertainties: The first type of uncertainty affecting the design procedure is uncertainty of the underlying model basis. In literature it is treated quite often and classified as internal or endogenous uncertainties [71]. The mathematical models used for e.g. reaction kinetics can naturally not perfectly match the real behavior due to e.g. insufficient data for the parameter estimation or an inaccurate model structure or measurement noise. Thus, the result of a deterministic dynamic optimization not taking these uncertainties into account will deviate from the real behavior with high probability. For instance, uncertain reaction kinetics changes the actual rates within the network and, thus, the performance of the process. In Fig. 4.1 it is exemplarily illustrated, where this type of uncertainty affects the fluid element. Accounting for an inaccurate model structure within the design process is hardly possible and has to be done by suitable model discrimination during the model identification. Whereas model parameter uncertainties originating from insufficient data and the resulting lack of identifiability of the parameters can be considered more easily during the design process. Therefore, the knowledge about their nominal values has to be augmented during the parameter estimation by information about their probability distributions or at least their confidence intervals. In the latter case, at least a reasonable assumption with respect to probability distributions within the confidence intervals can be made. Since this type of uncertainty affects the entire design procedure, it is reasonable to

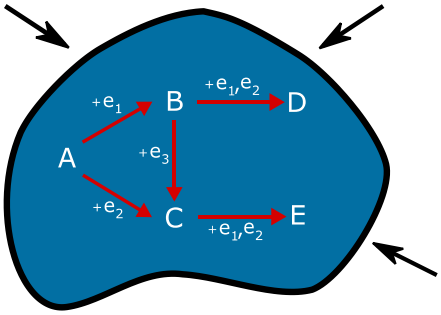

Figure 4.1: Fluid element with model uncertainties

associate it with the first design level of the reactor design approach of Peschel et al. [4] where the maximum potential of the process is identified, which is thereby extended by information about the risk to miss it.
Model parameter uncertainties are normally treated as static uncertainty as the model parameters do not change along the reaction coordinate.

- Non-ideal reactor characteristics: The second identified type of uncertainty during process design within the EPF framework is rather a consideration of non-ideality in the reactor behavior than a classical uncertainty. Originally, the fluid element is assumed to be ideally mixed. However, in a real reactor gradients arise either axial or radial, e.g. inside the flow field leading to a non-uniform residence time distribution (RTD), or in any other field such as pressure or temperature. This leads to a heterogeneous field in the notion of the fluid element (Fig. 4.2). Accounting for these phenomena within a reactor design procedure requires rigorous modeling resulting in higher computational effort. Moreover, the actual characteristic of the reactor is not known at this stage of the design procedure. Thus, it is reasonable to first analyze the impact of these phenomena on the reaction performance in order to assess whether a rigorous modeling of certain phenomena is crucial or the initial ideality assumption is sufficient. These phenomena come into play when transferring the fluid element into a distributed reactor, i.e. from batch to continuous operation where typically axial and radial gradients may arise, or a scale-up where a homogeneous mixing is complicated. Therefore it is associated with the second level within the reactor design approach of Peschel et al. [4]. Note, that the information of required modeling steps or impact of certain reactor characteristics are also very useful for the subsequent level of technical realization.
  Non-idealities in the reactor behavior can either be static or dynamic. In the former case they can be treated as parametric uncertainty, whereas in the latter case it becomes more complex to account for them, see discussion in subchapter 4.4.

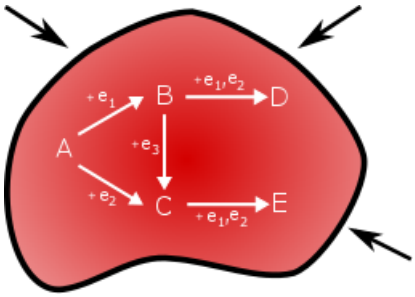

Figure 4.2: Fluid element with non-ideal field characteristics

- Imperfect control realizations: The third class of uncertainty corresponds to another characteristic feature of the EPF based reactor design, namely the realization of the optimal control profiles along the reaction coordinate. This uncertainty can be interpreted as a kind of noise on the realization of the control profiles and is a typical kind of disturbance treated in control of chemical processes. The origins of these disturbances are e.g. imperfectly working controllers or actuators. However, since the presented approach targets the design of a new reactor and not the control of an operating reactor, one can think additionally of inaccurate construction of the reactor unit, e.g. leading to a varying wall thickness or membrane permeability. To cope with those effects during the reactor design procedure, the control profiles are assumed to be deviating from the nominal optimal values at each point of the reaction coordinate (Fig. 4.3). As this type of uncertainty treats the imperfect realization of the optimal control profiles, it is associated

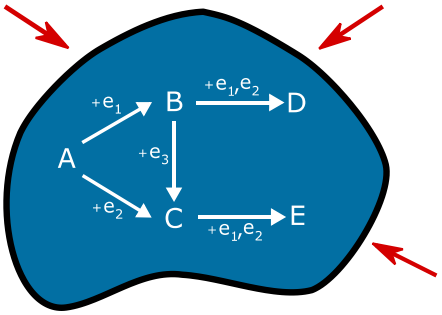

Figure 4.3: Fluid element with imperfect control realization

with the third level of the reactor design approach of Peschel et al. [4] where the technical realization is conducted. It allows to quantify the impact of control deviations on the possible realization options and the selection of more robust and, thus, easier controllable reactor realizations.
Due to the distributed nature of these imperfect control realizations, they are treated as dynamic uncertainty. In subchapter 4.1.3 it is elucidated how dynamic uncertainties are included within the dynamic optimization formulation in contrast to static uncertainties.

It has to be mentioned, that these types of uncertainty do not have to be treated separately. In practice it is rather likely that they affect the process simultaneously and, thus, a combined analysis is reasonable. This will be demonstrated in subchapter 4.3.3 for the hydroformylation process example. Moreover, although the previous association of the different types of uncertainties to the levels of the reactor design approach of Peschel et al. [4] is suitable and allows for uncertainty quantification of different kind on each level, latter can be carried out independently of these three design levels. Staying with the dynamic optimization formulation on level one, which corresponds to the basic dynamic optimization of the EPF methodology, the uncertainty quantification of the different types of uncertainty can be carried out each by each or in different combinations of interest without changing the model basis as done from level to level in the 3-level reactor design approach, see [166].

4.1.2 Propagation of uncertainties through the chemical process

The dynamic optimization problem of the EPF methodology has to be extended to include the aforementioned uncertainties. How to do this strongly depends on the available information about the uncertainty distributions. In process design studies under uncertainty it is widespread to consider lower and upper bounds of the uncertain variables or investigate a kind of worst and/or best case estimation. Therefore, mostly scenario based approaches, e.g. two-step stochastic programming [84], or Monte Carlo based approaches [81] are used. In case sufficient information about the distributions of the uncertainties is available, the same methods can be used and the scenarios are chosen to approximate these distributions as good as possible. Obviously, the accuracy of this procedure increases with the number of scenarios, i.e. samples from the distribution function, approximating the original distribution function and, thus, suffers from increasing computational effort. For the optimal reactor design within the EPF framework based on dynamic optimization, the approach of considering numerous scenarios is barely applicable. A smart way to overcome this problem is based on the assumption, that the main impacts of the uncertainties on the process performance can sufficiently be determined by taking characteristic information about the distributions of the uncertainties, i.e. the first two statistical moments, to describe the underlying PDF. A nonlinear transformation method, called *unscented transformation*, developed by Julier and Uhlmann [167] can be used to propagate these statistical moments of the uncertainty PDF through a nonlinear system such as a chemical process.

Unscented transformation

The basic idea of the *unscented transformation* (UT) is the representation of the moments of a PDF via so-called sigma points which, in case of appropriate choice, allow to describe the first and second statistical moments, i.e. the mean and the variance, of the output of a nonlinear system. The intuition of this idea is that “with a fixed number of parameters it should be easier to approximate a Gaussian distribution than it is to approximate an arbitrary nonlinear function” [167]. It can be seen as a minimalistic Monte Carlo method due to its superficial resemblance. However, instead of randomly drawing samples, the samples are deterministically chosen so that they capture specific information about the original distribution function. The procedure starts with generating $2n_{\boldsymbol{\theta}}$ sigma points $\boldsymbol{\theta}_i$ (Eq.

(4.2)) around the mean value $\boldsymbol{\theta}_0$ (Eq. (4.1)) describing precisely the variance matrix $Cov(\boldsymbol{\theta})$ and the mean value $E(\boldsymbol{\theta})$ of the symmetric, unimodal input density function $\rho_{\boldsymbol{\theta}}(\boldsymbol{\theta})$ of the $n_{\boldsymbol{\theta}}$-dimensional random variable vector $\boldsymbol{\Theta}$.

$$\boldsymbol{\theta}_0 = E(\boldsymbol{\theta}) \tag{4.1}$$

$$\boldsymbol{\theta}_i = \boldsymbol{\theta}_0 + sgn(n_{\boldsymbol{\theta}} - i)\sqrt{(n_{\boldsymbol{\theta}} + \lambda)}\sqrt{Cov(\boldsymbol{\theta})}_i, \qquad i = 1..2n_{\boldsymbol{\theta}} \tag{4.2}$$

In Eq. (4.2) $\sqrt{Cov(\boldsymbol{\theta})}_i$ is the ith row or column of the matrix square root of $Cov(\boldsymbol{\theta})$ and sgn is the signum function. The sigma points $\boldsymbol{\theta_i}$ with $i = 0, 1 \dots 2n_{\boldsymbol{\theta}}$ are transformed via the nonlinear transformation $\boldsymbol{h}(\boldsymbol{\theta_i}) = \boldsymbol{o_i}$ to yield the set of transformed sigma points in the range $\mathbb{R}^{n_{\boldsymbol{h}}=n_{\boldsymbol{o}}}$ of $\boldsymbol{h}$. With this set, mean and covariance in the range of $\boldsymbol{h}$ can be calculated via

$$E(\boldsymbol{o}) = \sum_{i=0}^{2n} w_i\, \boldsymbol{o}_i, \tag{4.3}$$

$$Cov(\boldsymbol{o}) = (1 - \alpha^2 + \beta)\{\boldsymbol{o}_0 - E(\boldsymbol{o})\}\{\boldsymbol{o}_0 - E(\boldsymbol{o})\}^{\mathrm{T}} + \sum_{i=1}^{2n} w_i \{\boldsymbol{o}_i - E(\boldsymbol{o})\}\{\boldsymbol{o}_i - E(\boldsymbol{o})\}^{\mathrm{T}}. \tag{4.4}$$

The weighting factors are

$$w_0 = \frac{\lambda}{n_{\boldsymbol{\theta}}+\lambda}, \quad w_i = \frac{1}{2(n_{\boldsymbol{\theta}}+\lambda)}, \quad i = 1 \dots 2n_{\boldsymbol{\theta}}. \tag{4.5}$$

The tuning parameter λ, with $\lambda \in \mathbb{R}$, is calculated via $\lambda = \alpha^2(n_{\boldsymbol{\theta}} + \kappa) - n_{\boldsymbol{\theta}}$. For selecting the tuning parameters α, β and κ Julier and coworkers suggested some rules of thumb depending on knowledge of the parameter distribution functions of the random variables. The tuning parameters β and κ are considered to include prior knowledge about the fourth and higher order moments of the input distribution function. The fourth statistical moment, i.e. the kurtosis k, can be accounted for by complying with the restriction $k = \kappa + n_{\boldsymbol{\theta}}$. For a Gaussian input PDF $\rho_{\boldsymbol{\theta}}(\boldsymbol{\theta}) \sim \mathcal{N}(E(\boldsymbol{\theta}), Cov(\boldsymbol{\theta}))$ the kurtosis is hence best matching for $3 = \kappa + n_{\boldsymbol{\theta}}$ [167]. Although there is no restriction for the sign of κ, a negative value might lead to a non-positive semi-definite $Cov(\boldsymbol{o})$. In this case, it is suggested to neglect the first part of Eq. (4.4), i.e. vanishing the impact of the zeroth sigma point on the $Cov(\boldsymbol{o})$ [168]. The parameter β is also a function of the kurtosis, but it only influences the weighting of the output variances and not, as κ, the choice of the sigma points. For Gaussian distributions it is recommended to use $\beta = 2$ [169]. In case $|\kappa + n_{\boldsymbol{\theta}}|$ becomes very small, the sigma points are very close to the mean values and the approximation merge to a Taylor approximation of second order, which requires the determination of the Jacobian and Hessian [168]. The parameter α is a scaling factor, which controls the spread of the sigma points. This spread increases with the number of random variables $n_{\boldsymbol{\theta}}$, though the spread in their PDFs do not change. This might lead to infeasible solutions for sigma points far away from the mean value in case of unscaled use of the UT. It should lie within $0 \leq \alpha \leq 1$. In case of $\alpha = 0$ the modified UT is achieved, whereas $\alpha = 1$ leads to the original formulation without scaling [170]. The suitable choice of the tuning parameters α, β, κ always depends on the specific problem and, thus, there exist no global optimal tuning or generic tuning rules [171]. The UT with sigma points has several advantages:

- The errors of the expectation estimate is of fourth and higher order, whereas the variance–covariance estimates have an error of fourth and higher order, too [167]. This only holds for scalars, ($n_{\boldsymbol{\theta}} = 1$), as elucidated by Gustafsson and Hendeby [172]. For higher numbers of $n_{\boldsymbol{\theta}}$ the tuning factors have to be adapted appropriately.
- There is no need for calculating the derivatives, i.e. Jacobian or even Hessian, which makes it a robust and efficient approach. Although additional function evaluations on the

sigma points are available, the computational cost is comparable to the gradient-based calculation of first order [173].

- Due to the deterministic sampling the computational effort scales linearly ($2n_{\boldsymbol{\theta}} + 1$) with the number of random variables $n_{\boldsymbol{\theta}}$ [167].
- Compared to linearization methods, the UT uses second and even higher order information, e.g. kurtosis, of the PDFs describing the random variables [167].
- Parallelization can easily be applied to speed up estimate calculation of the transformed expectation and variance–covariance, because each sigma point is independently propagated [174].
- Every kind of input PDF can be mapped via UT through a non-linear system by describing the PDF with Gaussian mixed distributions [173].

The UT was used for several applications in literature: Julier and Uhlmann applied it for filtering stochastic systems by incorporating noise to the nonlinear transformation [175]; the same authors used the UT for filtering of non-linear systems overcoming drawbacks of the extended Kalman filter [176]; Heine et al. [177] employed it for the design of robust model predictive controllers; the design of robust optimal process trajectories using the UT was introduced by Rossner et al. [178]; and other authors incorporated it in frameworks for optimal design of experiments ([179], [174]). By developing a generalized selection procedure of the sigma points, Julier and Uhlmann enable an approximation accuracy of fourth order using $2n_{\boldsymbol{\theta}}^2 + 1$ sigma points [180] or a minimalized formulation using $n_{\boldsymbol{\theta}} + 1$ sigma points within a $n_{\boldsymbol{\theta}}$-dimensional simplex [181]. Furthermore, Julier [182] extended the UT for the use of skewed input distribution functions.

Robust reactor design framework using unscented transformation

Embedding the *unscented transformation* within the dynamic optimization of the fluid element allows creating a framework for reactor design under uncertainty in which the different types of uncertainty, see subchapter 4.1.1, can be included and their impact on the reactor performance can be quantified or minimized. At first, the PDF of the uncertain variable is defined by its first two statistical moments, i.e. the mean and the variance. This information is used to create the sigma points with Eqs. (4.1)-(4.2) to approximate the PDF.

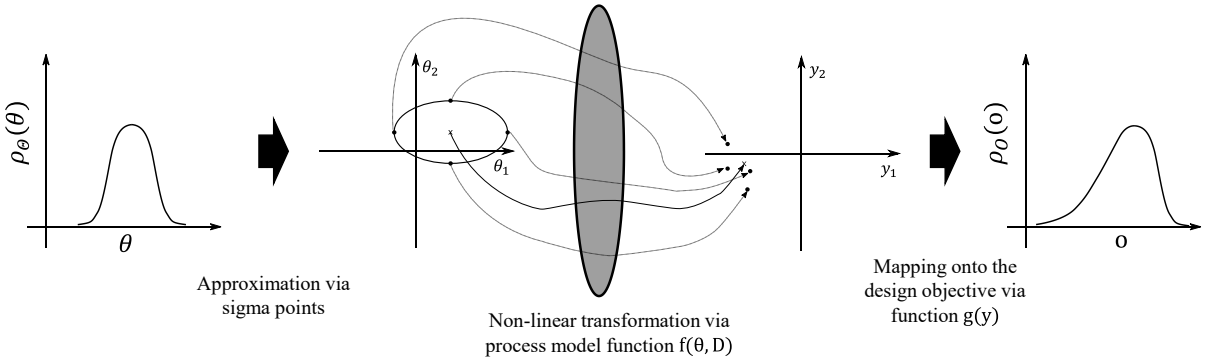

Figure 4.4: Nonlinear uncertainty propagation with *unscented transformation* on sigma points

Subsequently, the nonlinear transformation $\boldsymbol{h}(\boldsymbol{\theta}, D) = \boldsymbol{g}\big(\boldsymbol{f}(\boldsymbol{\theta}, D)\big)$ is carried out, whereby an optimal control of the process and optimal design parameters combined in the reactor design D are determined by the dynamic optimization under influence of the random variables $\boldsymbol{\theta}$. Note, that $\boldsymbol{h}(\boldsymbol{\theta}, D)$ is decomposed into a function $\boldsymbol{f}$, which maps random variables onto the model states, and a function $\boldsymbol{g}$, which maps the process state variables onto the space of design objectives. By changing the reactor

design D, the nonlinear transformation $\boldsymbol{O} = \boldsymbol{h}(\boldsymbol{\theta}, D)$ is varied and mean and variance of the objective are changed. The entire uncertainty propagation is illustrated in Fig. 4.4.

4.1.3 Mathematical formulation of dynamic optimization under uncertainty

The generic dynamic optimization problem formulated within the EPF methodology is introduced in subchapter 3.1 (Eqs. (3.1)-(3.6)). The extension of its formulation for inclusion of uncertainties depends on the type of uncertainty, especially whether it is of static or dynamic nature.

Static uncertainty

Static uncertainty indicates a parametric randomness, which does not change along the reaction coordinate, e.g. model parameter uncertainty. Their consideration requires an individual solving of all model equations on each sigma point and a final summation of the crucial states for determination of the objective, or rather its statistical moments. Therefore, the aforementioned generic, deterministic dynamic optimization problem is extended by: (i) the calculation of the sigma points from the moments of the uncertainty PDFs (Eqs. (4.12)-(4.13)); (ii) the parallelization of model equations evaluations on all sigma points (Eqs. (4.7)-(4.8)); and (iii) the final calculation of the statistical moments of the objective from the dependent states, which are distributed on the sigma points (Eqs. (4.14)-(4.16)). Moreover, the objective is changed to its expected value (Eq. (4.6)). The resulting robust dynamic optimization problem (RDOP) is stated as:

$$\min_{\boldsymbol{u}(t),\boldsymbol{\xi}} -E(\boldsymbol{o}) \tag{4.6}$$

$$\text{s.t. } \boldsymbol{C}\big(\boldsymbol{x}_i(t,\boldsymbol{\theta}_i)\big)\cdot\frac{d\boldsymbol{x}_i(t,\boldsymbol{\theta}_i)}{dt} = \boldsymbol{F}\cdot\boldsymbol{j}\big(\boldsymbol{x}_i(t,\boldsymbol{\theta}_i)\big), i \in SP \tag{4.7}$$

$$\boldsymbol{g}\big(\boldsymbol{x}_i(t,\boldsymbol{\theta}_i)\big) = \boldsymbol{0}, \boldsymbol{h}\big(\boldsymbol{x}_i(t,\boldsymbol{\theta}_i)\big) \le \boldsymbol{0}, i \in SP \tag{4.8}$$

$$\boldsymbol{u}^L \le \boldsymbol{u}(t) \le \boldsymbol{u}^U \tag{4.9}$$

$$\boldsymbol{\xi}^L \le \boldsymbol{\xi} \le \boldsymbol{\xi}^U \tag{4.10}$$

$$\boldsymbol{x}_i(t_0,\boldsymbol{\theta}_i) = \boldsymbol{x}_{0,i}(\boldsymbol{\theta}_i), \boldsymbol{x}\big(t_f,\boldsymbol{\theta}_i\big) = \boldsymbol{x}_{f,i}(\boldsymbol{\theta}_i), i \in SP \tag{4.11}$$

$$\boldsymbol{\theta}_0 = E(\boldsymbol{\theta}) \tag{4.12}$$

$$\boldsymbol{\theta}_i = \boldsymbol{\theta}_0 + sgn(n_{\boldsymbol{\theta}} - i)\sqrt{(n_{\boldsymbol{\theta}} + \lambda)}\sqrt{Cov(\boldsymbol{\theta})}_i, i = 1..2n_{\boldsymbol{\theta}} \tag{4.13}$$

$$E(\boldsymbol{o}) = \sum_{i=0}^{2n} w_i\, \boldsymbol{o}_i, i \in SP \tag{4.14}$$

$$Cov(\boldsymbol{o}) = (1 - \alpha^2 + \beta)\{\boldsymbol{o}_0 - E(\boldsymbol{o})\}\{\boldsymbol{o}_0 - E(\boldsymbol{o})\}^{\mathrm{T}} + \sum_{i=1}^{2n} w_i \{\boldsymbol{o}_i - E(\boldsymbol{o})\}\{\boldsymbol{o}_i - E(\boldsymbol{o})\}^{\mathrm{T}}, i \in SP \tag{4.15}$$

$$w_0 = \frac{\lambda}{n_{\boldsymbol{\theta}} + \lambda}, \quad w_i = \frac{1}{2(n_{\boldsymbol{\theta}} + \lambda)}, i = 1 \dots 2n_{\boldsymbol{\theta}} \tag{4.16}$$

$$\boldsymbol{o}_i = \int_0^{t_f} L\big(\boldsymbol{x}_i(t,\boldsymbol{\theta}_i)\big)dt + I\left(\boldsymbol{x}_{0,i}(\boldsymbol{\theta}_i)\right) + W\left(\boldsymbol{x}_{f,i}(\boldsymbol{\theta}_i)\right), i \in SP. \tag{4.17}$$

Dynamic uncertainty

In case of dynamic uncertainty, its influence is distributed along the reaction coordinate and has to be incorporated in each time evaluation of the model equations independently. Again, the objective is changed to its expected value (Eq. (4.18)) and the sigma points of the random variable(s)

are calculated according to the rules introduced in the previous subchapter (Eqs. (4.24)-(4.25)). However, due to the distributed influence of the uncertainty, the states do not evolve deterministically over time. Instead, the evaluation of the statistical moments is carried out for the states at every time step and the resulting expected value is propagated further over time, see Eqs. (4.19), (4.20) and (4.30). The resulting RDOP is stated as:

$$\min_{\boldsymbol{u}(t),\boldsymbol{\xi}} -E(\boldsymbol{o}) \tag{4.18}$$

$$\text{s.t. } \boldsymbol{C}\left(E\left(\boldsymbol{x}_i(t,\boldsymbol{\theta}_i)\right)\right)\cdot\frac{dE\left(\boldsymbol{x}_i(t,\boldsymbol{\theta}_i)\right)}{dt} = \boldsymbol{F}\cdot\boldsymbol{j}(E\left(\boldsymbol{x}_i(t,\boldsymbol{\theta}_i)\right)), i \in SP \tag{4.19}$$

$$\boldsymbol{g}\left(E\left(\boldsymbol{x}_i(t,\boldsymbol{\theta}_i)\right)\right) = \boldsymbol{0}, \boldsymbol{h}\left(E\left(\boldsymbol{x}_i(t,\boldsymbol{\theta}_i)\right)\right) \leq \boldsymbol{0}, i \in SP \tag{4.20}$$

$$\boldsymbol{u}^L \leq \boldsymbol{u}(t) \leq \boldsymbol{u}^U \tag{4.21}$$

$$\boldsymbol{\xi}^L \leq \boldsymbol{\xi} \leq \boldsymbol{\xi}^U \tag{4.22}$$

$$\boldsymbol{x}_i(t_0,\boldsymbol{\theta}_i) = \boldsymbol{x}_{0,i}(\boldsymbol{\theta}_i), \boldsymbol{x}\left(t_f,\boldsymbol{\theta}_i\right) = \boldsymbol{x}_{f,i}(\boldsymbol{\theta}_i), i \in SP \tag{4.23}$$

$$\boldsymbol{\theta}_0 = E(\boldsymbol{\theta}) \tag{4.24}$$

$$\boldsymbol{\theta}_i = \boldsymbol{\theta}_0 + sgn(n_{\boldsymbol{\theta}} - i)\sqrt{(n_{\boldsymbol{\theta}} + \lambda)}\sqrt{Cov(\boldsymbol{\theta})}_i, i = 1..2n_{\boldsymbol{\theta}} \tag{4.25}$$

$$E(\boldsymbol{o}) = \sum_{i=0}^{2n} w_i\, \boldsymbol{o}_i, i \in SP \tag{4.26}$$

$$Cov(\boldsymbol{o}) = (1 - \alpha^2 + \beta)\{\boldsymbol{o}_0 - E(\boldsymbol{o})\}\{\boldsymbol{o}_0 - E(\boldsymbol{o})\}^{\mathrm{T}} + \sum_{i=1}^{2n} w_i \{\boldsymbol{o}_i - E(\boldsymbol{o})\}\{\boldsymbol{o}_i - E(\boldsymbol{o})\}^{\mathrm{T}}, i \in SP \tag{4.27}$$

$$w_0 = \frac{\lambda}{n_{\boldsymbol{\theta}} + \lambda}, \quad w_i = \frac{1}{2(n_{\boldsymbol{\theta}} + \lambda)}, i = 1 \ldots 2n_{\boldsymbol{\theta}} \tag{4.28}$$

$$\boldsymbol{o}_i = \int_0^{t_f} L\left(\boldsymbol{x}_i(t,\boldsymbol{\theta}_i)\right)dt + I\left(\boldsymbol{x}_{0,i}(\boldsymbol{\theta}_i)\right) + W\left(\boldsymbol{x}_{f,i}(\boldsymbol{\theta}_i)\right), i \in SP \tag{4.29}$$

$$E\left(\boldsymbol{x}_i(t,\boldsymbol{\theta}_i)\right) = \textstyle\sum_{i=0}^{2n} w_i\, \boldsymbol{x}_i(t,\boldsymbol{\theta}_i), i \in SP. \tag{4.30}$$

Classically, process noise is considered as additive term in the balance equations. Thereby, at each time point of the process the states experience a certain simulated disturbance. Using the above presented formulation approximates this classical approach by describing the noise PDF with sigma points and only propagating the expected value of the states over time. That means, at every evaluated time step the expected values of the states of the previous time step is evaluated on the sigma point of the disturbed (random) variable and by applying the *unscented transformation* the expected values of the states at the current time step are determined. However, the objective evaluation is thereby not changed, see Eq. (4.26).

For solving these RDOP again a full discretization of the states and inputs using *orthogonal collocation on finite elements* is applied. The resulting discretized RDOPs both for the cases of static and dynamic uncertainty are given in the appendix (A.3) in detail, allowing the interested reader to comprehend the final implementation.

Multi-objective optimization

Both dynamic optimization problems for static and dynamic uncertainties are formulated for a robust optimization, i.e. the objective is optimized under the condition that all constraints are feasible for the considered uncertainty set. As outlined in the introduction of this chapter, a second important target of the design under uncertainty is the minimization of the uncertainty impact on the performance of the process. Therefore, the deviation from the predicted expected value has to be minimized

meaning a reduction of the corresponding variance. This can be understood as a minimization of risk to miss the predicted performance leading to a higher predictive power of the process. To include this risk measure, the variance of the objective, which is determined with the *unscented transformation*, is added to the objective of the RDOP stated above (Eq. (4.31)).

$$Obj = [-E(\boldsymbol{o}), Var(\boldsymbol{o})] \tag{4.31}$$

The resulting multi-objective optimization problem (MOOP) faces additional challenges. An excellent review on these in the field of process design can be found in 183 [183]. The major challenge is the simultaneous consideration of different objectives $J_i \in \mathbb{R}^m$ within the dynamic optimization leading to trade-offs between the m objectives. Therefore, the concept of *Pareto optimality* holds, which has the following definition: An optimal point of the decision variables $u^* \in U$, where U is the set of all feasible solutions, is Pareto optimal if and only if there does not exist another point $u \in U$ such that $J_i(u) \leq J_i(u^*)$ for all i and $J_i(u) < J_i(u^*)$ for at least one objective [184]. Following this definition, not only one unique optimal design exists. Instead, a bunch of Pareto optimal designs exist which form the Pareto set. The existing approaches for identifying the Pareto optimal solutions can be separated into vectorial methods and scalar methods. In the former case, the multi-objective optimization is directly solved with a vector-valued objective function, whereas in the latter case several objectives are transformed into a scalar function. These scalarization methods reformulate the underlying MOOP into a series of parametric single objective dynamic optimization problems. An approximation of the Pareto set is obtained by consistently varying the scalarization parameters. Several scalarization methods are reported in literature varying in complexity and accuracy, e.g. the *Method of Weighted Sum* (WS), the *ε-constraint Method* (ε-CM), *Normal Boundary Intersection* and *Enhanced Normalized Normal Constraint*, etc. For the sake of brevity not all available methods are discussed. Details can be found e.g. in [185], where a comprehensive survey is given. In the present work the *Method of Weighted Sum* and the *ε-constraint Method* are used. The WS associates the different objectives with weights allowing for an approximation of the Pareto set by varying the weights consistently. In case of the objectives stated in Eq. (4.31), the resulting scalar objective reads:

$$Obj = -\alpha E(\boldsymbol{o}) + (1-\alpha) Var(\boldsymbol{o}), \tag{4.32}$$

whereby α defines the scalarization parameter which can be varied between $0 \ldots 1$. Consequently, for $\alpha = 0$ the variance is minimized and the most robust design is identified, and for $\alpha = 1$ the highest performing design is determined corresponding to the result of the RDOPs with a single objective. In contrast to this method, the *ε-constraint Method* does not augment the original objective. Instead, it adds a constraint for the additional objectives forcing them to satisfy certain predefined bounds *ε*. For the objectives stated in Eq. (4.31), the objective and the additional constraint can have either the form:

$$Obj = -E(\boldsymbol{o}) \tag{4.33}$$
$$\text{s.t. } Var(\boldsymbol{o}) \leq \varepsilon \tag{4.34}$$

or the form:

$$Obj = Var(\boldsymbol{o}) \tag{4.35}$$
$$\text{s.t. } E(\boldsymbol{o}) \geq \varepsilon \tag{4.36}$$

whereby ε is varied to scan the desired range of the respective objective. The WS is suitable to find the extreme points of the Pareto set and to provide a first insight into the possible shape of the Pareto set.

Its drawback is, that one cannot identify concave regions and a suitable variation of the weighting parameter strongly depends on the specific problem. This might lead to kinks in the Pareto set. If the region of the Pareto set is roughly known, the ε-CM can be used to scan the Pareto set more precisely, whereby the values of ε can be chosen appropriately to the presumed shape of the Pareto set. Furthermore, it allows identifying concave regions by changing the optimized and constrained objectives, see Eqs. (4.33)-(4.34) and Eqs. (4.35)-(4.36). Due to these properties the Pareto sets in the presented work are determined by first using the WS to find reasonable ranges of the two objectives, where Pareto optimal solutions might exist, and subsequently calculate a more precise approximation of the Pareto set within these ranges via the ε-CM.

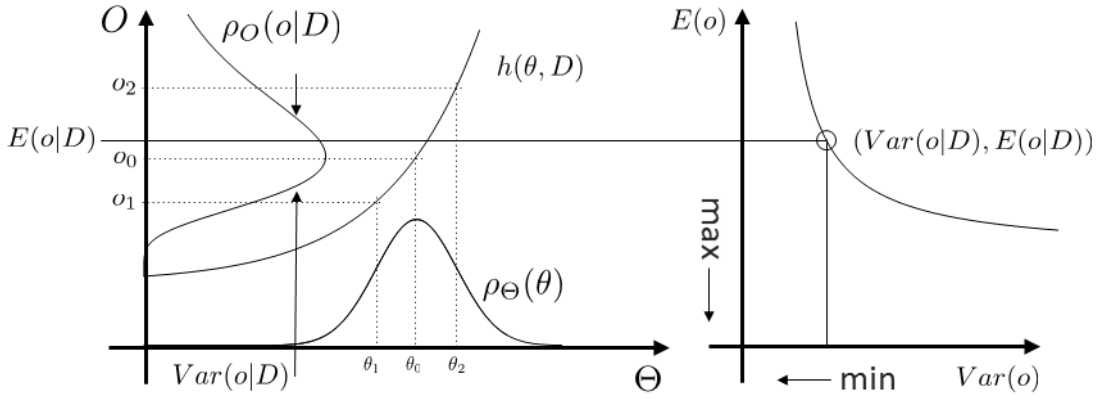

Figure 4.5: Scheme of the multi-objective robust dynamic optimization concept

The robust dynamic optimization problems introduced before (Eqs. (4.6)-(4.17) and Eqs. (4.18)-(4.30)) extended by the multi-objective optimization framework results in a multi-objective robust dynamic optimization problem (MORDOP). Its fundamental intention is schematically illustrated in Fig. 4.5. The considered uncertainty is introduced to the process design by its PDF $\rho_{\boldsymbol{\theta}}(\boldsymbol{\theta})$, which is approximately described by sigma points $\boldsymbol{\theta}_i$. Via the nonlinear transformation function $\boldsymbol{h}(\boldsymbol{\theta}, D)$, which combines the process model and the objective evaluation, the uncertainty is mapped to the objective yielding information about its expected value $E(\boldsymbol{o}|D)$ and its variance $Var(\boldsymbol{o}|D)$. This corresponds to a particular point in the Pareto set, see right side of Fig. 4.5. By varying the design D of the process, the nonlinear mapping changes, and another Pareto optimal point is found. With this approach one can find several process designs with different trade-offs between the performance of the process, i.e. the expected value, and the predictive power of the process performance, i.e. the variance, under influence of uncertainties.

4.2 Reactor design under model parameter uncertainties

In a first scenario the reactor design under uncertainty framework is applied for the case of uncertain model parameters. As example process the hydroformylation of 1-dodecene in a TMS system introduced in subchapter 2.3 is considered. Aiming at reactor designs, which are robust with respect to model parameter uncertainties, the respective parameters and their confidence intervals are introduced, and the MORDOP shown in the previous subchapter is derived and solved in subchapter 4.2.1. The Pareto set is determined, and a validation of the results is carried out using Monte Carlo simulations to achieve a qualitative and quantitative evaluation of the presented reactor design under uncertainty approach. Based on the validation results suitable tuning factors and modifications of the *unscented transformation* are identified and the determination of the Pareto set is repeated. Afterwards it is demonstrated, how the interdependency between two crucial performance measures, i.e. the

selectivity with respect to the desired product and the conversion of the main reactant, look like. In a subsequent step, the reactor design under uncertainty approach is extended by a global sensitivity analysis in order to identify the most sensitive model parameters of the process in subchapter 4.2.2.

4.2.1 Robust reactor design for the hydroformylation of 1-dodecene

Uncertain model parameters

For the uncertainty quantification of the model parameters in the process model equations additional knowledge about their uncertainty distributions is required. Hentschel et al. [157] provided confidence intervals for the estimated parameters in the reaction kinetics, which can be used to approximate their PDFs. In addition to these identified model parameters of the reaction kinetics, uncertainties in the equilibrium constants $\Delta G_2,\ \Delta G_3$ of the reactions r_2, r_3, respectively, and the Henry coefficients for the solubilities of the gaseous reactants $H_{CO}^0, H_{H2}^0, E_{A,H_{CO}}, E_{A,H_{H2}}$ are considered. The confidence intervals for the reaction rate parameters are adopted from Hentschel et al. [157] and given in Tab. 4.1. For the remaining uncertain model parameters no reference for confidence intervals is available. Thus, reasonable confidence intervals in a range of ± 10 % are assumed, see Tab. 4.2. To calculate the variances of the density functions of the uncertain model parameters the confidence intervals given in Tab. 4.1 and 4.2 are taken as two times the standard deviation

$$\sigma_{\boldsymbol{\theta}_i}{}^2 = \left(\frac{E(\boldsymbol{\theta}_i)\varepsilon_i}{2}\right)^2 \quad , \tag{4.37}$$

where $E(\boldsymbol{\theta}_i)$ are the expected values of the uncertain parameters, i.e. their deterministic values introduced in Tab. A.1, and ε_i are the confidence intervals from Tab. 4.1-4.2. Due to missing information about possible correlations, all covariances are assumed to be zero leading to a diagonal covariance matrix

$$Cov(\boldsymbol{\theta}) = diag(\sigma_{\boldsymbol{\theta}}{}^2). \tag{4.38}$$

Table 4.1: Confidence intervals of kinetic parameters and catalyst equilibrium

Variable	Eq.	$E_A\left[\frac{\text{kJ}}{\text{mol}}\right]$	k_0	Unit	$K_1\left[\frac{\text{ml}}{\text{mol}}\right]$	$K_2\left[\frac{\text{ml}}{\text{mol}}\right]$	$K_3\left[\frac{\text{ml}}{\text{mol}}\right]$
r_1	(2.2)	±33.0 %	±13.9 %	$\frac{\text{ml}^3}{\text{g min mol}^2}$	±355.0 %	±270.0 %	±1.0 %
r_2	(2.3)	±29.0 %	±9.7 %	$\frac{\text{ml}}{\text{g min}}$	±252.1 %	±21.0 %	-
r_3	(2.4)	±26.0 %	±8.5 %	$\frac{\text{ml}^2}{\text{g min mol}}$	±139.1 %	±97.2 %	±117.2 %
r_4	(2.5)	±13.0 %	±6832.3 %	$\frac{\text{ml}^2}{\text{g min mol}}$	-	-	-
r_5	(2.6)	±408.0 %	±5.1 %	$\frac{\text{ml}^3}{\text{g min mol}^2}$	-	-	-
r_6	(2.7)	-	±10.9 %	$\frac{\text{ml}^3}{\text{g min mol}^2}$	-	-	-
c_{cat}	(2.1)	-	-	-	±84.1%	-	±12.4%

Table 4.2: Assumed confidence intervals for solubility constants and equilibrium constants

Variable	ΔG_2	ΔG_3	H_{CO}^0	H_{H2}^0	$E_{A,H_{CO}}$	$E_{A,H_{H2}}$
	±10.0%	±10.0%	±10.0%	±10.0%	±10.0%	±10.0%

Robust dynamic optimization problem

The required model equations for the hydroformylation process are given in subchapter 2.3 and subchapter 3.2.3. The dynamic optimization problem, which was formulated in the course of the reactor-network synthesis in subchapter 3.2.3 (Eqs. (3.41)-(3.61)), is adopted and augmented by the model parameter uncertainties (Tab. 4.1 and 4.2, Eqs. (4.37)-(4.38)) and the *unscented transformation* equations according to subchapter 4.1.2 (Eqs. (4.1)-(4.5)). In contrast to the formulation in subchapter 3.2.3, the degree of freedom of distributed dosing of reactant is neglected and its initial value is predefined. Furthermore, the balancing of the storage tanks, the dosing constraints, and the differential selectivity calculation are removed. Following the adopted dynamic optimization problem, again the selectivity with respect to the desired linear aldehyde tridecanal S_{nC13al} is maximized subject to a preset conversion X_{nC12en} and a minimum constraint for the regio-selectivity n/iso. As elucidated in subchapter 4.1.3 the resulting MORDOP has to be solved several times for varying scalarization parameters both for the WS and the ε-CM to determine an adequate approximation of the Pareto set of the two opposite objectives, i.e. maximizing the expected value of $E(S_{nC13al})$ and minimizing the variance $Var(S_{nC13al})$. In the following the MORDOP using the ε-CM is given (Eqs. (4.39)-(4.59)), whereas the formulation using the WS can be simply achieved according to the explanation in subchapter 4.1.3.

$$\max_{T(t),p_{CO}(t),p_{H_2}(t),t_f} \; S_{nC13al}(t_f) \tag{4.39}$$

s.t. Component mass balances: $$\frac{dn_{\alpha,i}}{dt} = V_{liq}\left(c_{cat}M_{cat}\left(\sum_{m=1}^{M}\nu_{\alpha,m}r_m\right)\right), \alpha \in CH, i \in SP \tag{4.40}$$

Reaction kinetics: Eqs. (2.2)-(2.7), with $r_m = r_m(\boldsymbol{\theta}_i), m \in \{1 \dots M\}, i \in SP$ (4.41)

Catalyst equilibrium: Eq. (2.1), with $c_{cat} = c_{cat}(\boldsymbol{\theta}_i), i \in SP$ (4.42)

Constitutive equations: Eqs. (3.38)-(3.39) (4.43)

Gas solubilities: Eq. (2.11), with $H_j = H_j(\boldsymbol{\theta}_i), j \in \{CO, H_2\}, i \in SP$ (4.44)

Catalyst and solvent ratios: Eqs. (2.13)-(2.14) (4.45)

Path constraints: $\boldsymbol{n}_i(t) \geq 0, i \in SP$ (4.46)

$$10 \text{ bar} \leq p_t(t) = p_{CO}(t) + p_{H_2}(t) \leq 20 \text{ bar} \tag{4.47}$$

$$363.15 \text{ K} \leq T(t) \leq 388.15 \text{ K} \tag{4.48}$$

Terminal constraints: $$t_f \leq 100 \text{ min} \tag{4.49}$$

$$X_{nC12en,i} = \frac{n_{nC12en,i}(0) - n_{nC12en,i}(t_f)}{n_{nC12en,i}(0)} = 99\ \%, i \in SP \tag{4.50}$$

$$S_{nC13al,i} = \frac{n_{nC13al,i}(t_f) - n_{nC13al,i}(0)}{n_{nC12en,i}(0) - n_{nC12en,i}(t_f)}, i \in SP \tag{4.51}$$

$$n/iso_i = \frac{n_{nC13al,i}(t_f)}{n_{nC13al,i}(t_f) + n_{iC13al,i}(t_f)} \geq 95\ \%, i \in SP \tag{4.52}$$

Initial conditions: $$\boldsymbol{n}_i(t=0) = \boldsymbol{n}_{0,i} = \begin{cases} 1, & l \in \{nC12en\} \\ 0, & l \in \{CH/nC12en\} \end{cases}, i \in SP \tag{4.53}$$

Uncertain model parameters: $$\boldsymbol{\theta} = [k_1, k_2, k_3, k_4, k_5, k_6, K_{cat,1}, K_{cat,2}, \dots \Delta G_{r_2}, \Delta G_{r_3}, H^0_{CO}, H^0_{H2}, E_{A,H_{CO}}, E_{A,H_{H2}}]^{\mathrm{T}} \tag{4.54}$$

Unscented transformation: $$\boldsymbol{\theta}_0 = E(\boldsymbol{\theta}) \tag{4.55}$$

$$\boldsymbol{\theta}_i = \boldsymbol{\theta}_0 + sgn(n_{\boldsymbol{\theta}} - i)\sqrt{(n_{\boldsymbol{\theta}} + \lambda)}\sqrt{Cov(\boldsymbol{\theta})}_i, i \in SP \tag{4.56}$$

$$E(S_{nC13al}) = \sum_{i=0}^{2n} w_i\, S_{nC13al_i}, i \in SP \tag{4.57}$$

$$Var(S_{nC13al}) = (1-\alpha^2+\beta)\{S_{nC13al_0} - E(S_{nC13al})\}\{S_{nC13al_0} - E(S_{nC13al})\}^{\mathrm{T}} + \sum_{i=1}^{2n} w_i \{S_{nC13al_i} - E(S_{nC13al})\}\{S_{nC13al_i} - E(S_{nC13al})\}^{\mathrm{T}}, i \in SP \quad (4.58)$$

ε-CM constraint: $$Var(\boldsymbol{o}) \leq \varepsilon \quad (4.59)$$

The set of uncertain parameters is defined in Eq. (4.54). For those the sigma points (SP) are determined and the corresponding equality constraints, i.e. the reaction kinetics, the catalyst equilibrium, and the gas solubilities (Eqs. (4.41), (4.42), and (4.44)), are defined as function of the SP. The evaluation of the component mass balances and all state dependent constraints are conducted on the SP as well (Eqs. (4.40), (4.46), (4.50)-(4.53)).

Pareto set of optimal designs under model parameter uncertainties

For the different RDOPs solved to determine the set of Pareto optimal solutions, the tuning parameters of the UT are selected to be $\alpha = 1, \beta = 2$ and $\kappa = -11$. As elucidated in subchapter 4.1.2, $\alpha = 1$ yields the unscaled UT which seems to be a reasonable first choice since no heuristic knowledge about a suitable scaling is available. $\beta = 2$ is recommended for Gaussian distributions [169] and $\kappa = -11$ results from the heuristic rule that $n_\theta + \kappa = 3$ [167]. The Pareto set is constructed by optimization results for varying ε in bounds which are determined by a preliminary run with the WS method. The resulting Pareto set is depicted in Fig. 4.6 and shows the maximum expected values of the selectivity with respect to tridecanal, $E(S_{nC13al})$, over the variance of the same measure, $Var(S_{nC13al})$. Evidently, the set is convex implying that the first objective, $max\, E(S_{nC13al})$, cannot be improved without downgrading the second objective, $min\, Var(S_{nC13al})$.

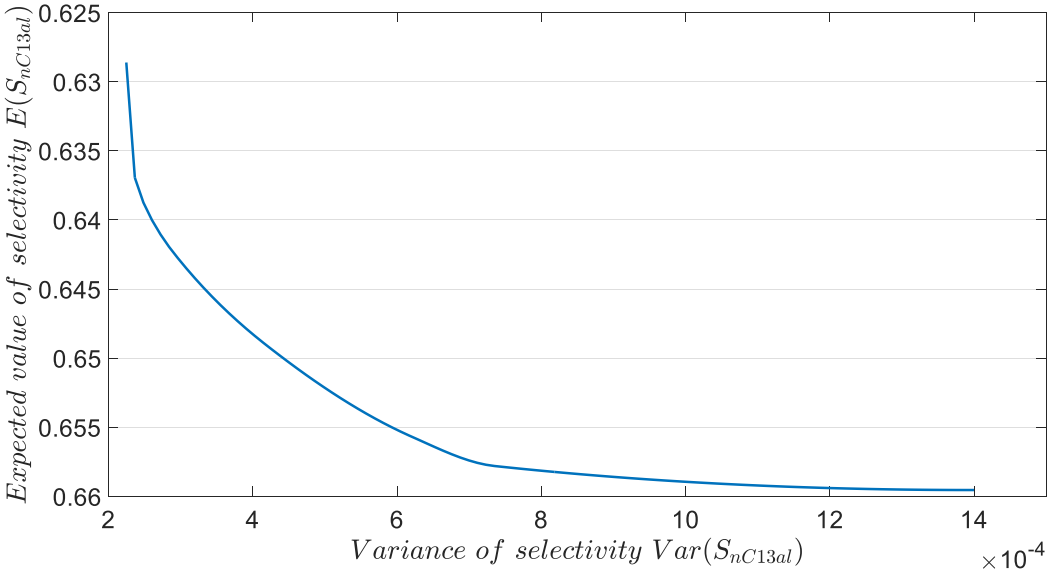

Figure 4.6: Set of Pareto optimal solutions resulting from the MORDOP for robust reactor design in Eqs. (4.39)-(4.59)

The highest performance is reached at $E(S_{nC13al}) = 65.95\,\%$ with a predicted variance of $Var(S_{nC13al}) = 14\,\%$. Thus, with a 95 % likelihood the selectivity would lie in the range of $58.47\,\% \leq S^{2\sigma}_{nC13al} \leq 73.43\,\%$, which means a very low predictive power of the reactor performance. This is highest when choosing the very left point at $E(S_{nC13al}) = 62.86\,\%$ with a variance $Var(S_{nC13al}) = 2.247\,\%$ which corresponds of a 2σ range of $59.88\,\% \leq S^{2\sigma}_{nC13al} \leq 65.84\,\%$. Since all points are optimal, or rather Pareto optimal, the decision-making about the best design is about

selecting the most acceptable trade-off. This decision requires either a clear bound for one of the objectives or more knowledge about their impacts on the overall process.

Validation via Monte Carlo simulations and tuning of UT parameters

Due to the approximate nature of the UT, the accuracy of the results of the MORDOP has to be quantified. Therefore, the predicted expected values and variances of the Pareto optimal designs are evaluated using Monte Carlo (MC) simulations. For $\#_{MC} = 10000$ samples of the Gaussian distributed model parameter uncertainties each design is simulated using the same model as employed for the MORDOP, see Eqs. (4.39)-(4.59). As result pairs $[E(S_{nC13al}), Var(S_{nC13al})]$ are achieved for each of the Pareto optimal designs, forming themselves a Pareto set. A comparison of the original solutions of the MORDOP and their corresponding MC results is shown in Fig. 4.7 a).

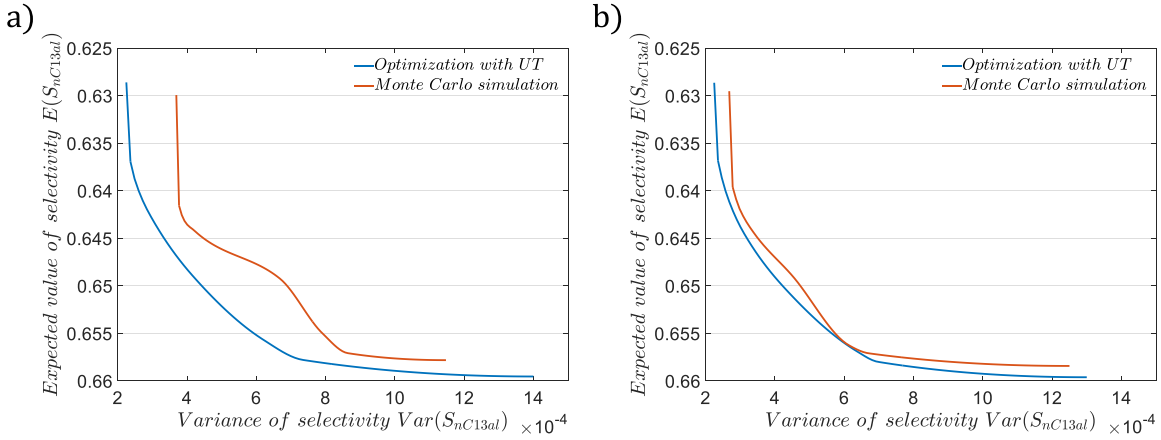

Figure 4.7: Comparison of the results achieved by solving a Monte Carlo simulation and the MORDOP for robust reactor design (Eqs. (4.39)-(4.59)) for: a) the original tuning factors and modification of the UT, and b) the refined tuning factors and modification of the UT

Although the values lie in a similar range, their matching is not very accurate, which means the Pareto optimal reactor designs determined with the UT are not highly reliable. To improve the accuracy of the approximation with the UT, several modifications and tuning factor configurations have been checked. The analysis revealed that due to the negative value of κ the approximation with the UT is improved using its modified version, which is recommended by Julier and Uhlmann [168] in this case. Following the formulation in Eqs. (4.56)-(4.58), $\alpha = 1$ and $\kappa = -11$ stay the same and β is set to 0 leading to $(1 - \alpha^2 + \beta) = 0$, which corresponds to the condition of the modified UT. The results of the RDOPs with this modification and their corresponding MC validations are illustrated in Fig. 4.7 b). Evidently, the matching has been improved significantly. Both the expected value and the variance of the objective are still slightly underestimated using the UT, but the quantitative and qualitative match allows a further use of the UT as a reliable approximation method for the dynamic optimization under uncertainty.

Interdependence of selectivity and conversion

So far, the quantification of the model parameter uncertainty impact is carried out only for the selectivity with respect to tridecanal for a predefined conversion. Following the analysis of the process potential, as it was introduced in chapter 3, it is expedient to seek for the robust optimal reactor design of the hydroformylation process as well investigating the impact of model parameter uncertainties on the conversion of 1-dodecene and carrying out the analysis in the $[S_{nC13al}, X_{nC12en}]$-space. Therefore, the MORDOP in Eqs. (4.39)-(4.59) is solved for several expected values of the conversion,

$E(X_{nC12en})$, still optimizing $E(S_{nC13al})$, and analyzing the variance of both the selectivity, $Var(S_{nC13al})$, and the conversion, $Var(X_{nC12en})$. The results are shown in the bar diagram in Fig. 4.8. The Pareto set for each $E(X_{nC12en})$ is illustrated with three grouped bars corresponding to characteristic points of the Pareto set, i.e. the point of maximum $E(S_{nC13al})$, medium $E(S_{nC13al})$, and minimum $E(S_{nC13al})$. The predictive powers are depicted in form of error bars using the standard deviation (STD) for both the selectivity and the conversion. To reach higher conversions the bound for the final time is changed to $t_f \leq 300$ min.

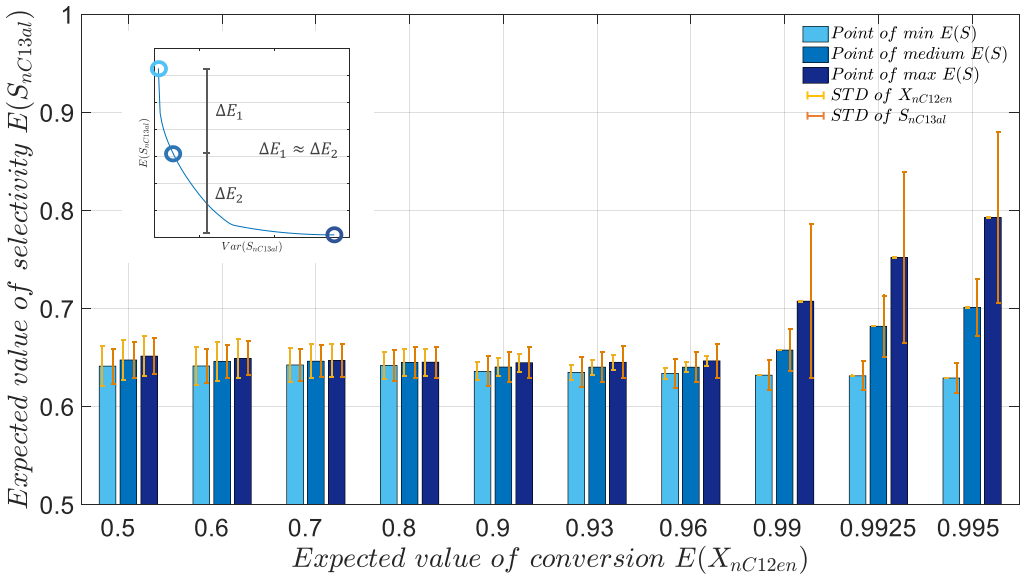

Figure 4.8: Bar diagram showing expected value of selectivity over the expected value of conversion, whereby the latter is depicted in grouped bars. Each bar corresponds to a characteristic point in the corresponding Pareto set, see scheme in the upper left corner. The error bars indicate the STD of conversion (yellow) and selectivity (orange), respectively.

For expected conversions $E(X_{nC12en}) \leq 96$ % the expected selectivities and the standard deviations of both the selectivity and the conversion are almost not changing. The Pareto sets are flat and, thus, the potential for robustification is small. Moreover, the STD of the selectivity stays constant, whereas the STD of the conversion decreases slightly with increasing $E(X_{nC12en})$. These characteristics significantly change for $E(X_{nC12en}) \geq 99$ %. The $E(S_{nC13al})$ and $STD(S_{nC13al})$ increases with $E(X_{nC12en})$ as its STD decreases to almost zero. The spread of the bars is increased implying a very noteworthy change of the designs from the point of the highest performance to the point of best predictive power.

The identification of a unique robust optimal reactor design requires again knowledge about the targeted bounds of the different objectives, either empirically predefined or imposed by the overall process requirements. Since the latter is not available for this design problem, the best design is chosen in order to achieve highest possible selectivity and conversion complying the condition $S_{nC13al}^{2\sigma} \leq 5$ %. The resulting optimal control trajectories of the robust optimal reactor design are shown in Fig. 4.9 a).The reaction time, t_f, is at its maximum at 300 min. The control of the temperature indicates three sections, i.e. a first section with lowest possible temperature, a second section of increasing temperature, and a third section with highest possible temperature. The partial pressures behave similarly, whereas their trajectories are contrary to each other, always maintaining the maximum overall pressure. The peaks in all control trajectories at $t = 0$ min might be negligible as they are present only for a few seconds and, thus, point to a numerical artifact.

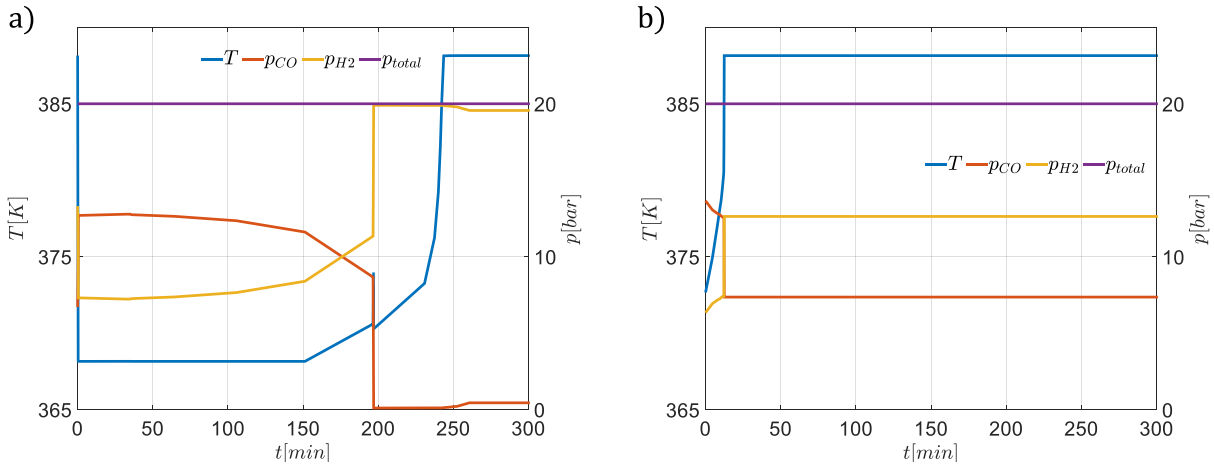

Figure 4.9: Optimal control trajectories for the hydroformylation reaction for: a) the best robust reactor design complying with the condition $S^{2\sigma}_{nC13al} \leq 5$ %; and b) for the deterministic case not considering model parameter uncertainties

The expected selectivity reaches 67.45 % at an expected conversion of 99.5 %. The 2σ condition stated above is satisfied and the STD of the conversion is almost zero. In case the model parameter uncertainties are not considered during the design procedure, the optimal control trajectories show a somehow similar behavior, see Fig. 4.9 b). The temperature starts at a lower point and directly increase to its maximum level, and the partial pressures start at similar points as in the robust design and switch their ratio when maximum temperature is set. Subsequently, they stay constant for more than 250 min until the final reaction time of 300 min is reached. Comparing these two designs, the deterministic design simply neglects the first section of the robust design, shrinks the transition section, and considerably increases the duration of the third section. Its performance is as well significantly increased reaching a selectivity of 82.43 % at a conversion of 99.5 %. However, this increased selectivity is accompanied by an indefinite uncertainty and both a design of a single reactor unit and, especially, the embedding of this unit in an integrated overall process are, thus, of indefinite risk.

The comparison of the robust optimal reactor design and the deterministic design indicates that the qualitative characteristics of different designs, especially of different robust designs within the same Pareto set, might be quite similar and, thus, allow to design a reactor unit, which is able to realize several of these designs by only shifting e.g. transition points. The knowledge about the unifying characteristics allows for determining the required flexibility of the reactor unit and its control and, therefore, supports the decision-making about the optimal reactor unit and/or operation, and necessary controller properties.

4.2.2 Identification of most sensitive model parameters via global sensitivity analysis

The introduced framework for reactor design under model parameter uncertainty has, in addition to the demonstrated determining of Pareto optimal reactor designs as function of one or more crucial performance measures, the potential to be used as basis for a sensitivity analysis with respect to the parameters of uncertainty. The sensitivity analysis aims at quantifying the contribution of each uncertain parameter to the predicted overall variance of the performance of a design. It will be demonstrated and discussed how this knowledge about the particular parameter impact on the performance can be applied. Furthermore, it will be illustrated how those parameter contributions change for the different designs of a Pareto set and, thus, identify which parameter uncertainty impacts are decreased by robustification.

Global sensitivity analysis via Sobol indices

In a fundamental work about global sensitivity analysis Sobol [186] introduced indices, further referred to as *Sobol indices*, which can be computed by Monte Carlo or quasi-Monte Carlo methods. They allow for estimating the influence of single or multiple variables on the output of a nonlinear mathematical model. This approach bases on the ANOVA (analysis of variances) representation which enables the decomposition of a model output variance $Var(Y) = Var_1 + Var_2 + \cdots + Var_k + R$, where Var_i are parts, which can be attributed to the different uncertain inputs θ_i individually, k is the number of uncertain inputs, and R is a residual. In a similar way, the FAST (Fourier amplitude sensitivity test) method decomposes the model output variance by use of spectral analysis instead of Monte Carlo methods [187]. Both approaches provide a framework for global sensitivity analysis and allow determining corresponding sensitivity indices. In chemical design one can more often find the use of local sensitivities analysis by calculating derivative based sensitivity indices, e.g. $S_i = \delta Y/\delta X_i$, for each uncertain input individually. They are determined usually using one-factor-at-a-time methods, which vary the ith input while fixing all others. However, these methods are only effective for determining the relative importance of the inputs when the model is linear in all inputs, which is not the case for nonlinear chemical reaction models [188]. Thus, the use of global sensitivity methods such as FAST and the ANOVA-based Sobol indices is necessary. As the representation introduced by Sobol (2001) bases on Monte Carlo or quasi-Monte Carlo methods and the *unscented transformation* used within the presented design framework under uncertainty can be associated as an approximate Monte Carlo method, *Sobol indices* are used for the following global sensitivity analysis. For a sound overview about these and further methods it is referred to [188].

The individual variance contributions of first order are determined via

$$Var_i = Var_{\theta_i}\left(E_{\theta_{-i}}(Y|\theta_i)\right), \tag{4.60}$$

where $E_{\theta_{-i}}$ is the expected value in case all inputs are of variation except of input i, and Var_{θ_i} defines the variance over θ_i. Thus, the expected value $E_{\theta_{-i}}$ has to be determined for several θ_i sampled from its specific PDF, so that the variance of these expected values can be calculated. The overall variance of the output is defined by

$$Var(Y) = E_{\theta_i}\left(Var_{\theta_{-i}}(Y|\theta_i)\right) + Var_{\theta_i}\left(E_{\theta_{-i}}(Y|\theta_i)\right), \tag{4.61}$$

whereby $Var_{\theta_{-i}}$ is, according to the aforementioned definition, the variance of the output in case all inputs are of variation except of input i. The quotient of Eq. (4.60) and Eq. (4.61) yields the input specific variance

$$D_i = Var_i/Var(Y). \tag{4.62}$$

This procedure can further be carried out for higher-order terms, i.e. Var_{ij}, Var_{ijl}, etc., which quantify the influence of combined inputs, see [188]. In practice these terms of higher order are often neglected, because the computational effort strongly increases, as long as the sum of the input specific variances D_i is close to 1, i.e. the contribution of combined inputs is negligible.

Finally, the global sensitivity indices are determined by

$$S_i = D_i/\sum D_i. \tag{4.63}$$

Identification and analysis of Sobol indices for Pareto optimal designs of the Hydroformylation process

The global sensitivity analysis is carried out for the Pareto optimal designs of the hydroformylation process determined for an expected conversion of $E(X_{nC12en}) = 99.5\ \%$ using the adapted UT parameters. The *Sobol indices* are determined for the selectivity and the conversion, to compare the changes induced by the robustification along the Pareto set. Aiming at a clear analysis, the previously introduced characteristic points along the Pareto set, see Fig. 4.8, are selected again and the corresponding *Sobol indices* are illustrated in pie diagrams Fig. 10 a)-f). The subfigures a)-c) show the *Sobol indices* for the selectivity at its highest expected value, medium expected value, and lowest expected value, respectively. The same holds for the conversion in the subfigures d)-f). The sum of D_i is close to one for all cases. Evidently, the highest impact on the overall variance of the selectivity and the conversion in case of maximum $E(S_{nC13al})$ originates from the catalyst equilibrium parameters $K_{cat,1}$ and $K_{cat,2}$, summing up to more than 90 %. In case of medium $E(S_{nC13al})$, i.e. a trade-off between good performance and good predictive power, the impact of these catalyst equilibrium parameters is significantly reduced, whereby their influence on the conversion is still higher. In the last case of minimum performance and maximum predictive power the catalyst equilibrium parameter impacts are further reduced and other parameter impacts become more substantial. For the selectivity those are especially the rate constants of reaction one and two, $k_{0,1}$ and $k_{0,2}$. Inasmuch as the objective of the robust dynamic optimization problems has been the reduction of the variance of the selectivity and not of the conversion, the analysis of the *Sobol indices* for the conversion is not so meaningful and serve only as comparing entity. However, the *Sobol indices* of the selectivity clearly indicate, that the main impact on the overall variance of the selectivity stems from the uncertainty of the catalyst equilibrium parameters and, thus, a more accurate identification of those is highly recommendable and would improve the predictive power of the process design significantly.

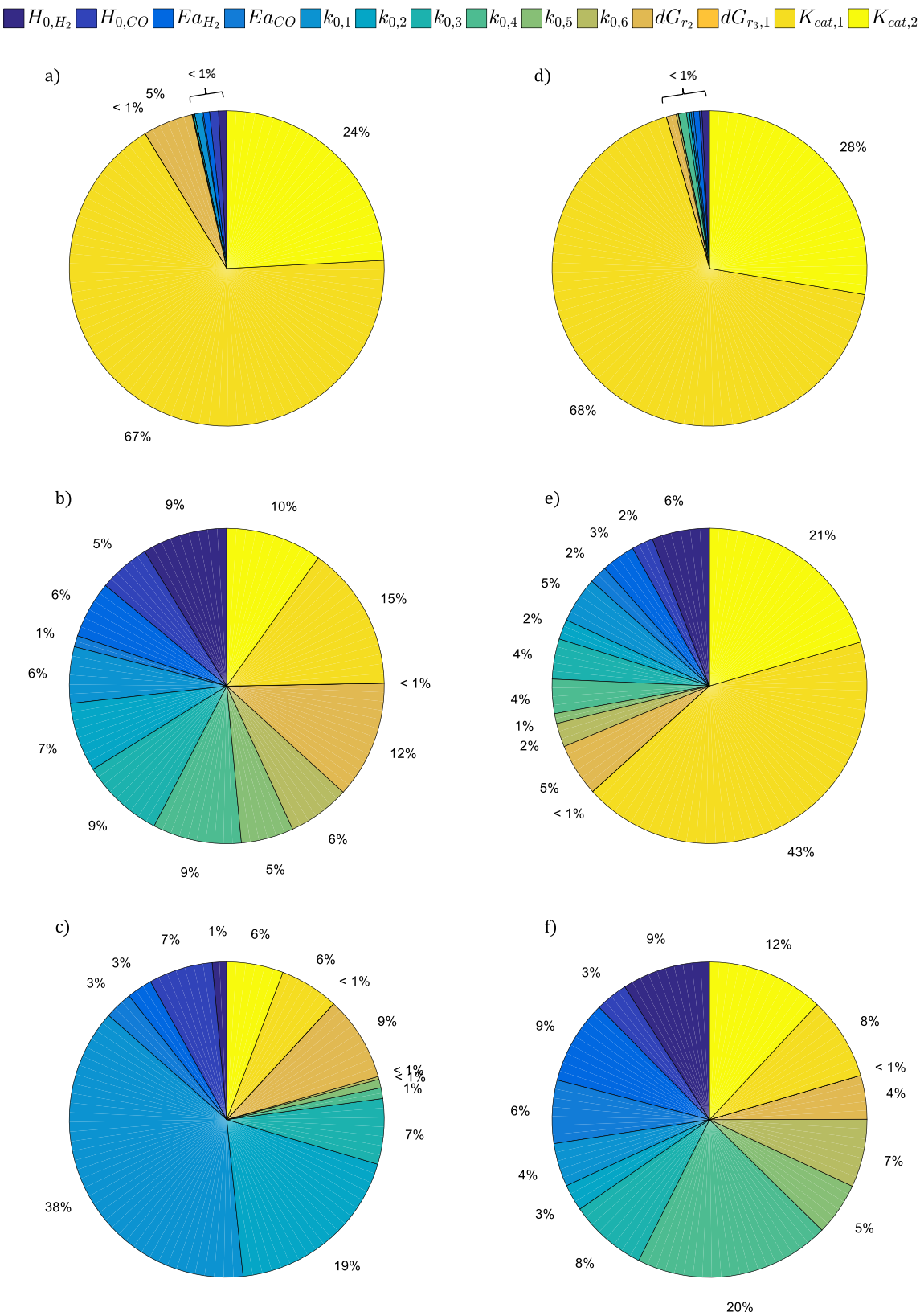

Figure 4.10: Pie diagrams illustrating the Sobol indices for the Pareto optimal designs at $E(X_{nC12en}) = 99.5$ %. Pie diagrams a)-c) for the variance of the selectivity correspond to the characteristic points in the Pareto set for maximum, medium and minimum $E(S_{nC13al})$, respectively. In the same way pie diagrams d)-f) correspond to the variance of the conversion.

4.3 Reactor design under imperfect control realizations

After introducing the use of the reactor design under uncertainty framework for model parameter uncertainties, it is now applied for analyzing the impact of imperfect realization of the optimal control trajectories on the predicted performance of the process. In contrast to the previously treated static model parameter uncertainties, the imperfect control realization effects the reaction as a distributed disturbance along the reaction coordinate and is, thus, a dynamic uncertainty. Again, the application and analysis of this type of uncertainty is demonstrated on the hydroformylation process. First, the concept of imperfect control realization of the EPF based design is elucidated in more detail in subchapter 4.3.1. In a second step the resulting robust dynamic optimization problem is derived and solved for different assumed standard deviations of the temperature control in subchapter 4.3.2. In a last step, the presented approach is used to compare the robustness properties of two different reactor realizations including both model parameter uncertainties and imperfect control realizations in subchapter 4.3.3. The results impressively indicate that this approach allows for a fast assessment of reactor realizations already in an early step of the design procedure using a rather simple model.

4.3.1 Imperfect control realizations as dynamic uncertainty along the reaction coordinate

The optimal state trajectories of the EPF fluid element along its way through the process are controlled by inputs of mass and energy, which are typically realized by dosing and temperature control, respectively (see subchapter 3.1). Independent of the kind of input it is, in contrast to the assumption of ideal control inputs within most design procedures, hardly possible to realize control inputs in a technical process perfectly. The main origins of these deviations are: (i) the controller and actuator accuracies, which are within an overall process design also a matter of cost; and (ii) the mass and energy transport limitations which, although considered in the model formulation, might still deviate from the assumed behavior e.g. due to model inaccuracy or time-variant process conditions such as degradation. However, a comprehensive analysis of these phenomena and their impact on the process requires a rigorous modeling and, thus, much more preliminary experimental and/or numerical effort to gather data and describe these phenomena appropriately. As an alternative way, the presented approach intends to neglect the distinct origin of the deviations and simply aims at quantifying the impact of possible deviations of the optimal control inputs on the process performance. The results are, therefore, independent of whether the deviation is based on e.g. varying wall thicknesses of a tube reactor, calibration errors of mass flow controllers, or non-homogeneous flow fields of a cooling medium. It intends to find robust reactor designs for a predefined overall deviation, which lumps all possible sources of randomness together. This lumped quantity can be compared to a kind of process noise $\varepsilon(t)$ which influences the process along the reaction coordinate with changing intensity.

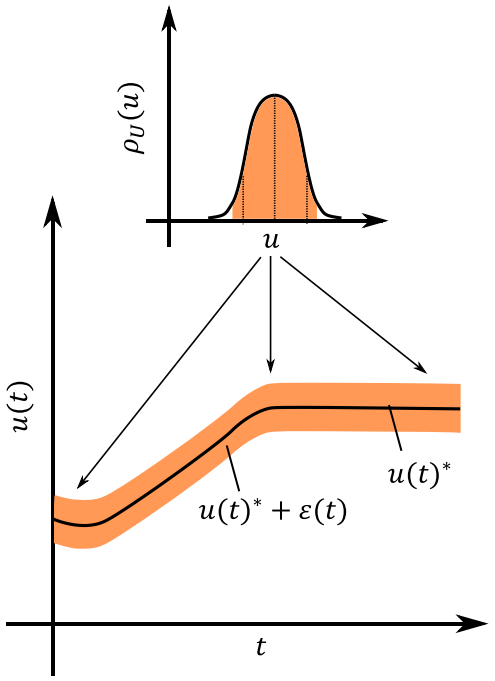

Figure 4.11: Uncertainty band caused by deviations of the optimal control

In the same way, as it is introduced for the model parameter uncertainties, the consideration of these imperfect control realization is based on the assumption that the imposed deviations can be characterized by a certain distribution function, which allows to simulate the aforementioned varying intensity of the deviations. Starting from the assumption of normally distributed deviations, the UT as introduced in subchapter 4.1.2 is used to sample the PDF $\rho_U(u)$ of the imperfect control u at characteristics points $u_i, i \in \mathbb{R}^n$. These samples are imposed on the process at each point along the reaction coordinate resulting in an uncertainty band around the nominal optimal solution $u(t)^*$, see Fig. 4.11. To ensure that the optimal control input is still complying with its constraints, the minimum and maximum bounds are shifted by $\pm 2\sigma$, respectively. In this way, roughly 95 % of the possible scenarios covered within the resulting RDOP are feasible within the original control bounds. Of course, one may select other uncertainty ranges. As the general RDOP in Eqs. (4.18)-(4.30) already indicates, the structure of the dynamic optimization and the use of the samples of the control PDF is changed in comparison to the static uncertainties. This also changes the operation of the optimizer. Instead of finding an optimal control trajectory which optimizes the given objective for all points within the uncertainty set, the optimizer seeks for the best control action at each point along the reaction coordinate considering the predicted result for different control actions represented by the samples of the control PDF. Hence the procedure is as following: At each point along the reaction coordinate, the solver evaluates all model equations for the samples of the imperfect control and the states of the previous step. The resulting states are taken to determine their expected values which are on the one hand transferred to the next step and on the other hand used by the optimizer to find the expected value of the imperfect control input which is, together with its corresponding samples of the control PDF, imposed on the process optimizing the given objective. This procedure is illustrated in Fig. 4.12 for an arbitrary step i along the reaction coordinate. Due to the simultaneous optimization framework, this procedure is carried out simultaneously for all points along the reaction coordinate resulting in a robust optimal trajectory of expected control values.

4.3.2 Impact of temperature control deviations on hydroformylation reaction

In the following, the optimal design of a chemical reactor for the hydroformylation of 1-dodecene in a TMS system is supposed to be analyzed with respect to the impact of deviations within the optimal temperature control. The temperature is preferred to be the subject of analysis over the partial pressures, since on the one hand it is expected to have a higher sensitivity with respect to the process performance, and on the other hand it is probably the most general type of control found in almost every chemical reaction. In order to identify the particular impact of the temperature deviation, the model parameter uncertainties are not considered simultaneously in this step but treated in an additional analysis in subchapter 4.3.3.

Robust dynamic optimization problem

The robust dynamic optimization problem is constructed by adapting the RDOP in Eqs. (4.39)-(4.59) of the model parameter uncertainty quantification of the hydroformylation process for dynamic uncertainties as elucidated in subchapter 4.1.3, see Eqs. (4.64)-(4.83). As mentioned above, the model parameter uncertainties are neglected and the time dependent expected values of the states, i.e. the molar amounts of the hydrocarbons, with respect to the samples of the temperature deviation are determined (Eq. (4.65)) and used within the balance equations. Moreover, the model equations are evaluated for all temperatures $T_i, i \in TP$, with TP being the set of temperature samples of the UT.

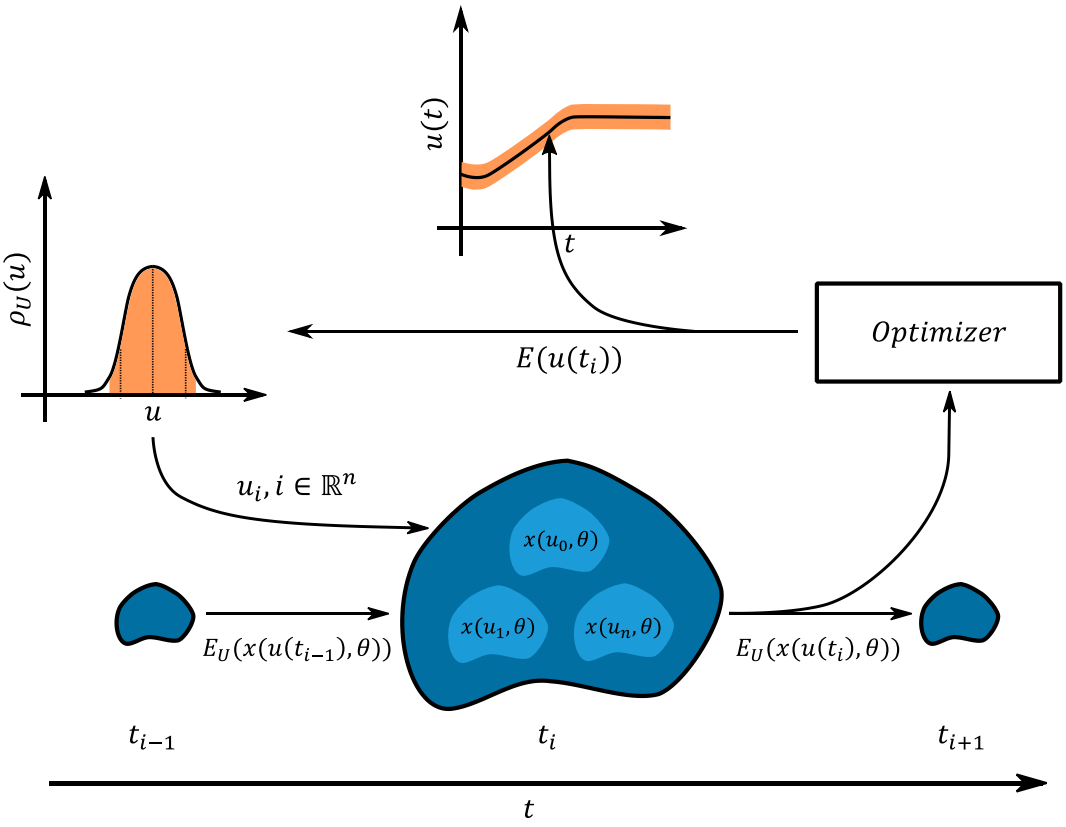

Figure 4.12: Scheme of optimal control action on the EPF fluid element for consideration of imperfect control realization following the discretized solution scheme of the orthogonal collocation on finite elements

$$\max_{E(T(t)),p_{CO}(t),p_{H_2}(t),t_f} \; E\left(S_{nC13al}(t_f)\right) \tag{4.64}$$

s.t. Component mass balances: $$\frac{dn_{\alpha,i}}{dt} = V_{liq}\left(c_{cat}M_{cat}\left(\sum_{m=1}^{M}\nu_{\alpha,m}r_m\right)\right), \quad \alpha \in CH, i \in TP \tag{4.65}$$

Reaction kinetics: Eqs. (2.2)-(2.7), with $r_m = r_m(T_i), m \in \{1 \dots M\}, i \in TP$ (4.66)

Catalyst equilibrium: Eq. (2.1) (4.67)

Constitutive equations: Eqs. (3.38)-(3.39), with $\boldsymbol{\rho} = \boldsymbol{\rho}(T_i)\,, i \in TP$ (4.68)

Gas solubilities: Eq. (2.11), with $H_j = H_j(T_i), j \in \{CO, H_2\}, i \in TP$ (4.69)

Catalyst and solvent ratios: Eqs. (2.13)-(2.14) (4.70)

Path constraints: $\boldsymbol{n}_i(t) \geq 0, i \in TP$ (4.71)

$$10\text{ bar} \leq p_t(t) = p_{CO}(t) + p_{H_2}(t) \leq 20\text{ bar} \tag{4.72}$$

$$363.15\text{ K} + 2 \cdot STD\big(T(t)\big) \leq T(t) \leq 388.15\text{ K} - 2 \cdot STD\big(T(t)\big) \tag{4.73}$$

Terminal constraints: $t_f \leq 300\text{ min}$ (4.74)

$$X_{nC12en,i} = \frac{n_{nC12en,i}(0) - n_{nC12en,i}(t_f)}{n_{nC12en,i}(0)} = 99.5\,\%, i \in TP \tag{4.75}$$

$$S_{nC13al,i} = \frac{n_{nC13al,i}(t_f) - n_{nC13al,i}(0)}{n_{nC12en,i}(0) - n_{nC12en,i}(t_f)}, i \in TP \tag{4.76}$$

$$n/iso_i = \frac{n_{nC13al,i}(t_f)}{n_{nC13al,i}(t_f) + n_{iC13al,i}(t_f)} \geq 95\,\%, i \in TP \tag{4.77}$$

Initial conditions: $$\boldsymbol{n}_i(t=0) = \boldsymbol{n}_{0,i} = \begin{cases} 1, & l \in \{nC12en\} \\ 0, & l \in \{CH/nC12en\} \end{cases}, i \in TP \quad (4.78)$$

Unscented transformation: $$T_0 = E(T(t)) \quad (4.79)$$

$$T_i = T_0 + sgn(n_{\boldsymbol{\theta}} - i)\sqrt{(n_{\boldsymbol{\theta}} + \lambda)}\sqrt{Var(T)}_i, i \in TP \quad (4.80)$$

$$E(S_{nC13al}) = \sum_{i=0}^{2n} w_i \, S_{nC13al_i}, i \in TP \quad (4.81)$$

$$Var(S_{nC13al}) = (1 - \alpha^2 + \beta)\{S_{nC13al_0} - E(S_{nC13al})\}\{S_{nC13al_0} - E(S_{nC13al})\}^{\mathrm{T}} + \sum_{i=1}^{2n} w_i \{S_{nC13al_i} - E(S_{nC13al})\}\{S_{nC13al_i} - E(S_{nC13al})\}^{\mathrm{T}}, i \in TP \quad (4.82)$$

$$E(\boldsymbol{n}_i(t)) = \sum_{i=0}^{2n} w_i \, \boldsymbol{n}_i(t, T_i) \quad (4.83)$$

Pareto optimal solutions for different temperature deviations

The RDOP in Eqs. (4.64)-(4.83) is solved for different standard deviations of the temperature control PDF, $STD(T)$. To present the results compactly, the final expected values are illustrated within an uncertainty band indicating $2 \cdot STD(S_{nC13al})$, i.e. 95 % confidence interval. The result on the left for $STD(T) = 0$ K corresponds to the deterministic solution without an uncertainty influence and has, thus, no variation of the objective. As expected, with increasing temperature deviation a clear tendency of decreasing expected selectivity values and increasing selectivity deviation is indicated, which is on the one hand caused by the shift of the temperature bounds within the optimization problem formulation and on the other hand by the impact of noisy temperature realization. However, the impact is fairly small compared to the impact of the previously investigated model parameter uncertainties, and the standard deviations can only be analyzed in relation to each other, since their absolute sizes might depend on the discretization scheme.

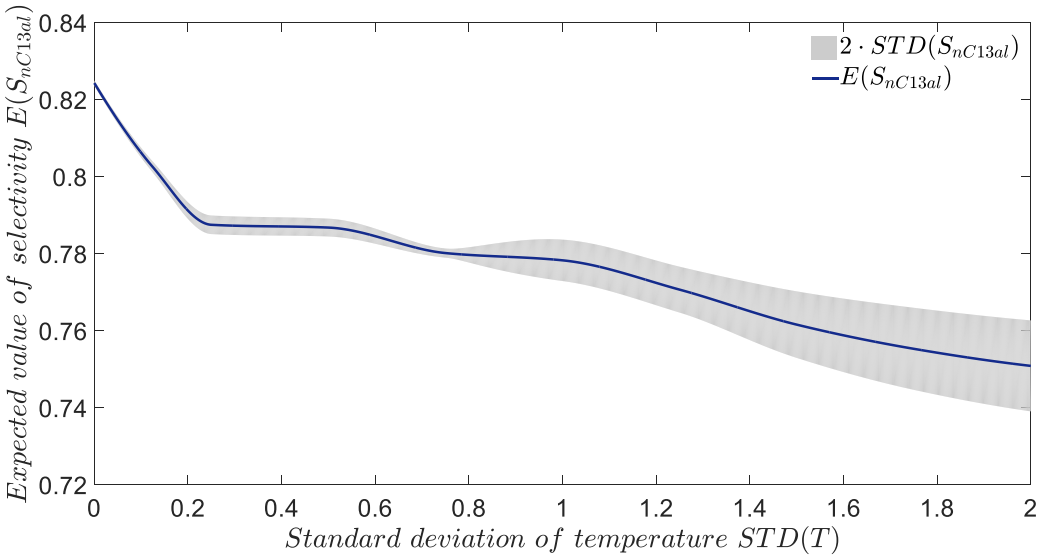

Figure 4.13: Expected value of selectivity for different deviations of the optimal temperature control. The grey uncertainty band indicates $2 \cdot STD(S_{nC13al})$.

A closer look to the formulated robust dynamic optimization problem reveals that the main target of this type of analysis is the identification of a control trajectory which ensures feasibility under consideration of possible control deviations. The results of this analysis quantify the impact of

different control deviations and indicate which performance can be expected and how large the risk is to miss it. In light of a robust design optimization, it is more reasonable to investigate the impact of the temperature deviation on an already uncertain process, e.g. originated from model parameter uncertainties, and analyze the arising interdependencies; see the following subchapter.

4.3.3 Comparison of robustness properties of two reactor realizations

As the previous result indicated, the imperfect realization of the temperature control of the hydroformylation reaction has an obvious effect on the optimal design and its expected reaction performance. However, in the real application the model parameter uncertainties and their effect on the optimal design procedure should not be neglected, and in the course of the analysis of the impact of control deviations on the optimal design they should be included. This allows for an identification of combined effects. As the classification of the different types of uncertainties within the 3-level design procedure of Peschel et al. [4] in subchapter 4.1.1 indicated, the imperfect control realizations arise in the third level, when the focus lies on the technical realization of the optimal control trajectories. Therefore, the presented approach is in the following used to compare the robustness properties of two different technical realizations of an optimal design under consideration of both model parameter uncertainties and temperature control deviations. Without conducting a detailed reactor-network synthesis, as introduced in chapter 3, two possible reactor realizations are chosen which differ regarding particular benefits:

- PFR with side dosing of gas components: This reactor realizations corresponds to the assumptions underlying the RDOP in Eqs. (4.39)-(4.59) and allows for an exact realization of the control trajectories shown in Fig. 4.9 (a).
- Cascade of four CSTRs: The realization with a CSTR cascade requires an approximation of the continuous control trajectories with discrete reaction zones, which is simpler to realize in a real application. In addition, this realization includes possible back-mixing benefits.

Robust dynamic optimization problem

For the derivation of the robust dynamic optimization problem for this analysis, the RDOP in Eqs. (4.64)-(4.83) is augmented by the model parameter uncertainties as shown in Eqs. (4.39)-(4.59). Consequently, the model equations have to be evaluated on the sigma points of both the uncertain model parameter set and the set of temperature samples, see Eqs. (4.85), (4.86), (4.89), (4.91), (4.98). The target of the following analysis is the quantification of the uncertainty impact when optimizing the expected objective and not the identification of more robust design alternatives by reducing the objective deviation. Hence, the RDOP in Eqs. (4.84)-(4.107) is solved once for both reactor realizations and no MORDOP arises.

$$\max_{E(T(t)),p_{CO}(t),p_{H_2}(t),t_f} \; E\left(S_{nC13al}(t_f)\right) \tag{4.84}$$

s.t. Component mass balances:
$$\frac{dn_{\alpha,i,j}}{dt} = V_{liq}\left(c_{cat}M_{cat}\left(\sum_{m=1}^{M}\nu_{\alpha,m}r_m\right)\right), \quad \alpha \in CH, \; i \in SP, j \in TP \tag{4.85}$$

Reaction kinetics: Eqs. (2.2)-(2.7),with $r_m = r_m(\boldsymbol{\theta}_i, T_j)$, $m \in \{1 \dots M\}, i \in SP, j \in TP$ (4.86)

Catalyst equilibrium: Eq. (2.1), with $c_{cat} = c_{cat}(\boldsymbol{\theta}_i), i \in SP$ (4.87)

Constitutive equations: Eqs. (3.38)-(3.39), with $\boldsymbol{\rho} = \boldsymbol{\rho}(T_j)$, $j \in TP$ (4.88)

Gas solubilities: Eq. (2.11), with $H_j = H_j(\boldsymbol{\theta}_i, T_j), j \in \{CO, H_2\}, i \in SP, j \in TP$ (4.89)

Catalyst and solvent ratios: Eqs. (2.13)-(2.14) (4.90)

Path constraints:
$$\boldsymbol{n}_{i,j}(t) \geq 0, i \in SP, j \in TP \quad (4.91)$$
$$10 \text{ bar} \leq p_t(t) = p_{CO}(t) + p_{H_2}(t) \leq 20 \text{ bar} \quad (4.92)$$
$$363.15 \text{ K} + 2 \cdot STD\big(T(t)\big) \leq T(t) \leq 388.15 \text{ K} - 2 \cdot STD\big(T(t)\big) \quad (4.93)$$

Terminal constraints:
$$t_f \leq 300 \text{ min} \quad (4.94)$$
$$X_{nC12n,i} = \frac{n_{nC12en,i}(0) - n_{nC12en,i}(t_f)}{n_{nC12en,i}(0)}, i \in SP \quad (4.95)$$
$$S_{nC13al,i} = \frac{n_{nC13al,i}(t_f) - n_{nC13al,i}(0)}{n_{nC12en,i}(0) - n_{nC12en,i}(t_f)}, i \in SP \quad (4.96)$$
$$n/iso_i = \frac{n_{nC13al,i}(t_f)}{n_{nC13al,i}(t_f) + n_{iC13al,i}(t_f)} \geq 95\ \%, i \in SP \quad (4.97)$$

Initial conditions:
$$\boldsymbol{n}_{i,j}(t=0) = \boldsymbol{n}_{0,i,j} = \begin{cases} 1, & l \in \{nC12en\} \\ \boldsymbol{0}, & l \in \{CH/nC12en\} \end{cases}, i \in SP, j \in TP \quad (4.98)$$

Uncertain model parameters:
$$\boldsymbol{\theta} = [k_1, k_2, k_3, k_4, k_5, k_6, K_{cat,1}, K_{cat,2}, \ldots \Delta G_{r_2}, \Delta G_{r_3}, H^0_{CO}, H^0_{H2}, E_{A,H_{CO}}, E_{A,H_{H2}}]^{\mathrm{T}} \quad (4.99)$$

Unscented transformation:
$$T_0 = E(T(t)) \quad (4.100)$$
$$T_j = T_0 + sgn(n_T - j)\sqrt{(n_{\boldsymbol{\theta}} + \lambda)}\sqrt{Var(T)}_j, j \in TP \quad (4.101)$$
$$E\left(\boldsymbol{n}_j(t)\right) = \sum_{j=0}^{2n} w_j \boldsymbol{n}_j(t, T_j), j \in TP \quad (4.102)$$
$$\boldsymbol{\theta}_0 = E(\boldsymbol{\theta}) \quad (4.103)$$
$$\boldsymbol{\theta}_i = \boldsymbol{\theta}_0 + sgn(n_{\boldsymbol{\theta}} - i)\sqrt{(n_{\boldsymbol{\theta}} + \lambda)}\sqrt{Cov(\boldsymbol{\theta})}_i, i \in SP \quad (4.104)$$
$$E(S_{nC13al}) = \sum_{i=0}^{2n} w_i S_{nC13al_i}, i \in SP \quad (4.105)$$
$$Var(S_{nC13al}) = (1 - \alpha^2 + \beta)\{S_{nC13al_0} - E(S_{nC13al})\}\{S_{nC13al_0} - E(S_{nC13al})\}^{\mathrm{T}} + \sum_{i=1}^{2n} w_i \{S_{nC13al_i} - E(S_{nC13al})\}\{S_{nC13al_i} - E(S_{nC13al})\}^{\mathrm{T}}, i \in SP \quad (4.106)$$

For the optimization of the CSTR cascade the balance equation is replaced by

$$n_{\alpha,i,j,k} = n^0_{\alpha,i,j,k} + \tau_k V_{liq,k}\left(c_{cat} M_{cat}\left(\sum_{m=1}^{M} \nu_{\alpha,m} r_{m,k}\right)\right), \quad \alpha \in CH, i \in SP, j \in TP, \quad k \in n_{CSTR} \quad (4.107)$$

where n_{CSTR} is the number of CSTRs in the cascade. The initial conditions for $k = 1$ are equal to the initial conditions in Eq. (4.98). The control variables are not continuous anymore and instead defined on discrete points k.

Optimization results for reactor realization comparison

The comparison of the optimization results under model parameter uncertainties and temperature control deviations for both reactor realization, the PFR with gas side dosing and the CSTR cascade, are carried out for different expected conversions $E(X_{nC12en})$. The results are again depicted in the $[S_{nC13al}, X_{nC12en}]$-space allowing for a compact illustration, see Fig. 4.14. To reveal the impact of the temperature control deviation, which was set to $STD(T) = 1$ K, on the uncertain process, the RDOP in Eqs. (4.84)-(4.107) was solved as well for the case without imposed disturbance on the temperature control. The analysis indicates:

- The expected selectivity is slightly decreased by the temperature control deviation for both reactor realizations, see Fig. 4.14 a). The CSTR cascade approximates the PFR quite close and even exceeds its performance in a particular range of expected conversions ($0.94 \leq E(X_{nC12en}) \leq 0.99$). This finding matches the results in subchapter 3.2.3 that the second reaction zone benefits from back-mixing. However, the decreasing effect of the temperature control deviation on the performance becomes high for the CSTR cascade at high expected conversions. Evidently, the CSTR cascade suffers more from the imposed temperature control deviation, because it is harder to approximate the more complex temperature profile at high expected conversions with small amount of disturbed temperature control inputs. For very high expected conversions the CSTR cascade with temperature control disturbance finally collapses.
- The predicted standard deviations of the selectivity are as well very close for expected conversions smaller 90 %, see Fig. 4.14 b). In the subsequent region, in which the CSTR cascade outperforms the PFR, also its standard deviations of the selectivity increase. Interestingly, the temperature control deviations reduce this effect. For very high expected conversions ($\leq$ 99 %) the CSTR cascade indicates again smaller variations of the objective than the PFR.
- The standard deviations of the conversion of the CSTR cascade are smaller than those of the PFR for all expected conversions, see Fig. 4.14 c). The imposed temperature control deviations show almost no effect for both realizations. Hence, the observed characteristics of these curves are similar to what was found in subchapter 4.2.1.

It becomes obvious, that the decision making about the better reactor realization is again a question of the most desirable trade-off since more than one objective is of interest. The performance benefit at high conversions of the PFR is accompanied by a very high increase of the corresponding standard deviation, whereas the more moderate selectivity deviations of the CSTR cascade for high expected conversions is to the detriment of smaller expected selectivities. The standard deviations of the conversion are only of interest for medium expected conversions as they overlap at high expected values where the real performance differences occur. Nevertheless, the analysis revealed advantages and disadvantages of both reactor realizations and allows for determining the more suitable one in case more knowledge about the requirements or bounds of the overall process is available. A similar analysis, which in addition considers non-ideal residence time distributions in the reactor realizations, is carried out in Kaiser et al. [166].

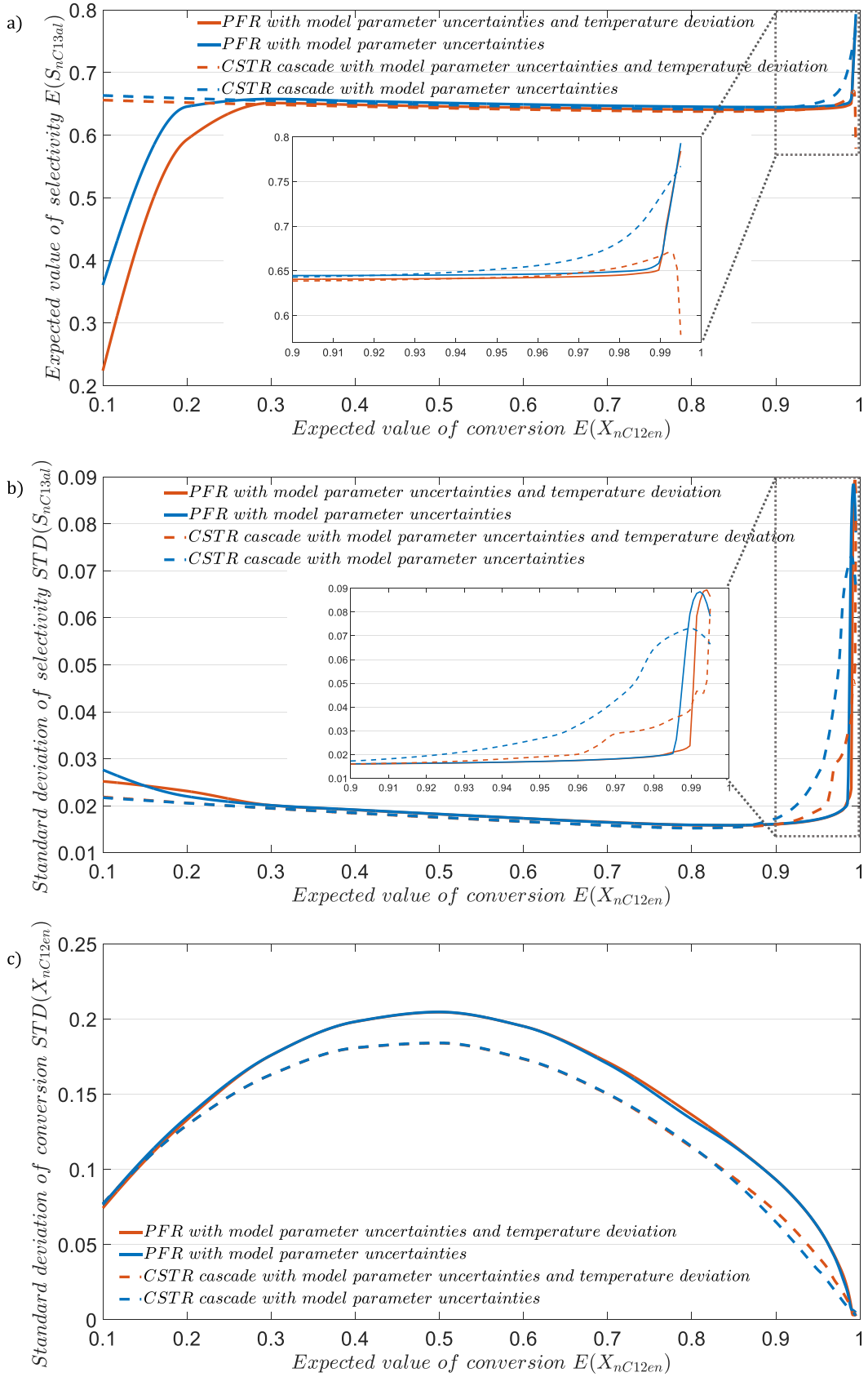

Figure 4.14: Results of robust optimization of the PFR with gas side dosing (solid lines) and the cascade of four CSTRs (dashed lines) for the cases of model parameter uncertainties (blue lines) and additional temperature deviation of $STD(T) = 1$ K (orange lines): The expected value of the selectivity a), the standard deviation of the selectivity b), and the standard deviation of the conversion c), are all illustrated over the expected value of the conversion.

4.4 Discussion

In this chapter a probabilistic reactor design framework is introduced, which allows for considering static and dynamic types of uncertainties within the reactor design procedure of the EPF methodology. Three general types of uncertainty are classified: (i) model parameter uncertainties; (ii) non-ideal reactor characteristics; and (iii) imperfect control realizations. On the hydroformylation of 1-dodecene in a TMS system as example process it is demonstrated how these uncertainties are embedded within the dynamic optimization problem for reactor design using the *unscented transformation* for nonlinear propagation of statistical moments of the uncertainty's probability density functions. For the solution of the resulting robust dynamic optimization problems a full probabilistic orthogonal collocation approach is developed for both random and stochastic variables (see A.3). As the results of the reactor design under uncertainty for the hydroformylation process are already discussed in the corresponding subchapters, the following discussion focuses on the methodological aspects of the probabilistic reactor design approach, debate its advantages and disadvantages, and points out interesting future perspectives.

Model parameter uncertainties

The design of chemical reactors, and in the next step of entire chemical processes, under consideration of model parameter uncertainties is generally of vital importance. This is remarkably confirmed by the results for the hydroformylation reaction indicating a significant impact of the model parameter uncertainties on the optimal design of the reactor and its predicted performance. The *unscented transformation* for nonlinear propagation of statistical moments of the uncertainties through the process model proves to be a powerful and efficient way to include model parameter uncertainties into a dynamic optimization based design procedure. Nevertheless, it became obvious that a validation of the therewith yielded approximate results with a more accurate method such as Monte Carlo simulations is necessary to identify the accuracy of the UT based approximation and, in case of unacceptable deviation, initiate an expedient adjustment of the UT tuning parameters. However, a consecutive procedure of optimization and simulation based validation is still more efficient than an optimization with integrated Monte Carlo simulation. In this work the validation and subsequent improvement of the UT tuning factors or rather selection of suitable modification of the method was carried out manually. An automated, iterative implementation would be desirable, but is not trivial to create, since there exists no heuristic for suitable selection of the tuning factor or modification of the UT [171]. A drawback of the use of sigma points for robust reactor design is the fact that the upper and lower bound of the parameter uncertainty ranges are not checked for feasibility. Feasibility is rather ensured for the chosen sigma points, which lie, depending on the chosen scaling and the number of random variables, not on the bound of the PDF. If the robust optimization targets to higher feasibility ranges, the sigma points have to be selected accordingly. In contrast to methods including the best and worst case scenario, this approach is hence less conservative.

For the purpose of reactor design the use of a robust optimization approach instead of a stochastic programming approach is recommended [71], since no recourse actions over a long term operation are required. As the target of the presented design under uncertainty approach, stated in the introduction of chapter 4, considers the identification of robust designs and designs of increased predictive power, it is expedient to pursuit a robust design optimization instead of a reliability-based optimization. The use of the *unscented transformation* with sigma points has been reported in literature before and their application on problems of this kind was successful, see e.g. [174], [189]. Alternatively, one can apply other approaches for the approximate description of uncertainty probability density functions and their nonlinear transformation, e.g. cubature rules. They numerically approximate the multi-dimensional integrals of the means and variances of the output function, see

e.g. [190]. It is out of the scope of the present work to compare different approximation approaches for probabilistic design. The interested reader is referred to a recent and thorough comparison study found in [191].

The objective of the design procedure was again the selectivity with respect to tridecanal, and the varied constraint for identifying different process windows was the conversion of 1-dodecene. However, the presented approach is not restricted to those measures and hence can as well be used for other objectives simply adapting the objective and the relevant constraints within the MORDOP. Moreover, the design procedure allows for including multiple objectives which are not statistical moments of a single focused measure. The resulting multi-objective optimization follows the same rules as introduced in subchapter 4.1.3. It is out of scope of this work to carry out the design procedure analyzing multiple objectives and their interdependencies. Furthermore, the presented approach does not intend to be a new framework for multi-objective optimization. It is only used as tool to quantify the statistical moments of a single objective and analyze their trade-offs.

The analysis of the global sensitivity indices led to interesting insights about the crucial model parameters of the process indicating an evident need of a more accurate identification of the catalyst activity model parameters. However, the use of sigma point based UT for this purpose is accompanied by possible approximation errors, which e.g. result in $\sum D_i > 1$. Hence, for a more accurate determination of the *Sobol indices* the use of e.g. Monte Carlo simulations is recommended, although implying unequally higher computational effort.

A very promising way to utilize the knowledge about the relative importance of each uncertain model parameter with respect to the predictive power of the process performance might further be to improve the parameter identification procedure of the underlying model. More precisely, the additionally gained knowledge is used to identify experimental conditions, which increase the identifiability of the highly sensitive model parameters. After conducting these experiments, either numerically or physically, the additional results are used to repeat the parameter identification and, thus, refine the model aiming at an increased predictive power of the resulting process design. This procedure is schematically illustrated in Fig. 4.15. It can be repeated iteratively until the improvement reaches a predefined threshold value. For lack of time, this approach has not been applied for the hydroformylation process and is hence only discussed briefly in the following. The main purpose of this approach is the improvement of the prediction quality for the optimal process design. Normally, an optimal experimental design (OED) is carried out to decrease the amount of necessary experiments ensuring a certain level of identifiability of a model and its parameters. The suggested approach intends to feed additional information about the most crucial parameters for the design procedure to the OED, and include the OED into an iterative procedure instead of carrying it out only for kinetic measurements. However, this gained information is only valid for the design, which results from the dynamic optimization, and might be different for designs obtained for other process conditions. Thus, the integrated process design and parameter identification has to be carried out for specific constraints or requirements of the design procedure, which are not changed from iteration to iteration. For changing conditions, the results of the global sensitivity analysis still have a qualitative value to get a rough understanding of the relative importance of the model parameters, but cannot be quantitatively used for a reliable next iteration. Furthermore, it can hardly be assessed whether the resulting process design changes significantly from iteration to iteration, since the optimization of the nonlinear reaction models with new parameters is not predictable.

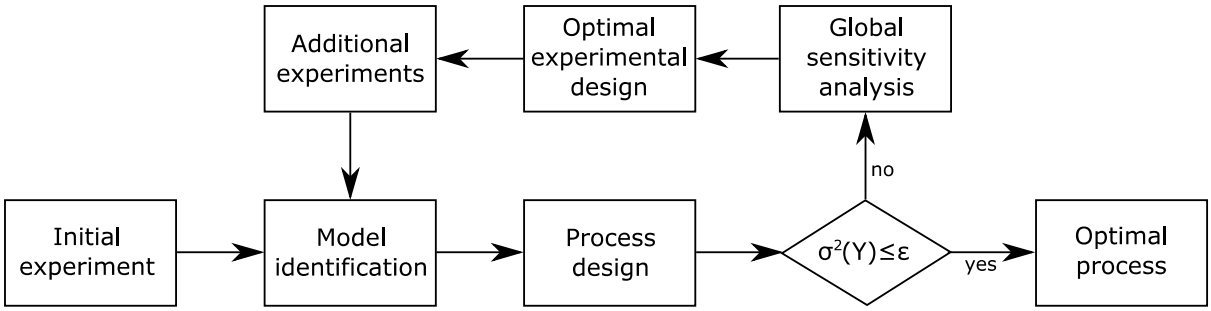

Figure 4.15: Schematic workflow for an integrated process design and parameter identification procedure

Imperfect control deviations

In contrast to the model parameter uncertainties, the deviation of the optimal control trajectories is of dynamic nature along the reaction coordinate leading to a different notion of their influence and resulting embedding within the DOP. Imagining the fluid element on its way through the process it is at every point along the reaction coordinate manipulated by an optimized control input, e.g. the temperature. In case this control input is randomly varying around the optimal input value at each point, the process becomes stochastic. To obtain a solution of a dynamic process with stochastic input, a stochastic differential equation has to be solved, which is unlikely more complex than solving an ODE as for the pure deterministic problem. A superposed optimization of this stochastic input makes it even more complex and could be solved by applying the Hamilton-Jacobi-Bellman equation for stochastic differential equations using the Ito formula [192]. To reduce the complexity and to stay within the deterministic formulation, the presented approach simplifies the problem by assuming that the impact of the stochastic input around its nominal optimal value on the process can be approximated again by the UT. Hence, the PDF describing the set of possible state variables at each point induced by the corresponding stochastic input is described by characteristic sigma points. Furthermore, instead of propagating all characteristic sigma points of the arising PDF for each state variable to the next step along the reaction coordinate, which would lead to a tremendously large problem suffering from the curse of dimensionality, only the expected values of the state variables are passed. Of course, this procedure only approximates the real stochastic process, but in enables the quantification of these control deviations within a dynamic optimization with a reasonable computational effort.

The knowledge about the impact of certain control deviations on the process performance is valuable and can be used on different ways, e.g. comparing the sensitivity of different control variables, or quantifying the effect of various deviation sizes on the performance as demonstrated in subchapter 4.3.2. However, to use that information for decision-making regarding the final process design, additional information about the cost and complexity of the realization of a particular control accuracy is required. This leads to trade-offs between accuracy and costs and allows to make profound decisions or to create a cost-optimizing design procedure.

An interesting aspect for further investigations is, how the presented approach can be used to reduce the control burdens of the final reactor or process. The robust designs resulting from the design under uncertainty compensate uncertainty influences and, thus, possibly reduce the range or the amount of necessary controller actions in the operating process. Hence, it could be reasonable to include the arising control burdens as an additional objective, e.g. in form of controllability indices, within the robust design optimization and create an alternative framework for simultaneous design and control. In contrast to classical approaches in this field, it would rather try to check for controllability and reduce the required amount and range of control actions instead of designing the particular controller simultaneously to the process.

Non-ideal reactor characteristics

The second type of uncertainty arising during the reactor design procedure introduced in subchapter 4.1.1 are non-ideal reactor characteristics. For the lack of time it is not demonstrated in detail in this work, but was published partly in Kaiser et al. [166] for the case of non-uniform residence time distribution (RTD) as deviation of the ideal plug flow assumption, which is used in the 3-level reactor design approach of Peschel et al. [4]. In the following it is discussed for the case of the RTD how this type of uncertainty can be treated.

First of all one can distinguish between three cases: (i) the nominal residence time is fixed as the mean of the assumed RTD aiming at a RDOP which investigates the impact of different deviations from this nominal value; or (ii) the mean residence time is a decision variable as well as its variance and the approach intends to find the best RTD optimizing the given objective; and (iii) the intention lies in quantifying the impact on the reaction performance of a particular RTD, e.g. of a given reactor setup, which is known in advance. In case this RTD is not normally distributed one could use Gaussian mixed distributions to realize more complex distributions with the UT [178].

For this type of uncertainty it is very important to discuss the role of the distributed character of the underlying reactor unit and its state of mixing. A concentrated system or a system of ideal mixing such as e.g. a batch reactor or an ideally mixed CSTR, respectively, are not subject of interest for this type of uncertainty quantification. Strictly speaking, it is only valid for distributed reactor systems, in which gradients can lead to axial or radial distribution of a certain measure of interest. The residence time is such a measure and its axial gradients emerge by the flow field. A second important aspect of this type of uncertainty, which decides about its treatment within the dynamic optimization, can be well elucidated on the example of the RTD. It is the question about the degree of diffusion or mixing along the radial coordinate. There exist two extreme cases, which are well known in reaction engineering. The first case is the complete segregation, which describes a degree of no radial mixing. Parallel streams, which exchange no material, flow with different velocities through the process and, thus, experience the optimal control with various degrees of distortion. The fast fluid elements experience the optimal control in shrunk manner and the slow fluid elements in an expanded manner. Due to the absence of radial mixing, the parallel streams can be treated as parallel reactors [193]. The RTD is approximated by characteristic points, the sigma points, and each stream is associated with one of these residence times leading to a certain flow velocity. For the optimization, all streams are evaluated individually but with the same optimal control, and finally the streams, containing the fluid elements of different ages, are mixed and the reactor output is determined using the UT. In this way Kaiser et al. [166,194] investigated the impact of the RTD as deviation from the optimal residence time on the hydroformylation reaction example. Note, that this approach neglects the forming of the flow field and assumes, that the flow field is stable along the reaction coordinate. The second case, which describes the other extreme, is the total mixedness, i.e. the radial mixing is so fast, that even when the fluid elements have different velocities, their concentrations are instantaneously mixed and cannot be distinguished anymore. Thus, they do not experience the optimal control differently. Between these two extreme cases, the fluid elements experience the optimal control with different ages and exchange their material with different transfer rates.

As a future perspective it might be interesting to describe the latter case with the help of the probabilistic reactor design approach for dynamic uncertainties. For a clear validation of its feasibility it should be validated using state-of-the-art models for RTD such as the axial dispersion model or the CSTR cascade approach. In contrast to the first it does not require the solving of a partial differential equation, which can lead to numerical problems in the context of dynamic optimization. In addition, it is promising in comparison to the second, since the degree of mixing is not accompanied by a limitation of control inputs due to a small number of units in the cascade.

Conclusion

Since almost every kind of uncertainty can be associated within the here presented classification, they can as well be included in the reactor design procedure. One can think of uncertain compositions of recycle streams, gradients in the radial temperature field, uncertain mass transfer rates, or catalyst degradation. Furthermore, the presented approach is not limited to chemical reactors. The underlying DAE system can also describe other units in a chemical process, e.g. distillation columns, or other kind of processes, e.g. mechanical or fluid mechanical problems. In any case, the uncertainty quantification and the associated robustification of the process, as introduced in this chapter, opens new vistas for a process designer and still reserves interesting potential for improvement and extension.

5 Optimal reactor design for the retrofit of an integrated hydroformylation miniplant

The final subject of this work is the application of the qualitative reactor synthesis approach and the reactor design under uncertainty framework, presented in chapter 3 and 4, respectively, on a real process design problem. For an existing miniplant setup of the hydroformylation of 1-dodecene in a TMS system an optimal reactor is sought complying with the given restrictions for residence time, recycle conditions, and control options. Since the methodical details and the discussion of the introduced approaches are already carried out in the previous chapters, the focus in this chapter lies on a straightforward application aiming at a technical realization of the optimal reactor design, which is embedded in the existing miniplant and experimentally tested. As far as the process conditions and the main structure of the miniplant is not changed, and only the reaction step is improved by replacing or extending reaction sections and control actions, this endeavor is called a retrofit.

In a first step the existing miniplant setup and the corresponding process conditions are presented and based on these the retrofit problem definition is derived in subchapter 5.1. Following this problem definition and the knowledge about the given process, a dynamic optimization problem for the synthesis is derived in subchapter 5.2 considering the restrictions and limitations of the miniplant process. By applying the *flux profile analysis* on the results of the dynamic optimization promising reactor-(recycle)-networks are derived and compared with regard to their $[S_{nC13al}, X_{nC12en}]$-behavior. Subsequently, the most promising reactor-(recycle)-network is technically designed in detail in subchapter 5.3. To evaluate the predicted performance of the technical design in comparison to the existing setup, both are optimized within the integrated overall process in subchapter 5.4. Thereby, model parameter uncertainties are included to ensure the final design to be robust against those and, furthermore, to identify designs with higher predictive power of the performance. In subchapter 5.5 a brief comparison of first experimental results of the retrofitted miniplant process with the *in silico* predicted results are presented. And finally, the design procedure and the results are discussed in subchapter 5.6.

5.1 Existing hydroformylation process in miniplant-scale

The miniplant for the hydroformylation of 1-dodecene in a TMS system consisting of n-decane and N-,N-dimethylformamide was constructed and operated as part of the CRC/TR63 “InPROMPT” project introduced in chapter 1. The experiments in miniplant-scale allow for investigation of recycle effects, effects by continuous operation and scale-up effects. In contrast to a pilot-scale, it is not a downsized copy of the later production plant, but a highly flexible, experimental setup including various possible scenarios of the future process [195]. The first setup of the hydroformylation miniplant consisted of a CSTR unit and a decanter unit for liquid-liquid phase separation of the polar and nonpolar solvents containing the catalyst and the products, respectively (see subchapter 2.3.2), whereby the polar phase was recycled to the reactor and the nonpolar phase further treated in a flash unit for gas separation [196,197]. In a subsequent step, a distillation column was added to the downstream path of the nonpolar phase allowing for a separation and a recycling of the nonpolar solvent, side products, and remaining reactant [198]. These two cases serve as reference for the derivation of the presented retrofit problem and are, thus, introduced in more detail.

5.1.1 Process conditions and experimental setup

The technical flow sheet of the complete process is illustrated in Fig. 5.1, wherein the gray box highlights the reduced process. A special property of the miniplant is the pressure level connection between the CSTR and the decanter maintaining a total pressure of 20 bar in both units. Before entering the distillation column, the nonpolar phase is unpressurized in a flash unit to the level of the distillation column. The distillate stream of the distillation column is treated in an additional liquid-liquid separation due to the formation of an azeotrope in the distillation column. The subsequent tank in the second recycle is installed to mix the recycle stream with required make-up stream of the nonpolar solvent and enables a controlled feed to the reactor.

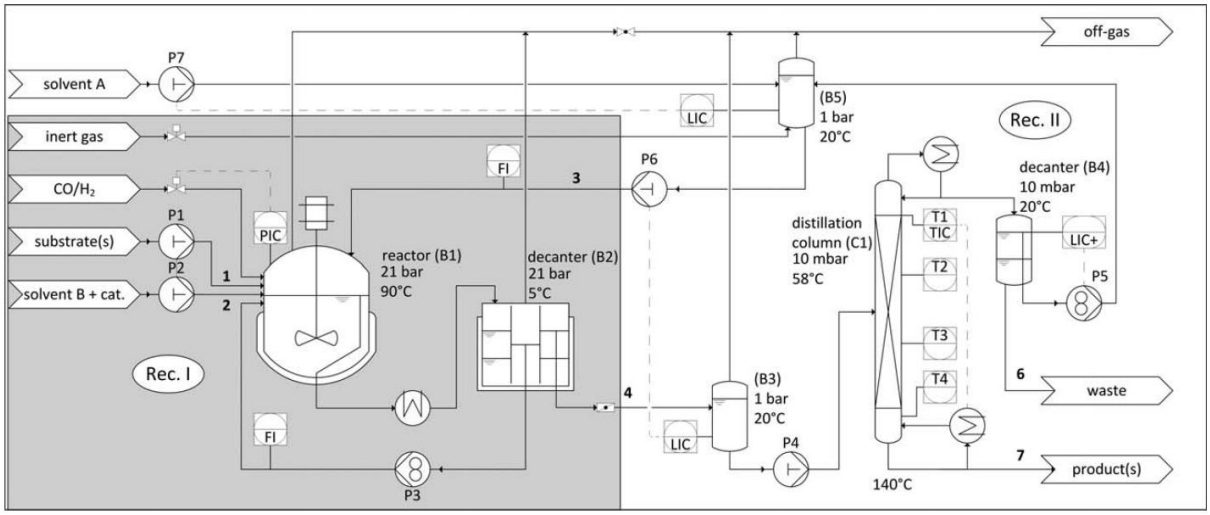

Figure 5.1: Technical flow sheet of the hydroformylation miniplant [198]

Table 5.1: Operational conditions of hydroformylation miniplant [197]

T_R	90°C
$w_{1-dodecene}$	0.16
$w_{n-decane}$	0.42
w_{DMF}	0.42
p_{total}	20 bar
CO/H_2	1:1
$n_{dodecene}/n_{Rh}$	4000/1
$n_{biphephos}/n_{Rh}$	5/1
T_S	5°C
$\dot{m}_{1-dodecene}$	12.2 g/h
$\dot{m}_{n-decane}$	32.1 g/h
$\dot{m}_{make-up}$	4.28125 g/h
$w_{DMF}^{make-up}$	0.9927
$w_{Rh(acac)(CO)_2}^{make-up}$	$0.0584 \cdot 10^{-3}$
$w_{Biphephos}^{make-up}$	0.0072
V_R	1000 ml
ε_R^{liq}	0.32
m_R^{liq}	244.3 g

The process conditions are summarized in Tab. 5.1. The reaction is not optimally controlled and the reaction conditions have been determined manually during operation. The same holds for the make-up

streams. The catalyst and solvent ratios have been identified in preliminary investigations in lab-scale experiments [199].

5.1.2 Retrofit problem definition

The miniplant process indicates specific properties, which lead to certain restrictions for the synthesis and design procedure of an optimal reactor unit or network. In addition, several requirements are set intending a proper comparison of the existing setup and the targeted retrofit. The following conditions and restrictions have to be complied with:

- The separation unit structure is fixed and no additional separators are supposed to be added.
- The envisaged reactor-network should be optimal for both realizations of the flow sheet, i.e. for the case of the complete operation scheme with a distillation column and resulting side product recycle, and the case of the reduced operation scheme considering only the recycle of the polar catalyst solvent phase.
- The residence time within the reaction section of the retrofitted process should not be higher than the residence time in the CSTR of the existing process.
- The catalyst amount and ratio, and the solvent composition have to be the same as used in the miniplant experiments.
- The amount of control inputs and reactor units should be kept as small as possible to avoid high construction effort and costs.
- The operating conditions of the separation units are fixed to ensure that possible performance improvements are not originated from better separation performance.
- The objective of the optimization is the maximization of the yield of tridecanal. It combines the selectivity and the conversion, which both are supposed to be improved by the retrofit.

Following the first two aspects, the synthesis will aim at an optimal reactor-recycle-network, which is as well highly performing without the recycle. The third point is taken into account by adding a residence time constraint and simultaneously setting the volume and the inlet streams of the optimal reactor-network as a degree of freedom in the design procedure. The fourth aspect was already considered in the previous design optimizations in chapter 3 and 4, and is taken into consideration easily as well for the upcoming optimizations. The fifth condition is part of the decision-making regarding the final choice of the best suitable reactor-network candidate and will be discussed in subchapters 5.2 and 5.3. The last aspect is taken into account when evaluating the optimal reactor-network within the integrated overall process in subchapter 5.4.

Considering the liquid mass inside the reactor, m_R^{liq}, and the mass flow rates given in Tab. 5.1, the residence time in the CSTR is 192 min. Note, that the total mass inlet flow has to contain the same amount of DMF as of n-decane to keep the solvent ratios constant. Hence, the maximum residence time of the retrofit optimization is set to $\tau_{set}^{max} = 192$ min.

5.2 Synthesis of optimal reactor-(recycle)-networks

Following the aforementioned restrictions and requirements of the retrofit problem, two dynamic optimization problems arise, i.e. one for the case of reactor-network synthesis and a second for the case of reactor-recycle-network synthesis for the reduced and the complete operation scheme, respectively. As the model formulation does not change in comparison to the reactor synthesis steps in chapter 3, the dynamic optimization problems formulated in Eqs. (41)-(61) and Eqs. (94)-(114) are adopted for the RNS and RRNS, respectively. However, the results cannot be adopted as well, because the residence time and the objective are changed. Hence, within both DOPs the constraint for the final

time, Eq. (55) and Eq. (107), is adjusted to set its maximum bound to the predefined value introduced before, i.e. $t_f \leq 192$ min. The objective is changed to the yield of tridecanal, Y_{nC13al}, and the conversion in both DOPs is unfixed.

5.2.1 Flux profile analysis for reactor-network synthesis and reactor-recycle-network synthesis

Results of reactor-network synthesis

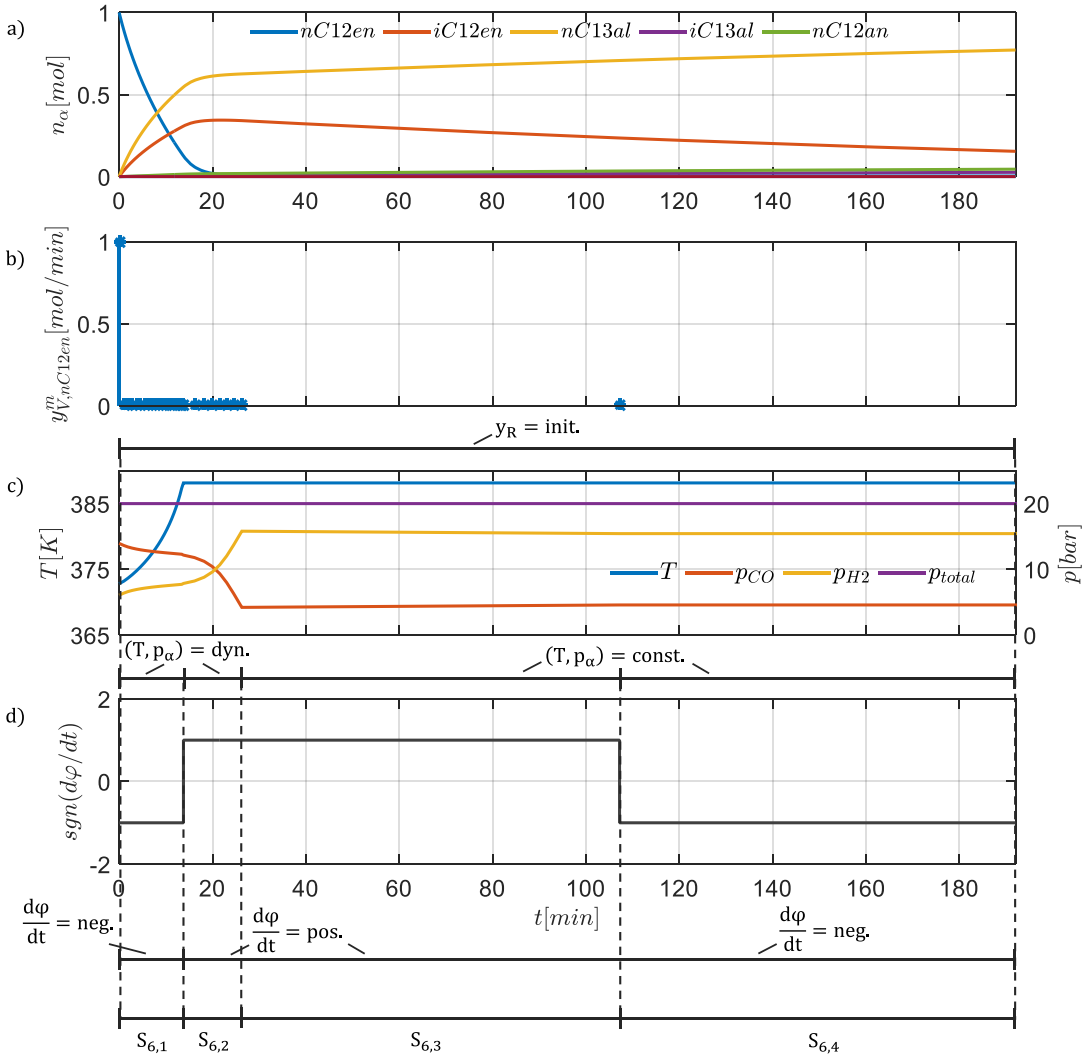

Figure 5.2: *Flux profile analysis* results of the RNS for the retrofit of the hydroformylation miniplant

The results of the dynamic optimization for RNS are illustrated in Fig. 5.2. Evidently, the reaction progress and the control fluxes are the same as shown in Fig. 3.7, at least up to $t = 100$ min. From there on, the temperature and partial pressure controls are kept constant until the end of the reaction at $t_f = 192$ min. However, the differential selectivity indicates a change in this last section. Due to the similarities to the results in subchapter 3.2.3, the sections $S_{6,1}$ - $S_{6,3}$ are not discussed in detail again. The fourth section, $S_{6,4}$, is supposed to be realized in an additional PFR, since no reactant dosing takes place and the gradient of the differential selectivity is negative. However, the control profiles are equal to the previous section and, thus, a merger of the last two sections in one unit seems

promising. Taking the knowledge from the discussion in subchapter 3.2.3 additionally into account, the realization of the second section, $S_{6,2}$, with a cascade of CSTRs is not beneficial. Hence, the resulting reactor-network candidates for further investigation are a PFR+CSTR network and a PFR+CSTR+PFR network.

Results of reactor-recycle-network synthesis

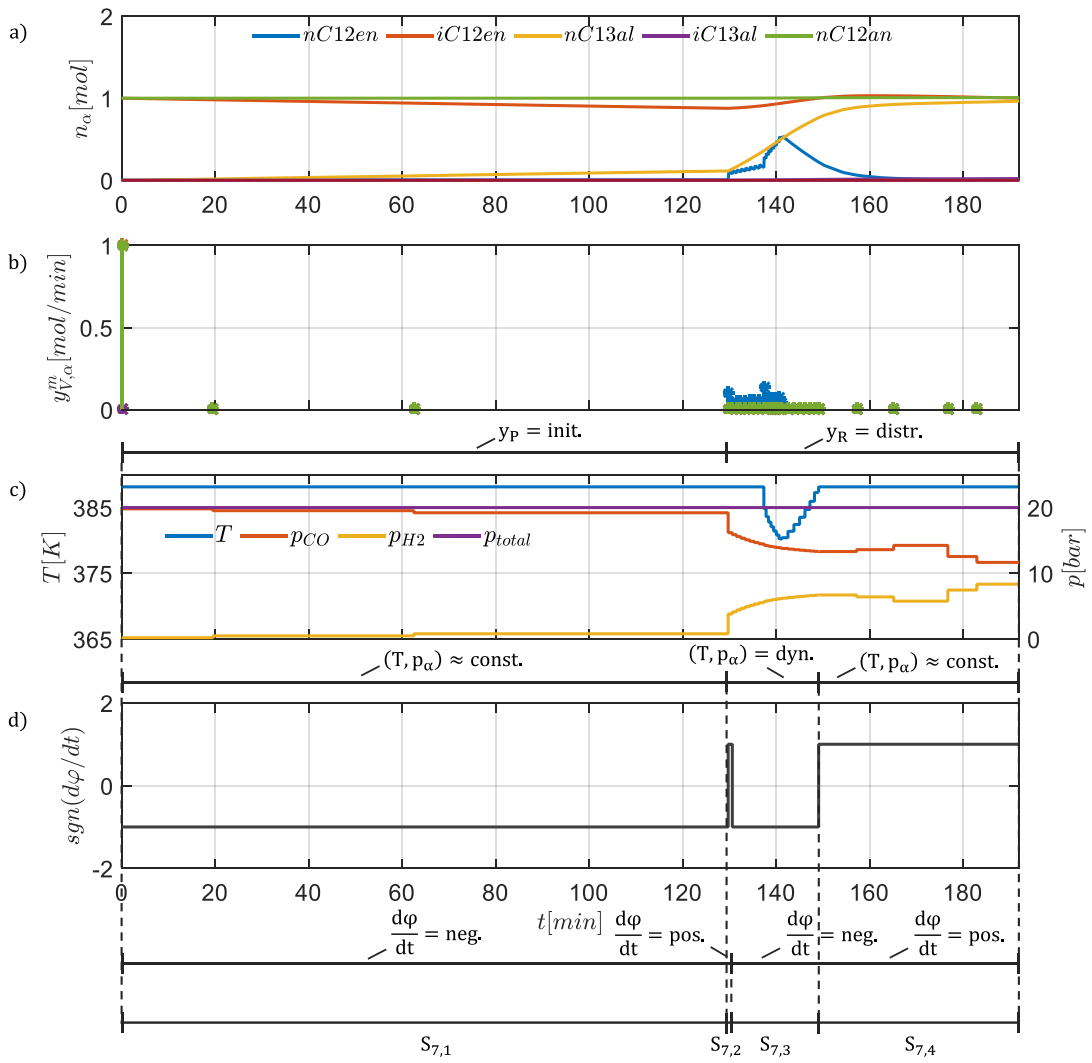

Figure 5.3: *Flux profile analysis* results of the RRNS for the retrofit of the hydroformylation miniplant

In the second step the product dosing is enabled in order to identify optimal candidates of reactor-recycle-networks. The results of the corresponding dynamic optimization are shown in Fig. 5.3 and indicates once more clear similarities to the optimization results discussed in subchapter 3.3.3, see Fig. 3.16. A first long reaction section $S_{7,1}$ with small progress and almost constant control profiles indicates again a benefit from recycling of the two reversible side products, n-dodecane and iso-dodecenes. Although the gradient of the differential selectivity is here of different sign, the character and hence the impact of this section is expected to be comparably low, as the results of subchapter 3.3.3 point out. Therefore, it is neglected with respect to the derivation of optimal reactor-recycle-network candidates. The second section $S_{7,2}$ is very small and only arises due to a change in the gradient of the differential selectivity. Although it might be a numerical artefact, it is considered

within one of the further investigated candidates, to check for its influence on the reaction performance. The third reaction section $S_{7,3}$ clearly indicates the realization with a DSR and the fourth section $S_{7,4}$ is supposed to be approximated with a CSTR. The final reaction time is again at its maximum. Thus, the RRNS results in two promising candidates, namely an IR-CSTR+DSR+CSTR network and an IR-DSR+CSTR network. Together with the candidates obtained from the RNS, the four reactor-(recycle)-network candidates, which are supposed to be compared to identify the final most promising network for technical realization, are depicted in Fig. 5.4.

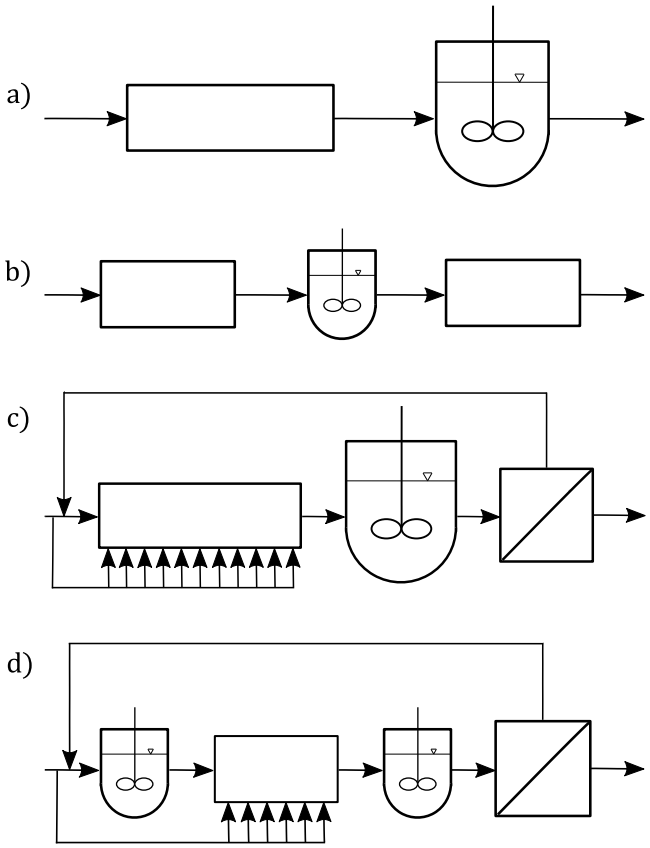

Figure 5.4: Optimal reactor-network candidates a) and b), and optimal reactor-recycle-network candidates c) and d) considered for the further design procedure

5.2.2 Comparison of reactor-(recycle)-network candidates

The derived reactor-(recycle)-network candidates are once again compared with respect to their performance in the $[S_{nC13al}, X_{nC12en}]$-space. Since the final reactor-network is supposed to be operated in a scenario with and a scenario without recycling of side products, the target of this comparison is to identify the candidate which performs well in both cases. Hence, the candidates a) and b) in Fig. 5.4 are as well investigated with closed global recycle and the candidates c) and d) without closed global recycle. In addition, the performance of the single PFR with gas dosing, which was suggested in Hentschel et al. [159] as optimal choice, is determined as reference.

To determine the characteristic $[S_{nC13al}, X_{nC12en}]$-curves, a dynamic optimization of each candidate is carried out maximizing the selectivity for varying predefined conversions. The results for the case without closed global recycle given in Fig. 5.5 indicate that the two candidates with the DSR (purple and green line) perform best for all conversions. However, a closer look to the dosing and control fluxes for different conversions reveals that these high selectivities at all conversions is reasoned by a global bypass effect. This means, that the degree of freedom to dose reactant everywhere along the reaction coordinate leads to a dosing strategy that initially doses the amount of

reactant, which is almost completely converted, and add a final dosing required to achieve the predefined conversion. The optimal control of temperature and partial pressures is thereby similar to those obtained for the high conversion of the initially dosed reactant, without the final addition of remaining reactant. This behavior is exemplarily illustrated in Fig. 5.6 for the DSR+CSTR network at a conversion of $X_{nC12en} = 50\%$. The increase of selectivity with decreasing conversion originates from the slightly improved ratio of reactant to formed side products which supports the reaction. Comparing the remaining three candidates, it becomes obvious that the PFR+CSTR (red line) shows again the increased selectivity in the conversion range between 90 % and 99 % in comparison to the single PFR (blue line), which was already discovered in subchapter 3.2.3. An added PFR to this network does not improve the performance noticeably (yellow line).

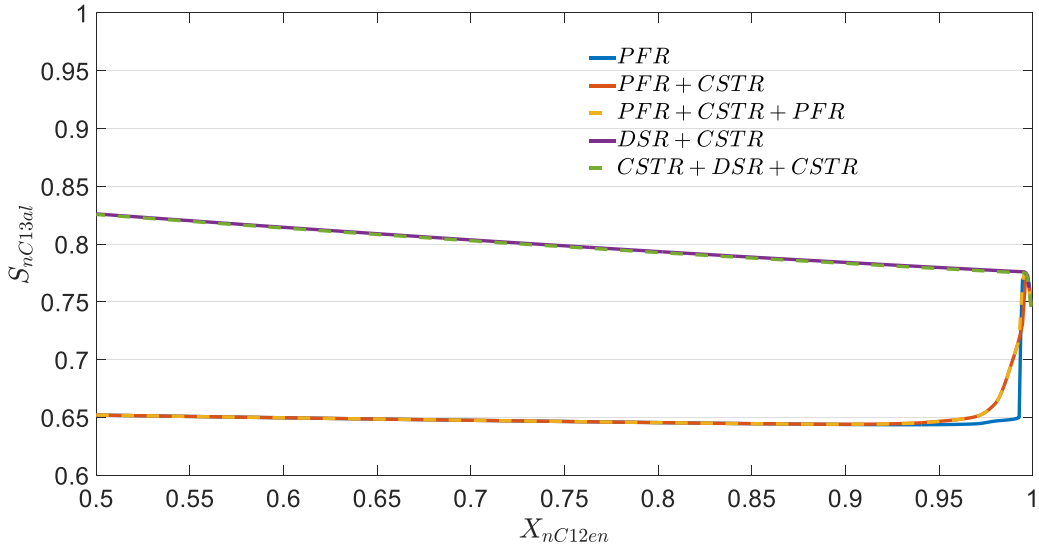

Figure 5.5: Selectivity with respect to tridecanal over conversion of 1-dodecene for optimal reactor-network candidates

The same procedure is carried out for the same network candidates for the case of closed global recycle. The corresponding results are depicted in Fig. 5.7. Evidently, the qualitative characteristics of the performance of the network candidates are the same. The two candidates containing a DSR show once more the high selectivity for all conversions due to the global bypass effect, and the IR-PFR+CSTR outperforms the single IR-PFR, whereas its performance is not increased by addition of an initial CSTR. As already shown in subchapter 3.3.3, the initially recycled side products increase the selectivity significantly for all candidates and all conversions. Since the target of this retrofit is the maximization of the yield of tridecanal, including the conversion of reactant and the selectivity with respect to tridecanal, the benefit of the network candidates containing a DSR for medium to high conversions is not useful. Moreover, their performance gain for high conversions in comparison to the candidates without distributed reactant dosing is rather small. Hence, the additional effort of realizing a distributed reactant dosing is not reasonable. Following the previous discussions about the remaining three network candidates, the (IR-)PFR+CSTR seems to be most promising.

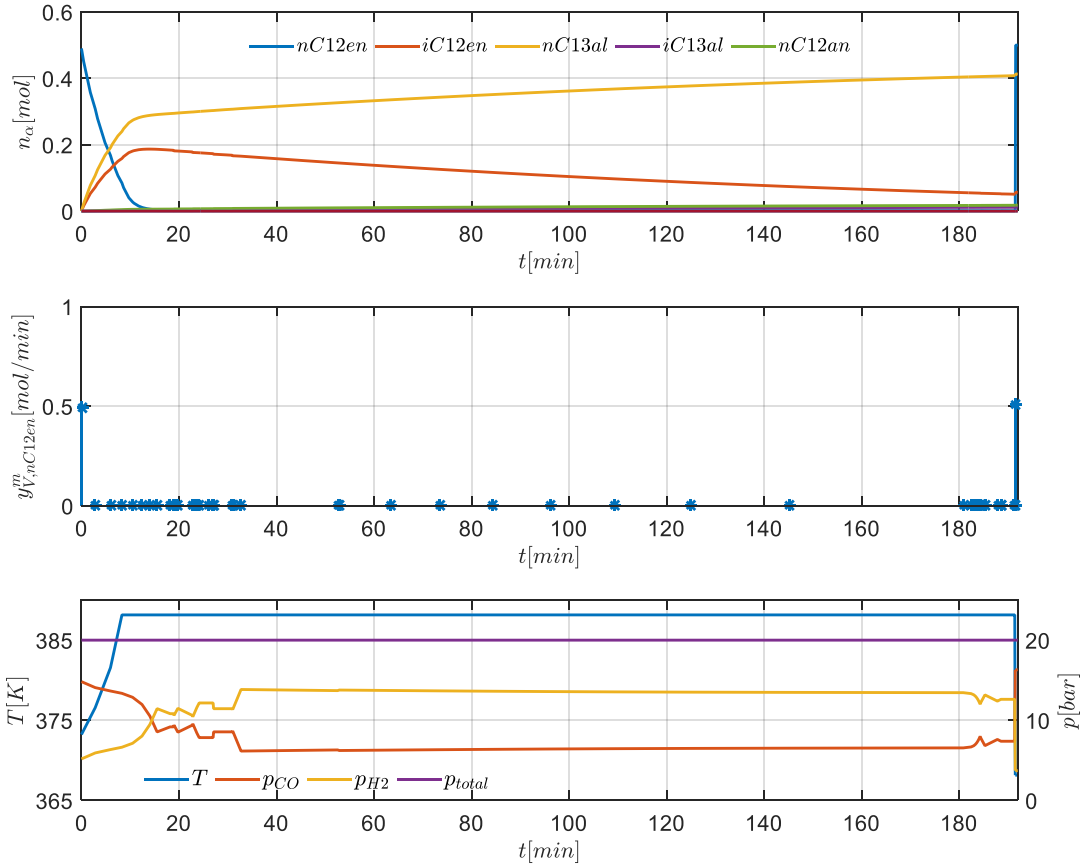

Figure 5.6: Optimal fluxes of the DSR+CSTR network at $X_{nC12en} = 50\%$ indicating the global bypass effect

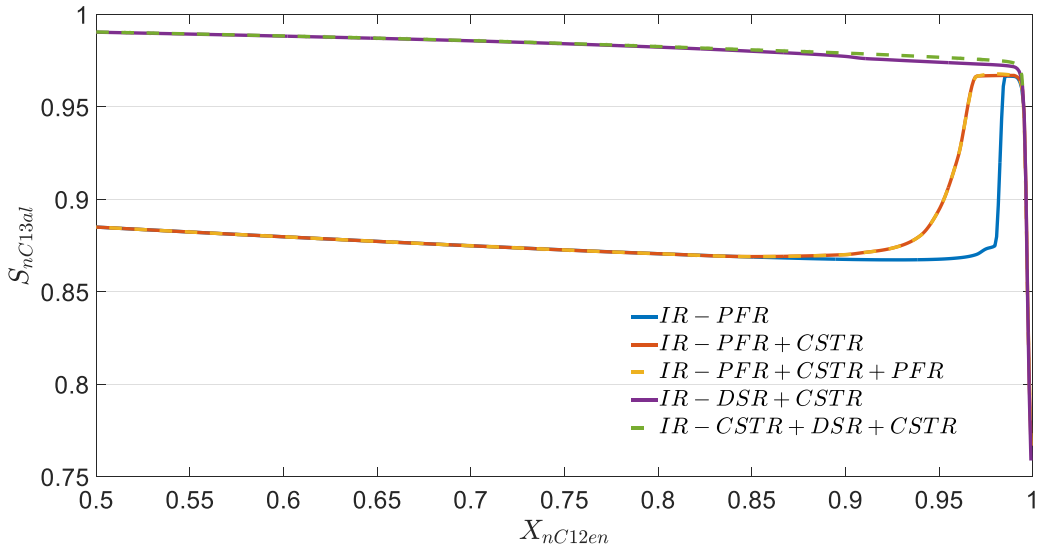

Figure 5.7: Selectivity with respect to tridecanal over conversion of 1-dodecene for optimal reactor-recycle-network candidates

The broader range of conversions with high selectivity and its smoother transition into this region in comparison to the (IR-)PFR indicate a higher potential for finding a robust design in the next step when considering model parameter uncertainties, since the investigations in subchapter 4.2.1 have

shown that the predictive power of the performance is strongly decreasing at very high conversions. In addition, the constant control profiles in the second reaction section are easier to realize in a CSTR than in a PFR. Thus, the (IR-)PFR+CSTR is chosen for further detailed design and embedding in the integrated miniplant process. Note, that the total residence times at the desired high conversions are always at the maximum bound and, thus, the technical design is carried out for the targeted residence time of $\tau_f = 192$ min.

5.3 Technical realization

In order to design the (IR-)PFR+CSTR network, identified as most suitable for the retrofit of the integrated miniplant process, in detail aiming at its technical realization, several aspects have to be investigated. At first it is discussed in subchapter 5.3.1 how the selected reactor-(recycle)-network might basically be realized with respect to its operational mode and its embedding in the existing miniplant process. Secondly, the main control variables, i.e. partial pressures and temperature, are analyzed with regard to the required number of control inputs for a sufficient approximation of the optimal control profiles in subchapter 5.3.2. As a result of these first steps, a rough realization of the optimal reactor-(recycle)-network is obtained. In subchapter 5.3.3 aspects of dimensioning of the individual units are considered, what includes mainly the investigation of flow patterns of the first unit.

5.3.1 Design options for embedding in miniplant process

The design of the synthesized reactor-(recycle)-network starts with deriving basic realization options. The first reaction section is supposed to be realized in a PFR since it indicates a dynamic control of the partial pressures and temperature and has no benefit from back-mixing. The initial recycling of side products does, thereby, not influence the possible realization options. Following these requirements, this reaction section can either be realized in a continuous flow reactor with distributed control or a discontinuous, i.e. batch wise, operated semi-batch reactor, see Fig. 5.8. The latter has the advantage that it is inherently free of back-mixing and, thus, has an analogous residence time behavior than a PFR. Furthermore, the dynamic control trajectories of the first reaction section can be realized accurately over time in the semi-batch reactor instead of approximating them discretely along the length of a continuous flow reactor. However, the integration of a discontinuously operated unit within a continuous process comes along with additional challenges, e.g. complex cyclic operation. A short overview of advantages and disadvantages of both realization options is given in Tab. 5.2, not striving for comprehensiveness. The second reaction section is supposed to be realized in a CSTR with constant control values. Since this is already the simplest way to realize this section in one unit, it is not sought for more complex alternatives.
In order to keep the construction effort small, the existing CSTR in the miniplant can be used to realize the second reaction section. Following the flow sheet in Fig. 5.1, the CSTR has a temperature control and equipment for maintaining a predefined partial pressure level and, thus, fulfills the given requirements of the optimal reactor-(recycle)-network. Although the size of the CSTR is fixed, when adopting the existing unit, the possible performance loss is expected to be acceptable in comparison to the reduction of realization effort. Its mass transfer rates are assumed to be sufficiently high as the hydroformylation was already operated in this vessel. Moreover, the required mass transfer rates in the second reaction section, which will be realized in the CSTR, are rather small as the reaction therein is slow. Hence, the CSTR does not require an individual technical design and the design procedure focuses mainly on the first reaction section.

Table 5.2: Advantages and disadvantages of realizations with cyclic semi-batch reactor and continuous flow reactor

Cyclic semi-batch reactor	
+	-
Continuous realization of control trajectories over time	Require buffer tanks for embedding in continuous overall process
Inherently free of back-mixing	Cyclic operation is more complex than steady-state operation
Accurate mass transfer controlled by stirring	Preparation time of each batch has to be considered leading to loss of reaction time
Easier to control as only one input has to be controlled for a concentrated system	Preparation has to be carried out very properly to avoid residues or oxygen input
Continuous flow reactor	
+	-
Less units to control since no additional buffer tanks are required	Requires suitable flow regime to approximate PFR characteristics
Simple embedding in continuous overall process	Control trajectories have to be approximated discretely along the reactor length with several control inputs
Steady-state operation, no preparation time needed	Pressure losses
Mass transfer can be increased by advanced flow regimes	Mass transfer is dependent and limited by possible flow regimes

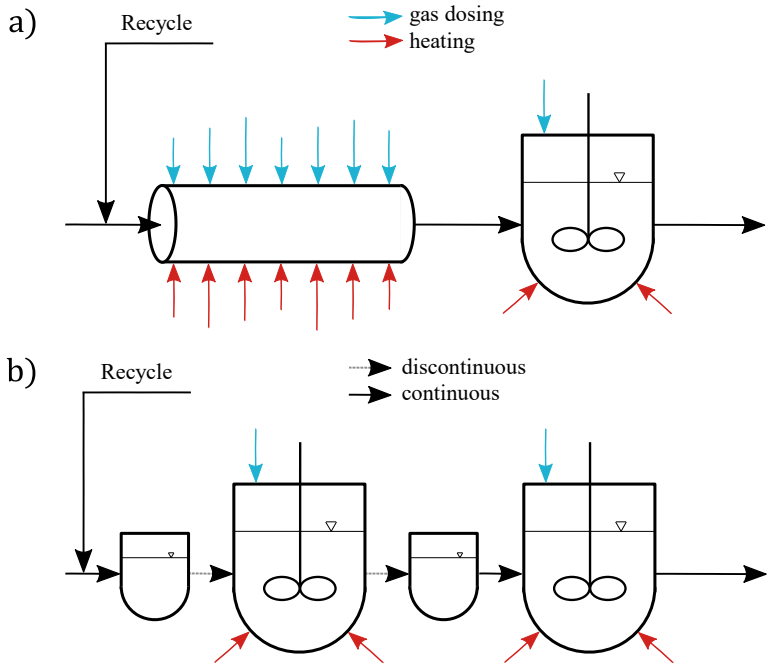

Figure 5.8: Realization options for (IR-)PFR+CSTR network: a) Continuous flow reactor with CSTR; b) Cyclic semi-batch reactor with CSTR and buffer tanks for embedding in overall process

Within this work the detailed design will be carried out only for the purely continuous realization option in which the first reaction section is realized in a continuous flow reactor (CFR).

Although the hybrid batch-continuous realization in a cyclic semi-batch reactor (CSBR) has promising potential, it is also accompanied by several challenges which require a comprehensive and detailed investigation. For the lack of time this research is not included in this thesis. The interested reader is referred to the work of Kaiser et al. [200] and Raetze et al. [201], who investigated this realization of the CSBR with model-based optimizations, and Jokiel et al. [202] who carried out the experimental validation of the CSBR both stand-alone and embedded in the integrated miniplant setup. Their work is complementary to this work and part of the same collaborative research center project introduced in chapter 1.

5.3.2 Sensitivity analysis with respect to number of control inputs

The technical realization of the (IR-)PFR+CSTR network requires exact knowledge about the number of control inputs which have to be realized. Within the previous synthesis and design steps the number of control inputs was assumed to be infinite resulting in continuous control trajectories. For the technical realization with a CFR these trajectories have to be approximated with discrete control inputs along the reactor length. In the following it is investigated, how many control inputs are required for the partial pressure control and the temperature control in order to keep the performance loss caused by the spatial approximation small. These investigations focus mainly on the (IR-)PFR unit, since the CSTR unit has only one control input for the temperature and one constant partial pressure level.

Realization of partial pressure profiles

As the partial pressures are directly linked to the amount of gas and its holdup, the controls of the partial pressures require a control of those measures. The holdup is assumed to evolve due to the reaction along the reactor length and is not controlled individually. However, the amount of gas can be controlled via dosing streams and in this way the holdup is somehow indirectly changed wherever a dosing is realized. The inclusion of dosing streams of gas components requires the modeling of the gas phase, the mass transfer from gas phase to liquid phase, and the balancing of the gaseous components within the liquid phase. The gas phase is balanced via

$$\frac{dn_\alpha^{gas}}{dt} = y_{V,\alpha}^m - k_L a\, V_{liq}(c_\alpha^* - c_\alpha), \quad \alpha \in GAS\,, \tag{5.1}$$

with $k_L a$ being the volumetric mass transfer coefficient and c_α^* corresponding to the liquid concentration of the gas components at the interphase, see Eq. (2.11). Thereby it is assumed, that the mass transfer is modelled with a stagnant film model and the mass transfer resistance is completely located in the liquid phase. In addition, the molar balance for the gas components in the liquid phase is stated as

$$\frac{dn_\alpha^{liq}}{dt} = V_{liq}\left(c_{cat} M_{cat}\left(\sum_{m=1}^{M} \nu_{\alpha,m} r_m\right)\right) + k_L a\, V_{liq}(c_\alpha^* - c_\alpha), \quad \alpha \in GAS. \tag{5.2}$$

Within the dynamic optimization problem the partial pressures as control variable are replaced by the molar dosing streams of gas components $y_{V,\alpha}^m, \alpha \in GAS$ and the partial pressures within the model are determined via the ideal gas law. Within the following investigations the $k_L a$ value is set to a very high value to avoid an influence of mass transfer resistance on the sensitivity analysis. This influence is later investigated individually. To approximate the optimal partial pressure profiles, four scenarios are investigated:

- Approximation case 1: Only one initial dosing of gas at the inlet of the (IR-)PFR is realized.
- Approximation case 2: An initial gas dosing for the first reactor and a gas dosing stream for the second reactor are considered.
- Approximation case 3: The (IR-)PFR has and initial and an intermediate gas dosing stream and the CSTR is controlled individually.
- Reference case: All results are compared with the ideal case of optimal dynamic partial pressure control, as determined in subchapter 5.2.2 and illustrated in Fig. 5.5 and Fig. 5.7 for the operation scenarios without and with side product recycling, respectively.

The results of the dynamic optimizations for the reference case and the three approximation cases are depicted in the $[S_{nC13al}, X_{nC12en}]$-space in Fig. 5.9.

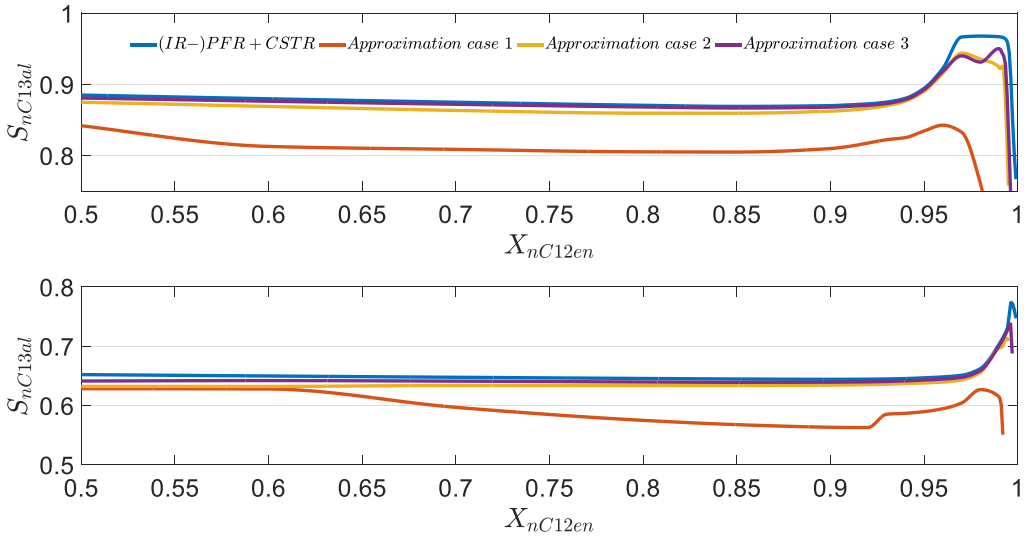

Figure 5.9: Sensitivity analysis for number of control inputs realizing the optimal partial pressure profiles of the (IR-)PFR+CSTR network for: a) the operation scenario with closed side product recycle; and b) without closed side product recycle.

Evidently, the realization with only one initial gas dosing stream in approximation case 1 is accompanied with an unacceptable performance loss. Approximation case 2 and 3 come quite close to the performance of the reference case and indicate only at high conversions a significant gap. The slightly higher performance of approximation case 3 in comparison to case 2 does not justify its additional constructional effort and, thus, the initial gas dosing in the (IR-)PFR and the individual gas dosing for the CSTR suffice for an accurate approximation of the optimal partial pressure control.

Realization of temperature profile

In the same way as the sensitivity of the number of control inputs for the partial pressures are investigated, the realization of the temperature profile is tested for different scenarios. However, in contrast to the partial pressures the temperature is not assumed to be controlled by discrete heating/cooling streams. Instead it is assumed that the temperature is controlled within sections of constant temperature. On the miniplant scale this is simply realizable and avoids the laborious inclusion of an energy balance, which describes the heat absorption and release along the reactor length of the (IR-)PFR and the vessel wall of the CSTR. This negligence bases moreover on the assumption that the required heating fluxes are rather small as the reaction is only slightly endothermic and the operation range of the temperature encloses only 20 K. Again, four scenarios are tested which are inspired by the previous approximation cases:

- Approximation case 1: Only one temperature level along the entire reaction coordinate, i.e. for both reactor units.
- Approximation case 2: Individual temperature levels for both reactor units.
- Approximation case 3: The (IR-)PFR has two temperature levels and the CSTR one.
- Reference case: All results are again compared with the ideal case of optimal dynamic temperature control, as determined in subchapter 5.2.2 and illustrated in Fig. 5.5 and Fig. 5.7 for the operation scenarios without and with side product recycling, respectively.

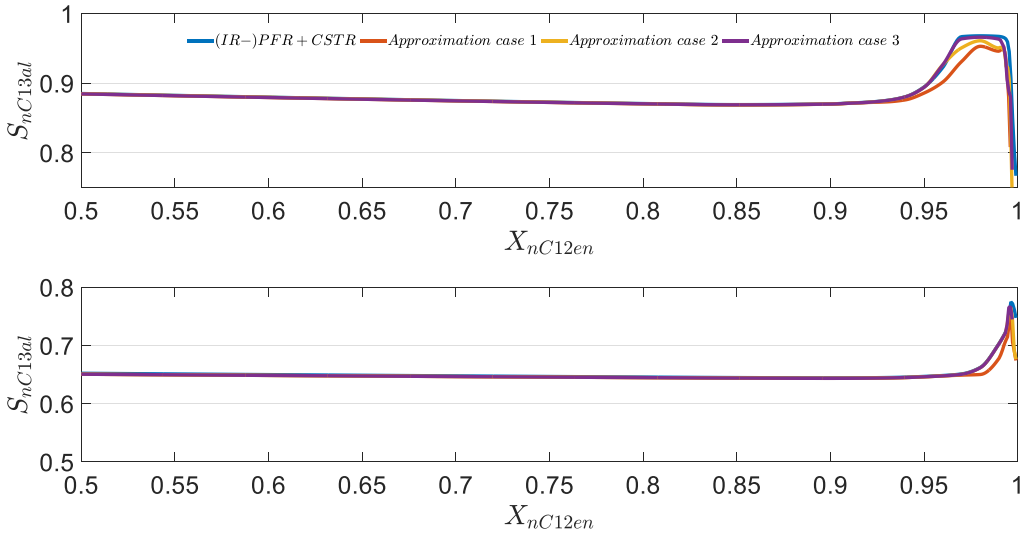

Figure 5.10: Sensitivity analysis for number of control inputs realizing the optimal temperature profile of the (IR-)PFR+CSTR network for: a) the operation scenario with closed side product recycle; and b) without closed side product recycle.

The results in Fig. 5.10 indicate that the performances of all approximation cases are almost equal to the reference case for conversions ≤ 93 %. For higher conversion the approximation improves with every additional temperature section. The gap for approximation case 1 at high conversions is of several percent and, thus, its realization is neglected. Since approximation case 3 is almost exactly matching the reference performance, a further increase of temperature sections is not necessary. Hence the optimal temperature profile is approximated with two constant temperature sections along the (IR-)PFR and one in the CSTR.

Following the previously discussed results, the technical realization of the optimal (IR-)PFR+CSTR network is conducted with an initial gas dosing for the (IR-)PFR and an individual gas dosing for the CSTR, and the temperature is realized with two temperature sections for the first and one for the second reactor unit.

5.3.3 Designing the continuous flow reactor

In this step the detailed design of the continuous flow reactor is carried out. Therefore, two aspects are emphasized whose accurate consideration decide about the performance of the continuous flow reactor.

- Mass transfer: Since the hydroformylation is a gas-liquid multiphase process, it is important to investigate the mass transfer requirements in order to ensure that sufficient gas reactant is supplied as the reaction progresses.

- Back-mixing: The continuous flow reactor is supposed to approximate the residence time behavior of the ideal plug flow reactor as good as possible, i.e. minimizing the axial dispersion.

Both properties mainly depend on the mixing characteristics of the continuous flow reactor and, thus on its flow regime. First, sensitivity studies are carried out to identify the minimum required mass transfer rates and the maximum allowed deviation from the plug flow behavior. Based on that a suitable flow regime is chosen and corresponding reactor dimensions are determined.

Mass transfer

In order to investigate the impact of the mass transfer rates on the performance of the optimal (IR-)PFR+CSTR network, its dynamic optimization is carried out for varying volumetric mass transfer coefficients $k_L a$. In this way a minimum required $k_L a$ value is identified.

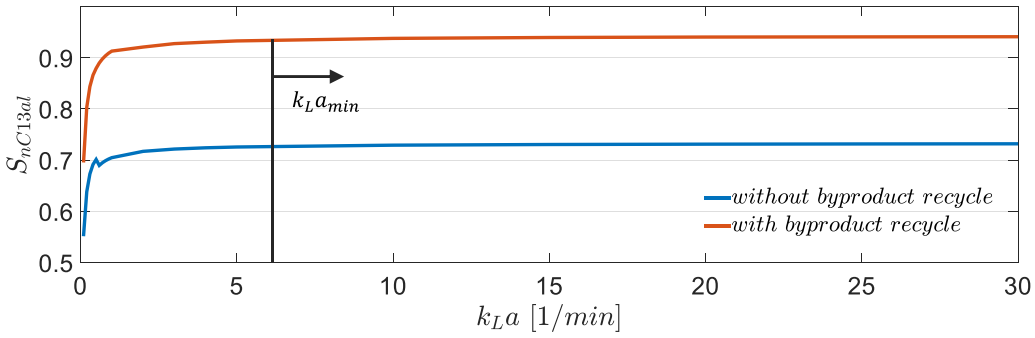

Figure 5.11: Sensitivity analysis quantifying the impact of the volumetric mass transfer coefficient on reaction performance

As can be seen in Fig. 5.11, the mass transfer limits the performance noticeably for small $k_L a$ values. In both operation scenarios, i.e. without and with side product recycle, the performance loss for $k_L a \leq 6\ 1/\text{min}$ increases to more than 1 %. Hence, this value is chosen as minimum required $k_L a$ value for the technical design of the continuous flow reactor.

Back-mixing

The impact of back-mixing on the reactor performance is supposed to be treated as deviation from optimal plug flow reactor and, thus, the concept of axial dispersion is considered. Since the final dimensions of the continuous flow reactor are not yet known, a dimensionless number is used, namely the Péclet number (*Pé*), to describe the axial dispersion coefficient D_{ax} in dependence of the reactor length l and the fluid velocity v (Eq. (5.3)).

$$Pé = \frac{l * v}{D_{ax}} \tag{5.3}$$

Hence, for a given length the *Pé* number increases with decreasing axial dispersion. In order to investigate the impact of varying *Pé* numbers on the reactor performance, a cascade model of equally sized CSTRs is used as kind of surrogate model for the PFR [193]. With a known heuristic the number of CSTRs N in this cascade is linked with the *Pé* number (Eq. (5.4)).

$$\frac{Pé}{2} = N \tag{5.4}$$

The equally sized CSTRs are modeled via the mass balances for the liquid phase components (Eq. (A.37)), the dissolved gas components in the liquid phase (Eq. (A.38)), and the gas phase components (Eq. (A.39)). In addition, continuity conditions are formulated connecting the CSTRs (Eqs. (A.40)-(A.41)). Based on this model, the dynamic optimizations are carried out for varying number of CSTRs approximating the (IR-)PFR for different *P*é numbers.

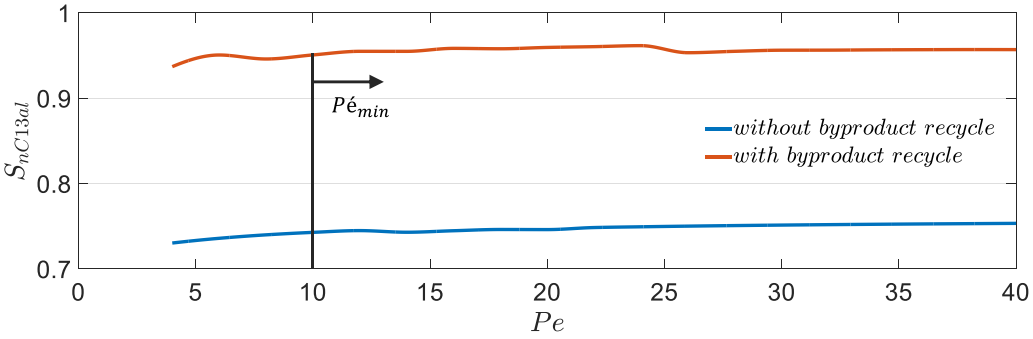

Figure 5.12: Sensitivity analysis quantifying impact of axial dispersion on reaction performance using the dimensionless ***P***é number

The results in Fig. 5.12 indicate that the impact of axial dispersion on the selectivity with respect to tridecanal is moderately high. For $Pé \leq 10$ the performance loss is again higher than 1 % and, thus, this is the minimum allowed *P*é number for the technical design of the continuous flow reactor.

Identifying suitable flow regime

The search for a suitable flow regime in the CFR that satisfies the above derived requirements is strongly dependent on the available range of dimensions, in particular the tube diameter. According to Tab. 5.1 the volumetric inlet flow is determined to $\dot{V}_{CSTR,in}^{liq} \approx 100$ ml/h. Since the residence time is supposed to be maintained, but an additional reactor unit is added to the existing CSTR, the volumetric flow rate has to be increased. The corresponding decision-making depends on the length the first reaction section is supposed to have. Based on the knowledge about the reaction sections indicated by the FPA and the insights of the shift of the reaction sections when searching for a robust design under model parameter uncertainties in subchapter 4.2.1, see Fig. 4.9, it seems reasonable to assume the first reaction section to be half as long as the second. Thus, the volumetric inlet flow rate is set to $\dot{V}_{CFR,in}^{liq} \approx$ 150 ml/h. Together with an assumed liquid hold-up of $\varepsilon_{liq}^{CFR} = 0.33$, the overall volumetric flow rate is considered around $\dot{V}_{CFR,in}^{tot} \approx 450$ ml/h. Considering further the overall residence time of $\tau_{tot} =$ 192 min, and the volume and liquid hold-up of the existing CSTR, $V_{CSTR}^{tot} = 1$ l and $\varepsilon_{liq}^{CSTR} = 0.32$, respectively, the overall volume of the CFR can be determined to $V_{CFR}^{tot} \approx 0.49$ l.

To achieve high mass transfer rates and a small axial dispersion in a tube reactor of ≈ 0.5 l, the flow regime has to provide a large specific surface of the gas-liquid interphase and high radial mixing, respectively. This can be induced by e.g. turbulent flow or static mixers. However, the volumetric flow rates are very small, e.g. for tube diameters between $1\,\text{mm} \leq d_{tube} \leq 10\,\text{mm}$ the superficial fluid velocity is in the range of $7.08 \cdot 10^{-4}\,\text{m/s} \leq v_s \leq 0.0708\,\text{m/s}$. The latter do not enable the use of static mixers or the generation of turbulent flows and, hence, both are not practical. According to Coleman and Garimella [203] the flow patterns being formed in such small diameter tubes are stratified flow, intermittent flow, dispersed flow, or annular flow. These in turn can be subdivided again into different special flow patterns. For similarly small gas and liquid superficial velocities the only flow pattern of interest is the intermittent flow pattern, also known as Taylor flow, due to the following advantageous properties: (i) the axial dispersion within the phases is reduced

significantly by the separation of the liquid bulk [204] and (ii) an internal recirculation within the liquid bulks is induced by the friction forces at the wall, which strongly enhances the mass transfer [205]. These are the two properties which were found to be important for the technical realization of the (IR-)PFR reactor section. According to literature, the volumetric mass transfer coefficients for the superficial velocities stated above are around $0.05..1.5\ \mathrm{s}^{-1}$ [206], and the Péclet numbers for the aforementioned liquid hold-up are higher than 100 [207]. Hence, the intermittent flow pattern is selected as most promising for the further design of the CFR.

In order to allow for the formation of intermittent flow, the tube diameters have to fulfill the condition $d_{tube} \leq 6\ \mathrm{mm}$ [203], and to limit the length of the tube reactor for the sake of a manageable construction effort concerning the tube length, the tube diameter should be not smaller than $1.5\ \mathrm{mm}$. Hence, the tube length will be in the range of $17.33\ \mathrm{m} \leq l_{CFR} \leq 277.28\ \mathrm{m}$. These tube lengths cannot be realized in form of a straight tube within the miniplant setup. Therefore, a bending of the tube to helices is favored. In addition to its compact construction such a reactor configuration has the additional advantage of a uniform pressure loss due to the regular bending [208].

Albeit the previously mentioned literature results already suggest the desired flow regime for these reactor dimensions, they were determined for species with different surface tensions and for higher superficial velocities. To ensure the formation of the desired flow regime for the used solvent system and volumetric flow rates of the hydroformylation miniplant, experiments are carried out under the corresponding conditions. A small setup was built to investigate the flow regime formed for volumetric flow rates in the range of $66\ \mathrm{ml/h} \leq \dot{V}_{CFR,in}^{liq} \leq 200\ \mathrm{ml/h}$ and tube diameters between $1.6\ \mathrm{mm} \leq d_{tube} \leq 3.2\ \mathrm{mm}$. The enable a visual observation a transparent tube material was used and, in addition, the pressure loss within this tube was determined in order to estimate the pressure loss of the intermittent flow inside the CFR. Details about the setup and the experimental results are given in the appendix (A.5). The results indicate that for a volumetric flow rate $\dot{V}_{CFR,in}^{liq} = 200\ \mathrm{ml/h}$ the intermittent flow shows a slight decomposition into a stratified flow and re-composition to an intermittent flow for $d_{tube} = 3.2\ \mathrm{mm}$, and stable intermittent flow for smaller tube diameters ($1.6\ \mathrm{mm}, 2\ \mathrm{mm}$). Due to this finding, no further experiments for larger tube diameters were conducted. For smaller volumetric flow rates ($66\ \mathrm{ml/h}, 102\ \mathrm{ml/h}$), the intermittent flow was stable in all of the tested tubes and, hence, as well for the volumetric flow rate of interest, $\dot{V}_{CFR,in}^{liq} = 150\ \mathrm{ml/h}$. As expected, the pressure loss $\Delta p/l$ increases with decreasing tube diameter and increasing volumetric flow rate. Thus, a trade-off has to be found between a small tube diameter, which ensures intermittent flow but leads to a longer tube, and a small pressure drop. For the technical design of the CFR, a maximum tube diameter of $d_{tube}^{max} = 3\ \mathrm{mm}$ is chosen to ensure the formation of an intermittent flow. On the one hand, the pressure drop for this configuration was measured as $\Delta p \approx 0.0017\ \mathrm{bar/m}$ which results in a negligible overall pressure drop in the CFR around $\Delta p \approx 0.12\ \mathrm{bar}$. And on the other hand, the length of the reactor stays with $l_{CFR} \approx 70\ \mathrm{m}$ in a manageable range.

Final technical design of the optimal reactor-(recycle)-network

Summarizing all findings with regard to the number of the required control inputs for an appropriate approximation of the optimal control profiles and the dimensioning of the PFR unit aiming at an intermittent flow regime providing sufficiently high mass transfer rates and only small axial dispersion, the final technical design is illustrated in Fig. 5.13. The helically coiled tube is oriented vertically, since preliminary studies about the characteristic flow patterns of a helically coiled tube have shown that for low volumetric flow rates a horizontal orientation suffers more from gravitational forces than a vertical orientation [209].

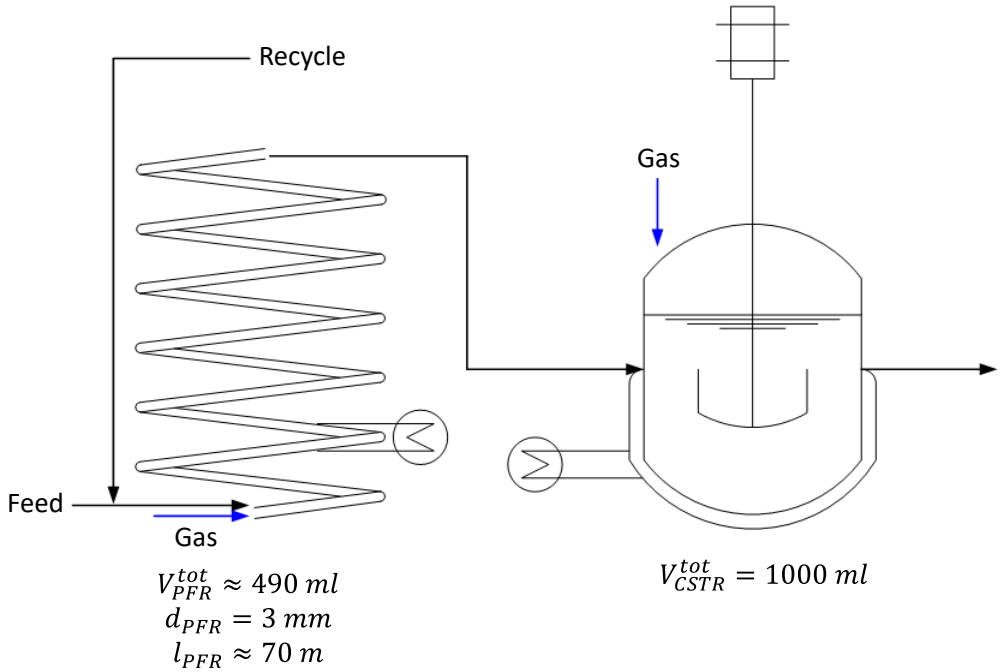

Figure 5.13: Technical design of the optimal reactor-(recycle)-network

5.4 Performance assessment of the technical reactor design in the overall process

The intention of retrofitting the miniplant setup by improving the reactor performance requires inherently the investigation of the optimal reactor-network embedded in the integrated overall process to reveal possible drawbacks and quantify the according performance losses. Moreover, the control inputs for achieving highest performance under real separation conditions are determined. Therefore, the technically designed reactor-network consisting of the helically coiled tube reactor (HCTR) and the CSTR derived in the previous subchapter is embedded in the process flow sheet of the integrated overall process. The flow sheet and the modeling of its units are introduced in subchapter 5.4.1. Subsequently, the dynamic optimization problem of the overall process optimization is derived and solved in subchapter 5.4.2. Therein, model parameter uncertainties for the reactor modeling as introduced in subchapter 4.2 are considered to allow for identifying robust control inputs. In addition, the overall process optimization is carried out for the single CSTR of the original miniplant setup to allow for an appropriate comparison.

5.4.1 Overall process modeling

In contrast to the flow sheet of the miniplant setup given in Fig. 5.1, the process flow sheet for the overall process optimization in Fig. 5.14 is slightly reduced. The second decanter at the distillate stream of the distillation column and the additional buffer tank for the subsequent nonpolar solvent recycle are neglected. The modeling includes the inlet streams, the reactor units, the decanter with its polar solvent recycle, and the distillation column with its nonpolar solvent recycle. The pumps and the flash unit are not modeled individually. The latter is only considered for pressure release and, thus, the molar flow rates of the liquid components fed from the decanter into the distillation column do not change.

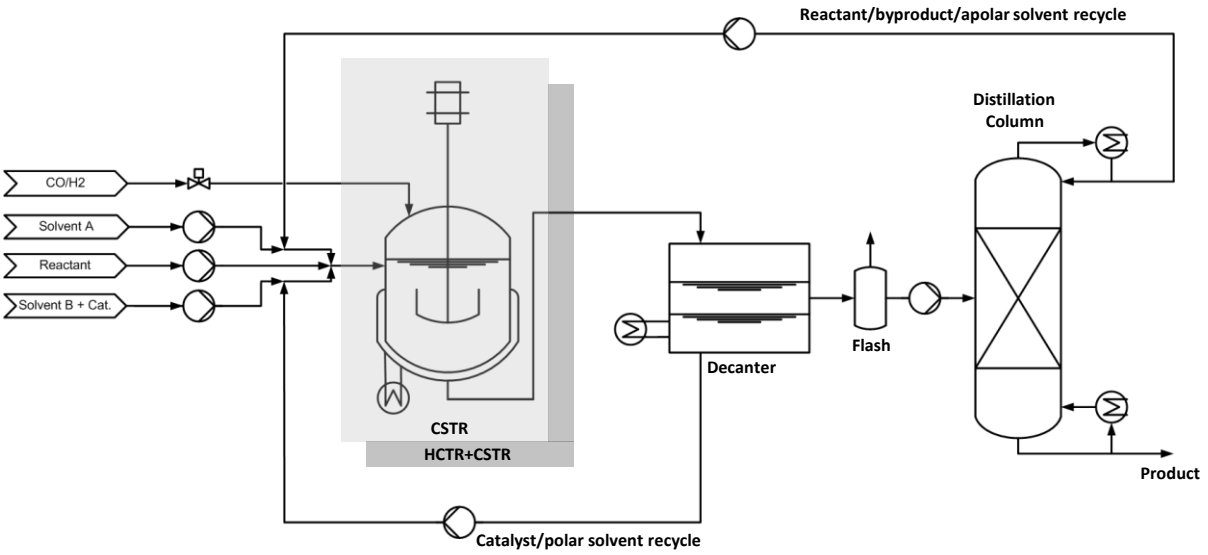

Figure 5.14: Flow sheet for the optimization of the integrated overall process

Inlet streams

The reactor section inlet streams are determined in dependence of the solvent system and catalyst conditions of the miniplant, see Tab. 5.1, and the volumetric inlet flow rates are defined in course of the technical design of the reactor-network in subchapter 5.3.3. In the process flow sheet it corresponds to $\dot{V}_{in}^{HCTR}$, which is calculated according to Eq. (5.5).

$$\dot{V}_{in}^{HCTR} = \dot{V}_{makeup}^{HCTR} + \dot{V}_{out,polar}^{dec} + \dot{V}_{out,D}^{col} \tag{5.5}$$

The calculation of the volumetric flow rate of the makeup stream (Eq. (5.6)) contains the corresponding molar flow rates of the reactant and solvents.

$$\dot{V}_{makeup}^{HCTR} = \frac{\sum_{\alpha}\left(\dot{n}_{\alpha,makeup}^{HCTR} M_{\alpha}\right)}{\rho_{\alpha}}, \alpha \in \{nC12en, DMF, C10an\} \tag{5.6}$$

These makeup streams are dependent of the recycled amounts of the components and the required reactor section inlet flow rates $\dot{n}_{\alpha,in}^{HCTR}$ of the reactant and the solvents (Eq. (5.7)).

$$\dot{n}_{\alpha,makeup}^{HCTR} = \dot{n}_{\alpha,in}^{HCTR} - \dot{n}_{\alpha,out,polar}^{dec} - \xi_{\alpha}\dot{n}_{\alpha,out,D}^{col}, \alpha \in \{nC12en, DMF, C10an\} \tag{5.7}$$

Here, a purge factor ξ_{α} is added to the distillate stream for each species, see subchapter 5.6. To ensure the desired ratio of reactant and solvents, the solvent streams are determined as function of the reactant inlet flow rate $\dot{n}_{nC12en,in}^{HCTR}$ (Eq. (5.8)).

$$\dot{n}_{\alpha,in}^{HCTR} = \dot{n}_{nC12en,in}^{HCTR} \frac{M_{nC12en}}{M_{\alpha}} \frac{w_{\alpha}}{w_{nC12en}}, \alpha \in \{DMF, C10an\} \tag{5.8}$$

The latter is thereby a degree of freedom for the dynamic optimization problem. By including the constraint of the volumetric liquid inlet flow rate $\dot{V}_{in,liq}^{HCTR} = 150$ ml/h, all streams are properly defined by the aforementioned equations. However, the catalyst makeup stream is, due to its negligible volumetric size, not included in this calculation procedure. Instead, it is calculated independently via Eq. (5.9).

$$\dot{n}_{cat,makeup}^{HCTR} = \dot{n}_{nC12en,in}^{HCTR} x_{cat} - \hat{\theta}_{BPP}^{polar} c_{cat}^{tot} \dot{V}_{in}^{HCTR} \tag{5.9}$$

Reactors

The HCTR model considers the balancing of the liquid phase (Eq. (5.10)), of the gas phase (Eq. (5.11)), and of the gas components in the liquid phase (Eq. (5.12)), whereby the latter two include the mass transfer between the phases.

$$\frac{d\dot{n}_{\alpha,liq}^{HCTR}}{dt} = \dot{V}_{liq}^{HCTR} \left(c_{cat} M_{cat} \left(\sum_{m=1}^{M} \nu_{\alpha,m} r_m^{HCTR} \right) \right), \quad \alpha \in CH \tag{5.10}$$

$$\frac{d\dot{n}_{\alpha,gas}^{HCTR}}{dt} = k_L a \, \dot{V}_{liq}^{HCTR} (c_\alpha^{*,HCTR} - c_\alpha^{HCTR}), \quad \alpha \in GAS \tag{5.11}$$

$$\frac{d\dot{n}_{\alpha,liq}^{HCTR}}{dt} = \dot{V}_{liq}^{HCTR} \left(c_{cat} M_{cat} \left(\sum_{m=1}^{M} \nu_{\alpha,m} r_m^{HCTR} \right) \right) + k_L a \, \dot{V}_{liq}^{HCTR} \left(c_\alpha^{*,HCTR} - c_\alpha^{HCTR} \right), \quad \alpha \in GAS \tag{5.12}$$

The CSTR model does not consider the mass transfer in detail since it is assumed that the reaction in the second reaction section taking place in the CSTR is rather slow and, thus, the amounts of gases in the liquid phase corresponds to its maximum solubility given by Eq. (2.11). Due to the assumption that the partial pressures in the CSTR are controlled by the pressure valve and the syngas ratio of the inlet gas stream, the gas phase is not balanced. Hence, the only remaining equation is the liquid phase balance (Eq. (5.13)).

$$\dot{n}_{\alpha,liq}^{CSTR} = \dot{n}_{\alpha,in}^{CSTR} + \tau_{CSTR} \, \dot{V}_{liq}^{CSTR} \left(c_{cat} M_{cat} \left(\sum_{m=1}^{M} \nu_{\alpha,m}{}^{CSTR} \right) \right), \quad \alpha \in CH \tag{5.13}$$

Decanter

For determining the liquid-liquid phase equilibria (LLE) in the decanter unit a Kriging model, introduced in McBride et al. [56], is considered. It makes use of a second order polynomial regression model with Gaussian correlation. As indicated in Eq. (5.14), the output variables $\hat{\theta}_\alpha^{polar}$ of the Kriging model, KR, are the molar fractions of N-,N-dimethylformamide, n-decane, 1-dodecene, tridecanal and Biphephos in the polar solvent phase. The input variables $\hat{x}_\beta$ are N-,N-dimethylformamide, n-decane and tridecanal. Note, that 2-methyl-dodecanal is added to the tridecanal fraction, n-dodecane to n-decane, and the iso-dodecenes to 1-dodecene for the input and output molar fractions. The latter can be calculated from the summation rule of the mole fractions to unity and is hence not given as particular input.

$$\begin{aligned} &\hat{\theta}_\alpha^{polar} = KR(\hat{x}_\beta, T), \\ &\alpha \in \{DMF, C10an, nC12en, nC13al, BPP\} \\ &\beta \in \{DMF, C10an\ nC13al\} \end{aligned} \tag{5.14}$$

The Kriging model is valid for temperatures between $-25°$ and $+25°C$. It shows very good accuracy in comparison to the LLE data calculated by a specially parameterized modified UNIFAC Dortmund model. The resulting output streams of the decanter unit are calculated via Eqs. (5.15)-(5.16).

$$\dot{n}_{\alpha,out,polar}^{dec} = \hat{\theta}_{\alpha}^{polar} \dot{n}_{\alpha,in}^{dec}\,,\ \epsilon \{CH, SOL, BPP\} \tag{5.15}$$

$$\dot{n}_{\alpha,out,apolar}^{dec} = \left(1 - \hat{\theta}_{\alpha}^{polar}\right) \dot{n}_{\alpha,in}^{dec}\,, \alpha \epsilon \{CH, SOL, BPP\} \tag{5.16}$$

Distillation column

The Fenske-Underwood correlations are used to determine the composition of the distillate and bottom streams, and the number of trays. Since the products degrade at temperatures higher than 180 °C, the distillation column is operated at vacuum pressure. For the sake of simplicity, no pressure loss is considered. Aiming at a quantitative separation of the iso-dodecenes and the desired product tridecanal, the first is defined as light key (*LK*) and the latter as heavy key (*HK*) with split fractions of $\zeta_{LK}^{D} = 0.99$ and $\zeta_{HK}^{D} = 0.01$, respectively. For the calculation of relative volatilities with Eq. (A.43), vapor pressure correlations were used given in Yaws [210] (see Eq. (A.41)). For the iso-dodecenes as well as the iso-aldehydes, fitted correlations from Hentschel et al. [159] are used (Eq. (A.42)). The corresponding parameters for Eqs. (A.41)-(A.42) are provided in Tab. A.5. A mean relative volatility is determined with Eq. (A.44) and used for the calculation of the minimum number of stages with Eq. (A.45). The resulting bottom stream is finally computed by Eq. (5.17), whereby the distillate can be determined using the summation condition in Eq. (5.18).

$$\dot{n}_{\alpha,out,B}^{col} = \frac{\dot{n}_{\alpha,in}^{col}}{1 + \frac{\zeta_{HK}^{D} * \dot{n}_{HK}^{in}}{\left(1 - \zeta_{HK}^{D}\right) * \dot{n}_{HK}^{in}}} \tag{5.17}$$

$$\dot{n}_{\alpha,in}^{col} = \dot{n}_{\alpha,out,D}^{col} + \dot{n}_{\alpha,out,B}^{col} \tag{5.18}$$

Flow sheet

The units within the flow sheets are interconnected with the conditions:

$$\dot{n}_{\alpha,in}^{HCTR} = \begin{cases} \dot{n}_{\alpha,makeup}^{HCTR} + \dot{n}_{\alpha,out,polar}^{dec} + \xi_{\alpha} \dot{n}_{\alpha,out,D}^{col}, \alpha \in \{nC12en, DMF, C10an\} \\ \dot{n}_{\alpha,out,polar}^{dec} + \xi_{\alpha} \dot{n}_{\alpha,out,D}^{col}, \alpha \in \{iC12en, nC13al, iC13al, nC12an\} \end{cases}, \tag{5.19}$$

$$\dot{n}_{\alpha,out}^{HCTR} = \dot{n}_{\alpha,in}^{CSTR}, \alpha \in \{CH, SOL\}, \tag{5.20}$$

$$\dot{n}_{\alpha,out}^{CSTR} = \dot{n}_{\alpha,out,polar}^{dec}, \alpha \in \{COM\}, \tag{5.21}$$

$$\dot{n}_{\alpha,out,apolar}^{dec} = \dot{n}_{\alpha,in}^{col}, \alpha \in \{CH, SOL\}. \tag{5.22}$$

5.4.2 Optimization of optimal reactor-network within the integrated overall process

The robust dynamic optimization problem for the optimization of the technically designed reactor-network considers not all model parameter uncertain, which have been considered in chapter 4.2.1. Instead, the insights of the global sensitivity analysis in subchapter 4.2.2 about the impact of the individual model parameters on the final reactor performance uncertainty are taken into account and, consequently, only the five most sensitive model parameters are considered uncertain. These are the kinetic constants $k_{0,1}$ and $k_{0,2}$, the catalyst equation parameters $K_{cat,1}$ and $K_{cat,2}$, and the Gibbs

energy of the chemical equilibrium of reaction two ΔG_{r_2}. Their expected values, confidence intervals, and the calculation of the corresponding variances are given in Tab. A.2.1, Tab. 4.1, and Eq. (4.37), respectively.

Robust dynamic optimization problem

The resulting RDOP for the overall process optimization under model parameter uncertainties is given in Eqs. (5.23)-(5.57).

$$\max_{T^{HCTR}(t),\dot{n}_{CO,in}^{HCTR},\dot{n}_{H_2,in}^{HCTR},T^{CSTR},p_{CO}^{CSTR},p_{H_2}^{CSTR},\dot{n}_{nC12en,in}^{HCTR}} \left\{E\left(S_{nC13al}(\tau_f)\right) * E\left(X_{nC12en}(\tau_f)\right)\right\} \quad (5.23)$$

s.t.

Component mass balances of HCTR:	Eqs. (5.10)-(5.12), with $\dot{n}_{\alpha}^{HCTR} = \dot{n}_{\alpha,i}^{HCTR}, i \in SP$	(5.24)
Component mass balances of CSTR:	Eq. (5.13), with $\dot{n}_{\alpha}^{CSTR} = \dot{n}_{\alpha,i}^{CSTR}, i \in SP$	(5.25)
Reaction kinetics:	Eqs. (2.2)-(2.7), with $r_m = r_m(\boldsymbol{\theta}_i), m \in \{1,2\}, i \in SP$	(5.26)
Catalyst equilibrium:	Eq. (2.1), with $c_{cat} = c_{cat}(\boldsymbol{\theta}_i), i \in SP$	(5.27)
Catalyst and solvent ratios:	Eqs. (2.13)-(2.14), Tab. 5.1	(5.28)
Constitutive equations:	Eqs. (3.38)-(3.39)	(5.29)
Gas solubilities:	Eq. (2.11)	(5.30)
Path constraints:	$\dot{\boldsymbol{n}}_i(t) \geq 0, i \in SP$	(5.31)
	$10 \text{ bar} \leq p_t^{HCTR}(t) = p_{CO}^{HCTR}(t) + p_{H_2}^{HCTR}(t) \leq 20 \text{ bar}$	(5.32)
	$363.15 \text{ K} \leq T^{HCTR}(t) \leq 388.15 \text{ K}$	(5.33)
	$10 \text{ bar} \leq p_t^{CSTR} = p_{CO}^{CSTR} + p_{H_2}^{CSTR} \leq 20 \text{ bar}$	(5.34)
	$363.15 \text{ K} \leq T^{CSTR} \leq 388.15 \text{ K}$	(5.35)
Terminal constraints:	$\tau_f = \tau^{HCTR} + \tau^{CSTR} = 192 \text{ min}$	(5.36)
	$\tau^{HCTR} = V^{HCTR}/\dot{V}^{HCTR}, \tau^{CSTR} = V^{CSTR}/\dot{V}^{CSTR}$	(5.37)
	$X_{nC12en,i} = \frac{\dot{n}_{nC12en,in,i}^{HCTR} - \dot{n}_{nC12en,i}^{CSTR}}{\dot{n}_{nC12en,in,i}^{HCTR}} = 99\ \%, i \in SP$	(5.38)
	$S_{nC13al,i} = \frac{\dot{n}_{nC13al,i}^{CSTR} - \dot{n}_{nC13al,in,i}^{HCTR}}{\dot{n}_{nC12en,in,i}^{HCTR} - \dot{n}_{nC12en,i}^{CSTR}}, i \in SP$	(5.39)
	$n/iso_i = \frac{\dot{n}_{nC13al,i}^{CSTR}}{\dot{n}_{nC13al,i}^{CSTR} + \dot{n}_{iC13al,i}^{CSTR}} \geq 95\ \%, i \in SP$	(5.40)
Initial conditions:	Eq. (5.19), with $\dot{n}_{\alpha,liq}^{HCTR}(\tau = 0) = \dot{n}_{\alpha,liq,in}^{HCTR} = \dot{n}_{\alpha,liq,in,i}^{HCTR}, \alpha \in CH, i \in SP$	(5.41)
	$\dot{n}_{\alpha,gas}^{HCTR}(\tau = 0) = \dot{n}_{\alpha,gas,in,i}^{HCTR} = \dot{n}_{\alpha,in}^{HCTR}, \alpha \in CH, i \in SP$	(5.42)
	$\dot{n}_{\alpha,liq}^{HCTR}(\tau = 0) = \dot{n}_{\alpha,liq,in,i}^{HCTR} = 0, \alpha \in GAS, i \in SP$	(5.43)
Uncertain model parameters:	$\boldsymbol{\theta} = [k_1, k_2, , K_{cat,1}, K_{cat,2}, \Delta G_{r_2}]^{\mathrm{T}}$	(5.44)
Unscented transformation:	$\boldsymbol{\theta}_0 = E(\boldsymbol{\theta})$	(5.45)
	$\boldsymbol{\theta}_i = \boldsymbol{\theta}_0 + sgn(n_{\boldsymbol{\theta}} - i)\sqrt{(n_{\boldsymbol{\theta}} + \lambda)}\sqrt{Cov(\boldsymbol{\theta})}_i, i \in SP$	(5.46)
	$E(S_{nC13al}) = \sum_{i=0}^{2n} w_i S_{nC13al_i}, i \in SP$	(5.47)
	$Var(S_{nC13al}) = (1 - \alpha^2 + \beta)\{S_{nC13al_0} -$	(5.48)

$$E(S_{nC13al})\}\{S_{nC13al_0} - E(S_{nC13al})\}^{\mathrm{T}} + \sum_{i=1}^{2n} w_i \{S_{nC13al_i} - E(S_{nC13al})\}\{S_{nC13al_i} - E(S_{nC13al})\}^{\mathrm{T}}, i \in SP$$

$$E(X_{nC12en}) = \sum_{i=0}^{2n} w_i X_{nC12en_i}, i \in SP \tag{5.49}$$

$$Var(X_{nC12en}) = (1 - \alpha^2 + \beta)\{X_{nC12en_0} - E(X_{nC12en})\}\{X_{nC12en_0} - E(X_{nC12en})\}^{\mathrm{T}} + \sum_{i=1}^{2n} w_i \{X_{nC12en_i} - E(X_{nC12en})\}\{X_{nC12en_i} - E(X_{nC12en})\}^{\mathrm{T}}, i \in SP \tag{5.50}$$

ε-CM constraint: $Var(\boldsymbol{o}) \leq \varepsilon$ (5.51)

Inlet conditions: Eqs. (5.5)-(5.9) (5.52)

$\dot{V}_{in,liq}^{HCTR} = 150$ ml/h (5.53)

Decanter: Eqs. (5.14)-(5.16) (5.54)

Distillation column: Eqs. (5.17)-(5.18), Eqs. (A.42)-(A.46) (5.55)

Purge condition: $\xi_\alpha = \begin{cases} \in \{0..1\} & , \alpha \in \{nC13al, iC13al\} \\ 1 & , \alpha \in \{CH, SOL\}/\{nC13al, iC13al\} \end{cases}$ (5.56)

Interconnection conditions: Eqs. (5.19)-(5.22) (5.57)

In the RDOP for the operation of the single CSTR in the integrated overall process the balance and model equations for the HCTR are neglected and the inlet condition for the volumetric liquid flow rate is set to $\dot{V}_{in,liq}^{CSTR} = 100$ ml/h. This value corresponds to the experimental conditions in the original miniplant setup [197]. As the retrofit initially intended to improve the process performance for the operation with and without distillation column, the single CSTR and the HCTR+CSTR-network are optimized as well for the reduced operation scheme without the distillation column and the corresponding side product recycle. Therefore, the molar recycle flow rates of the distillate stream in Eq. (5.19) are set to zero, $\dot{n}_{\alpha,out,D}^{col} = 0, \alpha \in \{CH, SOL\}$.

Results

For varying scalarization parameter ε the RDOP in Eqs. (5.23) – (5.57) is solved, resulting in the Pareto sets in Fig. 5.15 a) and b) for the reduced and the complete operation scheme, respectively. These Pareto sets indicate all Pareto optimal performance points $[E(S_{nC13al}), Var(S_{nC13al})]$ the HCTR+CSTR-network can reach when operating in the integrated overall process given in Fig. 5.14. Evidently, the recycle of side products and the according optimal process control lead to a higher predictive power of the process performance than the operation with the reduced scheme. In both cases a clear potential is revealed to decrease the performance uncertainty by means of the optimal control. Thereby, the improvement of predictive power of the performance is higher for the reduced operation scheme than for the complete operation scheme, what emphasizes the potential of the robust design optimization to find designs of increased robustness, since their finding is, evidently, highly non-intuitive.

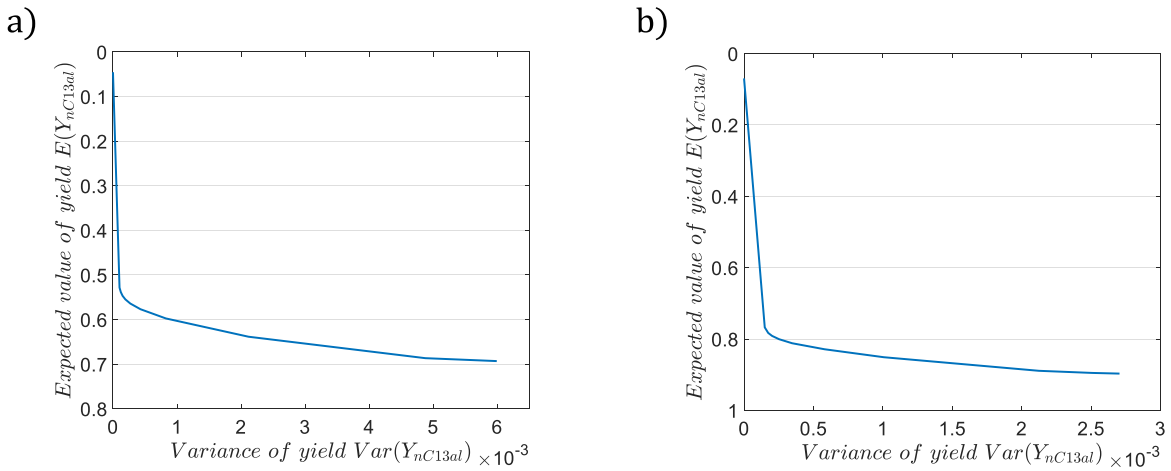

Figure 5.15: Sets of Pareto optimal solutions of the HCTR+CSTR-network for a) the reduced operation scheme without distillation column, and b) the complete operation scheme

All of the solutions are robust against the considered model parameter uncertainties and, thus, lead to a feasible realization within the integrated overall process. Since the main target of the retrofit is the maximization of the product yield, the designs with the highest expected yields, rightmost in the Pareto sets in Fig. 5.15, are chosen for the following performance comparison and subsequent experimental validation. The reaction progress and the control variables of these optimal performance points for the complete operation scheme and the reduced operation scheme are depicted in Fig. 5.16 and Fig. 5.17, respectively.

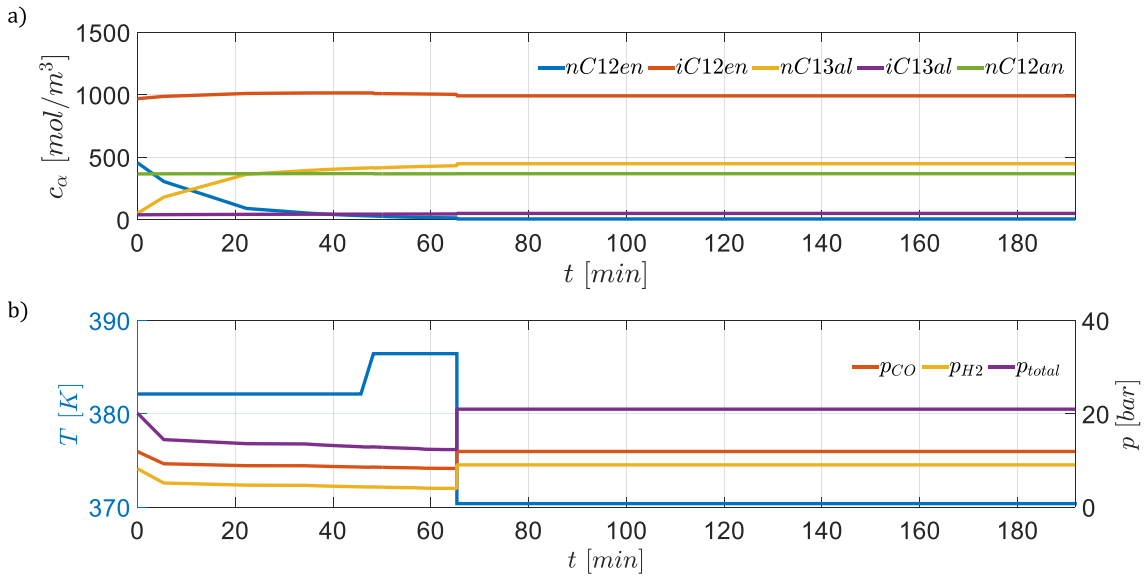

Figure 5.16: Reaction progress a) and control variables b) of the optimal performance point of the HCTR+CSTR-network in the integrated overall process in case of the complete operation scheme

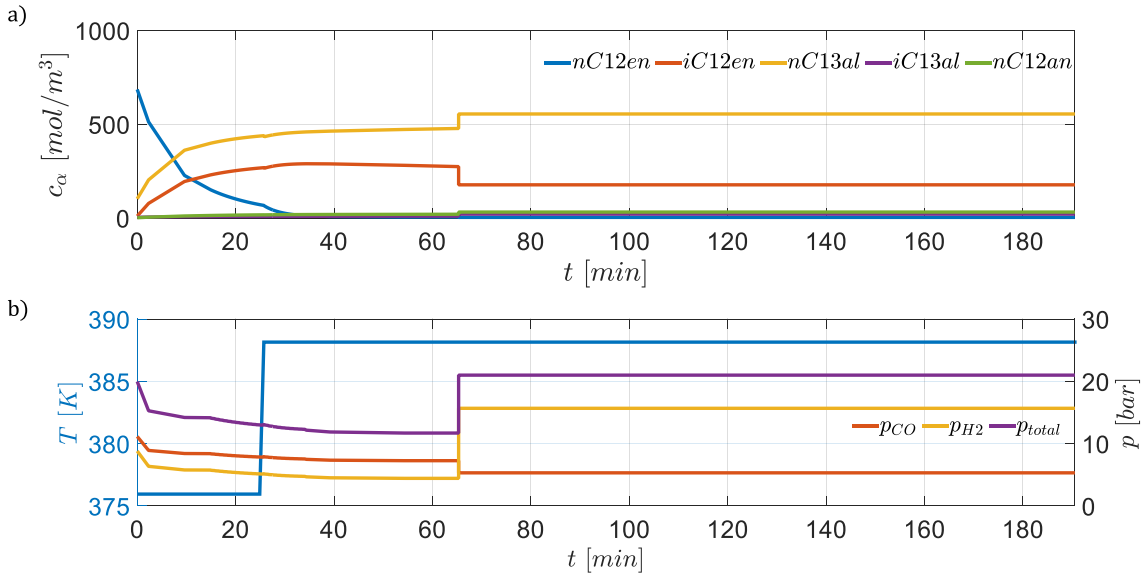

Figure 5.17: Reaction progress a) and control variables b) of the optimal performance point of the HCTR+CSTR-network in the integrated overall process in case of the reduced operation scheme

The optimal control and the reaction progress of the reduced operation scheme indicates qualitatively the same characteristics as the FPA results for this case in Fig. 5.2, especially regarding the temperature levels and partial pressure ratios. Hence, in this case the integration in the overall process and the limitations by the technical design had only a minor effect. In contrast, the control variables of the complete operation scheme look different in comparison to the FPA results in Fig. 5.3, in particular the temperature levels change. Within the limitations of the integrated overall process, the best performance is achieved by setting the temperature of the second reaction section to the minimum value. However, this does not change the course of the reaction progress significantly and, thus, does not lead to a contradiction to the predicted optimal fluxes of the FPA.

In order to assess how the retrofitted process performs in comparison to the existing miniplant setup, the results of the previous optimizations are compared to the simulation results of the existing miniplant on the one hand, and the best possible performance of the existing miniplant determined by means of the dynamic optimization tool on the other hand. This comparison is carried out for both the complete and the reduced operation scheme. The results are given in Fig. 5.18 a) and b), respectively. In case of the complete operation scheme a), i.e. with distillation column and closed side product recycle, the optimal yield of the HCTR+CSTR-network (blue diamond) is reached at $E(S_{nC13al}) = 91.2\ \%$ and $E(X_{nC12en}) = 98.3\ \%$ and is, thus, significantly higher than the maximum yield of the single CSTR (orange diamond) at $E(S_{nC13al}) = 88.3\ \%$ and $E(X_{nC12en}) = 93.3\ \%$. For both reactor realizations, their maximum potentials within the given integrated overall process (solid lines) indicate, that performance losses arise due to the considerations of model parameter uncertainties and the approximation of optimal control profiles. However, the comparison of the optimized CSTR performance (orange diamond) and the simulated performance of $E(S_{nC13al}) = 89.6\ \%$ and $E(X_{nC12en}) = 74.5\ \%$ under the heuristically adjusted experimental conditions (orange plus) show a significant increase using model-based optimization tools even for the heuristically chosen CSTR unit. The same characteristics of the results are indicated in case of the reduced operation scheme b). The HCTR+CSTR-network has the best performance at $E(S_{nC13al}) = 69.6\ \%$ and $E(X_{nC12en}) = 99.5\ \%$, although the optimized CSTR comes with $E(S_{nC13al}) = 66.6\ \%$ and $E(X_{nC12en}) = 98.0\ \%$ much closer to the retrofit performance. Again, both optimized cases show a significant improvement in comparison to the simulated performance of $E(S_{nC13al}) = 61.9\ \%$ and $E(X_{nC12en}) = 84.1\ \%$ under the heuristically chosen experimental conditions. This leads to the conclusion, that the optimization

based framework is a powerful tool to derive new promising reactor-networks on the one hand, and on the other hand allows improving the performance of the existing miniplant without changing the technical setup.

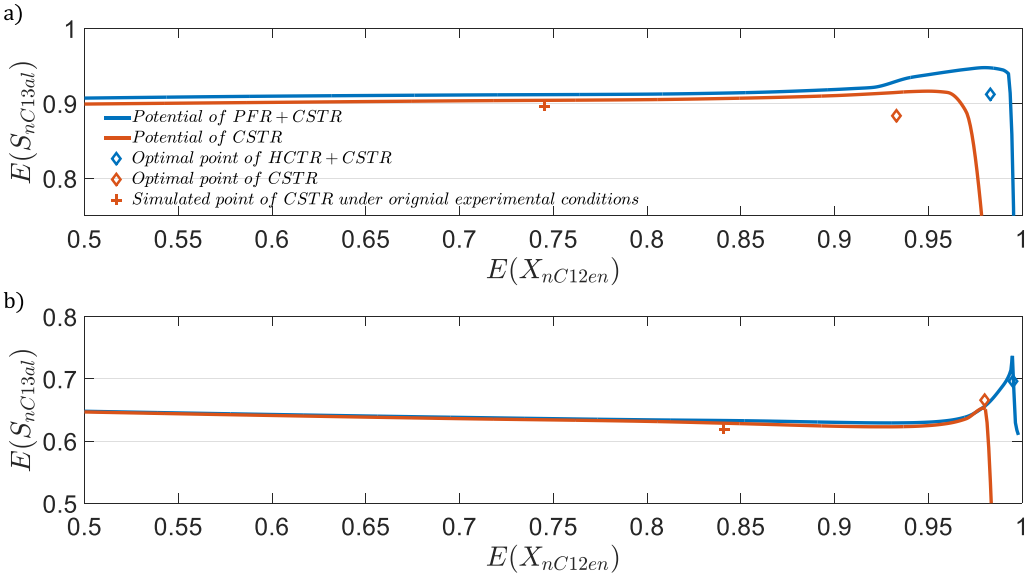

Figure 5.18: Optimal performances (diamonds), maximum potentials (solid lines), and performance under experimental conditions (pluses) of the HCTR+CSTR-network (blue) and the CSTR (orange) embedded in the integrated overall process for the cases a) of the complete operation scheme and b) of the reduced operation scheme

5.5 Experimental validation

In the experimental rig, the HCTR is, finally, built of a 3/16" stainless steel tube, whose diameter is with $d_{tube} = 2.98$ mm slightly smaller than the previously determined maximum, due to availability reasons. Because of the bending of the helices in a diameter of $d_{bend} \leq 30.6$ cm and a narrow arrangement of the helices the HCTR has a height of ≈ 2 m. For an appropriate sampling along the reactor length, eight sampling spots are arranged in a logarithmic grid from the inlet. The temperature control of the HCTR is realized by two heating sleeves and the pressure inside the tube is maintained by a backpressure regulator at the outlet of the HCTR. Two mass flow controllers, one for each gas, feed the optimal gas amount to the tube inlet via a T-junction. The temperature in the CSTR is controlled by a thermostat by means of a cooling medium in the tank jacket. Its pressure control is realized by a pressure valve, realizing a constant pressure of $p_{CSTR}^{tot} = 20$ bar. Thereby, two mass flow controllers adjust the gas inlet streams of H_2 and CO into the CSTR in the ratio of the optimal partial pressures. A sufficient gas-liquid contacting in the CSTR is ensured by the use of a gassing stirrer operated at 650 rpm.

The experimental setup is supposed to investigate the optimal reactor-network in the reduced operation scheme, i.e. without distillation column and side product recycle. Hence, only the decanter is operated and the nonpolar, product rich solvent recycle is closed. The reaction mixture from the CSTR is led to the decanter by a mass flow controller. Again, temperature and partial pressures in the vessel are controlled by a thermostat and two mass flow controllers, respectively. The polar solvent phase is continuously pumped to the inlet of the HCTR and the nonpolar product rich phase is removed into a storage tank using a relief valve. In order to obtain a single phasic TMS mixture in the HCTR inlet, the inlet pipe is heated up to 95°C.

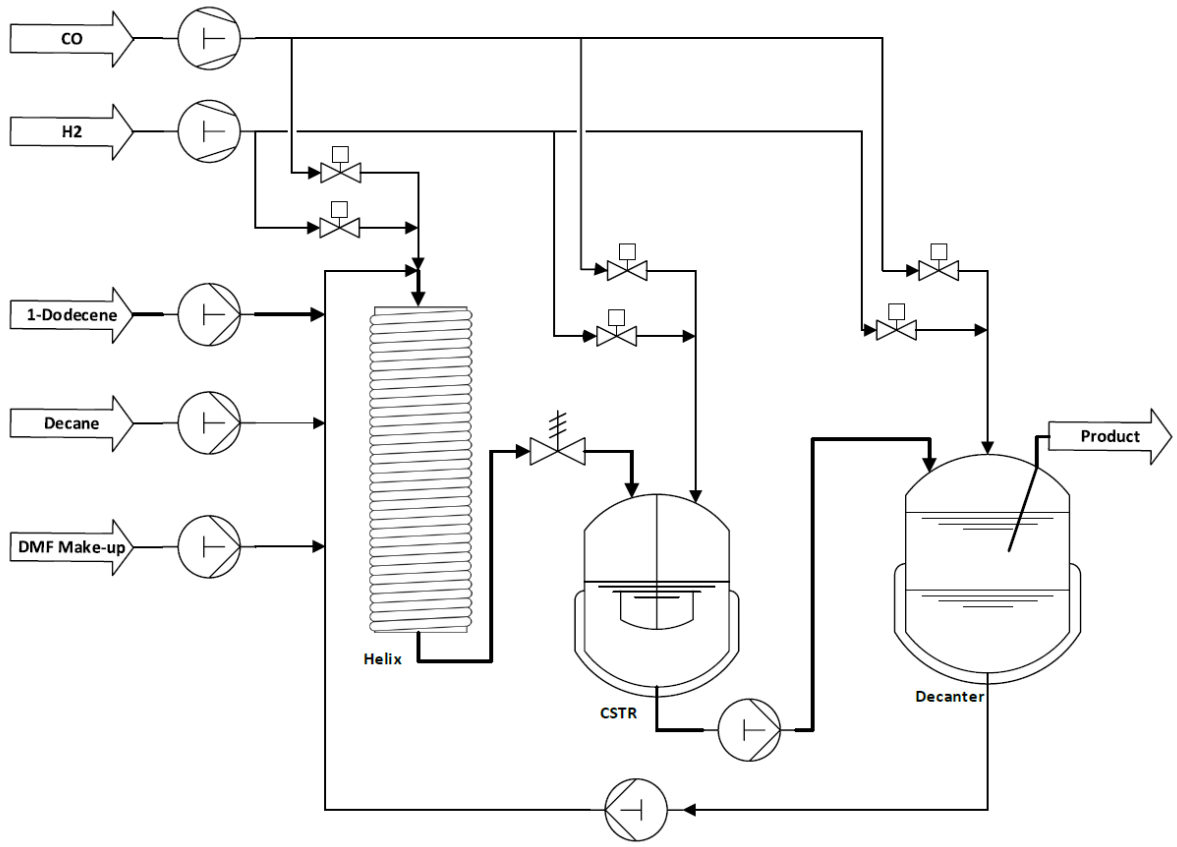

Figure 5.19: Simplified flow sheet of the experimental setup of the retrofitted process for the reduced operation scheme

The entire process, illustrated in a simplified form in Fig. 5.19, has been monitored by a process control system (Siemens PCS7 V.8.1) and samples have been taken from inlet and outlet streams of all process units. To prevent undesired phase splitting at room temperature, the samples have been diluted with 2-propanol. They have been analyzed in a gas-chromatograph with a connected mass spectrometer for a better distinction of terminal and internal dodecenes. For detailed information about the experimental setup and conditions, it is referred to the original publication [202].

Table 5.3: Comparison of experimental and simulation results of the conversion of 1-dodecene and the selectivity with respect to tridecanal for the existing miniplant setup with a single CSTR unit and the retrofitted miniplant with the optimal HCTR+CSTR-network for both the reduced and the complete operation scheme

Reduced operation scheme			Complete operation scheme	
X_{nC12en}	S_{nC13al}		X_{nC12en}	S_{nC13al}
80 %	62.5 %	CSTR experimental	75 %	86.7 %
84.1 %	61.9 %	CSTR simulation	74.5 %	89.6 %
100 %	70 %	HCTR experimental	-	-
99.5 %	69.6 %	HCTR simulation	98.3 %	91.2 %

For the experimental investigations the continuous process has been operated for ≈ 110 h and regularly samples have been drawn and analyzed. For the last 8 h a stable process under optimal reaction conditions was established indicating a conversion of $X_{nC12en} \approx 100$ % and a selectivity with respect to tridecanal of $S_{nC13al} \approx 70$ %. As Tab. 5.3 shows, this is in very good agreement with the

predicted results of the dynamic optimization. In addition, the experimental results of the existing miniplant, i.e. with a single CSTR unit, published in Dreimann et al. [197,198] are given and compared to the model-based simulations which are made in subchapter 5.4 for the according experimental conditions. The latter are shown for both operation schemes, whereas the experimental results for the retrofitted process are only available for the reduced scheme. The experimental investigation of the retrofitted process in the complete operation scheme is subject of future work.

5.6 Discussion

The final results indicate a significant performance improvement by the retrofit for both operation schemes and the match of the experimental results to the model-based optimizations are very good. The retrofitted integrated process including the HCTR+CSTR-network showed a yield increase of 17 % in case of the reduced operation scheme and of 23 % in case of the complete operation scheme compared to the heuristically chosen reactor and reaction conditions used in literature [197,198]. Moreover, it was shown that the performance of the existing setup has as well the potential of a clear improvement without changing the technical setup by choosing optimal reaction conditions based on optimization calculations. This led to a yield increase of 13 % in case of the reduced operation scheme and of 16 % in case of the complete operation scheme. Both results emphasize the large potential of model-based optimization calculations for designing chemical processes, especially in contrast to classical heuristical approaches.

However, the entire synthesis and design procedure is established in a way that allows the engineer as decision-maker analyzing intermediate results and steering the remaining steps in a desired manner. For instance, the definition of the retrofit problem could have been stated differently, taking into account e.g. further separation options, optimization of the existing separation units, optimization of the space-time-yield independent of the original residence time, etc., leading to a different dynamic optimization problem for the FPA. Moreover, the *flux profile analysis* resulted in reactor-(recycle)-network candidates due to specific assumptions or negligence of certain characteristics. A different sectioning or focus on other characteristic features might have led to other candidates. Therefore, it is indispensable to be aware of the non-uniqueness of the derived results and, thus, to carry out a comparison of the candidates' performances aiming at a clear assessment of those. After the synthesis is finished, the detailed technical design has to be carried out. Herein, the decision-maker analyzes the results of sensitivity analyses regarding control input numbers and required reactor characteristics. Again, it is up to his expertise to decide which trade-off between approximation accuracy and construction effort is reasonable or not. Summarizing, the final result is a consequence of a plenty of decisions making it a complex task for which expertise is required. The major alternative is a simultaneous synthesis and design procedure, which tries to identify the best technical process including all decisions in one large optimization problem. The drawbacks of this simultaneous approach in comparison to the chosen step-by-step procedure are:

- The resulting optimization problem is large, including nevertheless detailed models, and has a lot of degrees of freedom at once.
- It is hardly possible to understand the final solution with regard to every individual aspect, since the solver chooses its own trade-offs. This is, in turn, strongly dependent on the weighting of the different aspects, which cannot be controlled properly when the solver decides about it.
- In case the designer wants to identify alternatives, the entire synthesis and design problem has to be solved again, even for small changes. One cannot go only one or two steps backwards.

- The numerical effort of such a large optimization problem is tremendous and it is, due to lack of knowledge about appropriate initial conditions and the size of the problem, not guaranteed that a feasible solution is found.

The computational costs and numerical complexity are also the reason, why the model parameter uncertainties are not all considered in the robust design optimization within the integrated overall process. The convergence of the dynamic optimization problem was complicated and resulted in a plenty of infeasible solutions. Hence, the amount of uncertain model parameters was reduced to the five most sensitive. In case of a large optimization problem within a simultaneous synthesis and design procedure, it would have been much harder to identify the uncertain model parameters as origin of the convergence problems. As an alternative to the consideration of the model parameter uncertainties at the final optimization within the integrated overall process, one could have taken them into account as well in previous steps, and even in the FPA, which might have led to interesting additional possible reactor-network candidates. However, it does not avoid the consideration of the model parameter uncertainties in the remaining steps, especially when determining the final technical design. Hence, to decrease the model complexity and ensure feasible results of the FPA, the model parameter uncertainties have been considered only in the final overall process optimizations.

Although presented in subchapter 4.3.2, the imperfect control realization was not considered in the final design study for the optimal hydroformylation process for two reasons. On the one hand, the complexity of the realization of the required temperature profile is low, since the profiles indicate only a few changes, which can easily be realized, as the reaction is rather slow. On the other hand, the accuracy of the thermostats on this miniplant-scale is very high and, thus, the expected deviations negligible.

The model quality of the reaction and the liquid-liquid phase separation is high using an experimentally validated kinetic model with confidence intervals for the model parameters and a Kriging model, which was trained on experimental data and compared to state-of-the-art database approaches, respectively. However, the model for the distillation column in the complete operation scheme is a short-cut model with limited accuracy and, thus, validity. This became obvious when carrying out the dynamic optimization for the complete operation scheme. The nonpolar solvent recycle, i.e. the distillate stream of the distillation column, could not been closed completely, because it contained too much aldehydes. The predicted distillate stream composition has been compared to the measured compositions in Dreimann et al. [198] indicating, that the real distillation column separates the aldehydes almost completely. Hence, an additional purge factor $\xi_\alpha \in \{0..1\}, \alpha \in \{nC13al, iC13al\}$ was added for each species to allow the solver to control the recycle of aldehydes aiming at a convergence of the overall process. For all other species the purge was not activated. As a result, the recycled distillate stream contained only very small amounts of aldehydes which matched to the experimental results shown in Dreimann et al. [198]. Since all model-based predictions are only as good as their least accurate parts, the distillation column has to be modeled rigorously, e.g. using the MESH equations (material balance - equilibrium conditions - summation conditions - heat balance), to overcome the makeshift with the adjusted purge factors and to increase the optimization accuracy.

6 Conclusion

6.1 Summary

Within the scope of this work the methodology of *elementary process functions* for process design has been extended with respect to two crucial aspects: (i) the possibility to synthesize reactor-network candidates from the optimal control profiles of the EPF based dynamic optimization; and (ii) the consideration of different types of uncertainty within the design procedure intending to find robust process designs. Furthermore, both approaches have been used successfully for the retrofit of the reactor of an integrated miniplant process for a complex multiphase reaction.

Qualitative reactor synthesis

In order to synthesize reactor-network candidates, i.e. finding promising structures of crucial functions such as reaction, separation, mixing, and recycling, the *flux profile analysis* was developed, which stands out by:

- Serving as tool for rational selection of promising conceptual designs based on reaction engineering fundamentals allowing to derive reactor-networks, reactor-recycle-networks, or reactor-separator-recycle-networks depending on the frame of the synthesis and the operations, which are supposed to be included.
- A clear and straightforward three step procedure including (i) the fundamental dynamic optimization of the EPF methodology, which optimizes the external and internal mass and energy fluxes of an idealized fluid element; (ii) the subdivision of the obtained flux profiles into characteristic sections of dosing, removal, and heating/cooling; and (iii) the association of these characteristic sections with generic ideal reactors, which include different recycling and separation options.
- The derivation of several promising candidates of network structures, which on the one hand provide case-dependent reduction potentials, and on the other hand allow for comprehensive comparison studies and sensitivity analyses to identify the most promising candidate and to gain further insight into the reaction characteristics.

Since the final outcome of this analysis provides only structural information and rough estimations about quantitative relations, the FPA is introduced as qualitative reactor synthesis approach. In order to demonstrate its potentials and applicability, it was successfully applied on:

- The modified van-de-Vusse reaction indicating (i) that the FPA can be used to construct the attainable region of a simple two dimensional process example achieving the same results as given in literature, and (ii) that this approach is competitive to the AR approach with respect to the fast and direct identification of the optimal network configuration.
- The classical van-de-Vusse reaction aiming at a comparison with superstructure optimization literature results clearly indicating (i) that the FPA identifies the same and even additional promising reactor-network candidates, and (ii) that it can be used as sound basis for other rigorous optimization tools providing highly valuable knowledge about possible process structures, ranges for residence times, and bounds for control and state variables.
- The multiphase hydroformylation reaction of 1-dodecene in a thermomorphic solvent system yielding promising candidates for all synthesis levels, allowing for a systematic analysis of

benefits from back-mixing, recycling, and separation, partly confirming former results and partly outperforming them.

In course of the applications on the process examples, it was demonstrated and discussed in detail which kind of sensitivity analyses are required to reasonably asses the achieved results.

Reactor design under uncertainty

The second methodical achievement is the systematic inclusion of uncertainties into the design procedure with the EPF methodology resulting in a probabilistic reactor design framework which provides:

- The identification of (i) model uncertainties, which arise due to naturally not error-free description of real phenomena with mathematical models, (ii) non-ideal reactor characteristics, which consider deviations from the ideality assumptions often made in design procedures, and (iii) imperfect realization of the control profiles, which have their origin e.g. in limited actuator accuracy or manufacturing quality, as sources of uncertainty and randomness within the EPF design procedure and their classification with respect to their static or dynamic appearance.
- The inclusion of the *unscented transformation* with sigma points, which allows for the propagation of statistical moments of probability density functions in non-linear systems such as process system models, in order to account for the uncertainties within the dynamic optimization problem stated in the EPF method.
- The possibility to (i) find robust optimal designs, (ii) identify different designs of increased certainty, i.e. lower risk to miss the expected performance, and (iii) quantify the impact of uncertain variables on the overall process uncertainty and, thus, identify the most sensitive parameters.

It is demonstrated and discussed, that a design within such a probabilistic framework yields not one unique optimal solution, but a set of Pareto optimal solutions with different values for the two objectives, i.e. the expected value of the criterion on the one hand and its predictive power, e.g. quantified by its variance, on the other hand. The design under uncertainty approach was applied on the hydroformylation of 1-dodecene in a TMS system providing the following key features and results:

- The UT with sigma points was validated carrying out comparative Monte Carlo simulations for several designs within the Pareto set of robust optimal solutions under model parameter uncertainties. Thereby, the tuning factors and modifications have been chosen in a way such that the matching to the MC simulation results were improved significantly, what enabled a reliable further use of the UT.
- In order to demonstrate the possibility to analyze the interdependencies of several objectives, the reactor design under model parameter uncertainty study was carried out for two objectives, namely the selectivity to the desired product and the conversion of the main reactant, revealing clear robustification potentials for the selectivity at high conversions.
- The probabilistic design framework was used to determine global sensitivity indices, which quantify the impact of each individual uncertain variable or parameter on the uncertainty of the reactor performance. This study revealed the catalyst equilibrium parameters and the kinetic rate constants of the hydroformylation reaction and the isomerization reaction of 1-dodecene as most sensitive with respect to their impact on the variance of the selectivity of the desired aldehyde. Hence, the estimation of these model parameters should be improved to

increase the robustness of the predicted reactor performance. This is a very promising tool for further use in context of optimal experimental design since it provides information about parameters of high impact for improving the certain design of processes.

- In addition to the model parameter uncertainties, the imperfect control realization for the optimal reactor design of the hydroformylation process was treated. Therefore, the temperature control was impinged with different deviations from its nominal value indicating a clear impact on the expected value of the objective.
- In a last step both aforementioned uncertainty types, i.e. model parameter uncertainties and imperfect temperature control realization, have been considered simultaneously in a comparison study of two possible reactor realizations. Based on these results the benefits, each realization has, and suitable trade-offs, between high expected performance and high predictive power the realizations provide in different conversion ranges, have been identified.

Optimal reactor design for retrofit of an integrated miniplant process

Finally, the synthesis and design of an optimal reactor-network for the retrofit of an integrated miniplant for the hydroformylation of 1-dodecene in a thermomorphic solvent system was successfully conducted using the *flux profile analysis*. In addition, the probabilistic design framework using the *unscented transformation* was applied to consider model parameter uncertainties and their impact on the optimal reactor-network within the integrated overall process. The results indicate, that:

- A network of a PFR and a CSTR shows the highest performance and can be best technically designed by a helically coiled tube reactor and the already existing CSTR of the miniplant, respectively.
- This optimal reactor-network fulfills the requirement to show an optimized performance for both the reduced operation scheme, without distillation column and side product recycle, and the complete operation scheme.
- The technical design of the reactor-network is robust against the most sensitive model parameters and the determined Pareto sets provide promising trade-offs between the expected performance of the process and its predictive power.
- The performance (conversion, selectivity, yield) of the retrofitted overall process is significantly improved for both operation schemes, i.e. (i) in case of the reduced operation scheme, the retrofitted process with the HCTR+CSTR-network showed a yield increase of 17 % compared to the heuristically chosen reactor and reaction conditions used in literature [198], and (ii) in case of the complete operation scheme, even a yield improvement of 23 % is achieved compared to the reaction conditions and miniplant setup from literature [197].
- Even without changing the technical setup only using the dynamic optimization framework to optimize the reaction conditions of the existing miniplant, the yield could be improved by 13 % for the reduced operation scheme and by 16 % for the complete operation scheme.

These results impressively demonstrate, how model-based optimization calculations allow for finding non-intuitive process designs providing the potential to outperform classical heuristics significantly.

6.2 Outlook

In course of the presented work it has been debated in several discussion which challenges still remain and which potentials are worth it to be exploited. In the following, these remarks are summarized and classified within three main topics of challenging and promising future prospects.

Methodical extensions

Within this work the process design methodology of *elementary process functions* has been extended for the qualitative synthesis of reactor-networks based on optimal control profile analysis and for the design under uncertainty including different uncertainty types and appearances. The benefits of these methodical extensions have been demonstrated and their drawbacks and challenges for further improvement have been discussed. However, beside of these extensions the dynamic optimization based design within the framework of *elementary process functions* has still dormant potentials.

Up to now, the considered design problems had only one reactive phase and, in some cases, a support phase. The next step is the development of a comprehensive model basis that allows for the consideration of an arbitrary number of phases, which are either reactive or non-reactive. This includes the challenging consideration of appearing and disappearing phases inside the dynamic optimization problem, the modeling and inclusion of mass and heat interchange fluxes along the reaction coordinate, and the simultaneous balancing of states of different phases. This would, for instance, allow for the simultaneous reaction and separation within multiphase processes such as the hydroformylation reaction presented in this work. Therefore, e.g. a solvent is chosen in a way that enables a controllable phase split, a stripping, or precipitation during reaction to remove certain species. This suggestion leads directly to the next interesting methodical extension for the EPF based design procedure, namely the design of integrated reaction-separation units. For sure, the first step should be to use the methodology for the design of functional modules including separation tasks. When the dynamic optimization problem is reliably extended for multiple reactive and non-reactive phases, the main challenge is the inclusion of phase equilibria and/or heat balances to appropriately describe separation tasks. Then the subsequent step of integration of both reaction and separation tasks is highly promising with respect to process intensification purposes.

The main limitations for the presented and future methodical extensions are numerical issues of feasibility and convergence of the derived dynamic optimization problems. Available state-of-the-art NLP solvers provide already highly performing environments for local optimization using interior point or active set approaches. However, the successful solving of these DOPs requires well-chosen initial guesses for states and controls especially for the cases of increased problem size e.g. when considering uncertainties in the design procedure. As this complexity would increase unlikely in case of integer decisions, the problem formulation should avoid the inclusion of those. Hence, an experienced engineer is still indispensable. For a systematic improvement of feasibility and convergence, possibilities of model reduction and surrogate modeling play a crucial role as well as the suitable extension of the solver capacities. This requires an expedient collaboration of engineers and mathematicians and makes it a highly complex interdisciplinary challenge.

Development of practical tools

The fundamental research in process systems engineering is supposed to develop tools that enable the efficient design of process systems from the scratch to the plant. In the last decades this research field gained popularity and with increasing computational power more and more approaches have been presented. Unfortunately, although providing sound methods and promising frameworks, most of the approaches have not yet been used outside of academia or even their home institutions since they are not embedded in practical tools, e.g. software environments. As the EPF methodology celebrates its 10^{th} birthday this year and several interesting advances are made in its use for different process types, it might be a reasonable step to focus on the development of a practical tool.

One way to provide a practical framework for the EPF based reactor synthesis approach might be the derivation of heuristics for fast synthesis and design of process systems. These heuristics would

base on thorough analyses of the reaction engineering characteristics of various classes of reactions, e.g. with respect to the reaction order, the topology of the reaction network, the temperature dependencies, the supply of reactants with support phases, etc. Examples of such typical reaction characteristics have been provided within this work, i.e. the benefit of recycled reversible side products to control the chemical equilibrium within the hydroformylation reaction, or the sharp temperature profile exploiting the activation energy relations of the van-de-Vusse reaction. A comprehensive analysis of these characteristics would result in a pool of typically arising optimal control profiles and corresponding reactor-networks which provide the heuristical basis. For the described analysis no real processes have to be analyzed. Instead, one could fall back on the use of e.g. dimensionless numbers to describe the reaction characteristics and vary them.

A second way could be the development of a software tool, which provides an environment for model-based reactor synthesis. Basic reaction information such as reaction network topology, reaction rates, and basic thermodynamic data are entered, and suggestions for reactor-networks as a result of numerical optimizations are provided to the engineer. The required automation of the EPF based synthesis procedure is mainly hindered by the intermediate steps which require the decision-making of an expert. To avoid these, either the aforementioned heuristics are included, or the emergence of ambiguous cases are prevented by presetting certain decision rules or by restricting the number of possible units by use of e.g. parsimonious parameterization of the control vectors. The resulting reactor synthesis procedure should consider only the most crucial phenomena which are identified by suitable use of sensitivity analyses.

Interdisciplinary, multi-scale process development

The trans-regional project (InPROMPT), this work was a part of, intended to develop new process structures for the production of long chain alkenes, which allow for the substitution of petrochemical feedstocks. Thereby, natural scientists and engineers from various research fields have been involved and had to collaborate and exchange numerical, experimental, and model data. This was accompanied by a plenty of challenges, e.g. coordination of data transfer, definition of reaction and process fundamentals, creation of an expedient and efficient working plan etc. However, due to the various scales on which the involved parties worked, the different scientific languages they spoke including definitions of measures etc., and the diverse ways of data repository they used especially with respect to the form the data is defined and stored, the efficiency of the process development procedure was strongly decreased. The experiences from the tedious interactions in this project as well as other projects should be used to create an interdisciplinary, multi-scale process development procedure which defines clearly (i) in which order working steps are conducted, (ii) how data of any kind is edited and which interphases are used for their provision for other project partners, (iii) which experimental conditions, analytics, and numerical solvers are supposed to be used, (iv) which milestones of achievements are crucial at which time of the project, and (v) how and when the resulting data and knowledge has to be provided to collaborators. The preliminary defined working procedure is supposed to include iterative exchange of knowledge of different detailedness at different time points ensuring that every subproject has always the amount of data and knowledge it requires to continue its tasks. For instance, the model-based synthesis and design presented in this work requires reaction kinetics. At the very beginning of the overall project these data are not yet available since other subprojects are currently investigating it. Hence, for an efficient workflow it is necessary to consider this lack of detailed models at the beginning and create a model-based synthesis and design procedure that is able to start working with less detailed models, such as stoichiometric knowledge about the reaction, and available data from other sources. The experimental data for kinetic and thermodynamic investigations should, furthermore, be provided directly to the dependent subprojects even when the mechanistic investigations and model discrimination for a detailed and reliable kinetic

and thermodynamic model is not finished. The raw data can already be used to create data-driven models and their use can support the progress towards a better understanding of e.g. time constants and control bounds for the synthesis and design procedure. An example for that has been shown in this work with the global sensitivity analysis of the model parameter impacts on the reaction performance. Summarizing, one has to be aware that, beside of the development of improved experimental analytics, more efficient numerical solvers, and flexible and expedient process design frameworks, the collaboration strategies of scientists and engineers from different disciplines working on various scales and investigating diverse phenomena have to be improved to identify synergy effects and efficiently use the available development time.

A Appendix

A.1 Model parameters of hydroformylation reaction

Table A.1: Parameters for rate equations and catalyst equilibrium (Eqs. (2.1)-(2.7))

Variable	Eq.	$E_A \left[\frac{\text{kJ}}{\text{mol}}\right]$	k_0	Unit	$K_1 \left[\frac{\text{ml}}{\text{mol}}\right]$	$K_2 \left[\frac{\text{ml}}{\text{mol}}\right]$	$K_3 \left[\frac{\text{ml}}{\text{mol}}\right]$
r_1	(2.2)	113.08	$4.904 \cdot 10^{16}$	$\frac{\text{ml}^3}{\text{g min mol}^2}$	574876	3020413	11732838
r_2	(2.3)	136.89	$4.878 \cdot 10^{6}$	$\frac{\text{ml}}{\text{g min}}$	38632	223214	-
r_3	(2.4)	76.11	$2.724 \cdot 10^{8}$	$\frac{\text{ml}^2}{\text{g min mol}}$	2661.2	7100	1280
r_4	(2.5)	102.26	$2.958 \cdot 10^{4}$	$\frac{\text{ml}^2}{\text{g min mol}}$	-	-	-
r_5	(2.6)	120.84	$3.702 \cdot 10^{10}$	$\frac{\text{ml}^3}{\text{g min mol}^2}$	-	-	-
r_6	(2.7)	113.08	$3.951 \cdot 10^{11}$	$\frac{\text{ml}^3}{\text{g min mol}^2}$	-	-	-
c_{cat}	(2.1)	-	-	-	$3.041 \cdot 10^{4}$	0	0.644

Table A.2: Parameters for equilibrium constants (Eqs. (2.9)-(2.10))

Variable	$a_0 \left[\frac{\text{kJ}}{\text{mol}}\right]$	$a_1 \left[\frac{\text{kJ}}{\text{mol K}}\right]$	$a_2 \left[\frac{\text{kJ}}{\text{mol K}^2}\right]$
ΔG_2	-11.0034	0	0
ΔG_3	-126.275	0.1266	$6.803 \cdot 10^{-6}$

Table A.3: Parameters for the solubility coefficient calculation in Eq. (2.12)

Component	$H_0 \left[\frac{\text{bar ml}}{\text{mol}}\right]$	$\Delta_S H \left[\frac{\text{kJ}}{\text{mol}}\right]$
H_2	66400	-3.06
CO	73900	-0.84

Table A.4: Parameters for density correlation and molar masses (Eqs. (3.38)-(3.39))

Component	$a_0 \left[\frac{\text{kg}}{\text{m}^3}\right]$	$a_1 \left[\frac{\text{kg}}{\text{m}^3\text{K}}\right]$	$M \left[\frac{\text{g}}{\text{mol}}\right]$
C10an	981.60	$-8.3536 \cdot 10^{-1}$	142.2817
DMF	1256.52	-1.0306	73.0938
nC12en	993.89	$-7.8875 \cdot 10^{-1}$	168.3190
nC12an	977.04	$-7.6743 \cdot 10^{-1}$	170.3348
nC13al	1068.12	$-8.0180 \cdot 10^{-1}$	198.3449
iC12en	993.89	$-7.8875 \cdot 10^{-1}$	168.3190
iC13al	1068.12	$-8.0180 \cdot 10^{-1}$	198.3449

A.2 Fundamental balance equations

According to Sundmacher and Freund [15] the state evolution of the fluid element within the EPF methodology is described by the fundamental balance equations:

Total mass balance: $$\frac{1}{V}\frac{d}{dt}(\rho V) = a_m \cdot m_A \tag{A.1}$$

Component mass balance: $$\frac{1}{V}\frac{d}{dt}(\rho \boldsymbol{w} V) = a_m \cdot (\boldsymbol{j}_A + \boldsymbol{w}_A m_A) + \boldsymbol{M} \cdot \boldsymbol{N} \cdot \boldsymbol{r}_V \tag{A.2}$$

z-Momentum balance: $$\frac{1}{V}\frac{d}{dt}\left((\rho v^2 + \boldsymbol{p})\frac{V}{v}\right) = a_\tau \cdot \tau_A + f_V \tag{A.3}$$

Total energy balance: $$\frac{1}{V}\frac{d}{dt}(\rho h_{tot} V) = a_m \cdot \left(\boldsymbol{h}_A^T \cdot \boldsymbol{j}_A + h_{A,t} m_A\right) + a_q \cdot q_A + w_t \tag{A.4}$$

Evolution of geometry: $$\frac{1}{V}\frac{dV}{dt} = g \tag{A.5}$$

A.3 Discretized dynamic optimization problem under uncertainty

The reactor design under uncertainty bases on a dynamic optimization problem, which is solved by means of orthogonal collocation on finite elements (see. subchapter A.7). In the following the dynamic optimization problem under uncertainty using sigma points is fully discretized resulting in a full probabilistic orthogonal collocation approach for both static and dynamic uncertainties, compare Eqs. (4.6)-(4.17) and Eqs. (4.18)-(4.30), respectively.

Static uncertainty

$$\min_{\boldsymbol{u}_{l=1\ldots n_{FE}}, \boldsymbol{\xi}} -E(\boldsymbol{o}) \tag{A.6}$$

s.t. $$\boldsymbol{C}\left(\boldsymbol{x}_{ilk}(t, \boldsymbol{\theta}_i)\right) \cdot \frac{d\boldsymbol{x}_{ilk}(t_{il}, \boldsymbol{\theta}_i)}{dt_{il}} = \boldsymbol{F} \cdot \boldsymbol{j}\left(\boldsymbol{x}_{ilk}(t_{il}, \boldsymbol{\theta}_i)\right), i \in SP, l \in FE, k \in CP \tag{A.7}$$

$$\boldsymbol{x}_{ilk} = \boldsymbol{x}_{il0} + dt_{il} \sum_{j=0}^{n_{CP}-1} \boldsymbol{A}_{kj} \boldsymbol{f}(\boldsymbol{x}_{ilj}, \boldsymbol{\theta}_i, \boldsymbol{u}_l, \boldsymbol{\xi}) \ , i \in SP, l \in FE, k \in CP \tag{A.8}$$

$$\boldsymbol{g}\left(\boldsymbol{x}_{ilk}(t_{il}, \boldsymbol{\theta}_i)\right) = \boldsymbol{0}, \boldsymbol{h}\left(\boldsymbol{x}_{ilk}(t_{il}, \boldsymbol{\theta}_i)\right) \leq \boldsymbol{0}, i \in SP, l \in FE, k \in CP \tag{A.9}$$

$$\boldsymbol{u}^L \leq \boldsymbol{u}_l(t) \leq \boldsymbol{u}^U, l \in FE \tag{A.10}$$

$$\boldsymbol{\xi}^L \leq \boldsymbol{\xi} \leq \boldsymbol{\xi}^U \tag{A.11}$$

$$\boldsymbol{x}_{i,l=1,k=0} = \boldsymbol{x}_{0,i}(\boldsymbol{\theta}_i), \boldsymbol{x}_{i,l=n_{FE},k=n_{CP}} = \boldsymbol{x}_{f,i}(\boldsymbol{\theta}_i), i \in SP \tag{A.12}$$

$$\boldsymbol{x}_{i,l-1,k=n_{CP}} = \boldsymbol{x}_{i,l,0}, i \in SP, l = 2 \ldots n_{FE} \tag{A.13}$$

$$dt_{il} = \frac{\tau_i}{n_{FE}}, l \in FE \tag{A.14}$$

$$\boldsymbol{\theta}_0 = E(\boldsymbol{\theta}) \tag{A.15}$$

$$\boldsymbol{\theta}_i = \boldsymbol{\theta}_0 + sgn(n_{\boldsymbol{\theta}} - i)\sqrt{(n_{\boldsymbol{\theta}} + \lambda)}\sqrt{Cov(\boldsymbol{\theta})}_i, i = 1..2n_{\boldsymbol{\theta}} \tag{A.16}$$

$$E(\boldsymbol{o}) = \sum_{i=0}^{2n} w_i \, \boldsymbol{o}_i, i \in SP \tag{A.17}$$

$$Cov(\boldsymbol{o}) = (1 - \alpha^2 + \beta)\{\boldsymbol{o}_0 - E(\boldsymbol{o})\}\{\boldsymbol{o}_0 - E(\boldsymbol{o})\}^{\mathrm{T}} + \sum_{i=1}^{2n} w_i \, \{\boldsymbol{o}_i - E(\boldsymbol{o})\}\{\boldsymbol{o}_i - E(\boldsymbol{o})\}^{\mathrm{T}}, i \in SP \tag{A.18}$$

$$w_0 = \frac{\lambda}{n_{\boldsymbol{\theta}} + \lambda}, \quad w_i = \frac{1}{2(n_{\boldsymbol{\theta}} + \lambda)}, i = 1 \ldots 2n_{\boldsymbol{\theta}} \tag{A.19}$$

$$\boldsymbol{o}_i = \int_0^{t_f} L\left(\boldsymbol{x}_{ilk}(t, \boldsymbol{\theta}_i)\right) dt_{il} + I\left(\boldsymbol{x}_{0,i}(\boldsymbol{\theta}_i)\right) + W\left(\boldsymbol{x}_{f,i}(\boldsymbol{\theta}_i)\right), i \in SP, l \in FE, k \in CP. \tag{A.20}$$

Dynamic uncertainty

$$\min_{\boldsymbol{u}_{l=1\ldots n_{FE}},\boldsymbol{\xi}} -E(\boldsymbol{o}) \tag{A.21}$$

$$\text{s.t. } \boldsymbol{C}\left(E\left(\boldsymbol{x}_{ilk}(t,\boldsymbol{\theta}_i)\right)\right)\cdot\frac{dE\left(\boldsymbol{x}_{ilk}(t,\boldsymbol{\theta}_i)\right)}{dt_{il}} = \boldsymbol{F}\cdot\boldsymbol{j}\left(E\left(\boldsymbol{x}_{ilk}(t,\boldsymbol{\theta}_i)\right)\right), \quad i\in SP, \; l\in FE, k\in CP \tag{A.22}$$

$$\boldsymbol{x}_{ilk} = E(\boldsymbol{x}_{il0}) + dt_{il}\sum_{j=0}^{n_{CP}-1}\boldsymbol{A}_{kj}\boldsymbol{f}(E(\boldsymbol{x}_{lj}),\boldsymbol{\theta}_i,\boldsymbol{u}_l,\boldsymbol{\xi}) \;, i\in SP, l\in FE, k\in CP \tag{A.23}$$

$$\boldsymbol{g}\left(E\left(\boldsymbol{x}_{ilk}(t,\boldsymbol{\theta}_i)\right)\right) = \boldsymbol{0}, \boldsymbol{h}\left(E\left(\boldsymbol{x}_{ilk}(t,\boldsymbol{\theta}_i)\right)\right)\le\boldsymbol{0}, i\in SP, l\in FE, k\in CP \tag{A.24}$$

$$\boldsymbol{u}^L \le \boldsymbol{u}_l(t) \le \boldsymbol{u}^U, l\in FE \tag{A.25}$$

$$\boldsymbol{\xi}^L \le \boldsymbol{\xi} \le \boldsymbol{\xi}^U \tag{A.26}$$

$$\boldsymbol{x}_{i,l=1,k=0} = \boldsymbol{x}_{i,0}(\boldsymbol{\theta}_i), \boldsymbol{x}_{i,l=n_{FE},k=n_{CP}} = \boldsymbol{x}_{f,i}(\boldsymbol{\theta}_i), i\in SP \tag{A.27}$$

$$E\left(\boldsymbol{x}_{i,l-1,k=n_{CP}}\right) = \boldsymbol{x}_{i,l,0}, i\in SP, l = 2\ldots n_{FE} \tag{A.28}$$

$$dt_{il} = \frac{\tau_i}{n_{FE}}, l\in FE \tag{A.29}$$

$$\boldsymbol{\theta}_0 = E(\boldsymbol{\theta}) \tag{A.30}$$

$$\boldsymbol{\theta}_i = \boldsymbol{\theta}_0 + sgn(n_{\boldsymbol{\theta}}-i)\sqrt{(n_{\boldsymbol{\theta}}+\lambda)}\sqrt{Cov(\boldsymbol{\theta})}_i, i = 1..2n_{\boldsymbol{\theta}} \tag{A.31}$$

$$E(\boldsymbol{o}) = \sum_{i=0}^{2n} w_i\,\boldsymbol{o}_i, i\in SP \tag{A.32}$$

$$Cov(\boldsymbol{o}) = (1-\alpha^2+\beta)\{\boldsymbol{o}_0 - E(\boldsymbol{o})\}\{\boldsymbol{o}_0 - E(\boldsymbol{o})\}^{\mathrm{T}} + \sum_{i=1}^{2n} w_i\,\{\boldsymbol{o}_i - E(\boldsymbol{o})\}\{\boldsymbol{o}_i - E(\boldsymbol{o})\}^{\mathrm{T}}, i\in SP \tag{A.33}$$

$$E\left(\boldsymbol{x}_{ilk}(t_{il},\boldsymbol{\theta}_i)\right) = \textstyle\sum_{i=0}^{2n_\theta} w_i\,\boldsymbol{x}_{ilk}\,(t_{il},\boldsymbol{\theta}_i), i\in SP, l\in FE, k\in CP \tag{A.34}$$

$$w_0 = \frac{\lambda}{n_{\boldsymbol{\theta}}+\lambda}, \quad w_i = \frac{1}{2(n_{\boldsymbol{\theta}}+\lambda)}, i = 1\ldots 2n_{\boldsymbol{\theta}} \tag{A.35}$$

$$\boldsymbol{o}_i = \textstyle\int_0^{t_f} L\left(\boldsymbol{x}_{ilk}(t,\boldsymbol{\theta}_i)\right)dt_{il} + I\left(\boldsymbol{x}_{0,i}(\boldsymbol{\theta}_i)\right) + W\left(\boldsymbol{x}_{f,i}(\boldsymbol{\theta}_i)\right), i\in SP, l\in FE, k\in CP. \tag{A.36}$$

A.4 Balance equations for CSTR cascade

The sensitivity analysis for the axial dispersion by means of varying Péclet numbers is carried out employing a CSTR cascade model, see subchapter 5.3.3. The corresponding balance equations for the liquid phase, the gas components in the liquid phase, and the gas phase are given in Eqs. (A.37), (A.38), and (A.39), respectively. The connectivity conditions are shown in Eqs. (A.40)-(A.41).

$$n_{\alpha,i}^{liq} = n_{\alpha,i}^{0,liq} + \tau_{CSTR,i}\,V_{liq,i}\left(c_{cat}M_{cat}\left(\textstyle\sum_{m=1}^{M}\nu_{\alpha,m}r_{m,i}\right)\right), \quad \alpha\in CH, i\in 1..N \tag{A.37}$$

$$n_{\alpha,i}^{gas} = n_{\alpha,i}^{0,gas} + y_{V,\alpha}^{m} - k_L a\,V_{liq}(c_\alpha^* - c_\alpha), \quad \alpha\in GAS, i\in 1..N \tag{A.38}$$

$$n_{\alpha,i}^{liq} = n_{\alpha,i}^{0,liq} + \tau_{CSTR,i}\,V_{liq,i}\left(c_{cat}M_{cat}\left(\sum_{m=1}^{M}\nu_{\alpha,m}r_{m,i}\right)\right) + k_L a\,V_{liq}(c_\alpha^* - c_\alpha), \alpha\in GAS, i\in 1..N \tag{A.39}$$

$$n_{\alpha,i-1}^{liq} = n_{\alpha,i}^{0,liq}, \alpha \in \{CH, GAS\} \quad \text{(A.40)}$$

$$n_{\alpha,i-1}^{gas} = n_{\alpha,i}^{0,gas}, \alpha \in GAS \quad \text{(A.41)}$$

A.5 Preliminary experiments for flow regime testing

The experimental setup consists of a helically coiled tube made of silicon, PFA or PTFE, to enable visual observation of the flow patterns, with diameters of $d_{tube} = 1.6\,\text{mm}, 2.0\,\text{mm}$ and $3.0\,\text{mm}$ and a length between $2\,\text{m} \leq l \leq 6\,\text{m}$. The coils have a diameter of $d_{coil} = 10\,\text{cm}$ and are coiled around a yellow PVC cylinder. The liquid phase is fed to the helically coiled tube by a pump (Smartline 1050, KNAUER Wissenschaftliche Geräte GmbH) and the gas phase is fed using a rotameter (DK800, Krohne Messtechnik GmbH). For determining the pressure loss two pressure transducers (CPT6200, Wika Alexander Wiegand SE & Co. KG) are installed at the tube inlet and outlet. The pressure inside the tube is maintained on a level which ensures the desired liquid hold-up of $\varepsilon_{liq}^{PFR} = 0.33$. This is managed using a needle valve at the outlet and the measurements obtained by the transducers. A scheme of the setup is shown in Fig. A.1. For a simplified handling, the flow investigation experiments were carried out with the substitute species 2-propanol, which has a lower surface tension than the original solvent system (DMF, n-decane). Thus, if the desired intermittent flow regime is stable for 2-propanol, it will a fortiori be stable for the original solvent system. The synthesis gas was replaced with air. The experimental results are shown in Fig. A.2.

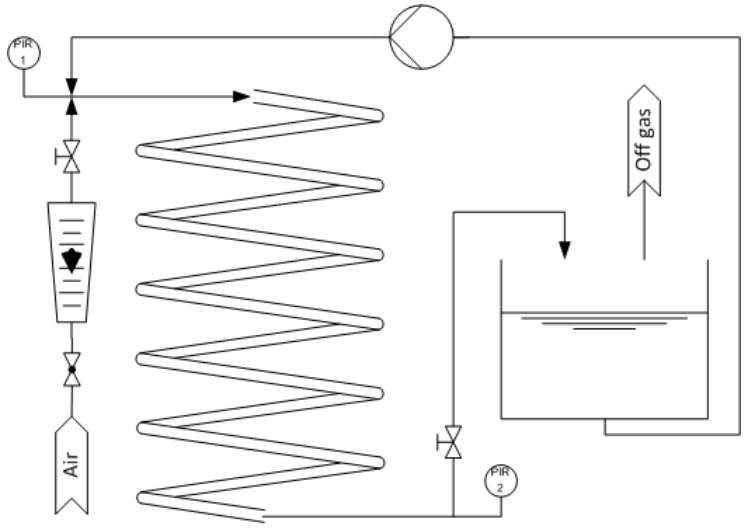

Figure A.1: Scheme of the experimental setup consisting of a helically coiled tube of different radii and a storage tank for the mixture of water and 2-propanol; air is dosed via rotameter to the helix and liquid phase via pump from the storage tank; pressure transducers are installed at the inlet and outlet for pressure drop registration

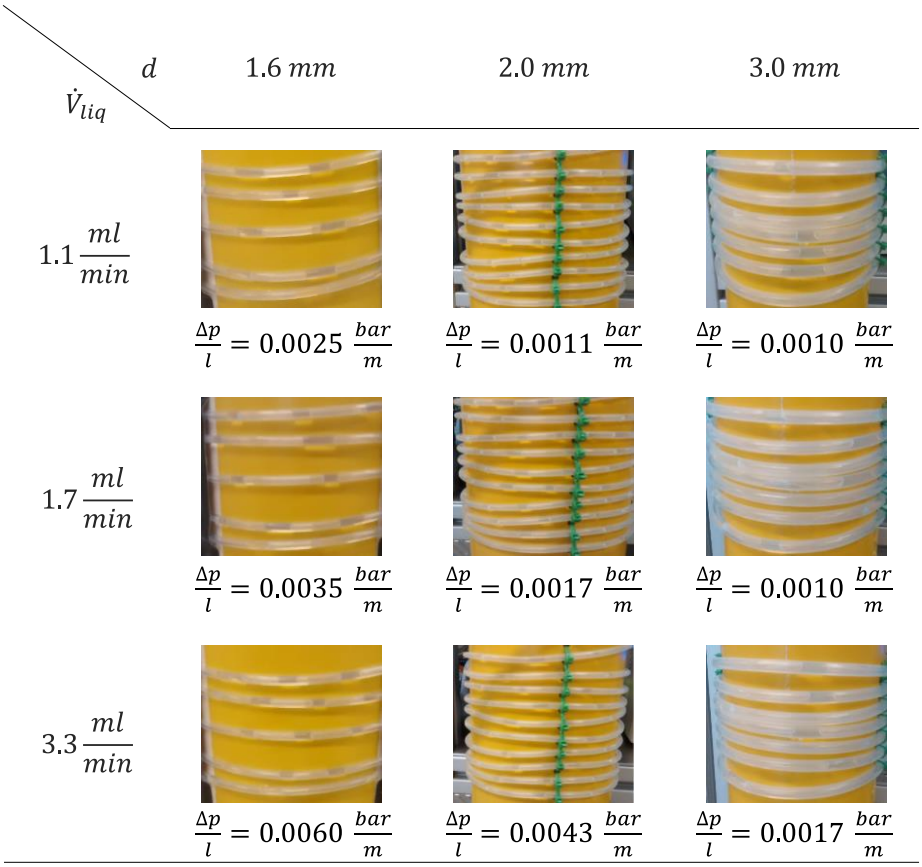

Figure A.2: Photographs of the flow regimes within the test setup (Fig. A.1) for different flow regimes $\dot{V}_{PFR,in}^{liq}$ and tube diameters ***d***; the transparent tubes are coiled around the yellow PVC cylinder and fixed with the green cable tie.

A.6 Modeling of distillation column

The modeling of the distillation column with the Fenske-Underwood equations requires information about the relative volatilities of the liquid components. Therefore, the vapor pressures of all components are determined using the correlations in Eqs. (A.42)-(A.43). The corresponding parameter are given in Tab. A.5.

$$p_\alpha^{vap} = 10\left(a_0 + \frac{a_1}{T} + a_2 \log_{10}(T) + a_3 T + a_4 T^2\right) \cdot 133.322 \cdot 10^{-6}, \quad \alpha \in \{nC12en, nC13al, nC12an, DMF, C10an\} \tag{A.42}$$

$$p_\alpha^{vap} = exp\left(a_0 + \frac{a_1}{T} + a_2 \ln(T) + a_3 T^{a_4}\right) \cdot 0.1, \quad \alpha \in \{iC12en, iC13al\} \tag{A.43}$$

$$\kappa_{\alpha,\beta} = \frac{p_\alpha^{vap}(T)}{p_\beta^{vap}(T)} \tag{A.44}$$

$$\bar{\kappa}_{\alpha,\beta} = \sqrt{\kappa_{\alpha,\beta}(T_D)\kappa_{\alpha,\beta}(T_B)} \tag{A.45}$$

$$N_{min} = \frac{\log\left(\frac{\dot{n}_{LK}^D \dot{n}_{HK}^B}{\dot{n}_{LK}^B \dot{n}_{HK}^D}\right)}{\log\left(\bar{\kappa}_{LK,HK}\right)} \tag{A.46}$$

Table A.5: Coefficients for vapour pressure correlations (Eqs. (A.42)-(A.43))

Components	Eq.	a_0	a_1	a_2	a_3	a_4
DMF	(A.42)	-47.99	-2385	28.80	$-5.86 \cdot 10^{-2}$	$3.139 \cdot 10^{-5}$
C10an	(A.42)	26.51	-3358	-6.12	$-3.32 \cdot 10^{-10}$	$4.855 \cdot 10^{-7}$
nC12en	(A.42)	-8.59	-3524	10.81	$-2.82 \cdot 10^{-2}$	$1.427 \cdot 10^{-5}$
nC12an	(A.42)	-5.65	-3470	9.03	$-2.32 \cdot 10^{-2}$	$1.124 \cdot 10^{-5}$
nC13al	(A.42)	161.50	-9766	-55.59	$2.10 \cdot 10^{-2}$	$5.550 \cdot 10^{-13}$
iC12en	(A.43)	75.79	-9964	-8.97	$4.94 \cdot 10^{-18}$	6
iC13al	(A.43)	10.42	-6149	0.20	$-2 \cdot 10^{-4}$	1

A.7 Numerical solution method

The dynamic optimization problems derived within this work are transformed into nonlinear programming problems by full discretization of states and controls via orthogonal collocation. The basic principle of collocation is the expansion of the unknown exact solution of the differential equations into a series of known functions, typically polynomials [211]

$$y(x) = \sum_{i=1}^{N+2} a_i y_i(x). \tag{A.47}$$

The more terms are included in the series the better its approximation of the exact solution is. This expansion is substituted in the original differential equation as a residual which is set to zero at a set of points called collocation points

$$F\left[\sum_{i=1}^{N+2} a_i y_i(x_j)\right] = 0, \quad j = 2, \dots, N+1 \tag{A.48}$$

with F being the differential equation and N the amount of collocation points. In addition to these N equations, two equations arise from the boundary conditions. This procedure is improved when the solution process is carried out in terms of the solution at the collocation points instead of the coefficients in the expansion. The coefficients in terms of the solution of the collocation points result in

$$a_i = \sum_{j=1}^{N+2} \left[y_i(x_j)\right]^{-1} y(x_j), \qquad j = 1, \dots, N+2. \tag{A.49}$$

By differentiation of Eq. (A.47) at all collocation points one can write the first derivative in terms of the values at the collocation points

$$\frac{dy}{dx}(x_j) = \sum_{i=1}^{N+2} a_i \frac{dy_i}{dx}(x_j) = \sum_{i,k=1}^{N+2} A_{jk} y(x_k), \qquad j = 1, \dots, N+2. \tag{A.50}$$

In the same way the second derivative can be obtained. Hence, ordinary and partial differential equations can be transformed into a set of algebraic equations to approximate their solution via collocation.

In case of orthogonal collocation, orthogonal polynomial functions are used and the collocation points are the root to one of the orthogonal polynomials, e.g. Legendre polynomials. The solution horizon is therefore normalized between $0..1$ and the collocation points are ordered such that the boundary points are included. Knowing the exact position of the collocation points, since they are roots of the polynomials, the expressions in Eq. (A.49) can be evaluated on the collocation points. In terms of this solution, again, the derivative at any collocation points can be determined. For the use of the orthogonal collocation methods, one requires the collocation matrix A. Depending on the chosen roots or polynomials and the resulting number of collocation points N, they differ in size and values. In the present work the Legendre roots for an initial value problem with three collocation points (Eq. (A.51)) are used.

$$\zeta = (0.155051025721682 \quad 0.644948974278318 \quad 1.0) \tag{A.51}$$

The resulting collocation matrix is defined as

$$A = \begin{pmatrix} 0.196815477223661 & -0.065535425850198 & 0.023770974348220 \\ 0.394424314739087 & 0.292073411665228 & -0.041548752125998 \\ 0.376403062700467 & 0.512485826188421 & 0.111111111111111 \end{pmatrix}. \tag{A.52}$$

The solution procedure and the practicability of the approach are further improved, when the domain is preliminary subdivided into finite elements of either the same lengths or varying lengths. The orthogonal collocation is then carried out on each finite element and the elements are connected via connectivity conditions to ensure a feasible overall solution [212]. Depending on the number of finite elements n_{FE} and the number of collocation points n_{CP} the system needs to be evaluated at $n_{FE} * (n_{CP} + 1) + 1$ points.

This approach is classified as direct simultaneous approach since the solution on all points is determined simultaneously and the Karush-Kuhn-Tucker optimality conditions are directly complied with. Its advantage is the applicability for a wide range of problems, especially large-sparse problems often arising in engineering, and the availability of powerful NLP solvers. The main drawback is the trade-off one has to make between the feasibility of the program and the accuracy of the underlying approximation of the exact solution, since the constraints are only satisfied on the collocation points and the controls are discretized and, thus, approximated.

Alternative methods are direct sequential methods such as single shooting, and indirect methods such as Pontryagin's Minimum Principle (PMP) or the Hamilton-Jacobi-Bellman (HJB) equation. Direct sequential methods only discretize the control vector and solve the evolution of the states via ODE solvers. They have the advantage, that the balance equations and constraints are not approximated and, hence, strictly satisfied. However, the evaluation of the ODEs might be very computationally expensive and the convergence of these approaches is low in case of several distributed control vectors and the inclusion of complex algebraic constraints. The indirect methods transform the dynamic optimization problem using the Hamiltonian function and define the constraints as a part of it including co-states. A recent, thorough study about the use of PMP for dynamic optimization of chemical processes can be found in [213]. The application of the HJB equation results in a formulation of a partial differential equation, which is often even harder to solve than the DAE systems described above. It is of special interest for optimal control calculations providing both information for feed forward and feedback control, see e.g. [214].

All NLPs in this work are solved with the interior-point optimizer IPOPT 3.11.9 including the linear solver ma27. The solver is a local optimizer, which cannot guarantee global optimal solutions. To ensure, that no suboptimal local optima were found, all optimizations were carried out for different initial values. The results presented in this work were the only local optima found within the studies.

References

[1] J.-C. Charpentier, "Modern Chemical Engineering in the Framework of Globalization, Sustainability, and Technical Innovation †", *Industrial & Engineering Chemistry Research*, vol. 46, no. 11, pp. 3465–3485, 2007.

[2] A. C. Dimian, "Renewable Raw Materials: chance and challenge for Computer-Aided Process Engineering", *17th European Symposium on Computer Aided Process Engineering - ESCAPE 17*, vol. 24, pp. 309–318, 2007.

[3] H. Freund and K. Sundmacher, "Towards a methodology for the systematic analysis and design of efficient chemical processes", *Chemical Engineering and Processing: Process Intensification*, vol. 47, no. 12, pp. 2051–2060, 2008.

[4] A. Peschel, H. Freund, and K. Sundmacher, "Methodology for the Design of Optimal Chemical Reactors Based on the Concept of Elementary Process Functions", *Industrial & Engineering Chemistry Research*, vol. 49, no. 21, pp. 10535–10548, 2010.

[5] A. Peschel, A. Jörke, K. Sundmacher et al., "Optimal reaction concept and plant wide optimization of the ethylene oxide process," *Chemical Engineering Journal*, 207-208, pp. 656–674, 2012.

[6] A. El Sibai, L. K. Rihko Struckmann, and K. Sundmacher, "Model-based Optimal Sabatier Reactor Design for Power-to-Gas Applications," *Energy Technology*, vol. 5, no. 6, pp. 911–921, 2017.

[7] J.-C. Charpentier, "Perspective on multiscale methodology for product design and engineering," *Computers & Chemical Engineering*, vol. 33, no. 5, pp. 936–946, 2009.

[8] H. Freund and K. Sundmacher, *Process Intensification, 1. Fundamentals and Molecular Level*, Wiley-VCH Verlag GmbH & Co. KGaA, Weinheim, 2011.

[9] J. J. Lerou and K. M. Ng, "Chemical reaction engineering: A multiscale approach to a multiobjective task," *Chemical Engineering Science*, vol. 51, no. 10, pp. 1595–1614, 1996.

[10] J. C. Charpentier and T. F. McKenna, "Managing complex systems: Some trends for the future of chemical and process engineering," *Chemical Engineering Science*, vol. 59, 8-9, pp. 1617–1640, 2004.

[11] J. M. Douglas, "A hierarchical decision procedure for process synthesis," *AIChE Journal*, vol. 31, no. 3, pp. 353–362, 1985.

[12] R. Smith and B. Linnhoff, "The design of separators in the context of overall processes," *Chemical Engineering Research and Design*, vol. 66, no. 3, pp. 195–228, 1988.

[13] J. A. Arizmendi-Sánchez and P. N. Sharratt, "Phenomena-based modularisation of chemical process models to approach intensive options," *Chemical Engineering Journal*, vol. 135, 1-2, pp. 83–94, 2008.

[14] M. Mangold, S. Motz, and E. Gilles, "A network theory for the structured modelling of chemical processes," *Chemical Engineering Science*, vol. 57, no. 19, pp. 4099–4116, 2002.

[15] K. Sundmacher and H. Freund, "Chemical Process Design: Moving Matter ElementsAlong Optimal Travel Routes in the Thermodynamic State Space," *The 5th International Symposium on Design, Operation and Control of Chemical Processes*, 2010.

[16] F. Karst, H. Freund, M. Maestri et al., "Multiscale Chemical Process Design Exemplified for a PEM Fuel Cell Process," *Chemie Ingenieur Technik*, vol. 86, no. 12, pp. 2075–2088, 2014.

[17] M. Feinberg and D. Hildebrandt, "Optimal reactor design from a geometric viewpoint—I. Universal properties of the attainable region," *Chemical Engineering Science*, vol. 52, no. 10, pp. 1637–1665, 1997.

[18] G. F. Froment, J. d. Wilde, and K. B. Bischoff, *Chemical reactor analysis and design*, Wiley, Hoboken, N.J., 2011.

[19] T. Dröge, G. Schembecker, U. Westhaus et al., “Heuristisch-numerisches Beratungssystem für die Reaktorauswahl bei der Verfahrensplanung,” *Chemie Ingenieur Technik*, vol. 66, no. 8, pp. 1043–1050, 1994.

[20] J. Till, G. Sand, S. Engell et al., “ReadOpt– Reaktor-Design- Optimierung durch Heuristik-gestützte MINLP-Methoden,” *Chemie Ingenieur Technik*, vol. 76, no. 8, pp. 1105–1110, 2004.

[21] F. Horn, *Attainable and non-attainable regions in chemical reaction technique*, Pergamon Press, London, UK, 1964.

[22] D. Glasser, C. Crowe, and D. Hildebrandt, “A geometric approach to steady flow reactors: The attainable region and optimization in concentration space,” *Industrial & Engineering Chemistry Research*, vol. 26, no. 9, pp. 1803–1810, 1987.

[23] W. C. Rooney, B. P. Hausberger, L. T. Biegler et al., “Convex attainable region projections for reactor network synthesis,” *Computers & Chemical Engineering*, vol. 24, 2-7, pp. 225–229, 2000.

[24] T. K. Abraham and M. Feinberg, “Kinetic Bounds on Attainability in the Reactor Synthesis Problem,” *Industrial & Engineering Chemistry Research*, vol. 43, no. 2, pp. 449–457, 2004.

[25] S. Balakrishna and L. T. Biegler, “Targeting strategies for the synthesis and energy integration of nonisothermal reactor networks,” *Industrial & Engineering Chemistry Research*, vol. 31, no. 9, pp. 2152–2164, 1992.

[26] S. Balakrishna and L. T. Biegler, “A unified approach for the simultaneous synthesis of reaction, energy, and separation systems,” *Industrial & Engineering Chemistry Research*, vol. 32, no. 7, pp. 1372–1382, 1993.

[27] S. Kauchali, W. C. Rooney, L. T. Biegler et al., “Linear programming formulations for attainable region analysis,” *Chemical Engineering Science*, vol. 57, no. 11, pp. 2015–2028, 2002.

[28] B. J. Davis, L. A. Taylor, and V. I. Manousiouthakis, “Identification of the Attainable Region for Batch Reactor Networks,” *Industrial & Engineering Chemistry Research*, vol. 47, no. 10, pp. 3388–3400, 2008.

[29] W. Zhou and V. I. Manousiouthakis, “Automating the AR construction for non-isothermal reactor networks,” *Computers & Chemical Engineering*, vol. 33, no. 1, pp. 176–180, 2009.

[30] D. Ming, D. Glasser, and D. Hildebrandt, “Application of attainable region theory to batch reactors,” *Chemical Engineering Science*, vol. 99, pp. 203–214, 2013.

[31] R. Jackson, “Optimization of chemical reactors with respect to flow configuration,” *Journal of Optimization Theory and Applications*, vol. 2, no. 4, pp. 240–259, 1968.

[32] L. E. K. Achenie and L. T. Biegler, “Algorithmic synthesis of chemical reactor networks using mathematical programming,” *Industrial & Engineering Chemistry Fundamentals*, vol. 25, no. 4, pp. 621–627, 1986.

[33] L. Achenie and L. T. Biegler, “A superstructure based approach to chemical reactor network synthesis,” *Computers & Chemical Engineering*, vol. 14, no. 1, pp. 23–40, 1990.

[34] A. C. Kokossis and C. A. Floudas, “Optimization of complex reactor networks—II. Nonisothermal operation,” *Chemical Engineering Science*, vol. 49, no. 7, pp. 1037–1051, 1994.

[35] E. C. Marcoulaki and A. C. Kokossis, “Scoping and screening complex reaction networks using stochastic optimization,” *AIChE Journal*, vol. 45, no. 9, pp. 1977–1991, 1999.

[36] A. Lakshmanan and L. T. Biegler, “Synthesis of Optimal Chemical Reactor Networks,” *Industrial & Engineering Chemistry Research*, vol. 35, no. 4, pp. 1344–1353, 1996.

[37] C. A. Schweiger and C. A. Floudas, "Optimization Framework for the Synthesis of Chemical Reactor Networks," *Industrial & Engineering Chemistry Research*, vol. 38, no. 3, pp. 744–766, 1999.

[38] O. Bilous and N. R. Amundson, "Optimum temperature gradients in tubular reactors—I," *Chemical Engineering Science*, vol. 5, no. 2, pp. 81–92, 1956.

[39] O. Bilous and N. R. Amundson, "Optimum temperature gradients in tubular reactors—II," *Chemical Engineering Science*, vol. 5, no. 3, pp. 115–126, 1956.

[40] F. Horn, "C1. Optimale Temperatur- und Konzentrationsverläufe," *Chemical Engineering Science*, vol. 14, no. 1, pp. 77–88, 1961.

[41] R. Aris, "Studies in optimization—II," *Chemical Engineering Science*, vol. 13, no. 1, pp. 18–29, 1960.

[42] R. Bellman, *Dynamic Programming*, Princeton University Press, Princeton, USA, 1957.

[43] M. Soroush and C. Kravaris, "Optimal design and operation of batch reactors. 1. Theoretical framework," *Industrial & Engineering Chemistry Research*, vol. 32, no. 5, pp. 866–881, 1993.

[44] M. Soroush and C. Kravaris, "Optimal design and operation of batch reactors. 2. A case study," *Industrial & Engineering Chemistry Research*, vol. 32, no. 5, pp. 882–893, 1993.

[45] O. Abel, A. Helbig, W. Marquardt et al., "Productivity optimization of an industrial semi-batch polymerization reactor under safety constraints," *Journal of Process Control*, vol. 10, no. 4, pp. 351–362, 2000.

[46] E. Johannessen and S. Kjelstrup, "Minimum entropy production rate in plug flow reactors: An optimal control problem solved for SO2 oxidation," *Energy*, vol. 29, 12-15, pp. 2403–2423, 2004.

[47] M. Hillestad, "A systematic generation of reactor designs," *Computers & Chemical Engineering*, vol. 28, no. 12, pp. 2717–2726, 2004.

[48] M. Hillestad, "A systematic generation of reactor designs," *Computers & Chemical Engineering*, vol. 29, no. 5, pp. 1101–1112, 2005.

[49] J. M. Douglas, *Conceptual design of chemical processes*, McGraw-Hill Book Co, New York, 1988.

[50] A. A. Upadhye, W. Qi, and G. W. Huber, "Conceptual process design: A systematic method to evaluate and develop renewable energy technologies," *AIChE Journal*, vol. 57, no. 9, pp. 2292–2301, 2011.

[51] W. L. Luyben, "Heuristic Design of Reaction/Separation Processes," *Industrial & Engineering Chemistry Research*, vol. 49, no. 22, pp. 11564–11571, 2010.

[52] M. Feinberg, "Toward a Theory of Process Synthesis," *Industrial & Engineering Chemistry Research*, vol. 41, no. 16, pp. 3751–3761, 2002.

[53] M. Feinberg and P. Ellison, "General Kinetic Bounds on Productivity and Selectivity in Reactor−Separator Systems of Arbitrary Design: Principles," *Industrial & Engineering Chemistry Research*, vol. 40, no. 14, pp. 3181–3194, 2001.

[54] P. Linke and A. Kokossis, "Attainable reaction and separation processes from a superstructure-based method," *AIChE Journal*, vol. 49, no. 6, pp. 1451–1470, 2003.

[55] S. Kossack, A. Refinius, S. Brüggemann et al., "Konzeptioneller Entwurf von Reaktions-Destillations-Prozessen mit Näherungsverfahren," *Chemie Ingenieur Technik*, vol. 79, no. 10, pp. 1601–1612, 2007.

[56] K. McBride, N. M. Kaiser, and K. Sundmacher, "Integrated reaction–extraction process for the hydroformylation of long-chain alkenes with a homogeneous catalyst," *Computers & Chemical Engineering*, 2016.

[57] O. Ryll, S. Blagov, and H. Hasse, "Thermodynamic analysis of reaction-distillation processes based on piecewise linear models," *Chemical Engineering Science*, vol. 109, pp. 284–295, 2014.

[58] B. Gross and P. Roosen, “Total process optimization in chemical engineering with evolutionary algorithms,” *Computers & Chemical Engineering*, vol. 22, pp. S229-S236, 1998.

[59] M. Vázquez-Ojeda, J. G. Segovia-Hernández, S. Hernández et al., “Design and optimization of an ethanol dehydration process using stochastic methods,” *Separation and Purification Technology*, vol. 105, pp. 90–97, 2013.

[60] L. M. Rios and N. V. Sahinidis, “Derivative-free optimization: A review of algorithms and comparison of software implementations,” *Journal of Global Optimization*, vol. 56, no. 3, pp. 1247–1293, 2013.

[61] J. A. Caballero and I. E. Grossmann, “An algorithm for the use of surrogate models in modular flowsheet optimization,” *AIChE Journal*, vol. 54, no. 10, pp. 2633–2650, 2008.

[62] A. C. Kokossis and C. A. Floudas, “Synthesis of isothermal reactor—separator—recycle systems,” *Chemical Engineering Science*, vol. 46, 5-6, pp. 1361–1383, 1991.

[63] I. E. Grossmann, J. A. Caballero, and H. Yeomans, “Mathematical programming approaches to the synthesis of chemical process systems,” *Korean Journal of Chemical Engineering*, vol. 16, no. 4, pp. 407–426, 1999.

[64] A. W. Westerberg, “A retrospective on design and process synthesis,” *Computers & Chemical Engineering*, vol. 28, no. 4, pp. 447–458, 2004.

[65] A. W. Dowling and L. T. Biegler, “A framework for efficient large scale equation-oriented flowsheet optimization,” *Computers & Chemical Engineering*, vol. 72, pp. 3–20, 2015.

[66] S. Recker, M. Skiborowski, C. Redepenning et al., “A unifying framework for optimization-based design of integrated reaction–separation processes,” *Computers & Chemical Engineering*, vol. 81, pp. 260–271, 2015.

[67] J. A. Fox, D. Hildebrandt, D. Glasser et al., “A graphical approach to process synthesis and its application to steam reforming,” *AIChE Journal*, vol. 59, no. 10, pp. 3714–3729, 2013.

[68] P. Lutze, A. Román-Martinez, J. M. Woodley et al., “A systematic synthesis and design methodology to achieve process intensification in (bio) chemical processes,” *Computers & Chemical Engineering*, vol. 36, pp. 189–207, 2012.

[69] H.-G. Beyer and B. Sendhoff, “Robust optimization – A comprehensive survey,” *Computer Methods in Applied Mechanics and Engineering*, vol. 196, 33-34, pp. 3190–3218, 2007.

[70] V. Gabrel, C. Murat, and A. Thiele, “Recent advances in robust optimization: An overview,” *European Journal of Operational Research*, vol. 235, no. 3, pp. 471–483, 2014.

[71] I. E. Grossmann, R. M. Apap, B. A. Calfa et al., “Recent advances in mathematical programming techniques for the optimization of process systems under uncertainty,” *Computers & Chemical Engineering*, vol. 91, pp. 3–14, 2016.

[72] A. Urbina, S. Mahadevan, and T. L. Paez, “Quantification of margins and uncertainties of complex systems in the presence of aleatoric and epistemic uncertainty,” *Reliability Engineering & System Safety*, vol. 96, no. 9, pp. 1114–1125, 2011.

[73] N. V. Sahinidis, “Optimization under uncertainty: State-of-the-art and opportunities,” *Computers & Chemical Engineering*, vol. 28, 6-7, pp. 971–983, 2004.

[74] J. R. Birge and F. V. Louveaux, “A multicut algorithm for two-stage stochastic linear programs,” *European Journal of Operational Research*, vol. 34, no. 3, pp. 384–392, 1988.

[75] J. L. Higle and S. Sen, “Stochastic Decomposition: An Algorithm for Two-Stage Linear Programs with Recourse,” *Mathematics of Operations Research*, vol. 16, no. 3, pp. 650–669, 1991.

[76] A. Shapiro and Y. Wardi, “Convergence analysis of gradient descent stochastic algorithms,” *Journal of Optimization Theory and Applications*, vol. 91, no. 2, pp. 439–454, 1996.

[77] M. A. H. Dempster, M. L. Fisher, L. Jansen et al., "Analytical Evaluation of Hierarchical Planning Systems," *Operations Research*, vol. 29, no. 4, pp. 707–716, 1981.

[78] G. Laporte and F. V. Louveaux, "The integer L-shaped method for stochastic integer programs with complete recourse," *Operations Research Letters*, vol. 13, no. 3, pp. 133–142, 1993.

[79] C. C. Carøe and J. Tind, "A cutting-plane approach to mixed 0–1 stochastic integer programs," *European Journal of Operational Research*, vol. 101, no. 2, pp. 306–316, 1997.

[80] C. C. Carøe and R. Schultz, "Dual decomposition in stochastic integer programming," *Operations Research Letters*, vol. 24, 1-2, pp. 37–45, 1999.

[81] L. L. Sakalauskas, "Nonlinear stochastic programming by Monte-Carlo estimators," *European Journal of Operational Research*, vol. 137, no. 3, pp. 558–573, 2002.

[82] Y. P. Li and G. H. Huang, "Interval-parameter Two-stage Stochastic Nonlinear Programming for Water Resources Management under Uncertainty," *Water Resources Management*, vol. 22, no. 6, pp. 681–698, 2008.

[83] Y. Shastri and U. Diwekar, "An efficient algorithm for large scale stochastic nonlinear programming problems," *Computers & Chemical Engineering*, vol. 30, no. 5, pp. 864–877, 2006.

[84] J. Steimel and S. Engell, "Conceptual design and optimization of chemical processes under uncertainty by two-stage programming," *Computers & Chemical Engineering*, vol. 81, pp. 200–217, 2015.

[85] S. Ahmed and N. V. Sahinidis, "Robust Process Planning under Uncertainty," *Industrial & Engineering Chemistry Research*, vol. 37, no. 5, pp. 1883–1892, 1998.

[86] Z. S. Guo, Y. P. Li, G. H. Huang et al., "An interval robust stochastic programming method for planning carbon sink trading to support regional ecosystem sustainability—A case study of Zhangjiakou, China," *Ecological Engineering*, vol. 104, pp. 99–115, 2017.

[87] X. M. Liu, G. H. Huang, S. Wang et al., "Water resources management under uncertainty: Factorial multi-stage stochastic program with chance constraints," *Stochastic Environmental Research and Risk Assessment*, vol. 30, no. 3, pp. 945–957, 2016.

[88] M. Delgado, F. Herrera, J. L. Verdegay et al., "Post-optimality analysis on the membership functions of a fuzzy linear programming problem," *Fuzzy Sets and Systems*, vol. 53, no. 3, pp. 289–297, 1993.

[89] H. Tanaka, T. Okuda, and K. Asai, "On Fuzzy-Mathematical Programming," *Journal of Cybernetics*, vol. 3, no. 4, pp. 37–46, 1974.

[90] H. Tanaka and K. Asai, "Fuzzy linear programming problems with fuzzy numbers," *Fuzzy Sets and Systems*, vol. 13, no. 1, pp. 1–10, 1984.

[91] R. E. Bellman and L. A. Zadeh, "Decision-Making in a Fuzzy Environment," *Management Science*, vol. 17, no. 4, pp. B-141-B-164, 1970.

[92] M. L. Liu and N. V. Sahinidis, "Optimization in Process Planning under Uncertainty," *Industrial & Engineering Chemistry Research*, vol. 35, no. 11, pp. 4154–4165, 1996.

[93] R. R. Tan and D. E. Cruz, "Synthesis of robust water reuse networks for single-component retrofit problems using symmetric fuzzy linear programming," *Computers & Chemical Engineering*, vol. 28, no. 12, pp. 2547–2551, 2004.

[94] H.-J. Park, J.-S. Lim, and J. M. Kang, "Optimization of Gas Production Systems Using Fuzzy Nonlinear Programming and Co-evolutionary Genetic Algorithm," *Energy Sources, Part A: Recovery, Utilization, and Environmental Effects*, vol. 30, no. 9, pp. 818–825, 2008.

[95] D. H. S. Tay, D. K. S. Ng, N. E. Sammons et al., "Fuzzy Optimization Approach for the Synthesis of a Sustainable Integrated Biorefinery," *Industrial & Engineering Chemistry Research*, vol. 50, no. 3, pp. 1652–1665, 2011.

[96] C.-L. Chen, T.-W. Yuan, and W.-C. Lee, “Multi-criteria fuzzy optimization for locating warehouses and distribution centers in a supply chain network,” *Journal of the Chinese Institute of Chemical Engineers*, vol. 38, 5-6, pp. 393–407, 2007.

[97] G. I. Schuëller and H. A. Jensen, “Computational methods in optimization considering uncertainties – An overview,” *Computer Methods in Applied Mechanics and Engineering*, vol. 198, no. 1, pp. 2–13, 2008.

[98] K. P. Halemane and I. E. Grossmann, “Optimal process design under uncertainty,” *AIChE Journal*, vol. 29, no. 3, pp. 425–433, 1983.

[99] R. E. Swaney and I. E. Grossmann, “An index for operational flexibility in chemical process design. Part I: Formulation and theory,” *AIChE Journal*, vol. 31, no. 4, pp. 621–630, 1985.

[100] Q. Zhang, I. E. Grossmann, and R. M. Lima, “On the relation between flexibility analysis and robust optimization for linear systems,” *AIChE Journal*, vol. 62, no. 9, pp. 3109–3123, 2016.

[101] G. Taguchi and M. S. Phadke, “Quality Engineering through Design Optimization,” in *Quality Control, Robust Design, and the Taguchi Method,* K. Dehnad, Ed., pp. 77–96, Springer US, Boston, MA, 1988.

[102] M.-h. Suh and T.-y. Lee, “Robust Optimization Method for the Economic Term in Chemical Process Design and Planning,” *Industrial & Engineering Chemistry Research*, vol. 40, no. 25, pp. 5950–5959, 2001.

[103] F. Logist, B. Houska, M. Diehl et al., “Robust multi-objective optimal control of uncertain (bio)chemical processes,” *Chemical Engineering Science*, vol. 66, no. 20, pp. 4670–4682, 2011.

[104] D. E. Majewski, M. Wirtz, M. Lampe et al., “Robust multi-objective optimization for sustainable design of distributed energy supply systems,” *Computers & Chemical Engineering*, vol. 102, pp. 26–39, 2017.

[105] P. Li, H. Arellano-Garcia, and G. Wozny, “Chance constrained programming approach to process optimization under uncertainty,” *Computers & Chemical Engineering*, vol. 32, 1-2, pp. 25–45, 2008.

[106] P. Li, M. Wendt, and G. Wozny, “Robust model predictive control under chance constraints,” *Computers & Chemical Engineering*, vol. 24, 2-7, pp. 829–834, 2000.

[107] G. M. Ostrovsky, N. N. Ziyatdinov, and T. V. Lapteva, “One-stage optimization problem with chance constraints,” *Chemical Engineering Science*, vol. 65, no. 7, pp. 2373–2381, 2010.

[108] G. M. Ostrovsky, N. N. Ziyatdinov, T. V. Lapteva et al., “Optimization of Chemical Process with Joint Chance Constraints,” *Industrial & Engineering Chemistry Research*, vol. 56, no. 12, pp. 3309–3331, 2017.

[109] K.-D. Wiese and D. Obst, “Hydroformylation,” in *Catalytic Carbonylation Reactions*: *Hydroformylation,* M. Beller, Ed., vol. 18, pp. 1–33, Springer Berlin Heidelberg, 2006.

[110] van Leeuwen and Claver, *Rhodium catalyzed hydroformylation*, Kluwer Academic Publishers, New York, 2002.

[111] A. Behr and L. Johnen, *Alternative Feedstocks for Synthesis*, Wiley-VCH Verlag GmbH & Co. KGaA, 2012.

[112] H.-W. Bohnen and B. Cornils, “Hydroformylation of alkenes: An industrial view of the status and importance,” vol. 47, pp. 1–64, Elsevier, 2002.

[113] J. Hibbel, E. Wiebus, and B. Cornils, “75 Jahre Hydroformylierung - Oxoreaktoren und Oxoanlagen der Ruhrchemie AG und der Oxea GmbH von 1938 bis 2013,” *Chemie Ingenieur Technik*, vol. 85, no. 12, pp. 1853–1871, 2013.

[114] R. Jennerjahn, I. Piras, R. Jackstell et al., “Palladium-catalyzed isomerization and hydroformylation of olefins,” *Chemistry (Weinheim an der Bergstrasse, Germany)*, vol. 15, no. 26, pp. 6383–6388, 2009.

[115] R. van Duren, van der Vlugt, Jarl Ivar, H. Kooijman et al., “Platinum-catalyzed hydroformylation of terminal and internal octenes,” *Dalton transactions (Cambridge, England : 2003),* no. 10, pp. 1053–1059, 2007.

[116] J. Pospech, I. Fleischer, R. Franke et al., “Alternative Metalle für die homogen katalysierte Hydroformylierung,” *Angewandte Chemie*, vol. 125, no. 10, pp. 2922–2944, 2013.

[117] B. Cornils and W. A. Herrmann, “Concepts in homogeneous catalysis: The industrial view,” *Journal of Catalysis*, vol. 216, 1-2, pp. 23–31, 2003.

[118] D. Obst, *Untersuchungen zur Synthese linearer Aldehyde durch isomerisierende Hydroformylierung innenständiger n-Alkene petro- und oleochemischer Herkunft*, Cuvillier, Göttingen, 2005.

[119] H. J. Beckers, J. M. de Rijke, and R. D. Garton, *Hydroformylation process employing loop reactors*.

[120] R. Tudor and M. Ashley, “Enhancement of Industrial Hydroformylation Processes by the Adoption of Rhodium-Based Catalyst: Part I,” *Platinum Metals Review*, vol. 51, no. 3, pp. 116–126, 2007.

[121] B. R. Tudor and M. Ashley, “Enhancement of Industrial Hydroformylation Processes by the Adoption of Rhodium-Based Catalyst: Part II,” *Platinum Metals Review*, vol. 51, no. 4, pp. 164–171, 2007.

[122] H. Bahrmann, H. Bach, and G. D. Frey, “Oxo Synthesis,” *Ullmann's Encyclopedia of Industrial Chemistry*, 2003.

[123] W. H. Summerlin, *Method for removing hydroformylation catalyst*.

[124] K. Winnacker, L. Küchler, and R. Dittmeyer, *Chemische Technik: Prozesse und Produkte. Band 4: Energieträger, Organische Grundstoffe*, Wiley-VCH, Weinheim, Great Britain, 2004-.

[125] C. W. Kohlpaintner, R. W. Fischer, and B. Cornils, “Aqueous biphasic catalysis: Ruhrchemie/Rhône-Poulenc oxo process,” *Applied Catalysis A: General*, vol. 221, 1-2, pp. 219–225, 2001.

[126] D. I. Enache, W. Thiam, D. Dumas et al., “Intensification of the solvent-free catalytic hydroformylation of cyclododecatriene: Comparison of a stirred batch reactor and a heat-exchange reactor,” *Catalysis Today*, vol. 128, 1-2, pp. 18–25, 2007.

[127] K.-D. Wiese, O. Möller, G. Protzmann et al., “A new reactor design for catalytic fluid–fluid multiphase reactions,” *Catalysis Today*, 79-80, pp. 97–103, 2003.

[128] A. Behr, G. Henze, L. Johnen et al., “Advances in thermomorphic liquid/liquid recycling of homogeneous transition metal catalysts,” *Journal of Molecular Catalysis A: Chemical*, vol. 285, 1-2, pp. 20–28, 2008.

[129] A. Behr and R. Roll, “Temperaturgesteuerte Mehrkomponenten-Lösungsmittelsysteme für homogene übergangsmetallkatalysierte Reaktionen,” *Chemie Ingenieur Technik*, vol. 77, no. 6, pp. 748–752, 2005.

[130] C. M. Hansen, *Hansen solubility parameters*: *A user's handbook*, CRC Press, Boca Raton, 2007.

[131] A. Behr and A. Wintzer, “Baukastensystem zur Auswahl von Lösungsmitteln in homogenkatalytischen Reaktionen,” *Chemie Ingenieur Technik*, vol. 83, no. 9, pp. 1356–1370, 2011.

[132] K. McBride, T. Gaide, A. Vorholt et al., “Thermomorphic solvent selection for homogeneous catalyst recovery based on COSMO-RS,” *Chemical Engineering and Processing: Process Intensification*, vol. 99, pp. 97–106, 2016.

[133] I. T. Horváth, G. Kiss, R. A. Cook et al., “Molecular Engineering in Homogeneous Catalysis: One-Phase Catalysis Coupled with Biphase Catalyst Separation. The Fluorous-Soluble HRh(CO){P[CH 2 CH 2 (CF 2) 5 CF 3] 3 } 3 Hydroformylation System,” *Journal of the American Chemical Society*, vol. 120, no. 13, pp. 3133–3143, 1998.

[134] M. Haumann, H. Koch, P. Hugo et al., “Hydroformylation of 1-dodecene using Rh-TPPTS in a microemulsion,” *Applied Catalysis A: General*, vol. 225, 1-2, pp. 239–249, 2002.

[135] F. Favre, H. Olivier-Bourbigou, D. Commereuc et al., “Hydroformylation of 1-hexene with rhodium in non-aqueous ionic liquids: How to design the solvent and the ligand to the reaction,” *Chemical Communications,* no. 15, pp. 1360–1361, 2001.

[136] B. Tan, J. Jiang, Y. Wang et al., “Thermoregulated ionic liquids and their application for the hydroformylation of 1-dodecene catalyzed by Rh/TPPTS complex,” *Applied Organometallic Chemistry*, vol. 22, no. 11, pp. 620–623, 2008.

[137] H.-P. Steinrück and P. Wasserscheid, “Ionic Liquids in Catalysis,” *Catalysis Letters*, vol. 145, no. 1, pp. 380–397, 2015.

[138] S. Giret, M. Wong Chi Man, and C. Carcel, “Mesoporous-Silica-Functionalized Nanoparticles for Drug Delivery,” *Chemistry (Weinheim an der Bergstrasse, Germany)*, vol. 21, no. 40, pp. 13850–13865, 2015.

[139] Y. Zhao, X. Zhang, J. Sanjeevi et al., “Hydroformylation of 1-octene in Pickering emulsion constructed by amphiphilic mesoporous silica nanoparticles,” *Journal of Catalysis*, vol. 334, pp. 52–59, 2016.

[140] K.-C. Song, J. Y. Baek, J. A. Bae et al., “Octene hydroformylation by using rhodium complexes tethered onto selectively functionalized mesoporous silica and in situ high pressure IR study,” *Catalysis Today*, vol. 164, no. 1, pp. 561–565, 2011.

[141] J. P. Arhancet, M. E. Davis, J. S. Merola et al., “Hydroformylation by supported aqueous-phase catalysis: A new class of heterogeneous catalysts,” *Nature*, vol. 339, no. 6224, pp. 454–455, 1989.

[142] A. Riisager, “Continuous fixed-bed gas-phase hydroformylation using supported ionic liquid-phase (SILP) Rh catalysts,” *Journal of Catalysis*, vol. 219, no. 2, pp. 452–455, 2003.

[143] A. Riisager, K. M. Eriksen, P. Wasserscheid et al., “Propene and 1-Octene Hydroformylation with Silica-Supported, Ionic Liquid-Phase (SILP) Rh-Phosphine Catalysts in Continuous Fixed-Bed Mode,” *Catalysis Letters*, vol. 90, 3/4, pp. 149–153, 2003.

[144] P. G. Jessop, T. Ikariya, and R. Noyori, “Homogeneous Catalysis in Supercritical Fluids,” *Chemical Reviews*, vol. 99, no. 2, pp. 475–494, 1999.

[145] D. Koch and W. Leitner, “Rhodium-Catalyzed Hydroformylation in Supercritical Carbon Dioxide,” *Journal of the American Chemical Society*, vol. 120, no. 51, pp. 13398–13404, 1998.

[146] C. J. Chang and A. D. Randolph, “Solvent expansion and solute solubility predictions in gas-expanded liquids,” *AIChE Journal*, vol. 36, no. 6, pp. 939–942, 1990.

[147] H. Jin and B. Subramaniam, “Homogeneous catalytic hydroformylation of 1-octene in CO 2 -expanded solvent media,” *Chemical Engineering Science*, vol. 59, 22-23, pp. 4887–4893, 2004.

[148] J. Fang, R. Jana, J. A. Tunge et al., “Continuous homogeneous hydroformylation with bulky rhodium catalyst complexes retained by nano-filtration membranes,” *Applied Catalysis A: General*, vol. 393, 1-2, pp. 294–301, 2011.

[149] Z. Xie, G. R. Akien, B. R. Sarkar et al., "Continuous Hydroformylation with Phosphine-Functionalized Polydimethylsiloxane Rhodium Complexes as Nanofilterable Homogeneous Catalysts," *Industrial & Engineering Chemistry Research*, vol. 54, no. 43, pp. 10656–10660, 2015.

[150] P. B. Webb, M. F. Sellin, T. E. Kunene et al., "Continuous flow hydroformylation of alkenes in supercritical fluid-ionic liquid biphasic systems," *Journal of the American Chemical Society*, vol. 125, no. 50, pp. 15577–15588, 2003.

[151] U. Hintermair, Z. Gong, A. Serbanovic et al., "Continuous flow hydroformylation using supported ionic liquid phase catalysts with carbon dioxide as a carrier," *Dalton transactions (Cambridge, England : 2003)*, vol. 39, no. 36, pp. 8501–8510, 2010.

[152] A. Behr, D. Obst, C. Schulte et al., "Highly selective tandem isomerization–hydroformylation reaction of trans-4-octene to n-nonanal with rhodium-BIPHEPHOS catalysis," *Journal of Molecular Catalysis A: Chemical*, vol. 206, 1-2, pp. 179–184, 2003.

[153] A. Behr, Y. Brunsch, and A. Lux, "Rhodium nanoparticles as catalysts in the hydroformylation of 1-dodecene and their recycling in thermomorphic solvent systems," *Tetrahedron Letters*, vol. 53, no. 22, pp. 2680–2683, 2012.

[154] E. Schäfer, Y. Brunsch, G. Sadowski et al., "Hydroformylation of 1-Dodecene in the Thermomorphic Solvent System Dimethylformamide/Decane. Phase Behavior–Reaction Performance–Catalyst Recycling," *Industrial & Engineering Chemistry Research*, vol. 51, no. 31, pp. 10296–10306, 2012.

[155] J. Markert, Y. Brunsch, T. Munkelt et al., "Analysis of the reaction network for the Rh-catalyzed hydroformylation of 1-dodecene in a thermomorphic multicomponent solvent system," *Applied Catalysis A: General*, 462-463, pp. 287–295, 2013.

[156] G. Kiedorf, D. M. Hoang, A. Müller et al., "Kinetics of 1-dodecene hydroformylation in a thermomorphic solvent system using a rhodium-biphephos catalyst," *Chemical Engineering Science*, vol. 115, pp. 31–48, 2014.

[157] B. Hentschel, G. Kiedorf, M. Gerlach et al., "Model-Based Identification and Experimental Validation of the Optimal Reaction Route for the Hydroformylation of 1-Dodecene," *Industrial & Engineering Chemistry Research*, vol. 54, no. 6, pp. 1755–1765, 2015.

[158] N. M. Kaiser, R. J. Flassig, and K. Sundmacher, "Reactor-network synthesis via flux profile analysis," *Chemical Engineering Journal*, vol. 335, pp. 1018–1030, 2018.

[159] B. Hentschel, A. Peschel, H. Freund et al., "Simultaneous design of the optimal reaction and process concept for multiphase systems," *Chemical Engineering Science*, vol. 115, pp. 69–87, 2014.

[160] O. Levenspiel, *The chemical reactor omnibook*, 1989.

[161] M. Metzger, B. Glasser, D. Glasser et al., "Teaching Reaction Engineering Using the Attainable Region," *Chemical Engineering Education*, vol. 41, no. 4, 2007.

[162] J. F. Burri, S. D. Wilson, and V. I. Manousiouthakis, "Infinite DimEnsionAl State-space approach to reactor network synthesis: Application to attainable region construction," *Computers & Chemical Engineering*, vol. 26, no. 6, pp. 849–862, 2002.

[163] M. Feinberg, "Optimal reactor design from a geometric viewpoint. Part II. Critical sidestream reactors," *Chemical Engineering Science*, vol. 55, no. 13, pp. 2455–2479, 2000.

[164] K. McBride and K. Sundmacher, "Data Driven Conceptual Process Design for the Hydroformylation of 1-Dodecene in a Thermomorphic Solvent System," *Industrial & Engineering Chemistry Research*, vol. 54, no. 26, pp. 6761–6771, 2015.

[165] J. Bremer, K. H. G. Rätze, and K. Sundmacher, “CO 2 methanation: Optimal start-up control of a fixed-bed reactor for power-to-gas applications,” *AIChE Journal*, vol. 63, no. 1, pp. 23–31, 2017.

[166] N. M. Kaiser, R. J. Flassig, and K. Sundmacher, “Probabilistic reactor design in the framework of elementary process functions,” *Computers & Chemical Engineering*, vol. 94, pp. 45–59, 2016.

[167] S. J. Julier, J. K. Uhlmann, and H. F. Durrant-Whyte, “A new approach for filtering nonlinear systems,” in *1995 American Control Conference - ACC'95*, pp. 1628–1632, 1995.

[168] S. J. Julier and J. K. Uhlmann, “A General Method for Approximating Nonlinear Transformations of Probability Distributions,” Technischer Bericht 7, Robotics Research Group, Department of Engineering Science.

[169] S. J. Julier and J. K. Uhlmann, “Unscented Filtering and Nonlinear Estimation,” *Proceedings of the IEEE*, vol. 92, no. 3, pp. 401–422, 2004.

[170] S. J. Julier, “The scaled unscented transformation,” in *Proceedings of 2002 American Control Conference*, p. 4555-4559 vol.6, 2002.

[171] R. van der Merwe, *Sigma-Point Kalman Filters for Probabilistic Inference in Dynamic State-Space Models*, 2004.

[172] F. Gustafsson and G. Hendeby, “On nonlinear transformation of stochastic variables and its application to nonlinear filtering,” *ICASSP 2008*, pp. 3617–3620, 2008.

[173] N. Rossner, *Robuste modellgestützte Prozessführung auf Basisvon Gauß’schen Mischdichten am Beispiel der Bray-Liebhafsky-Reaktion und der autotrophen Kultivierung von Ralstonia eutropha H16*, Berlin, 2014.

[174] R. J. Flassig and K. Sundmacher, “Optimal design of stimulus experiments for robust discrimination of biochemical reaction networks,” *Bioinformatics (Oxford, England)*, vol. 28, no. 23, pp. 3089–3096, 2012.

[175] S. Julier, J. Uhlmann, and H. F. Durrant-Whyte, “A new method for the nonlinear transformation of means and covariances in filters and estimators,” *IEEE Transactions on Automatic Control*, vol. 45, no. 3, pp. 477–482, 2000.

[176] S. J. Julier and J. K. Uhlmann, “New extension of the Kalman filter to nonlinear systems,” in *AeroSense '97,* I. Kadar, Ed., p. 182, SPIE, 1997.

[177] T. Heine, M. Kawohl, and R. King, “Robust model predictive control using unscented transformation,” *2006 IEEE Conference on Computer*, pp. 224–230, 2006.

[178] N. Rossner, T. Heine, and R. King, “Quality-by-Design Using a Gaussian Mixture Density Approximation of Biological Uncertainties,” *IFAC Proceedings Volumes*, vol. 43, no. 6, pp. 7–12, 2010.

[179] R. Schenkendorf, A. Kremling, and M. Mangold, “Optimal experimental design with the sigma point method,” *IET systems biology*, vol. 3, no. 1, pp. 10–23, 2009.

[180] S. J. Julier and J. K. Uhlmann, “A Consistent, Debiased Method for Converting Between Polar and Cartesian Coordinate Systems,” *Proceedings of AeroSense: 11th International Symposium on Aerospace/Defense Sensing, Simulation and Controls*, pp. 110–121, 1997.

[181] S. J. Julier and J. K. Uhlmann, “Reduced sigma point filters for the propagation of means and covariances through nonlinear transformations,” *Proceedings of the 2002 American Control conference,* no. 2, pp. 887–892, 2002.

[182] S. J. Julier, “<title>Skewed approach to filtering</title>,” in *Aerospace/Defense Sensing and Controls,* O. E. Drummond, Ed., pp. 271–282, SPIE, 1998.

[183] V. Bhaskar, S. K. Gupta, and A. K. Ray, “APPLICATIONS OF MULTIOBJECTIVE OPTIMIZATION IN CHEMICAL ENGINEERING,” *Reviews in Chemical Engineering*, vol. 16, no. 1, pp. 1–54, 2000.

[184] V. Pareto, *Manual of political economy*, Scholars Book Shelf, 1971.

[185] R. T. Marler and J. S. Arora, “Survey of multi-objective optimization methods for engineering,” *Structural and Multidisciplinary Optimization*, vol. 26, no. 6, pp. 369–395, 2004.

[186] I. Sobol’, “Global sensitivity indices for nonlinear mathematical models and their Monte Carlo estimates,” *Mathematics and Computers in Simulation*, vol. 55, 1-3, pp. 271–280, 2001.

[187] R. I. Cukier, C. M. Fortuin, K. E. Shuler et al., “Study of the sensitivity of coupled reaction systems to uncertainties in rate coefficients. I Theory,” *The Journal of Chemical Physics*, vol. 59, no. 8, pp. 3873–3878, 1973.

[188] A. Saltelli, M. Ratto, S. Tarantola et al., “Sensitivity analysis for chemical models,” *Chemical reviews*, vol. 105, no. 7, pp. 2811–2828, 2005.

[189] M. Vallerio, D. Telen, L. Cabianca et al., “Robust multi-objective dynamic optimization of chemical processes using the Sigma Point method,” *Chemical Engineering Science*, vol. 140, pp. 201–216, 2016.

[190] J. Lu and D. L. Darmofal, “Higher-Dimensional Integration with Gaussian Weight for Applications in Probabilistic Design,” *SIAM Journal on Scientific Computing*, vol. 26, no. 2, pp. 613–624, 2004.

[191] J. Maußner and H. Freund, “Optimization under uncertainty in chemical engineering: Comparative evaluation of unscented transformation methods and cubature rules,” *Chemical Engineering Science*, vol. 183, pp. 329–345, 2018.

[192] B. K. Øksendal, *Stochastic differential equations*: *An introduction with applications / Bernt Øksendal*, Springer, Berlin, London, 2003.

[193] M. Baerns, *Technische Chemie*, Wiley-VCH, Weinheim, 2006.

[194] N. M. Kaiser, R. J. Flassig, and K. Sundmacher, “Design and Comparison of Optimal Reactor Concepts for the Hydroformylation of Olefins by Use of a Probabilistic Design Framework,” in *26th European Symposium on Computer Aided Process Engineering*, vol. 38, pp. 1365–1370, Elsevier, 2016.

[195] A. Behr, H. Witte, and M. Zagajewski, “Scale-up durch Miniplant-Technik: Anwendungsbeispiele aus der homogenen Katalyse,” *Chemie Ingenieur Technik*, vol. 84, no. 5, pp. 694–703, 2012.

[196] M. Zagajewski, J. Dreimann, M. Thönes et al., “Rhodium catalyzed hydroformylation of 1-dodecene using an advanced solvent system: Towards highly efficient catalyst recycling,” *Chemical Engineering and Processing: Process Intensification*, vol. 99, pp. 115–123, 2016.

[197] J. Dreimann, P. Lutze, M. Zagajewski et al., “Highly integrated reactor–separator systems for the recycling of homogeneous catalysts,” *Chemical Engineering and Processing: Process Intensification*, vol. 99, pp. 124–131, 2016.

[198] J. M. Dreimann, H. Warmeling, J. N. Weimann et al., “Increasing selectivity of the hydroformylation in a miniplant: Catalyst, solvent, and olefin recycle in two loops,” *AIChE Journal*, vol. 62, no. 12, pp. 4377–4383, 2016.

[199] M. Zagajewski, J. Dreimann, and A. Behr, “Verfahrensentwicklung vom Labor zur Miniplant: Hydroformylierung von 1-Dodecen in thermomorphen Lösungsmittelsystemen,” *Chemie Ingenieur Technik*, vol. 86, no. 4, pp. 449–457, 2014.

[200] N. M. Kaiser, M. Jokiel, K. McBride et al., “Optimal Reactor Design via Flux Profile Analysis for an Integrated Hydroformylation Process,” *Industrial & Engineering Chemistry Research*, vol. 56, no. 40, pp. 11507–11518, 2017.

[201] K. Raetze, M. Jokiel, N. M. Kaiser et al., “Cyclic Operation of a Semi-Batch Reactor for the Hydroformylation of Long-Chain Olefins and Integration in a continuous Production Process,” *International Symposia on Chemical Reaction Engineering 25*, 2018.

[202] M. Jokiel, N. M. Kaiser, P. Kovats et al., “Helically Coiled Segmented Flow Tubular Reactor for the Hydroformylation of Long-Chain Olefins in a Thermomorphic Multicomponent Solvent System,” *International Symposia on Chemical Reaction Engineering 25*, 2018.

[203] J. W. Coleman and S. Garimella, “Characterization of two-phase flow patterns in small diameter round and rectangular tubes,” *International Journal of Heat and Mass Transfer*, vol. 42, no. 15, pp. 2869–2881, 1999.

[204] H. Pedersen and C. Horvath, “Axial dispersion in a segmented gas-liquid flow,” *Industrial & Engineering Chemistry Fundamentals*, vol. 20, no. 3, pp. 181–186, 1981.

[205] R. Gruber and T. Melin, “Radial mass-transfer enhancement in bubble-train flow,” *International Journal of Heat and Mass Transfer*, vol. 46, no. 15, pp. 2799–2808, 2003.

[206] S. Haase, D. Y. Murzin, and T. Salmi, “Review on hydrodynamics and mass transfer in minichannel wall reactors with gas–liquid Taylor flow,” *Chemical Engineering Research and Design*, vol. 113, pp. 304–329, 2016.

[207] I. R. Chughtai, W. Iqbal, G. U. Din et al., “Investigation of liquid phase axial dispersion in Taylor bubble flow by radiotracer residence time distribution analysis,” *EPJ Web of Conferences*, vol. 50, p. 1002, 2013.

[208] A. M. Fsadni and J. P. Whitty, “A review on the two-phase pressure drop characteristics in helically coiled tubes,” *Applied Thermal Engineering*, vol. 103, pp. 616–638, 2016.

[209] M. Jokiel, L.-M. Wagner, M. Mansour et al., “Measurement and simulation of mass transfer and backmixing behavior in a gas-liquid helically coiled tubular reactor,” *Chemical Engineering Science*, 2017.

[210] C. L. Yaws, *Chemical properties handbook*: *Physical, thermodynamic, environmental, transport, safety, and health related properties for organic and inorganic chemicals / Carl L. Yaws*, McGraw-Hill, New York, London, 1999.

[211] B. A. Finlayson, L. T. Biegler, and I. E. Grossmann, *Ullmann's modeling and simulation*: *Mathematics in Chemical Engineering*, Wiley-VCH; Chichester : John Wiley [distributor], Weinheim, 2007.

[212] J. S. Logsdon and L. T. Biegler, “Accurate solution of differential-algebraic optimization problems,” *Industrial & Engineering Chemistry Research*, vol. 28, no. 11, pp. 1628–1639, 1989.

[213] E. Aydin, D. Bonvin, and K. Sundmacher, “Dynamic optimization of constrained semi-batch processes using Pontryagin’s minimum principle—An effective quasi-Newton approach,” *Computers & Chemical Engineering*, vol. 99, pp. 135–144, 2017.

[214] C. Hermosilla, R. Vinter, and H. Zidani, “Hamilton–Jacobi–Bellman equations for optimal control processes with convex state constraints,” *Systems & Control Letters*, vol. 109, pp. 30–36, 2017.

List of figures

List of tables